

**Exploring the Potentials and
Limitations of Solid Tumor Treatment
by Thermosensitive Liposomes
and Hyperthermia**

Wouter Jacobus Marinus Lokerse

ISBN: 978-94-6361-006-3

Cover and printing: Optima Grafische Communicatie, Rotterdam, the Netherlands

© W.J.M. Lokerse, Rotterdam, 2017

All rights reserved. No part of this thesis may be reproduced or transmitted in any form by any means, without permission of the author or corresponding author.

This thesis is part of NanoNextNL, a micro and nanotechnology innovation consortium of the Government of the Netherlands and 130 partners from academia and industry. More information on www.nanonextnl.nl



Exploring the Potentials and Limitations of Solid Tumor Treatment by Thermosensitive Liposomes and Hyperthermia

**Het verkennen van de mogelijkheden en beperkingen van
thermosensitieve liposomen en hyperthermie voor de behandeling van
solide tumoren**

Thesis

To obtain the degree of Doctor from the Erasmus University of Rotterdam
by command of the rector magnificus
Prof.dr. H.A.P. Pols
and in accordance with the decision of the Doctorate board

The public defense shall be held on
Friday 22 December 2017 at 09:30 h

by

Wouter Jacobus Marinus Lokerse
born in Terneuzen, the Netherlands

Erasmus University Rotterdam



DOCTORAL COMMITTEE

Promoters: Prof.dr. A.M.M. Eggermont
Prof.dr. H. Grüll

Other members: Prof.dr. M de Jong
Prof.dr. L.H. Lindner
Prof.dr. T. Lammers

Copromoter: Dr. G.A. Koning

TABLE OF CONTENTS

Chapter 1:	General Introduction	7
Chapter 2:	In depth study on thermosensitive liposomes: Optimizing formulations for tumor specific therapy and <i>in vitro</i> to <i>in vivo</i> relations	29
Chapter 3:	Investigation of particle accumulation, chemosensitivity and thermosensitivity for effective solid tumor therapy using thermosensitive liposomes and hyperthermia	59
Chapter 4:	Comparing the therapeutic potential of thermosensitive liposomes and hyperthermia in two distinct subtypes of breast cancer	85
Chapter 5:	Development and validation of an isolated limb infusion model for investigation of drug delivery kinetics to solid tumors by thermosensitive liposomes and hyperthermia	109
Chapter 6:	Feasibility study on magnetic nanoparticle-entrapping liposomes for localized hyperthermia and image-guided drug delivery to solid tumors	127
Chapter 7:	General Discussion	143
	Summary	163
	List of publications	172
	PhD portfolio	173
	Acknowledgements	175
	Curriculum Vitae	179

CHAPTER 1

General Introduction



SOLID TUMOR TREATMENT

Cancer is a malignancy that will become more prevalent due to the demographic change towards an aging society [1-3]. When diagnosed early at a local stage, some cancers have a good prognosis for cure, while a diagnosis at a late stage makes treatment challenging and remains often palliative. As a tumor originates from the patient's own tissue, it can evade immune response and do not offer distinct targets for a more cancer specific treatment [4].

The classical cancer therapies used in the clinic are surgery, radiotherapy and chemotherapy. Surgery, although invasive, is a successful option if a tumor is diagnosed at an early stage in its development. However, resection of a tumor frequently includes removal of a margin of healthy tissue to reduce the chance of recurrence. In some cases, tumors are not resectable or only partly resectable, when vital organs or tissues are involved [5, 6]. Often chemotherapy or radiotherapy is given before or after surgery to reduce the local recurrence from residual cancer cells. Radiotherapy makes use of high energy photon radiation to treat cancers. The principle is based on cancer cells being less capable of recovering from damage induced by radiation than healthy cells. Therefore, radiotherapy is often given in multiple treatment rounds with sufficient recovery time in between for irradiated healthy tissues to recover [7, 8]. As radiation is intrinsically carcinogenic, it is dose limited and may even induce secondary cancers at a later stage. Chemotherapy is a method that makes use of drugs that interfere with cell division by interactions with DNA and can consequently cause cancer cell death [9, 10]. Because cancers have a more rapid growth rate than healthy tissues and are less capable of repairing DNA, chemotherapy causes a higher cytotoxic effect on cancer cells than healthy cells [11]. However, other healthy cell types with high growth rates are also affected by chemotherapy. This can cause side effects like hair loss, toxic effects in the intestine and bone marrow, which results in anemia. Next to these disadvantages, the DNA damaging effect of chemotherapy can also result in carcinogenic effects in healthy tissues.

Although cancer therapy has substantially improved over the last decades, a lot of cancers still are unsuccessfully treated by the conventional therapies. The conventional therapies do not act tumor specific and pose a risk to the patient as they cause side effects in healthy tissue. Because of these reasons, novel and more targeted therapies need to be investigated [12, 13].

LIPOSOMAL CHEMOTHERAPY FOR SOLID TUMORS

Traditional chemotherapy implies the intravenous (i.v.) administration of a chemotherapeutic drug which ideally has a more cytotoxic effect on cancers than on healthy

tissues. This is caused by the effect of chemotherapy on the cellular level as described above, but also due to specific microenvironmental factors within a tumor. Solid tumors have various typical characteristics like a necrotic core, high interstitial fluid pressure because of the absence of lymphatic drainage and a chaotically and tortuously developed vascular network. Fast developing tumors have the tendency to develop immature blood vessels which are chaotically organized [14], are variable in blood flow rate and direction [15] and contain gaps in the endothelial cell lining [16]. These gaps allow materials in the blood stream to diffuse into the tumor interstitium, a process which was first shown for macromolecules by Matsumura and Maeda in 1986 [17] and was termed as the “enhanced permeability and retention” (EPR) effect. In traditional chemotherapy, small chemotherapeutic molecules can penetrate the endothelium of blood vessels in the majority of tissues. However, because of their small size, the retention of these molecules in the tumor interstitium is low since blood flow mediated convection also removes the drug relatively quickly before it can get taken up by tumor cells [18-20]. Furthermore, chemotherapeutic drugs have a short circulation half-life and this prevents sufficient amount of drug from reaching the tumor and be therapeutically effective [21]. To increase the circulation time and reduce side effects of chemotherapeutic drugs, liposomes were proposed as drug carriers in the 70s [22]. The average diameter of commonly used liposomes is ~100 nm and was considered sufficiently small to accumulate in solid tumors by the EPR effect [23-25]. One of the best described liposomal chemotherapeutics which has reached the clinic is Doxil®, a liposome encapsulating doxorubicin (Dox) (Figure 1) [26]. This liposomal formulation is composed of the hydrogenated soy phosphatidylcholine (HSPC), cholesterol and 1,2-distearoyl-*sn*-glycero-3-phosphoethanolamine-N-(amino(polyethylene glycol)-2000) (DSPE-PEG₂₀₀₀). The natural product HSPC is a 9:1 mixture of 1,2-distearoyl-*sn*-glycero-3-phosphocholine (DSPC) and 1,2-dipalmitoyl-*sn*-glycero-3-phosphocholine (DPPC), respectively and is the main lipid building block of the liposome. Cholesterol is added to increase membrane stability [27]. The PEG₂₀₀₀ polymer conjugated to the DSPE lipid provides a steric coating on the surface of the liposome, which reduces interaction with serum opsonins, blood cells and cells of the reticuloendothelial system, which improves circulation time over not “pegylated” liposomes [28-30]. Liposomes can be loaded with Dox by a pH [31] or ion gradient [32], which is also known as active loading. Here the liposome aqueous core has an excess of protons relative to the external media that causes Dox that enters the liposome to become protonated and is therefore unable to migrate back out. Exceeding a certain interior concentration, Dox will precipitate and crystallize inside the core of the liposome (Figure 1).

When tested in patients, the half-life of Doxil® in the bloodstream was approximately 45h whereas free Dox was totally cleared within minutes after i.v. administration [33]. Furthermore, pegylated liposomes containing Dox also reduced side effects and showed

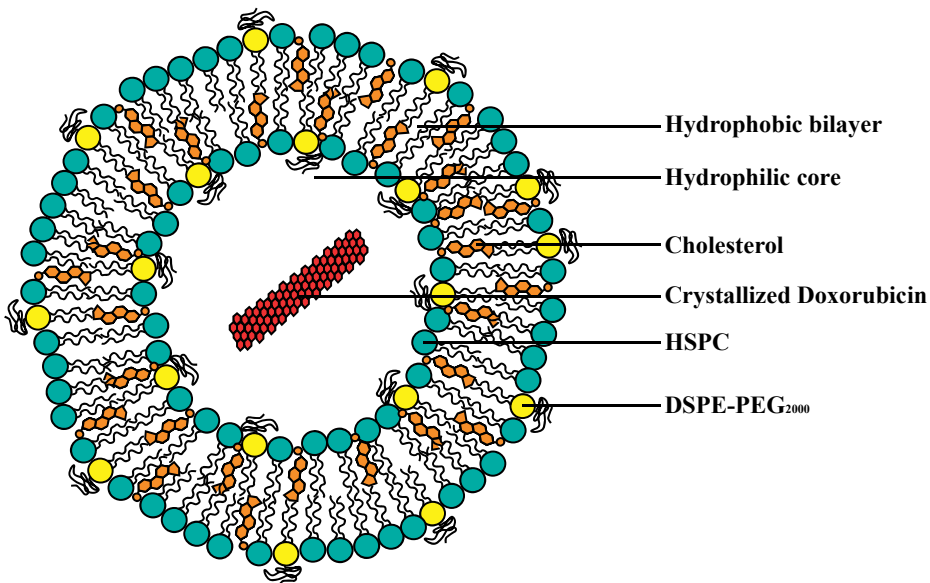


Figure 1. Schematic representation of the Doxil® liposome. The liposome is composed of a hydrophobic lipid bilayer with an entrapped aqueous compartment. Hydrogenated soy phosphatidylcholine (HSPC) is the main lipid used in the formulation and cholesterol provides higher stability of the lipid bilayer. The polyethylene glycol (PEG) 2000 group on the 1,2-distearoyl-*sn*-glycero-3-phosphoethanolamine (DSPE) lipid reduces interaction of the liposomes with proteins and cells of the reticuloendothelial system, thereby prolonging circulation time of the liposome. Doxorubicin is actively loaded into the hydrophilic core of the liposome where it resides in a crystallized form.

higher intratumoral Dox concentrations [34-36]. However, despite the indicated accumulation of liposomes in tumors in various pre-clinical [37, 38] and clinical occasions [25, 39], a significant therapeutic response of Doxil® over conventional chemotherapy in a clinical setting is lacking [40-43]. These findings can be explained by the EPR effect being highly variable between tumor types [25] and within patient populations [44]. Furthermore, discussion remained if the encapsulated Dox becomes bioavailable to the tumor cell nucleus to have its therapeutic effect or whether Dox is retained in the liposome and be therapeutically ineffective [45]. This resulted in a demand for liposomal formulations that could release their contents more effectively in a solid tumor, and thereby possibly being more effective in a broader set of cancer malignancies.

THERMOSENSITIVE LIPOSOMES

The research on developing liposomal formulations which release contents under influence of an environmental trigger focused on several options. Some examples of stimuli which have been investigated for drug release from liposomes are pH, ultrasound and

temperature [46]. The last-mentioned has the advantage that it can also influence the tumor in multiple ways, which will be further described in the next section. When designing a thermosensitive liposome (TSL), one has to select the appropriate lipids for drug release at a preferred temperature [47]. Each phospholipid has a melting temperature (T_m) that when approached, causes a lipid bilayer to undergo a phase transition from a solid gel phase to a liquid crystalline phase and thereby increases membrane permeability. In the solid gel phase, the lipid molecules are well organized with carbon chains largely in a stretched orientation and polar lipid head groups being immobile. Just below the T_m , at the pre-melting temperature, the enthalpy of the lipid molecules decrease and this increases mobility of the lipid head groups thereby slightly increasing the permeability of the membrane. A further increase in temperature will induce the carbon chains to become more flexible and thereby greatly increases fluidity and thus permeability of the membrane [48]. Furthermore, heating the lipid bilayer around the T_m will induce grain boundaries between lipid rafts that underwent phase transition and others that have not [49, 50]. This creates structural packing defects which further increase permeability of the membrane, thereby facilitating more pronounced transmembrane movement of any compound [51]. Greatly exceeding the T_m will cause the entire membrane to reach the liquid crystalline phase and grain boundaries will not be present anymore, this will cause the membrane permeability to decrease again [52, 53]. The chemical structure of the carbon chain of a lipid is the most important factor that determines the T_m of a lipid bilayer and by mixing different lipids in specific ratios; one can design a liposome with an optimal T_m based on the selected lipids and the quantities of each. Experiments on the feasibility of using mild hyperthermia (40–43°C; HT) for release of compounds from liposomes were first described by Yatvin and Weinstein in 1978, where they showed that the release of neomycin or carboxyfluorescein from a 1,2-dipalmitoyl-*sn*-glycero-3-phosphocholine (DPPC; $T_m = 41^\circ\text{C}$) liposome can be shifted to the mild hyperthermia range by adding 33 % (mol) of 1,2-distearoyl-*sn*-glycero-3-phosphocholine (DSPC; $T_m = 55^\circ\text{C}$) to the lipid composition of the particle [54].

In the late 80s and early 90s, the encapsulation of chemotherapeutics was investigated for cancer therapy and showed the first promising results in terms of stability at body temperature, release of the drug at mild HT, induction of cytotoxic effects on cancer cells *in vitro* and increased drug levels in heated tumors *in vivo* (Figure 2A) [55–57]. After pegylation proved to give higher circulation half-lives for stable liposomes (e.g. Doxil®), PEG made its introduction into thermosensitive liposomes (TSL) as well [58, 59]. This pegylated TSL is in literature often termed as the traditional thermosensitive liposome (TTSL), which next to the basic lipids, also contained cholesterol for increased membrane stability (Figure 2B). However, Needham and Dewhirst hypothesized that the TTSL had to be altered in order to ensure total drug release which is fast enough considering the short transition time of a liposome migrating through the vasculature of

a heated tumor [60, 61]. In order to do so, cholesterol and DSPC were removed in order to reduce membrane rigidity and lower the overall T_m of the liposome, respectively. More importantly, lysolipid was added to the formulation. This “low temperature sensitive liposome” (LTSL) relies on the micelle forming capacity of the lysolipid to generate pores at the grain boundaries which induces a higher drug release rate than a lysolipid-lacking TSL (Figure 2C) [48, 62]. Therefore, the LTSL showed higher Dox delivery to tumors than the TTSL [63] and resulted in a significant therapeutic response in multiple tumor types [64]. The LTSL formulation is undergoing commercialization by Celsion Corporation under the name ThermoDox® and is currently tested in clinical trials for liver cancers [65-67], breast [68], and pediatric cancers [69]. The clinical trials on liver cancer where LTSL was tested in combination with radiofrequency thermal ablation (RFA; see next section) showed no increase in progression free survival versus RFA treatment alone. The clinical trial on breast cancers has not provided survival data so far, but did show a 48% local overall (partial and complete) response rate for tumors treated with LTSL

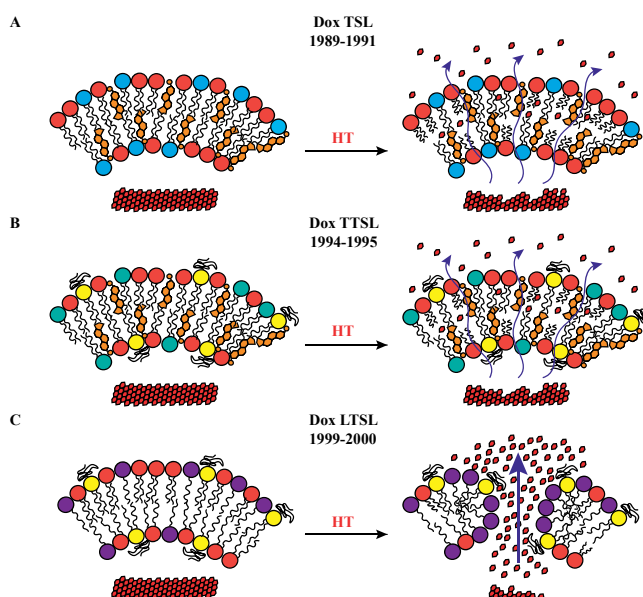


Figure 2. Schematic representation of Dox release from different TSL formulations described through time. The first Dox loaded TSL (A) was composed of dipalmitoyl-phosphatidylcholine (DPPC; red), distearoylphosphatidylcholine (DSPC; blue) and cholesterol (orange). At HT, the melting temperature (T_m) of the DPPC lipid is exceeded and the hydrocarbon chains (black tails) become disordered, creating grain boundaries with adjacent lipids through which the drug can cross the bilayer of the TSL. The “traditional TSL” (TTSL; B) closely resembles Doxil® in lipid makeup (Figure 1), where hydrogenated soy phosphatidylcholine (HSPC) is replaced by a mix of DPPC and DSPC with the appropriate net T_m to ensure drug release in a similar fashion as the first described Dox loaded TSL. The low TSL (LTSL; C) is by removing DSPC, HSPC and cholesterol more optimized for rapid drug release. The LTSL is composed of DPPC, DSPE-PEG₂₀₀₀ and the lysolipid monostearoylphosphatidylcholine (MSPC; purple). Initially, the same grain boundaries are formed at HT as for the previously mentioned TSLs. However, the additional lysolipids can migrate across the liposomal bilayer, forming a pore at the grain boundary, which can be further stabilized by PEG, through which Dox is released.

and mild HT. These findings implicate that clinical cancer treatment with LTSL and HT is not conclusive and that optimization of the therapy is required. The first factor to investigate for optimization of the therapy is the liposome formulation. Banno et al [70] and Paoli et al [71] described that LTSLs have a significantly shorter circulation half-life than TSL that did not contain lysolipid. Their findings, combined with *in vitro* and *in vivo* experiments from others [72, 73], also suggested that lysolipids may not stay associated with the liposome in circulation.

Additionally, Li and colleagues showed that by removing lysolipids from the formulation, the stability of the formulation can be increased without losing much of the thermosensitivity for rapid drug release. This increase in TSL stability also caused the formulation to be therapeutically more effective than LTSL [74]. These findings suggest that more investigation on alternatives for LTSL can be beneficial for optimizing the therapy.

Other examples of promising LTSL alternatives are TSL formulations with a detergent as a lysolipid replacement [75] or usage of pegylation alternatives for longer circulation time, without losing thermosensitivity [76]. The above-mentioned findings on TSLs illustrate that TSL-mediated drug delivery is a treatment with high potential for many types of solid tumors. However, there is still a demand for an optimal formulation that shows 1) high drug retention inside the liposomal carrier in circulation at body temperature, 2) high circulation half-life of the particle and 3) instant release at HT. A second factor that might be responsible for the above-mentioned results of the first clinical trials of LTSL is the infusion and HT workflow. Here, the LTSLs are infused before the RFA is applied and because of the relatively poor stability and circulation half-life of these particles, much of the administered dose can already be cleared before the tumor is brought to the desired temperature.

HYPERTHERMIA IN DRUG DELIVERY

Next to using HT as a trigger for drug release from thermosensitive liposomes, HT can also directly influence the tumor and its microenvironment. The first descriptions of using HT for cancer treatment date back to the writings of Hippocrates [77]. Additionally, findings where tumors appeared to shrink due to high fevers have also been described over a century ago [78, 79]. In cancer therapy, HT can be used solely to treat cancers [80, 81]. The effectiveness of this form of therapy depends on the specific heating protocol, duration of heating and the tissue type that is exposed [82, 83]. RFA is an example of a treatment that relies on only the heating of tissues for therapy. Here, a RFA probe is placed inside the tumor to induce heating up to 100 °C, thereby inducing local cell death [84]. However, HT is usually applied in the clinic in the mild range (40-43 °C)

as an additive to radiotherapy or chemotherapy where it has been shown to enhance therapeutic effect of these classical treatments [85, 86]. The increased sensitivity of cancers to chemotherapeutic drugs when exposed to HT is suggested to be caused by an increase in permeability of the cancer cell membrane and consequently higher drug uptake [87, 88]. In the field of drug delivery to solid tumors by nanomedicine, it is the influence on the tumor microenvironment that proved to be an interesting feature. HT influences the tumor microenvironment in multiple ways e.g. increasing blood flow and oxygenation [89-92]. But more importantly, HT appeared to improve tumor vessel permeability to small molecules [93], proteins [94], antibodies [95, 96] and liposomes [97-99]. The improved accumulation of these compounds in heated tumors is caused by increased perfusion [93] and a broadening of gaps in the endothelial lining of the affected blood vessels [97, 100, 101]. Although increased liposome accumulation by HT solely is interesting to exploit for cancer therapy [102, 103], the combination with direct cytotoxicity, enhanced chemosensitivity and the local triggered drug release from TSL by HT, is likely a more promising multi-edged therapy (Figure 3) [63, 104]. Currently, novel methods are developed to heat tumors more specifically and reduce heating of surrounding tissues. HT by high-intensity focused ultrasound (HIFU) is one example that is non-invasive and can be specifically directed to the tumor, a method that has gained attention as an effective tool for drug delivery in combination with TSL [105]. There are also examples of nanoparticles that can generate heat by an external trigger e.g. gold nanorods that generate heat by a near-infrared laser for Dox release by TSL [106] or liposomes that next to the encapsulated drug, contain magnetic nanoparticles (MNPs) that can generate heat by exposure to an alternating magnetic field (AMF), thereby releasing the drug [107, 108].

IMAGE-GUIDED DRUG DELIVERY

The previously mentioned results show that TSLs in combination with HT have high potential for clinical translation. However, there is a need for a better understanding on how injected particles behave when entering blood circulation, their pharmacokinetics, biodistribution, the interaction and behavior within the heated tumor and how this affects the drug that it carries. A suitable approach is the use of non-invasive imaging using e.g. positron emission tomography (PET), single-photon emission computed tomography (SPECT), magnetic resonance imaging (MRI) or fluorescence to follow and possibly quantify nanomedicines that carry a contrast and/ or imaging tracer *in vivo*. This field of image-guided drug delivery has become very broad and consists of a large amount of different types of particles, imaging techniques and drug delivery methodologies [109, 110]. For local drug release therapies, an ideal nanoparticle and its

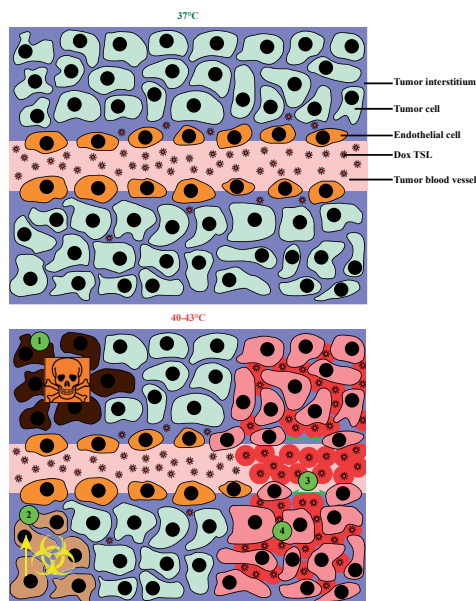


Figure 3. Schematic representation of factors influencing therapeutic response of a tumor to drug delivery by thermosensitive liposomes (TSL) and hyperthermia (HT). At 37°C (A), TSLs migrate through the tumor blood stream with particles accumulating in the tumor interstitium by gaps in the endothelial cell lining. When the tumor is heated to mild hyperthermic temperatures (40–43°C; B), direct apoptosis can be induced when given with the right timing, duration and intensity (1). Furthermore, chemosensitivity of the tumor can be increased (2). The gaps in the endothelial lining are broadened (3) and more particles can extravasate deeper into the tumor interstitium. Finally, HT causes a rapid drug release from TSLs (4), which is taken up by the cells in the area.

encapsulated cargo should be able to be imaged by one or more of the above-mentioned techniques (Figure 4). Using nuclear or optical imaging has shown that HT can increase the intratumoral uptake of the particle when a tumor was heated during [99] or before i.v. administration [100], respectively. However, imaging the drug remains the most important parameter to consider and this has been intensively investigated in various cases by encapsulating MRI contrast agents into TSLs [111, 112]. Here, the paramagnetic contrast agent is encapsulated inside the TSL limiting its interaction with the outside water pool. Upon release, the contrast agent generates an increase in T_1 relaxation time when it regains exposure to the surrounding water, which is visualized by MRI *in vivo*, thereby providing a representative indicator for the release and localization of Dox in an actual tumor. This concept was introduced by Viglianti et al [113, 114] where MnSO_4 was coencapsulated with Dox in TSLs. They showed by MRI that the contrast agent was highly released in the well-perfused periphery of the heated tumor and this was in good correlation with Dox measurements in the same tissues by fluorescence or high-performance liquid chromatography (HPLC). Other studies where $\text{Gd(HPDO3A)(H}_2\text{O)}$ was used as MRI contrast agent showed comparable results and thereby indicates the robustness of the methodology [99, 101, 115–117]. MnSO_4 and $\text{Gd(HPDO3A)(H}_2\text{O)}$

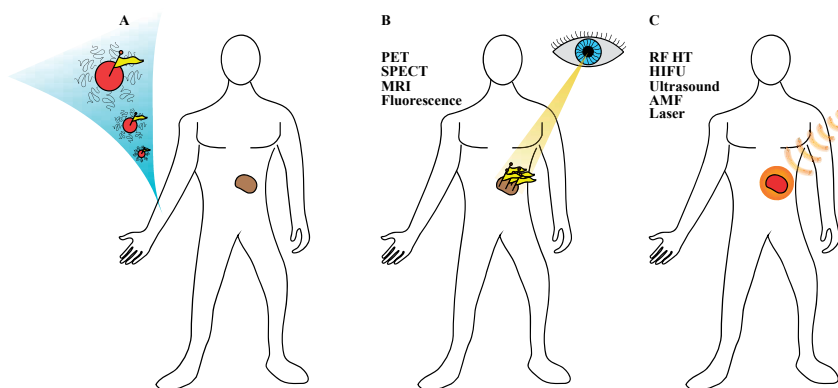


Figure 4. Representation of an ideal image guided drug delivery scenario. A nanomaterial can be tagged with a compound e.g. MRI contrast agent, radioactive compound or fluorescent dye (yellow flag) prior to intravenous administration (A). The tag can represent the nanoparticle or the incorporated drug and accumulates in the tumor which can be imaged by e.g. PET, SPECT, MRI or fluorescence imaging (B). Thirdly, the carrier needs to be susceptible to a non-invasive trigger for drug release at the target site e.g. HT induced directly by radiofrequency (RF HT) or HIFU, or indirectly by exposing accumulated MNPs or gold nanorods to an AMF or laser light, respectively. Other triggers like ultrasound or light can also be used for drug release (C).

were recently compared as imaging agents for Dox release from TSL [118]. Although both agents can represent Dox remarkably well, Mn^{2+} showed impairment in Dox release at 41°C and higher drug leakage at body temperature, leaving $\text{Gd}(\text{HPDO3A})(\text{H}_2\text{O})$ as the most suitable choice for imaging Dox release in a potentially future clinical setting. MRI for visualizing drug release and HIFU as the HT source (MR-HIFU) is currently getting more attention as a very promising theranostic methodology for treatment with Dox loaded TSL that could be translated to clinical use. Several studies in a rabbit model have shown high drug delivery to solid tumors that resulted in significant therapeutic efficacy [119-121] and recently, phase I clinical trials were initiated for pediatric refractory solid tumors that will further investigate the therapeutic potential of MR-HIFU with LTSL [69].

AIM OF THE THESIS

This thesis is focused on improving drug delivery by TSL and HT, and gaining a better understanding of the therapy and robustness of its efficacy. Throughout this thesis, Dox was used as a drug compound.

In [Chapter 2](#), different TSL formulations and Dox loading methods is compared in order to obtain a TSL with optimal Dox retention at 37°C and instant total release at 42°C . Furthermore, the correlation between *in vitro* stability tests and the actual *in vivo* outcome is investigated extensively.

In Chapter 3, the intravascular Dox release from TSLs is compared to a delivery scheme that comprises interstitial drug release after liposomal accumulation that is achieved in preheated tumors. Further investigation is performed on factors influenced by HT that improved local drug delivery and the role of the tumor microenvironment herein.

In Chapter 4, the therapeutic response of two different orthotopic breast cancer models to temperature induced Dox delivery by TSLs is investigated. The motivation is to understand how differences in tumor microenvironment and growth rate between these tumors affect Dox delivery and therapeutic response.

In Chapter 5, an isolated limb infusion model is introduced to investigate release kinetics from TSL and the delivery of the drug after a single passage through a heated tumor. The preliminary data shows that a considerable amount of TSL passages through a heated tumor are required for the delivery of a therapeutically relevant Dox dose. With future optimization of the model and experimental design, more quantitative data can be obtained which will improve the understanding of the delivery dynamics of Dox to solid tumors by TSLs.

In Chapter 6, approaches for development of a magnetic nanoparticle containing liposome for image-guided drug delivery is described. Though no liposomes with a high payload of magnetic nanoparticles could be obtained, this chapter contains an in depth analysis on liposomal preparations which could serve as a starting point for future successful production of magnetoliposomes.

REFERENCES

1. Mathers CD, Loncar D. Projections of global mortality and burden of disease from 2002 to 2030. *PLoS medicine*. 2006; 3: e442.
2. Stuckler D. Population causes and consequences of leading chronic diseases: a comparative analysis of prevailing explanations. *The Milbank quarterly*. 2008; 86: 273-326.
3. Smith BD, Smith GL, Hurria A, Hortobagyi GN, Buchholz TA. Future of cancer incidence in the United States: burdens upon an aging, changing nation. *Journal of clinical oncology : official journal of the American Society of Clinical Oncology*. 2009; 27: 2758-65.
4. Zindl CL, Chaplin DD. Immunology. Tumor immune evasion. *Science (New York, NY)*. 2010; 328: 697-8.
5. Quint LE. Lung cancer: assessing resectability. *Cancer Imaging*. 2004; 4: 15-8.
6. Wong JC, Raman S. Surgical resectability of pancreatic adenocarcinoma: CTA. *Abdominal Imaging*. 2010; 35: 471-80.
7. Bates T. A review of local radiotherapy in the treatment of bone metastases and cord compression. *International Journal of Radiation Oncology*Biophysics*. 1992; 23: 217-21.
8. Laperriere N, Zuraw L, Cairncross G. Radiotherapy for newly diagnosed malignant glioma in adults: a systematic review. *Radiotherapy and oncology : journal of the European Society for Therapeutic Radiology and Oncology*. 2002; 64: 259-73.
9. Brown JM, Attardi LD. The role of apoptosis in cancer development and treatment response. *Nature reviews Cancer*. 2005; 5: 231-7.
10. Ricci MS, Zong WX. Chemotherapeutic approaches for targeting cell death pathways. *The oncologist*. 2006; 11: 342-57.
11. Cheung-Ong K, Giaever G, Nislow C. DNA-damaging agents in cancer chemotherapy: serendipity and chemical biology. *Chemistry & biology*. 2013; 20: 648-59.
12. Peer D, Karp JM, Hong S, Farokhzad OC, Margalit R, Langer R. Nanocarriers as an emerging platform for cancer therapy. *Nature nanotechnology*. 2007; 2: 751-60.
13. Davis ME, Chen Z, Shin DM. Nanoparticle therapeutics: an emerging treatment modality for cancer. *Nat Rev Drug Discov*. 2008; 7: 771-82.
14. Jain RK. Determinants of tumor blood flow: a review. *Cancer Res*. 1988; 48: 2641-58.
15. Brurberg KG, Gaustad JV, Mollatt CS, Rofstad EK. Temporal heterogeneity in blood supply in human tumor xenografts. *Neoplasia*. 2008; 10: 727-35.
16. Hashizume H, Baluk P, Morikawa S, McLean JW, Thurston G, Roberge S, et al. Openings between defective endothelial cells explain tumor vessel leakiness. *Am J Pathol*. 2000; 156: 1363-80.
17. Matsumura Y, Maeda H. A new concept for macromolecular therapeutics in cancer chemotherapy: mechanism of tumoritropic accumulation of proteins and the antitumor agent smancs. *Cancer Res*. 1986; 46: 6387-92.
18. Primeau AJ, Rendon A, Hedley D, Lilge L, Tannock IF. The distribution of the anticancer drug Doxorubicin in relation to blood vessels in solid tumors. *Clinical cancer research : an official journal of the American Association for Cancer Research*. 2005; 11: 8782-8.
19. Patel KJ, Tredan O, Tannock IF. Distribution of the anticancer drugs doxorubicin, mitoxantrone and topotecan in tumors and normal tissues. *Cancer chemotherapy and pharmacology*. 2013; 72: 127-38.
20. Tredan O, Galmarini CM, Patel K, Tannock IF. Drug resistance and the solid tumor microenvironment. *Journal of the National Cancer Institute*. 2007; 99: 1441-54.

21. Speth PAVH, Q.G.; Haanen, C. Clinical pharmacokinetics of doxorubicin. *Clinical Pharmacokinetics*. 1988; 15: 15-31.
22. Kaye SB, Richardson VJ. Potential of liposomes as drug-carriers in cancer chemotherapy: a review. *Cancer Chemother Pharmacol*. 1979; 3: 81-5.
23. Koukourakis MI, Koukouraki S, Fezoulidis I, Kelekis N, Kyrias G, Archimandritis S, et al. High intratumoural accumulation of stealth liposomal doxorubicin (Caelyx) in glioblastomas and in metastatic brain tumours. *British journal of cancer*. 2000; 83: 1281-6.
24. Jain RK, Stylianopoulos T. Delivering nanomedicine to solid tumors. *Nat Rev Clin Oncol*. 2010; 7: 653-64.
25. Harrington KJ, Mohammadtaghi S, Uster PS, Glass D, Peters AM, Vile RG, et al. Effective targeting of solid tumors in patients with locally advanced cancers by radiolabeled pegylated liposomes. *Clinical cancer research : an official journal of the American Association for Cancer Research*. 2001; 7: 243-54.
26. Gabizon A, Shmeeda H, Barenholz Y. Pharmacokinetics of pegylated liposomal Doxorubicin: review of animal and human studies. *Clin Pharmacokinet*. 2003; 42: 419-36.
27. Silvander M, Johnsson M, Edwards K. Effects of PEG-lipids on permeability of phosphatidylcholine/cholesterol liposomes in buffer and in human serum. *Chem Phys Lipids*. 1998; 97: 15-26.
28. Senior J, Delgado C, Fisher D, Tilcock C, Gregoriadis G. Influence of surface hydrophilicity of liposomes on their interaction with plasma protein and clearance from the circulation: studies with poly(ethylene glycol)-coated vesicles. *Biochimica et biophysica acta*. 1991; 1062: 77-82.
29. Allen TM, Hansen C, Martin F, Redemann C, Yau-Young A. Liposomes containing synthetic lipid derivatives of poly(ethylene glycol) show prolonged circulation half-lives in vivo. *Biochimica et biophysica acta*. 1991; 1066: 29-36.
30. Allen TM, Austin GA, Chonn A, Lin L, Lee KC. Uptake of liposomes by cultured mouse bone marrow macrophages: influence of liposome composition and size. *Biochimica et biophysica acta*. 1991; 1061: 56-64.
31. Mayer LD, Bally MB, Cullis PR. Uptake of adriamycin into large unilamellar vesicles in response to a pH gradient. *Biochimica et biophysica acta*. 1986; 857: 123-6.
32. Haran G, Cohen R, Bar LK, Barenholz Y. Transmembrane ammonium sulfate gradients in liposomes produce efficient and stable entrapment of amphipathic weak bases. *Biochimica et biophysica acta*. 1993; 1151: 201-15.
33. Gabizon A, Catane R, Uziely B, Kaufman B, Safra T, Cohen R, et al. Prolonged circulation time and enhanced accumulation in malignant exudates of doxorubicin encapsulated in polyethylene-glycol coated liposomes. *Cancer Res*. 1994; 54: 987-92.
34. Hong RL, Huang CJ, Tseng YL, Pang VF, Chen ST, Liu JJ, et al. Direct comparison of liposomal doxorubicin with or without polyethylene glycol coating in C-26 tumor-bearing mice: is surface coating with polyethylene glycol beneficial? *Clinical cancer research : an official journal of the American Association for Cancer Research*. 1999; 5: 3645-52.
35. Barenholz Y. Doxil(R)--the first FDA-approved nano-drug: lessons learned. *Journal of controlled release : official journal of the Controlled Release Society*. 2012; 160: 117-34.
36. Wu NZ, Da D, Rudoll TL, Needham D, Whorton AR, Dewhirst MW. Increased microvascular permeability contributes to preferential accumulation of Stealth liposomes in tumor tissue. *Cancer Res*. 1993; 53: 3765-70.

37. Gabizon A, Papahadjopoulos D. Liposome formulations with prolonged circulation time in blood and enhanced uptake by tumors. *Proceedings of the National Academy of Sciences of the United States of America*. 1988; 85: 6949-53.
38. Yuan F, Leunig M, Huang SK, Berk DA, Papahadjopoulos D, Jain RK. Microvascular permeability and interstitial penetration of sterically stabilized (stealth) liposomes in a human tumor xenograft. *Cancer Res*. 1994; 54: 3352-6.
39. Harrington KJ, Lewanski C, Northcote AD, Whittaker J, Peters AM, Vile RG, et al. Phase II study of pegylated liposomal doxorubicin (Caelyx) as induction chemotherapy for patients with squamous cell cancer of the head and neck. *Eur J Cancer*. 2001; 37: 2015-22.
40. Northfelt DW, Dezube BJ, Thommes JA, Miller BJ, Fischl MA, Friedman-Kien A, et al. Pegylated-liposomal doxorubicin versus doxorubicin, bleomycin, and vincristine in the treatment of AIDS-related Kaposi's sarcoma: results of a randomized phase III clinical trial. *Journal of clinical oncology : official journal of the American Society of Clinical Oncology*. 1998; 16: 2445-51.
41. Garcia AA, Kempf RA, Rogers M, Muggia FM. A phase II study of Doxil (liposomal doxorubicin): lack of activity in poor prognosis soft tissue sarcomas. *Annals of oncology : official journal of the European Society for Medical Oncology*. 1998; 9: 1131-3.
42. Samantas E, Kalofonos H, Linardou H, Nicolaides C, Mylonakis N, Fountzilas G, et al. Phase II study of pegylated liposomal doxorubicin: inactive in recurrent small-cell lung cancer. A Hellenic Cooperative Oncology Group Study. *Annals of oncology : official journal of the European Society for Medical Oncology*. 2000; 11: 1395-7.
43. O'Brien ME, Wigler N, Inbar M, Rosso R, Grischke E, Santoro A, et al. Reduced cardiotoxicity and comparable efficacy in a phase III trial of pegylated liposomal doxorubicin HCl (CAELYX/Doxil) versus conventional doxorubicin for first-line treatment of metastatic breast cancer. *Annals of oncology : official journal of the European Society for Medical Oncology*. 2004; 15: 440-9.
44. Lee H, Shields AF, Siegel BA, Miller KD, Krop I, Ma CX, et al. ⁶⁴Cu-MM-302 Positron Emission Tomography Quantifies Variability of Enhanced Permeability and Retention of Nanoparticles in Relation to Treatment Response in Patients with Metastatic Breast Cancer. *Clinical cancer research : an official journal of the American Association for Cancer Research*. 2017.
45. Laginha KM, Verwoert S, Charrois GJ, Allen TM. Determination of doxorubicin levels in whole tumor and tumor nuclei in murine breast cancer tumors. *Clinical cancer research : an official journal of the American Association for Cancer Research*. 2005; 11: 6944-9.
46. Mura S, Nicolas J, Couvreur P. Stimuli-responsive nanocarriers for drug delivery. *Nat Mater*. 2013; 12: 991-1003.
47. Al-Ahmady Z, Kostarelos K. Chemical Components for the Design of Temperature-Responsive Vesicles as Cancer Therapeutics. *Chemical Reviews*. 2016; 116: 3883-918.
48. Landon CD, Park JY, Needham D, Dewhirst MW. Nanoscale Drug Delivery and Hyperthermia: The Materials Design and Preclinical and Clinical Testing of Low Temperature-Sensitive Liposomes Used in Combination with Mild Hyperthermia in the Treatment of Local Cancer. *The open nanomedicine journal*. 2011; 3: 38-64.
49. Kim DH, Costello MJ, Duncan PB, Needham D. Mechanical Properties and Microstructure of Polycrystalline Phospholipid Monolayer Shells: Novel Solid Microparticles. *Langmuir*. 2003; 19: 8455-66.

50. Kaasgaard T, Leidy C, Crowe JH, Mouritsen OG, Jørgensen K. Temperature-Controlled Structure and Kinetics of Ripple Phases in One- and Two-Component Supported Lipid Bilayers. *Biophysical Journal*. 2003; 85: 350-60.
51. Mouritsen OG, Zuckermann MJ. Model of interfacial melting. *Physical Review Letters*. 1987; 58: 389-92.
52. Papahadjopoulos D, Jacobson K, Nir S, Isac I. Phase transitions in phospholipid vesicles Fluorescence polarization and permeability measurements concerning the effect of temperature and cholesterol. *Biochimica et Biophysica Acta (BBA) - Biomembranes*. 1973; 311: 330-48.
53. Lu T, Ten Hagen TL. Inhomogeneous crystal grain formation in DPPC-DSPC based thermosensitive liposomes determines content release kinetics. *Journal of controlled release : official journal of the Controlled Release Society*. 2017; 247: 64-72.
54. Yatvin MB, Weinstein JN, Dennis WH, Blumenthal R. Design of liposomes for enhanced local release of drugs by hyperthermia. *Science*. 1978; 202: 1290-3.
55. Tomita T, Watanabe M, Takahashi T, Kumai K, Tadakuma T, Yasuda T. Temperature-sensitive release of adriamycin, an amphiphilic antitumor agent, from dipalmitoylphosphatidylcholine-cholesterol liposomes. *Biochimica et biophysica acta*. 1989; 978: 185-90.
56. Merlin JL. In vitro evaluation of the association of thermosensitive liposome-encapsulated doxorubicin with hyperthermia. *Eur J Cancer*. 1991; 27: 1031-4.
57. Iga K, Hamaguchi N, Igari Y, Ogawa Y, Toguchi H, Shimamoto T. Increased tumor cisplatin levels in heated tumors in mice after administration of thermosensitive, large unilamellar vesicles encapsulating cisplatin. *J Pharm Sci*. 1991; 80: 522-5.
58. Unezaki S, Maruyama K, Takahashi N, Koyama M, Yuda T, Suginata A, et al. Enhanced delivery and antitumor activity of doxorubicin using long-circulating thermosensitive liposomes containing amphipathic polyethylene glycol in combination with local hyperthermia. *Pharm Res*. 1994; 11: 1180-5.
59. Gaber MH, Hong K, Huang SK, Papahadjopoulos D. Thermosensitive sterically stabilized liposomes: formulation and in vitro studies on mechanism of doxorubicin release by bovine serum and human plasma. *Pharm Res*. 1995; 12: 1407-16.
60. Anyarambhatla GR, Needham D. Enhancement of the Phase Transition Permeability of DPPC Liposomes by Incorporation of MPPC: A New Temperature-Sensitive Liposome for use with Mild Hyperthermia. *Journal of Liposome Research*. 1999; 9: 491-506.
61. Needham D, Anyarambhatla G, Kong G, Dewhirst MW. A new temperature-sensitive liposome for use with mild hyperthermia: characterization and testing in a human tumor xenograft model. *Cancer Res*. 2000; 60: 1197-201.
62. Ickenstein LM, Arfvidsson MC, Needham D, Mayer LD, Edwards K. Disc formation in cholesterol-free liposomes during phase transition. *Biochimica et Biophysica Acta (BBA) - Biomembranes*. 2003; 1614: 135-8.
63. Kong G, Anyarambhatla G, Petros WP, Braun RD, Colvin OM, Needham D, et al. Efficacy of liposomes and hyperthermia in a human tumor xenograft model: importance of triggered drug release. *Cancer Res*. 2000; 60: 6950-7.
64. Yarmolenko PS, Zhao Y, Landon C, Spasojevic I, Yuan F, Needham D, et al. Comparative effects of thermosensitive doxorubicin-containing liposomes and hyperthermia in human and murine tumours. *International journal of hyperthermia : the official journal of European Society for Hyperthermic Oncology, North American Hyperthermia Group*. 2010; 26: 485-98.
65. Celsion. Phase 3 Study of ThermoDox With Radiofrequency Ablation (RFA) in Treatment of Hepatocellular Carcinoma (HCC). *ClinicalTrialsgov* NCT00617981; 2008.

66. Celsion. Study of ThermoDox With Standardized Radiofrequency Ablation (RFA) for treatment of Hepatocellular Carcinoma (HCC) (OPTIMA). ClinicalTrialsgov NCT02112656; 2014.
67. Poon RTP, Borys N. Lyso-thermosensitive liposomal doxorubicin: a novel approach to enhance efficacy of thermal ablation of liver cancer. *Expert Opinion on Pharmacotherapy*. 2009; 10: 333-43.
68. Zagar TM, Vujaskovic Z, Formenti S, Rugo H, Muggia F, O'Connor B, et al. Two phase I dose-escalation/pharmacokinetics studies of low temperature liposomal doxorubicin (LTLT) and mild local hyperthermia in heavily pretreated patients with local regionally recurrent breast cancer. *International journal of hyperthermia : the official journal of European Society for Hyperthermic Oncology, North American Hyperthermia Group*. 2014; 30: 285-94.
69. Kim A. A Phase I Study of Lyso-thermosensitive Liposomal Doxorubicin and MR-HIFU for Pediatric Refractory Solid Tumors. ClinicalTrialsgov NCT02536183; 2015.
70. Banno B, Ickenstein LM, Chiu GN, Bally MB, Thewalt J, Brief E, et al. The functional roles of poly(ethylene glycol)-lipid and lysolipid in the drug retention and release from lysolipid-containing thermosensitive liposomes in vitro and in vivo. *J Pharm Sci*. 2010; 99: 2295-308.
71. Paoli EE, Kruse DE, Seo JW, Zhang H, Kheirloomoom A, Watson KD, et al. An optical and microPET assessment of thermally-sensitive liposome biodistribution in the Met-1 tumor model: Importance of formulation. *Journal of controlled release : official journal of the Controlled Release Society*. 2010; 143: 13-22.
72. Sandstrom MC, Ickenstein LM, Mayer LD, Edwards K. Effects of lipid segregation and lysolipid dissociation on drug release from thermosensitive liposomes. *Journal of controlled release : official journal of the Controlled Release Society*. 2005; 107: 131-42.
73. Ickenstein LM. Triggered Drug Release from Thermosensitive Liposomes. Vancouver: University of British Columbia; 2003.
74. Li L, ten Hagen TL, Hossann M, Suss R, van Rhooen GC, Eggermont AM, et al. Mild hyperthermia triggered doxorubicin release from optimized stealth thermosensitive liposomes improves intratumoral drug delivery and efficacy. *Journal of controlled release : official journal of the Controlled Release Society*. 2013; 168: 142-50.
75. Tagami T, Ernstring MJ, Li SD. Optimization of a novel and improved thermosensitive liposome formulated with DPPC and a Brij surfactant using a robust in vitro system. *Journal of controlled release : official journal of the Controlled Release Society*. 2011; 154: 290-7.
76. Lindner LH, Eichhorn ME, Eibl H, Teichert N, Schmitt-Sody M, Issels RD, et al. Novel temperature-sensitive liposomes with prolonged circulation time. *Clinical cancer research : an official journal of the American Association for Cancer Research*. 2004; 10: 2168-78.
77. Hajdu SI. Greco-Roman thought about cancer. *Cancer*. 2004; 100: 2048-51.
78. Westermarck N. The Effect of Heat upon Rat-Tumorsl. *Skandinavisches Archiv Für Physiologie*. 1927; 52: 257-322.
79. Kienle GS. Fever in Cancer Treatment: Coley's Therapy and Epidemiologic Observations. *Global advances in health and medicine*. 2012; 1: 92-100.
80. Hildebrandt B, Wust P, Ahlers O, Dieing A, Sreenivasa G, Kerner T, et al. The cellular and molecular basis of hyperthermia. *Crit Rev Oncol Hematol*. 2002; 43: 33-56.
81. Vorotnikova E, Ivkov R, Foreman A, Tries M, Braunhut SJ. The magnitude and time-dependence of the apoptotic response of normal and malignant cells subjected to ionizing radiation versus hyperthermia. *Int J Radiat Biol*. 2006; 82: 549-59.
82. Roizin-Towle L, Pirro JP. The response of human and rodent cells to hyperthermia. *International journal of radiation oncology, biology, physics*. 1991; 20: 751-6.

83. Dewhirst MW, Vujaskovic Z, Jones E, Thrall D. Re-setting the biologic rationale for thermal therapy. *International journal of hyperthermia : the official journal of European Society for Hyperthermic Oncology, North American Hyperthermia Group.* 2005; 21: 779-90.
84. Wood BJ, Ramkaransingh JR, Fojo T, Walther MM, Libutti SK. Percutaneous Tumor Ablation with Radiofrequency. *Cancer.* 2002; 94: 443-51.
85. van der Zee J, Gonzalez Gonzalez D, van Rhooen GC, van Dijk JD, van Putten WL, Hart AA. Comparison of radiotherapy alone with radiotherapy plus hyperthermia in locally advanced pelvic tumours: a prospective, randomised, multicentre trial. *Dutch Deep Hyperthermia Group. Lancet.* 2000; 355: 1119-25.
86. Issels RD, Lindner LH, Verweij J, Wust P, Reichardt P, Schem BC, et al. Neo-adjuvant chemotherapy alone or with regional hyperthermia for localised high-risk soft-tissue sarcoma: a randomised phase 3 multicentre study. *Lancet Oncol.* 2010; 11: 561-70.
87. Bates DA, Mackillop WJ. Hyperthermia, Adriamycin Transport, and Cytotoxicity in Drug-sensitive and -resistant Chinese Hamster Ovary Cells. *Cancer Research.* 1986; 46: 5477-81.
88. Kawai H, Minamiya Y, Kitamura M, Matsuzaki I, Hashimoto M, Suzuki H, et al. Direct measurement of doxorubicin concentration in the intact, living single cancer cell during hyperthermia. *Cancer.* 1997; 79: 214-9.
89. Karino T, Koga S, Maeta M. Experimental studies of the effects of local hyperthermia on blood flow, oxygen pressure and pH in tumors. *Jpn J Surg.* 1988; 18: 276-83.
90. Horsman MR, Overgaard J. Can mild hyperthermia improve tumour oxygenation? *International journal of hyperthermia : the official journal of European Society for Hyperthermic Oncology, North American Hyperthermia Group.* 1997; 13: 141-7.
91. Song CW. Effect of local hyperthermia on blood flow and microenvironment: a review. *Cancer Res.* 1984; 44: 4721s-30s.
92. Song CW, Shakil A, Osborn JL, Iwata K. Tumour oxygenation is increased by hyperthermia at mild temperatures. 1996. *International journal of hyperthermia : the official journal of European Society for Hyperthermic Oncology, North American Hyperthermia Group.* 2009; 25: 91-5.
93. Lefor AT, Makohon S, Ackerman NB. The effects of hyperthermia on vascular permeability in experimental liver metastasis. *Journal of surgical oncology.* 1985; 28: 297-300.
94. Fujiwara K, Watanabe T. Effects of hyperthermia, radiotherapy and thermoradiotherapy on tumor microvascular permeability. *Acta Pathol Jpn.* 1990; 40: 79-84.
95. Hosono MN, Hosono M, Endo K, Ueda R, Onoyama Y. Effect of hyperthermia on tumor uptake of radiolabeled anti-neural cell adhesion molecule antibody in small-cell lung cancer xenografts. *J Nucl Med.* 1994; 35: 504-9.
96. Schuster JM, Zalutsky MR, Noska MA, Dodge R, Friedman HS, Bigner DD, et al. Hyperthermic modulation of radiolabelled antibody uptake in a human glioma xenograft and normal tissues. *International journal of hyperthermia : the official journal of European Society for Hyperthermic Oncology, North American Hyperthermia Group.* 1995; 11: 59-72.
97. Kong G, Braun RD, Dewhirst MW. Hyperthermia enables tumor-specific nanoparticle delivery: effect of particle size. *Cancer Res.* 2000; 60: 4440-5.
98. Kong G, Braun RD, Dewhirst MW. Characterization of the effect of hyperthermia on nanoparticle extravasation from tumor vasculature. *Cancer Res.* 2001; 61: 3027-32.
99. de Smet M, Langereis S, van den Bosch S, Bitter K, Hijnen NM, Heijman E, et al. SPECT/CT imaging of temperature-sensitive liposomes for MR-image guided drug delivery with high

- intensity focused ultrasound. *Journal of controlled release : official journal of the Controlled Release Society*. 2013; 169: 82-90.
100. Li L, ten Hagen TL, Bolkestein M, Gasselhuber A, Yatvin J, van Rhoon GC, et al. Improved intratumoral nanoparticle extravasation and penetration by mild hyperthermia. *Journal of controlled release : official journal of the Controlled Release Society*. 2013; 167: 130-7.
 101. de Smet M, Hijnen NM, Langereis S, Elevelt A, Heijman E, Dubois L, et al. Magnetic resonance guided high-intensity focused ultrasound mediated hyperthermia improves the intratumoral distribution of temperature-sensitive liposomal doxorubicin. *Investigative radiology*. 2013; 48: 395-405.
 102. Kong G, Dewhirst MW. Hyperthermia and liposomes. *International journal of hyperthermia : the official journal of European Society for Hyperthermic Oncology, North American Hyperthermia Group*. 1999; 15: 345-70.
 103. Matteucci ML, Anyarambhatla G, Rosner G, Azuma C, Fisher PE, Dewhirst MW, et al. Hyperthermia increases accumulation of technetium-99m-labeled liposomes in feline sarcomas. *Clinical cancer research : an official journal of the American Association for Cancer Research*. 2000; 6: 3748-55.
 104. Gaber MH, Wu NZ, Hong K, Huang SK, Dewhirst MW, Papahadjopoulos D. Thermosensitive liposomes: extravasation and release of contents in tumor microvascular networks. *Int J Radiat Oncol Biol Phys*. 1996; 36: 1177-87.
 105. Hijnen N, Langereis S, Grull H. Magnetic resonance guided high-intensity focused ultrasound for image-guided temperature-induced drug delivery. *Adv Drug Deliv Rev*. 2014; 72: 65-81.
 106. Agarwal A, Mackey MA, El-Sayed MA, Bellamkonda RV. Remote triggered release of doxorubicin in tumors by synergistic application of thermosensitive liposomes and gold nanorods. *ACS Nano*. 2011; 5: 4919-26.
 107. Tai LA, Tsai PJ, Wang YC, Wang YJ, Lo LW, Yang CS. Thermosensitive liposomes entrapping iron oxide nanoparticles for controllable drug release. *Nanotechnology*. 2009; 20: 135101.
 108. Nappini S, Bombelli FB, Bonini M, Norden B, Baglioni P. Magnetoliposomes for controlled drug release in the presence of low-frequency magnetic field. *Soft Matter*. 2010; 6: 154-62.
 109. Lammers T, Kiessling F, Hennink WE, Storm G. Nanotheranostics and Image-Guided Drug Delivery: Current Concepts and Future Directions. *Molecular Pharmaceutics*. 2010; 7: 1899-912.
 110. Terreno E, Uggeri F, Aime S. Image guided therapy: The advent of theranostic agents. *Journal of Controlled Release*. 2012; 161: 328-37.
 111. Tashjian JA, Dewhirst MW, Needham D, Viglianti BL. Rationale for and measurement of liposomal drug delivery with hyperthermia using non-invasive imaging techniques. *International journal of hyperthermia : the official journal of European Society for Hyperthermic Oncology, North American Hyperthermia Group*. 2008; 24: 79-90.
 112. Grull H, Langereis S. Hyperthermia-triggered drug delivery from temperature-sensitive liposomes using MRI-guided high intensity focused ultrasound. *Journal of controlled release : official journal of the Controlled Release Society*. 2012; 161: 317-27.
 113. Viglianti BL, Ponce AM, Michelich CR, Yu D, Abraham SA, Sanders L, et al. Chemodosimetry of in vivo tumor liposomal drug concentration using MRI. *Magnetic resonance in medicine*. 2006; 56: 1011-8.
 114. Viglianti BL, Abraham SA, Michelich CR, Yarmolenko PS, MacFall JR, Bally MB, et al. In vivo monitoring of tissue pharmacokinetics of liposome/drug using MRI: illustration of targeted delivery. *Magn Reson Med*. 2004; 51: 1153-62.

115. Peller M, Willerding L, Limmer S, Hossann M, Dietrich O, Ingrisich M, et al. Surrogate MRI markers for hyperthermia-induced release of doxorubicin from thermosensitive liposomes in tumors. *Journal of controlled release : official journal of the Controlled Release Society*. 2016; 237: 138-46.
116. Hijnen N, Kneepkens E, de Smet M, Langereis S, Heijman E, Grull H. Thermal combination therapies for local drug delivery by magnetic resonance-guided high-intensity focused ultrasound. *Proceedings of the National Academy of Sciences of the United States of America*. 2017; 114: E4802-e11.
117. Tagami T, Foltz WD, Ernstring MJ, Lee CM, Tannock IF, May JP, et al. MRI monitoring of intratumoral drug delivery and prediction of the therapeutic effect with a multifunctional thermosensitive liposome. *Biomaterials*. 2011; 32: 6570-8.
118. Yeo SY, de Smet M, Langereis S, Vander Elst L, Muller RN, Grull H. Temperature-sensitive paramagnetic liposomes for image-guided drug delivery: Mn(2+) versus [Gd(HPDO3A) (H₂O)]. *Biochimica et biophysica acta*. 2014; 1838: 2807-16.
119. Ranjan A, Jacobs GC, Woods DL, Negussie AH, Partanen A, Yarmolenko PS, et al. Image-guided drug delivery with magnetic resonance guided high intensity focused ultrasound and temperature sensitive liposomes in a rabbit Vx2 tumor model. *Journal of controlled release : official journal of the Controlled Release Society*. 2012; 158: 487-94.
120. Staruch RM, Ganguly M, Tannock IF, Hynynen K, Chopra R. Enhanced drug delivery in rabbit VX2 tumours using thermosensitive liposomes and MRI-controlled focused ultrasound hyperthermia. *International journal of hyperthermia : the official journal of European Society for Hyperthermic Oncology, North American Hyperthermia Group*. 2012; 28: 776-87.
121. Staruch RM, Hynynen K, Chopra R. Hyperthermia-mediated doxorubicin release from thermosensitive liposomes using MR-HIFU: therapeutic effect in rabbit Vx2 tumours. *International journal of hyperthermia : the official journal of European Society for Hyperthermic Oncology, North American Hyperthermia Group*. 2015; 31: 118-33.

CHAPTER 2

In depth study on thermosensitive liposomes: Optimizing formulations for tumor specific therapy and *in vitro* to *in vivo* relations

Wouter J.M. Lokerse

Esther C.M. Kneepkens

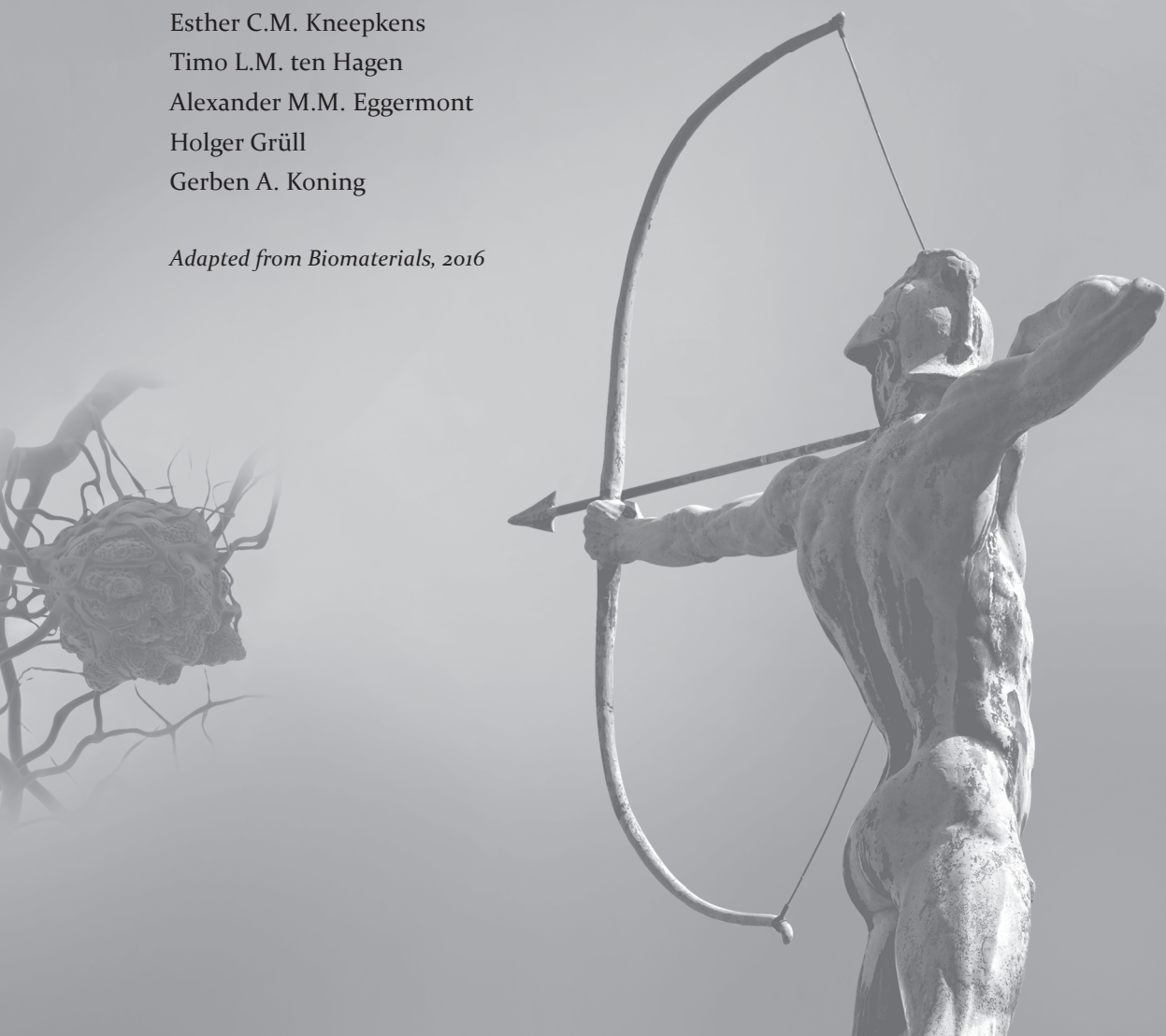
Timo L.M. ten Hagen

Alexander M.M. Eggermont

Holger Gröll

Gerben A. Koning

Adapted from Biomaterials, 2016



ABSTRACT

In numerous studies, thermosensitive liposomes (TSLs) for local heat-triggered delivery of Doxorubicin (Dox) to tumors have been investigated, with TSLs having different lipid formulations, drug loading methodology and testing procedures. To gain more insight in these parameters, we investigated TSLs with four variable DSPC-DPPC lipid ratios (50, 60, 70 or 80% DPPC and 5 mol% of DSPE-PEG₂₀₀₀) using either ammonium sulfate or a citrate buffer for Dox loading. Ammonium sulfate loading of Dox yielded more stable TSLs than citrate loading. At 37°C, leakage was unnoticeable for all ammonium sulfate TSLs. At 42°C, complete release occurred within seconds, except for 50% DPPC TSLs, where slow and incomplete release was observed *in vitro* but also *in vivo* using a dorsal skinfold window chamber. In contrast to *in vitro* assays, blood kinetics studies indicated a burst release of Dox upon injection and higher leakage for all TSLs. In therapeutic studies, hyperthermia in combination with TSLs repressed BFS-I sarcoma growth. Our study shows that prediction of therapeutic efficacy purely based on differences found *in vitro* is difficult, instead, parameters obtained from pharmacokinetic studies *in vivo*, and the exact timing of the delivery protocol need to be taken into account.

INTRODUCTION

Chemotherapy of solid tumors is complicated by the narrow therapeutic window typical for low molecular weight cytostatics like doxorubicin (Dox). Site-directed chemotherapy allows improving the therapeutic window by sparing the healthy organs from exposure to the drug while increasing drug concentrations in the targeted tissue. One approach for local drug delivery is the heat-triggered release of drugs that are encapsulated in aqueous lumen of temperature sensitive liposomes (TSLs). Upon heating, the lipid bilayer passes through a melting phase transition temperature (T_m) from a gel to a liquid-crystalline phase. The exact temperature and broadness of the phase transition depends on the exact lipid formulation and can be adjusted to be in the range of hyperthermic (HT) temperatures ($41 < T/^\circ\text{C} < 43$). As the phase transition is associated with a rapid increase in membrane permeability, TSLs can be exploited for rapid temperature-induced drug release. Stability at body temperature, release kinetics and T_m are strongly determined by the exact composition of the lipid bilayer, the chemical properties of the drug and other formulation aspects. Above concept was introduced by Yatvin and Weinstein et al. using a TSL based on 1,2-dipalmitoyl-sn-glycerophosphocholine (DPPC) and 1,2-distearoyl-sn-glycerophosphocholine (DSPC) for temperature-induced neomycin and methotrexate delivery, respectively [1,2]. Although they achieved a 3.6 times increase in tumor methotrexate levels when compared to free methotrexate or liposomal methotrexate without heating, the formulation showed poor blood circulation times and relatively slow release kinetics.

The most important goal in optimizing TSL formulations is to minimize drug leakage at body temperature while maximizing drug release at HT. The problem is that performance of TSL *in vitro* may not reflect their behaviour under *in vivo* conditions due to the more complex environment. Upon injection of the formulation *in vivo*, the liposomal release and stability might change and additionally, new parameters will come into play: e.g. time between injection and HT, the HT duration, the blood kinetics of the liposomal carrier and tumor characteristics e.g. perfusion [3–6]. A simplified equation describing the intricate balance between all these factors is depicted in Eq.1. [7].

$$[Dox]_{tumor} = \int_{t_{start}}^{t_{stop}} [liposome]_{plasma}(t) \cdot \left[\frac{Dox}{liposome} \right](t) \cdot Dox\ retention(t) \ dt \cdot \text{released fraction per } t_{res} \cdot \frac{\text{plasma flow tumor}}{\text{plasma volume tumor}} \quad \text{Eq.1}$$

The liposome plasma concentration ($[liposome]_{plasma}$) will decrease upon time after injection due to clearance by the reticulo-endothelial system (RES), while the rate of clearance depends on liposomal composition. The $[Dox/liposome]$ represents the fraction of Dox still present within the liposome and decreases when the Dox leaks out of the liposome (at 37°C) or gets released from the liposome (at 42°C). It is therefore related to

the liposome stability and release kinetics. The plasma flow in the tumor plasma space (plasma flow tumor/ plasma volume tumor) is dependent on the tumor type and its microenvironment. The released fraction of Dox per tumor residence time (t_{res}) depends on the combination of tumor perfusion, which will influence the t_{res} , and the release kinetics of the liposomal formulation. Furthermore, the Dox that is released from the liposomes within the tumor enters the interstitial space at a rate that is influenced by the Dox concentration already present in the tumor and when it enters, it can partially be washed out by blood flow mediated convection [7]. The Dox influx and outflux can be subsumed under the Dox retention parameter. Finally, the total Dox available to the tumor will depend on the total HT time ($t_{stop} - t_{start}$).

Over the years, different attempts have been made on improving the original TSL formulation used by Yatvin and Weinstein. Gaber et al. added pegylated lipids to the TSL formulation in order to increase its circulation time and therefore the $[liposome]_{plasma}$ parameter [8]. Later, Needham et al. and Li et al. showed that the incorporation of pegylated lipids not only increases the liposome circulation time but also influences their release kinetics [9,10]. Needham et al. greatly improved the rate of Dox release by the incorporation of lysolipids into low temperature sensitive liposomes (LTSLs, currently in clinical trials in a slightly different formulation as Thermodox® by Celsion) [11]. Unfortunately, the $[Dox/liposome]$ parameter of this formulation is still suboptimal due to premature leakage under physiological conditions [7]. In work previously published by our group, we have described a TSL consisting of DPPC, DSPC and 1,2-distearoyl-sn-glycero-3-phosphoethanolamine-N-[methoxy(polyethylene glycol)-2000] (DSPE-PEG₂₀₀₀) in a molar ratio of 80:15:5. The release of carboxyfluorescein and Dox from these liposomes was rapid and quantitative within seconds when exposed to a temperature of 42°C [10,12]. However, also this formulation displayed considerable leakage (up to 30% after one hour) under physiological conditions.

Aim of this study is to further improve above TSL formulation by systematic variation of its lipid composition and to investigate above explained parameters that contribute to the overall performance in drug delivery and relate them to the therapeutic efficacy of the formulations. Four TSL formulations were prepared by varying DPPC/DSPC ratio while maintaining a constant 5% mol:mol of DSPE-PEG₂₀₀₀. For all TSLs, the stability at 37°C and the release kinetics at 42°C were measured *in vitro* by fluorometry. The intraliposomal buffers ammonium sulphate ((NH₄)₂SO₄) or citrate were compared in their effect on Dox loading efficiency, stability and release kinetics [13,14]. The blood kinetics of the liposomal carrier and the leakage of these formulations were investigated *in vivo*. Further *in vivo* studies have been carried out in the form of murine dorsal skinfold intravital microscopy which showed the release patterns of these different liposomal formulations and the drug distribution in the tumor micro-environment. Finally, a therapeutic efficacy study was performed in a murine BFS-1 sarcoma (Figure 1). With

the presented data we aim to provide more insight in which parameters matter most in conducting an optimal therapy and to what extent *in vitro* data can be translated to *in vivo* therapeutic effect.

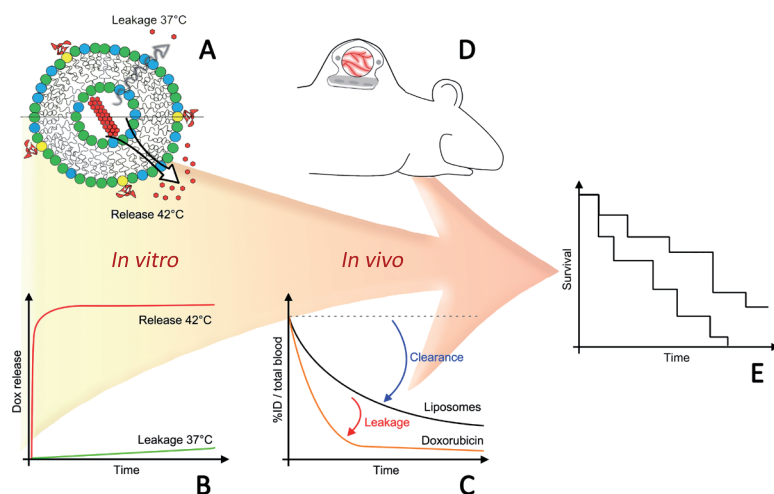


Figure 1. Schematic depiction of the presented workflow. *In vitro* characteristics like Dox release kinetics and leakage at physiological temperatures (A, B) were compared to release and leakage *in vivo* by studying Dox and carrier blood kinetics (C) and dorsal skinfold intravital microscopy (D). While these studies gave insight in the Dox supply to the tumor, a therapeutic study (E) was needed to study the result of the interplay of these factors with other therapeutically relevant factors like Dox tumor uptake, Dox tumor distribution and sensitivity of tumor cells to the drug.

MATERIALS AND METHODS

Materials

1,2-distearoyl-sn-glycero-3-phosphocholine (DSPC), 1,2-dipalmitoyl-sn-glycero-3-phosphocholine (DPPC) and 1,2-distearoyl-sn-glycero-3-phosphoethanolamine-N-[methoxy(polyethylene glycol)-2000] (DSPE-PEG₂₀₀₀) were purchased from Lipoid (Germany). DSPE-diethylenetriaminepentaacetic acid (DTPA) was obtained from Avanti polar lipids Inc. Doxorubicin-hydrochloride solution (2 mg/ml) was ordered from Accord Healthcare. All remaining chemicals were from Sigma Aldrich. PD-10 desalting columns were bought from GE-Healthcare Life Sciences.

Preparation of liposomes

Four liposomal formulations, were prepared with a different molar ratio of DPPC:DSPC but keeping a constant molar fraction of 5% DSPE-PEG₂₀₀₀. In detail, these formulations have molar ratios of DPPC:DSPC:DSPE-PEG₂₀₀₀ of 80:15:5 (TSL80), 70:25:5 (TSL70),

60:35:5 (TSL60) and 50:45:5 (TSL50). Liposomes were prepared by the film hydration and extrusion method at 60°C. The lipid film was hydrated in a 300 mM citrate buffer pH 4.5 or a 250 mM (NH₄)₂SO₄ buffer pH 5.5. Extrusion was done using a thermobarrel extruder (Northern Lipids, Vancouver, Canada). Samples were extruded 5 times through polycarbonate filters of 200, 100, 80 and 50 nm pore size. Liposomes were brought onto a PD-10 column and eluted with HEPES buffer pH 7.4. Subsequently, the phosphate concentration was determined with an ammonium molybdate spectrophotometric assay [15]. Dox loading was achieved by establishing as sample with a molar Dox:lipid ratio of 0.15:1 in HEPES buffer pH 7.4 that was incubated in a thermoshaker for 1 hour at 39°C and 300 rpm. Size and zeta potential measurements were carried out using dynamic light scattering (DLS) with a Zetasizer Nano ZS (Malvern Instruments, Worcestershire, UK). Transition temperatures (T_m) of liposomes were determined by differential scanning calorimetry (DSC).

Liposome radiolabeling

Measurement of the blood kinetics was performed using radiolabeled liposomes. TSLs incorporating 0.1 mol% DSPE-DTPA in the phospholipid bilayer were prepared and loaded with Dox in a similar fashion as described above. Subsequently, these TSLs were radiolabeled by 40 minutes incubation at 26°C with ¹¹¹InCl₃ in 2.5M sodium acetate pH 5.0. The radiochemical purity was tested with iTLC (running buffer: 10 mM EDTA in saline). After 10 minutes incubation with 10 mM EDTA at 26°C, the sample was washed 10 times with saline in a Amicon Ultra-0.5 mL centrifugal filter (50 kDa MWCO, Millipore) in order to dilute the sodium acetate and remove unbound ¹¹¹In to yield a radiochemical purity of ≥ 97%. No free Dox was observed in the supernatant.

Release kinetics of liposomes

For temperature dependent release testing, liposomes were added to preheated fetal bovine serum (FBS) (Sigma) and incubated for 5 min at designated temperatures in a thermoblock at 800 rpm. After measurement of the Dox fluorescence (excitation 482 nm; emission 594 nm), 50 µL 10% Triton-X100 (Sigma) was added to the sample and the sample was measured again to determine its 100% release signal. The resulting points per formulation were fitted with non-linear regression. Based on the fits, the temperature at which 50 % of the encapsulated Dox would be released after 5 min incubation in FBS was determined (R_{50}). The time dependent release analysis has been investigated in a largely similar fashion. A FBS containing cuvette was pre-heated to the temperature of choice and after 1 min of measurement, liposomes were spiked into the serum via surgical tubing and the sample was measured for 1 hour. Percentage release was calculated by: % release = $(S_n - S_{base}) / (S_{max} - S_{base}) * 100\%$, where S_n is the signal measured by a sample, S_{base} is the signal of a similar sample not exposed to elevated temperatures and S_{max} is the

maximum signal of a sample (either by exposure to HT, or adding Triton X-100). In an additional experiment, fluorescence measurements were performed with free Dox and empty liposomes at a Dox:lipid ratio of 0.15:1 in FBS in order to test for any quenching or scattering effects the presence of liposomes may have (Figure 2). All formulations were prepared in triplo and release assays were conducted in triplo for all formulations.

Cryo-Transmission Electron Microscopy

(NH₄)₂SO₄ TSL (50μL) samples in FBS (450μL) which were exposed to 42°C for 1 h were 1:1 diluted with distilled water before freezing. Sample preparation was performed by applying a 2 μl droplet of suspension to a lacy carbon film and subsequently plunge-freezing this sample into liquid ethane using a Vitrobot. The resulting amorphous ice film was prepared using the following blot conditions: blot time (2 sec), blot offset (2 mm) and blot total (1). Subsequently, cryo-TEM studies were performed using a FEI TECNAI F30ST (300kV, using a cryo-holder, keeping the sample at -173°C during the studies). Imaging was done in low-dose mode on a CCD camera (1k x 1k). For several locations on the sample, images were acquired at under-focus conditions.

In vivo experiments

BFS-1 tumors

BFS-1 sarcoma cells were grown *in vitro* in DMEM medium supplemented with 10% inactivated FBS and 5% penicillin/streptomycin. 1·10⁶ cells were injected subcutaneously into the flank of ten weeks old C57BL/6 mice (Harlan). When tumors reached the desirable size, 1 mm³ fragments were dissected and transplanted to the mice in the experimental groups. All BFS-1 animal study protocols were approved by the committee of Animal Research of Erasmus MC, Rotterdam, the Netherlands.

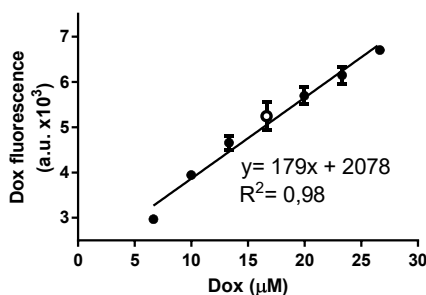


Figure 2. Dox fluorescence as a function of Dox concentration in the presence of empty liposomes, measured in FBS. The open circle represents the concentration of Dox at which all *in vitro* experiments were performed. N=3 for each concentration.

Blood kinetics and biodistribution

¹¹¹In-labeled TSLs (10 ± 2 MBq/mL TSL solution, $\sim 1.0 \pm 0.1$ MBq/mouse, 5 mg Dox/kg bodyweight in 96 ± 11 μ L) were injected via the tail vein of C57BL/6 mice under isoflurane anesthesia. Blood samples were taken according to two timelines. For the first timeline blood samples were drawn at 2, 10, 45, 150 and 210 minutes after injection ($n = 3$). During this period, the mice were kept under anesthesia and their temperature was maintained by a heated plate and heating pads, ensuring contact temperatures always $\leq 37^\circ\text{C}$. Body temperatures were always between 35 and 37°C as measured by a rectal probe. For the second timeline, animals were kept under anesthesia for 90 minutes while blood samples were drawn at 10, 30 and 60 minutes, followed by blood samples from the awake animals at 2, 3.5, 6 and 24 hours ($n = 3$). The blood samples and standards of the ¹¹¹In-labeled TSLs were weighed and their radioactivity was counted with a 1480 Automatic Gamma Counter (WizardTM 3", Perkin Elmer). Dox concentrations of the blood samples were determined according to the procedure outlined below. The percentage of the injected dose was calculated for the total organ or for the total blood assuming a total blood volume of 7.8% of the body weight. This relationship was derived by calculating the total blood volume of each mouse from the first group (first timeline) based on the blood level of liposomal carrier at the 2 min time point, by assuming the liposomal carrier was still fully present at this time point. The animal study protocols were approved by the committee of Animal Research of Maastricht University, Maastricht, the Netherlands.

Doxorubicin quantification

Blood samples (~ 10 -20 μ L/sample) and pieces of organs (~ 100 - 200 mg/organ) obtained during the blood kinetics and biodistribution experiments were analyzed for their Dox concentrations according to the protocol previously described [16]. An aqueous solution of daunorubicin (0.5 μ g/mL in 1 mL H₂O for the blood samples, 2 μ g/mL in 1.5 mL H₂O for the organ samples) was added to all samples as an internal standard for Dox quantification, followed by homogenization for 30 min at 30 Hz in a Qiagen TissueLyser. Subsequently, 125 μ L of the homogenized blood and tissue solutions were incubated with 50 μ L AgNO₃ in water (33% w/v) for 10 minutes at room temperature. The Dox was extracted by mixing with 1.25 mL chloroform/isopropanol (2:1 v/v). The organic phase was obtained by centrifugation (10 min at 3600 rpm) and transferred to a clean tube and evaporated to dryness at 40°C under N₂ flow. The resulting residue was dissolved in 200 μ L H₂O. HPLC analysis was performed on an Agilent Technologies system (1100 series) equipped with an autosampler and fluorescence detector ($\lambda_{\text{ex}} = 485$ nm and $\lambda_{\text{em}} = 590$ nm). 50 μ L of each sample was injected on an Eclipse XDB-C18 column (5 μ m, 4.6×150 mm² Agilent). The Dox and daunorubicin were eluted in 6 and 12 min respectively,

using an isocratic flow of 1 mL/min with 30% (v/v) acetonitrile in H₂O containing 0.1% TFA (v/v).

Pharmacokinetic parameter estimation

The blood kinetic data of the four different liposomal carriers (from both timelines) were fitted using a mono-exponential function to derive the blood half-lives as well as the clearance of the liposomal carrier by the reticuloendothelial system (RES) (k_{RES}).

$$c_{lip}(t) = c_{lip}(0) \cdot \exp(-k_{RES} \cdot t) \quad \text{Eq.2}$$

in which $c_{lip}(t)$ represents the liposomal concentration in the blood.

The leakage of the liposomes was estimated based on the Dox blood kinetics data from the first 3.5 h after injection of both timelines using on a simple pharmacokinetic model (Eq. 3 to 5, Figure 3).

$$F_{lip}(t) = F_{lip}(0) \cdot \exp(-\ln(2)/t_{1/2,leak} \cdot t) \quad \text{Eq.3}$$

$$c_{free}'(t) = k_{leak} \cdot (c_{lip}(t) \cdot F_{lip}(t)) - (\ln(2)/t_{1/2,dox}) \cdot c_{free}(t) \quad \text{Eq.4}$$

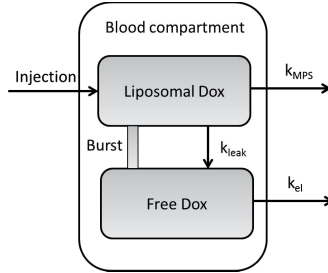


Figure 3. Schematic representation of the model used to estimate the burst and leakage half-lives ($\ln(2)/k_{leak}$) based on the total amount of Dox measured (Liposomal Dox + Free Dox), the Dox elimination constant k_{el} as derived from literature [16] and the liposomal clearance time ($\ln(2)/k_{leak}$) as derived from the liposomal carrier blood kinetic data.

$$c_{free}(0) = (1 - F_{lip}(0)) \cdot c_{lip}(0) = Burst \quad \text{Ep.5}$$

with $F_{lip}(t)$ representing the fraction of total Dox present in the liposome, $D_{free}(t)$ the concentration of free Dox in the blood stream, and $t_{1/2,leak}$ the leakage half-life of Dox from the liposomes, respectively. The parameter $t_{1/2,dox}$ is the half-life of free Dox in the bloodstream of mice, which is set to 1.2 min [17,18]. This model takes into account the measured $k_{clear,RES}$ as estimated based on the liposome blood kinetics and the blood level of total (free and liposomal) Dox as measured by HPLC.

Intravital imaging by murine dorsal skinfold window chamber model

Twelve weeks old C57BL/6 mice received a dorsal skinfold window chamber with a BFS-1 sarcoma implant and were imaged using intravital confocal microscopy within two weeks after placement of the window [19]. During imaging, the mice are under isoflurane anesthesia and body temperature was kept stable at 37°C using a thermal stage and was monitored by a rectal probe. 5 mg/kg liposomal Dox in 100 μ L phosphate buffered saline (PBS) was injected intravenously and liposomes were allowed to circulate for 15 min. The window was kept at 37°C using an external circular electric heating coil that was attached to the window glass on the back side of the window chamber. The temperature in the window was continuously monitored using a thermocouple that was inserted into the window chamber. The temperature was increased to 42°C and the imaging continued for another hour. Three animals were used per formulation.

Therapeutic efficacy in a murine BFS-1 sarcoma model

Ten weeks old C57BL/6 mice were given a $\pm 3 \text{ mm}^3$ murine BFS-1 tumor fragment, transplanted subcutaneously in the right hind limb. When the tumor reached 200 mm^3 within three weeks, the tumors were heated to hyperthermia (HT; 42°C) or normothermia (NT; 37°C) conditions for one hour under anesthesia. Each treatment group consisted of eight animals. In case of a HT experiment, the right hind limb was submerged into a 42.5°C water bath for 10 min to bring the intratumoral temperature to 42°C (Figure 4, comparable to previously published tumor heating by water bath [20]). Body temperature was checked by rectal insertion of a temperature probe and was averagely 35–37°C. 5 mg/kg Dox in 100 μ L PBS were intravenously injected and the tumor was kept at 42°C for an additional hour. In case of a NT experiment, the same procedure was applied while the mouse was kept at 34–36°C (temperature probe in rectum) by putting the mouse on a heating plate and an aluminum foil cover was used to prevent body temperature loss. 10 min after subjecting the mice to NT or HT conditions, an intravenous injection

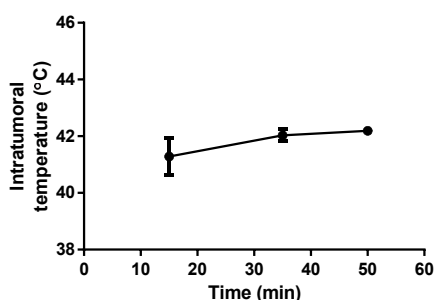


Figure 4. Intratumoral temperature measurement over time during heating of the tumor-bearing limb in a water bath at a temperature of 42.5 °C. Temperature was measured by introducing a thermocouple probe inside the center of the tumor. N=12 for each time point.

was performed with one of the four investigated liposome formulations or saline. Mice were sacrificed 30 days after treatment, or when the tumor exceeded the maximum allowed size (3375 mm^3 or 18 mm in one dimension), when the tumor became necrotic and caused an open wound. The efficacy of the treatment was judged based on tumor doubling time.

Statistics

All *in vitro* data are represented as mean \pm standard deviation of experiments performed in triplicates. The R_{50} and T_m values were analyzed by two-way ANOVA after equal variances were verified by Levene's test. Other *in vitro* data were analyzed by independent two-samples T-tests. The area under de curve (AUC) for Dox in different liposomal formulations was analyzed by one-way ANOVA after equal variances were verified by Levene's test. Tumor doubling times were analyzed by Mantel-Cox. All tests were performed using IBM SPSS Statistics for Windows v. 23. All statistical tests were two-sided and p-values below 0.05 were considered statistically significant.

RESULTS

In vitro release and stability assays on TSL formulations with varying DPPC:DSPC ratios and Doxorubicin loading techniques

The TSL formulations were prepared by film hydration and extrusion and Dox was loaded into every formulation by $(\text{NH}_4)_2\text{SO}_4$ (A) or citrate (C) loading. Four different TSL formulations were prepared by alternating DPPC:DSPC molar ratio while keeping a constant 5% molar fraction of DSPE-PEG₂₀₀₀. All batches were analyzed by DLS on size, zeta potential and polydispersity index (pdi). The results in Table I show that by changing the lipid ratio between DPPC:DSPC:DSPE-PEG₂₀₀₀, no differences in size, pdi or zeta-potential were observed. The Dox loading efficacy was 100%, regardless of whether

Table I. Size, surface charge and melting transition temperature of TSL formulations.

Formulation	Size (nm)	Pdi	Zeta potential (mV)	T_m ($^{\circ}\text{C}$)
TSL50A	82 \pm 5	0.07 \pm 0.03	-7.8 \pm 0.9	46.7 \pm 0.1
TSL60A	80 \pm 2	0.04 \pm 0.01	-8.0 \pm 0.7	45.3 \pm 0.6
TSL70A	78 \pm 1	0.04 \pm 0.01	-7.2 \pm 1.0	44.4 \pm 0.3
TSL80A	77 \pm 4	0.03 \pm 0.02	-6.8 \pm 0.7	43.0 \pm 0.2
TSL50C	83 \pm 2	0.03 \pm 0.01	-7.8 \pm 1.4	46.4 \pm 0.1
TSL60C	83 \pm 1	0.04 \pm 0.01	-8.4 \pm 1.6	45.2 \pm 0.7
TSL70C	83 \pm 2	0.04 \pm 0.01	-7.2 \pm 0.7	44.0 \pm 0.4
TSL80C	82 \pm 3	0.04 \pm 0.01	-7.8 \pm 0.4	42.8 \pm 0.4

citrate or $(\text{NH}_4)_2\text{SO}_4$ was used. DSC analysis indicated that T_m significantly decreased ($p < 0.001$, two-way ANOVA) with increasing DPPC fractions. There was no difference in T_m between $(\text{NH}_4)_2\text{SO}_4$ or citrate loading (Table 1; Figure 5) as tested by a two-way ANOVA procedure. To test their stability and release, the liposomal formulations (0.5 mM phosphate) were exposed to temperatures ranging from 37 to 45°C in FBS for 5 minutes. When the R_{50} values of these curves were determined by non-linear regression (Table 2), it became apparent that in all formulations, the $(\text{NH}_4)_2\text{SO}_4$ loaded liposomes were releasing Dox at slightly lower temperatures than when citrate was used (Fig. 6A, B, tested by two-way ANOVA). Fig. 6C indicates that the R_{50} values were consistently lower than T_m , yet a strong linear correlation existed between them regardless of the Dox loading method used ($R^2=0.990$ for $(\text{NH}_4)_2\text{SO}_4$ and 0.993 for citrate loaded liposomes). Next, the leakage at 37°C and the release kinetic at 42 °C in FBS was studied for all formulations (Figure 7). The fastest release at 42°C is observed for TSL70 and TSL80 formulations with half of the Dox already released ($R_{50\text{HT}}$) after approximately 5 seconds (Figure 7A, B). The TSL60 required approximately 20 s (TSL60A) to 30 s (TSL60C) to reach 50% release, while TSL50 formulations required 6 min heating (Figure 7C, D). The formulations TSL60-80 reached total release (>95%) after one hour at 42°C,

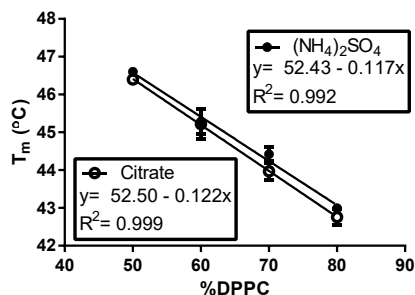


Figure 5. Linear regression of T_m versus % DPPC. Citrate loaded liposomes did not give significantly lower T_m values than $(\text{NH}_4)_2\text{SO}_4$.

Table 2. Different liposomal formulations and their corresponding R_{50} values calculated from the temperature dependent release assays shown in Fig. 6 A and B.

Formulation	R_{50} (°C)
TSL50A	42.48 ± 0.24
TSL60A	41.41 ± 0.16
TSL70A	40.34 ± 0.16
TSL80A	39.37 ± 0.13
TSL50C	42.89 ± 0.06
TSL60C	41.64 ± 0.09
TSL70C	40.56 ± 0.12
TSL80C	39.68 ± 0.08

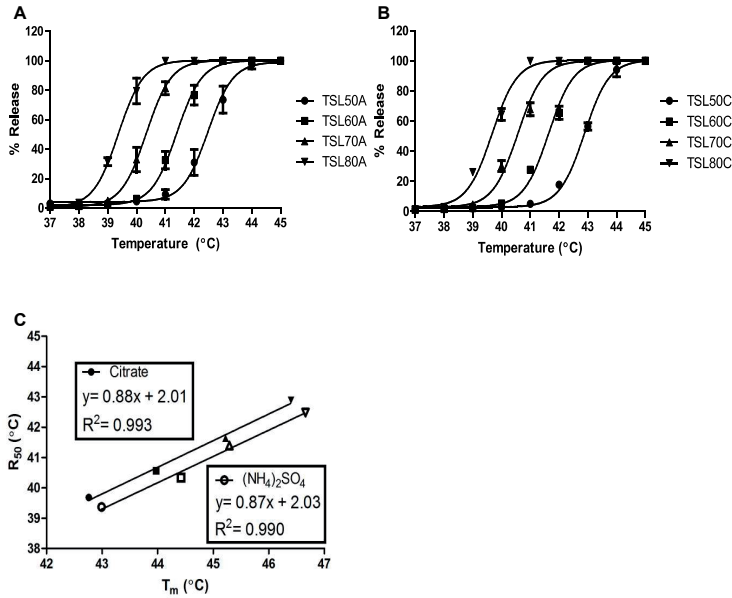


Figure 6. Temperature dependent release profiles after 5 min exposure to 37–45°C of the different liposomal formulations when (NH₄)₂SO₄ (A) or citrate (B) was used for Dox loading. For each formulation, three batches (n=3) were tested. Release (R₅₀) as a function of T_m for both Dox loading methods is shown (C).

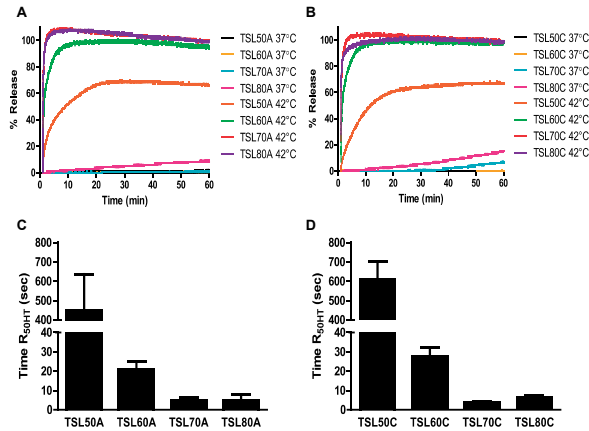


Figure 7. Time dependent release profiles of the different liposomal formulations when (NH₄)₂SO₄ (A) or citrate (B) was used for Dox loading. The time when R_{50HT} was reached for each formulation is shown in (C) for (NH₄)₂SO₄ and in (D) for citrate. For each formulation, three batches (n=3) were tested.

while TSL50 formulations showed with 66% incomplete release after one hour at 42°C (Table 3). At a physiological temperature of 37°C, citrate loaded TSLs displayed more leakage after one hour compared to the corresponding liposomes having an (NH₄)₂SO₄ internal buffer, i.e. $6 \pm 1\%$ versus $1 \pm 1\%$ for TSL70; independent samples T-test, $p = 2.2 \cdot 10^{-4}$, and $15 \pm 1\%$ versus $8 \pm 1\%$ for TSL80 independent samples T-test, $p = 0.002$,

respectively. Consequently, all the following studies described were carried out with TSL formulations with $((\text{NH}_4)_2\text{SO}_4)$ based Dox loading. Leakage at 37°C as well as release at 42°C from these liposomes was dependent on the presence of serum proteins since in HEPES buffer under HT conditions, leakage and release decreased (Figure 8A). This result was different compared to lysolipid containing formulations, where presence of serum was required to a lesser extent (Figure 8B).

Table 3. Different liposomal formulations and their corresponding Dox release percentage after 1h incubation in FBS at 37°C or 42°C.

Formulation	1h release 37°C (%)	1h release 42°C (%)
TSL50A	1±1.1	66±7.1
TSL60A	1±0.8	94±1.2
TSL70A	1±0.6	100±0.4
TSL80A	8±1.1	100±0.5
TSL50C	0±0.9	66±5.5
TSL60C	0±0.9	97±2.3
TSL70C	6±0.8	100±1.9
TSL80C	15±1.2	100±1.2

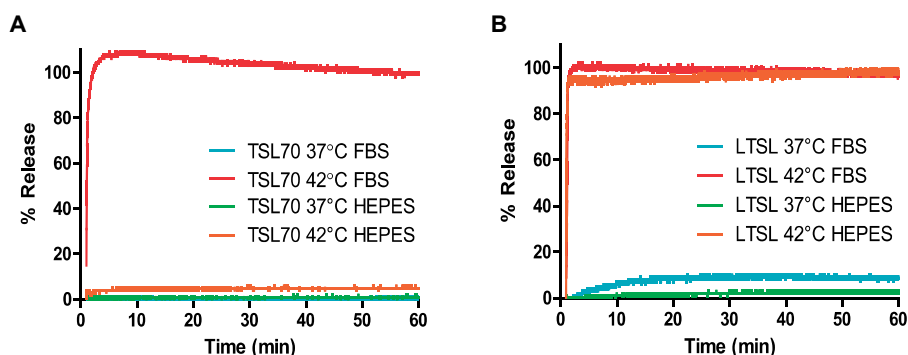


Figure 8. Comparison of Dox release between FBS and HEPES buffer pH 7.4. TSL70A shows instant total release at 42°C in FBS while the release in HEPES is not higher than 5% (A). LTSL prepared according to Needham et al [9] shows in FBS and HEPES a rapid release at 42°C which reached completion faster in FBS than in HEPES (B). All tests done at n=3.

Cryo-TEM analysis on Dox release from TSL formulations

The release characteristics for TSL50-80A formulations were further investigated using cryo-TEM images (Figure 9). The Dox crystals inside liposomes were quantified before and after heating to 42°C for 1 hour in FBS. At least five cryo-TEM recordings were made for each formulation and scored for the presence of Dox crystals after HT exposure. All liposomal formulations showed the presence of Dox crystals (Figure 10A-D) before heating. After heating, 70% of the TSL50A liposomes still showed presence of crystals inside though with an altered morphology (Figure 10E), while 30% of liposomes were

empty. For the TSL60A a higher fraction of empty liposomes was observed compared to liposomes with Dox crystals still present (Figure 10F). After heating, TSL70A and TSL80A (Figure 10G, H) displayed only empty liposomes, indicating complete release of Dox. The fraction of empty liposomes and liposomes with Dox crystals present in the inner lumen after heating is shown in Figure 10I for all formulations.

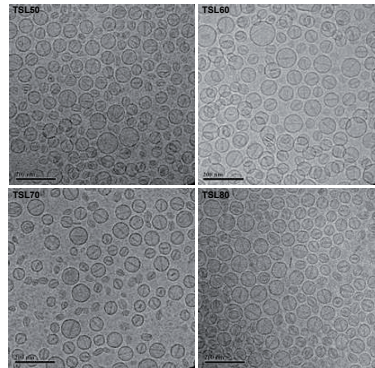


Figure 9. Cryo-TEM analysis of TSL50A, TSL60A, TSL70A and TSL80A at 20mM in HEPES buffer pH 7.4. Bars indicate 200nm.

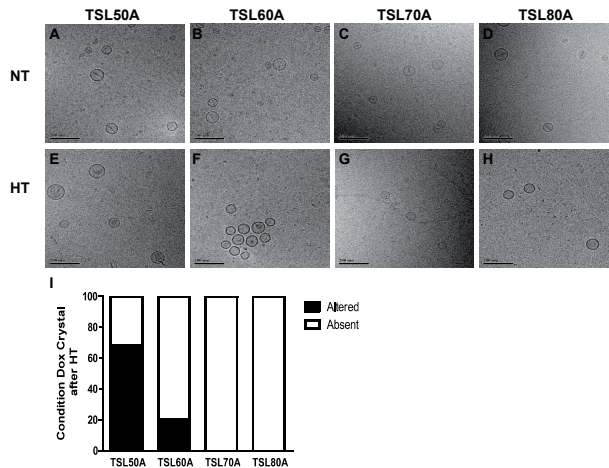


Figure 10. Cryo-TEM analysis of all TSLA formulations in FBS before (Normothermia; NT) and after 1h exposure to 42°C (HT). For the TSL50A formulation, the partial release profile after HT becomes apparent as the majority of liposomes contain an alteration in shape of the Dox-SO₄ crystal, whereas the other formulations show only empty liposomes after HT. Bars indicate 200nm. In I the condition of the Dox crystal in each liposome visualized was counted (at least 25 liposomes were counted per formulation).

Doxorubicin release visualized by intravital imaging

The *in vivo* release properties of the $(\text{NH}_4)_2\text{SO}_4$ TSL formulations were characterized with confocal microscopy in a BFS-1 tumor using a dorsal skinfold window model. In all cases a rapid increase in Dox fluorescent signal in the intravascular as well as the extra-vascular space was observed indicating the release of Dox from the liposomes. However, TSL50A had a slower release rate than the other formulations (Fig. II).

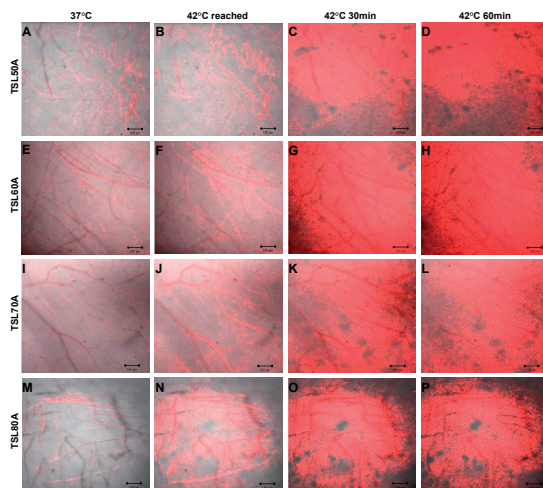


Figure II. Window images on the TSL50, 60, 70 and 80 formulations. All formulations showed a relatively quick increase in Dox fluorescence, within seconds after the temperature in the window reached 42°C. Bars indicate 100 μm . Temperature reached 42°C after 5 min using a heating ring.

Blood kinetics study on TSL and Doxorubicin circulation time

The blood kinetics of all four ^{111}In -labeled TSL formulations were studied in C57BL/6 mice. Incorporation of 0.1% DSPE-DTPA to the lipid composition resulted in 4% more leakage of the TSL80A after one hour incubation at 37°C in FBS, while TSL70A did not show any difference in leakage (Figure I2). The injected dose (%ID) per total blood volume for the liposomal carrier and Dox as a function of time for both time lines combined are depicted in Figure I3. TSL clearance from the blood could be described by single exponential kinetics. Liposomal blood half-lives reduced from 8.2 hours to ca. 4.4 h with DPPC fractions increasing from 50 to 80%. The liposome clearance was mainly caused by liver and splenic uptake (Figure I4). The overall Dox concentration found in plasma was always lower than that of the TSL, indicating release from its carrier. Upon injection, the Dox showed first a fast burst release followed by a more gradual, exponential leakage from its carrier at body temperature. A simple pharmacokinetic model was used to determine burst percentage (Eq. 5) and leakage half-lives, which are summarized in Table 4. A trend of increased leakage with increasing DPPC contents was observed, while burst release upon first blood

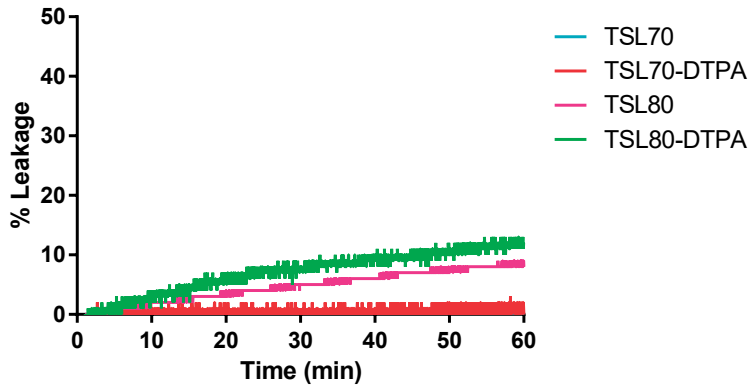


Figure 12. Stability comparison between TSL formulations with and without 0.1% DSPE-DTPA lipid incorporation needed for radiolabeling. Addition of 0.1% DSPE-DTPA to the TSL70A or TSL80A did not result in a major defect in stability for both cases.

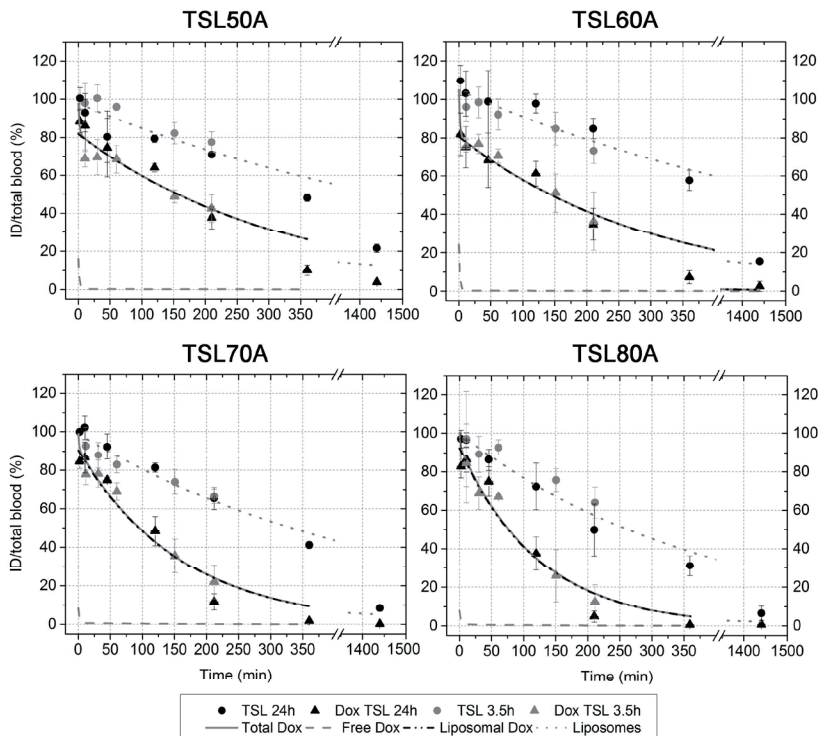


Figure 13. Blood kinetics for the liposomal carriers and Dox for all formulations expressed in % injected dose (ID) in the total blood volume. The data were fitted by a pharmacokinetic model and the resulting fits are indicated in the graph.

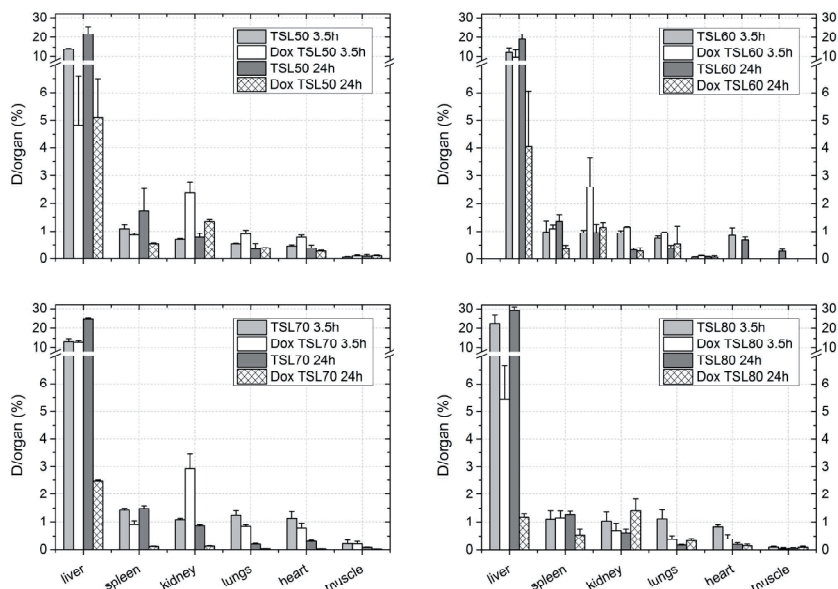


Figure 14. Biodistribution of Dox and the liposomal carrier for the TSL formulations. All liposomal carriers show predominantly liver and spleen clearance. The Dox ends up in liver and spleen as well, but additionally, a considerable amount of Dox can be observed in the kidney at the 3.5h time point.

contact reduced with increasing DPPC contents. From above blood kinetics data, the area under the curve (AUC) for Dox was calculated for all formulations, taking burst release and leakage into account (Table 4). The AUC for all formulations in the time range of 1 – 60 minutes was found to be in the range between 34 ± 4 to 42 ± 6 %ID·h/g with neither a statistical difference between the formulations (one-way ANOVA, equal variances, $p = 0.089$) nor a correlation with the fraction of DPPC. Calculated for a timeframe from 30–90 min, TSL70 shows a slightly higher AUC than TSL80 (one-way ANOVA, equal variances, $p = 0.045$, post-hoc Bonferroni $p = 0.042$).

Table 4. Pharmacokinetic parameters of the liposomal formulations. Values are depicted \pm the standard error of the fitted parameters. Liposome blood half-life is derived from mono-exponential fits of the blood kinetics data. Leakage half-lives are obtained from a pharmacokinetic model fitted to the total Dox blood kinetics, taking the liposomal and Dox clearance into account. Dox $t_{1/2}$ indicates the time point at which the total Dox concentration in the blood (both liposomal and free Dox) has reached 50%, as derived from the curves fitted by the model.

Formulation	AUC 1-60 min (%ID x h/g)	AUC 30-90 min (%ID x h/g)	Liposome $t_{1/2}$ (h)	Dox $t_{1/2}$ (h)	Dox leakage $t_{1/2}$ (h)	Dox burst (%)
TSL50A	36 ± 7	32 ± 5	8.2 ± 0.9	2.61	6.6 ± 1.6	16 ± 3
TSL60A	35 ± 4	32 ± 4	8.3 ± 0.9	2.41	5.0 ± 1.3	23 ± 3
TSL70A	42 ± 6	35 ± 6	5.6 ± 0.4	1.59	2.7 ± 0.3	8 ± 3
TSL80A	34 ± 4	27 ± 3	4.4 ± 0.5	1.28	2.1 ± 0.3	8 ± 4

Therapeutic efficacy study in a BFS-1 sarcoma model

The therapeutic efficacy of these formulations was tested in a subcutaneous murine BFS-1 sarcoma model. When no HT was applied, no significant reduction tumor size doubling time is observed for any of the formulations (Mantel-Cox test, $p > 0.32$; Figure 15 A, C, E, G, I, K & Table 5). When the BFS-1 tumors were subjected to HT, a reduction of

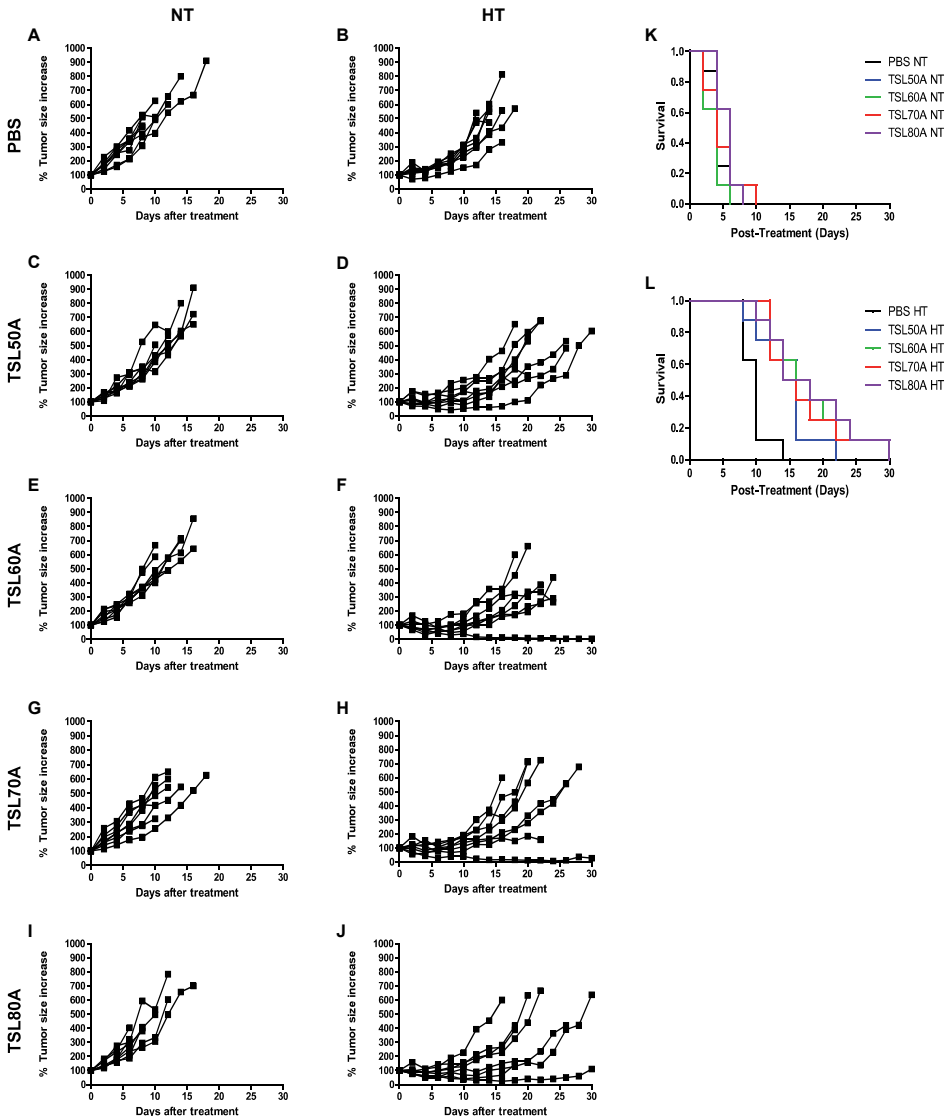


Figure 15. BFS-1 Tumor response to different kinds of TSL treatments. In A-J, the tumor growth of the individual mice for treatments with different liposomal formulations, at NT or HT are shown with a maximum follow up time up to 30 days. Kaplan-Meier plots were made for tumor doubling time for the NT (K) and HT groups (L). N=8 for all groups.

Table 5.

Group	PBS HT		TSL60 HT		TSL60 HT		TSL70 HT		TSL60 HT		PBS NT		TSL60 NT		TSL70 NT		TSL80 NT	
	Chi-Square	Sig.	Chi-Square	Sig.	Chi-Square	Sig.	Chi-Square	Sig.	Chi-Square	Sig.	Chi-Square	Sig.	Chi-Square	Sig.	Chi-Square	Sig.	Chi-Square	Sig.
Log Rank (Mantel-Cox)																		
TSL60 HT	2.788	.095			6.465	.025	5.026	.025	6.465	.011	6.628	.010	7.604	.006	2.300	.129	6.493	.008
TSL60 HT	6.465	.011	3.466	.075			2.152	.142	4.697	.030	7.886	.005	9.000	.003	5.026	.025	8.352	.004
TSL70 HT	5.026	.025	2.462	.142	3.20	.071	3.20	.071	1.907	.167	7.886	.005	9.000	.003	9.120	.003	8.352	.004
TSL60 HT	6.465	.011	4.697	.030	1.907	.167			.154	.595	7.886	.005	9.000	.003	9.120	.003	8.352	.004
PBS NT	6.628	.010	7.886	.005	7.886	.005	7.886	.005	7.886	.005	7.886	.005	7.886	.005	9.120	.003	8.352	.004
TSL60 NT	7.604	.006	9.000	.003	9.000	.003	9.000	.003	9.000	.003	4.310	.038	1.750	.186	.547	.460	2.798	.094
TSL70 NT	2.300	.129	5.026	.025	9.120	.003	9.120	.003	9.120	.003	5.47	.460	1.796	.180	1.796	.180	4.654	.031
TSL80 NT	6.543	.008	8.352	.004	8.352	.004	8.352	.004	8.352	.004	2.798	.094	4.654	.031	.031	.870		

tumor doubling time was observed (Figure 15 B, L) (Mantel-Cox test, $p = 3 \cdot 10^{-2}$), which was further enhanced by the use of any of the TSL formulations (Figure 15 D, F, H, J, L & Table 5) (Mantel-Cox test, TSL50A, $p = 3 \cdot 10^{-3}$; TSL60A, $p = 3 \cdot 10^{-4}$; TSL70A, $p = 1 \cdot 10^{-3}$; TSL80A $p = 2 \cdot 10^{-3}$), however, no difference could be detected between the TSL formulations when they were combined with HT (Mantel-Cox test, $p > 0.18$).

DISCUSSION

In this study, a set of eight different TSL formulations with respect to lipid composition and Dox loading method were prepared and tested *in vitro* and *in vivo*. For the tested formulations the presence of serum proteins was indispensable for adequate *in vitro* drug release, suggesting an interaction of the serum proteins with the TSLs, as shown in Figure 8. Increasing the DSPC fraction led to an increase in T_m values, which consequently influenced drug release and retention. The TSL60, 70 and TSL80 formulations displayed a rapid and total drug release at 42°C in FBS, except for the TSL50, which showed a much slower and only partial release (66% after 1 hour of HT). The internal buffer used for Dox loading turned out to be an important parameter, as $(\text{NH}_4)_2\text{SO}_4$ loaded formulations appeared more stable than their citrate loaded counterparts. Using citrate as a loading buffer seemed to slightly decrease T_m , which led to higher leakage at 37°C as well as higher R_{50} values. Based on these *in vitro* experiments, $(\text{NH}_4)_2\text{SO}_4$ loaded formulations were chosen over citrate loaded liposomes for all further experiments. TSL70A and TSL80A show nearly instant quantitative release at 42°C in FBS, comparable to LTSL [11,21,22]. However, the advantage of TSL70A when compared to LTSL is that the leakage of the TSL70A formulation is limited to $1 \pm 1\%$ after 60 min in FBS at 37°C making it slightly more stable than the LTSL formulation when tested under the same circumstances (Figure 8). For the TSL50A, Cryo-TEM images displayed a high fraction of liposomes still containing Dox crystals after heating. This fraction was less for the TSL60A formulation, and completely absent for TSL70A and TSL80A, where only empty liposomes were observed. As a result, above mentioned cryo-TEM findings were consistent with the fluorimetric assays.

Next, intravital microscopy studies were performed with TSL50A-TSL80A formulations in a BFS-1 sarcoma tumor using a dorsal skinfold window chamber model. In line with the *in vitro* data, the measurements revealed a comparable slow release for TSL50A *in vivo*, while release kinetics appeared comparable for all other formulations. For all formulations, intravascular release was obtained followed by rapid extravasation into the tumor tissue. Comparable results have been reported by our group in BFS-1 and other tumors for TSL80 and in FaDu tumors with LTSLs by Manzoor et al.[3,23]. Although the intravital microscopy can provide information about both *in vivo* release

kinetics and local tumor penetration depth, it has been shown by de Smet et al. [24] that it is paramount to study drug distribution also across the entire tumor. Although Dox penetration and distribution improves in the vicinity of blood vessels on cellular length scales upon heat treatment, it is important to realize that significant drug concentrations will only be reached in sufficiently perfused tumor areas, where the liposomes can enter.

Blood kinetics were assessed for all formulations using radiolabeled TSLs allowing to differentiate between the blood half-life of the liposomal carrier and that of Dox. All liposomal carriers showed a mono-exponential clearance, with blood circulation half-lives ranging from 4 to 8 hours with increasing DSPC content. This effect might be attributed to an increasing membrane rigidity with increasing DSPC content, which could lead to a decreasing affinity for serum opsonins and thus reduced clearance [25,26]. Similar behavior has been reported by Zisman et al. for cisplatin containing liposomes, where liposomes containing DPPC as the main constituent showed shorter blood half-lives compared to DSPC-rich formulations [27]. Upon injection, all TSLs showed a rapid “burst” release of Dox, followed by a further slow leakage of Dox from its liposomal carrier. While the burst release decreased with increasing DPPC content, the subsequent leakage rate (k_{leak}) increased. Taking the blood half-lives of the liposomal carriers into account, our pharmacokinetic model allowed calculating the AUC of Dox for all different formulations. Interestingly, over the time span of 1 hour p.i., the AUC is similar for all formulations. The ‘burst effect’ was unexpected based on the *in vitro* stability studies and also the *in vivo* leakage rates were higher compared to the data obtained *in vitro*. Needham and coworkers also observed a Dox burst release from DPPC-DSPE-PEG₂₀₀₀ TSLs, which they explained with an instantaneous release of membrane-bound Dox at T_m [9]. The lack of burst release in the *in vitro* data could be explained by both the absence of full blood and the difference in serum between species (bovine for *in vitro* and murine for *in vivo*) [8,28,29]. Although the TSL70A and TSL80A showed more leakage over time than the TSL50A and TSL60A, the leakage half-lives were still relatively long compared to LTSLs, leading to a better [Dox/liposome] parameter (Eq. 1). As Al Jamal et al. [30] showed, for LTSL the Dox:lipid ratio decreases to ~0.3 after 1 hour, compared to 0.7 for TSL80A.

A therapeutic study was performed in BFS-I tumor bearing mice testing the efficacy of the TSL50-80A formulations with and without HT. Notably, exposing the tumor to one hour HT already induces a therapeutic effect leading to a reduced tumor growth compared to untreated tumors. A possible explanation can be HT induced cytotoxicity and blood vessel shutdown [31–33]. HT in combination with all liposomes significantly increased the therapeutic effect further (TSL50A, $p = 3 \cdot 10^{-3}$; TSL60A, $p = 3 \cdot 10^{-4}$; TSL70A, $p = 1 \cdot 10^{-3}$; TSL80A $p = 2 \cdot 10^{-3}$). For all formulations, the AUC at 37°C was comparable, which can partly explain the lack of distinction between the formulations. Moreover, TSL60A, TSL70A and TSL80A all had similar *in vitro* release kinetics, whereas the

TSL50A formulation did show incomplete and slow release both *in vitro* as well as *in vivo* using the dorsal skinfold window model. The fact that this observed difference in release kinetics did not result in a significant therapeutic benefit might be caused by a saturation of the tumor tissue with Dox due to the long treatment duration and dosage.

In a current phase III clinical trial using LTSL in combination with radiofrequency ablation (RFA) of primary liver tumors, the treatment did not result in a significant increase in overall survival when compared to treatment by an RFA control (HEAT trial [34,35]). However, post-hoc subgroup analysis revealed a greater than two-year survival benefit for a subgroup of patients that received an optimized RFA treatment of 45 minutes or more [36,37]. This is indicative of the effect the treatment duration and other aspects of the clinical workflow could have on the performance of a TSL formulation.

Above analysis and pharmacokinetic model allows evaluation of formulations for possible clinical application, as well as the implications of the clinical workflow, such as infusion time and timing of HT. For example, in above mentioned HEAT trial [34] as well as the OPTIMA trial [38]), both using Thermodox® in combination with radiofrequency ablation of primary liver tumors, Thermodox® is administered by infusion over 15-30 minutes. According to the trial protocol, the tumor is heated by radiofrequency ablation which is initiated minimally 15 minutes and should be completed maximally 3 hours after the start of the infusion. With the Dox circulation time in mind, it is obvious that the Dox AUC will drop when the time between HT and TSL administration increases. Therefore, it is important to also assess the capabilities of a formulation at clinically relevant, later time points. While the Dox blood kinetics in our current study was comparable for the different TSL formulations in AUC from 1 – 60 minutes after injection, the AUC at a later time span, e.g. during a heating period from 30 to 90 minutes after injection, is actually larger for the TSL70A compared to all other formulations. Therefore, if heating is applied at a later time period after infusion, TSL70A might give a higher Dox accumulation in the tumor tissue than TSL60A or TSL80A. Another aspect to consider is that Dox accumulation in the tumor can be limited by saturation of drug uptake using a treatment dose of 5 mg / kg. This effect could allow slower releasing TSL formulations to yield similar intratumoral Dox concentrations as faster releasing TSL explaining the similar therapeutic efficacy observed for TSL60,70,80A [39,40]. From a clinical workflow perspective, a TSL formulation is preferred that ensures a reasonably high AUC of Dox also at later times after injection, which eases time constraints in a clinical application. In this respect, TSL70A seems to be the best candidate having a relatively low burst, low leakage, a high AUC at later time points and rapid release (Figure 16).

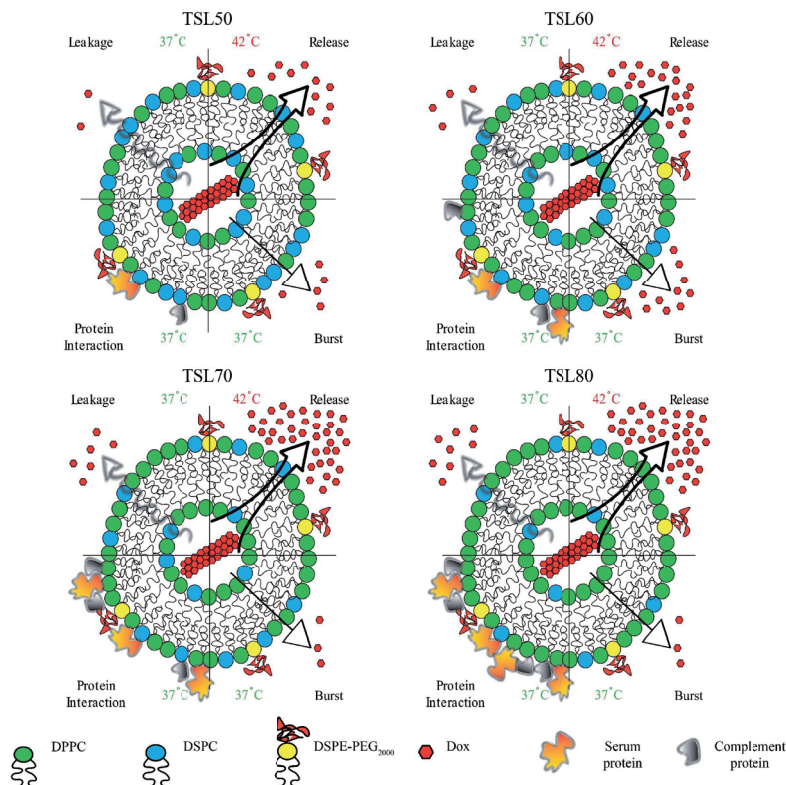


Figure 16. Schematic representation of the results found of TSL50, 60, 70 & 80. With increasing fraction of DPPC, the release kinetics at HT increases with similar release rates at 42°C. However, the leakage in circulation also increases with increasing amounts of DPPC. Furthermore, DPPC rich liposomes are more prone to interact with proteins in circulation, giving them a shorter circulation time which has been indicated in various studies [26–28]. When liposomes contain more DSPC (TSL50 & TSL60), there is a larger likelihood for a burst release that takes place as soon as the particles enter circulation.

CONCLUSION

In search for an optimized Dox-TSL formulation, it is crucial to acknowledge that stability and release kinetics of the formulation might not fully reflect its *in vitro* behavior. In the current study, different Dox-TSL formulations were subjected to rigorous *in vitro* and *in vivo* testing. A burst in Dox release was observed *in vivo* which was not predicted based on the *in vitro* stability and release assays. Moreover, the differences in Dox release between TSL formulations that were observed *in vitro*, were less apparent *in vivo*. This indicates that an optimal treatment with Dox-TSL is not solely dependent on an optimal TSL formulation alone and is likely to be influenced by the interplay between release kinetics, Dox saturation in the tumor area and effective tumor Dox uptake, topics which require further investigation. The formulations presented here display a relatively slow

Dox leakage and a long liposome half-life which could be beneficial in a clinical setting where formulations with high AUC values are demanded because of variable time spans between TSL infusion and HT treatment. The optimal Dox-TSL formulation needs to be designed keeping the clinical workflow in mind and should be selected based on extensive *in vivo* tests combined with blood kinetics modelling.

REFERENCES

1. Yatvin MB, Weinstein JN, Dennis WH, Blumenthal R. Design of liposomes for enhanced local release of drugs by hyperthermia. *Science*. 1978;202(4374):1290-1293. doi:10.1126/science.364652.
2. Weinstein JN, Magin RL, Yatvin MB, Zaharko DS. Liposomes and local hyperthermia: selective delivery of methotrexate to heated tumors. *Science*. 1979;204(October 1978):188-191. doi:10.1126/science.432641.
3. Li L, Ten Hagen TLM, Bolkestein M, et al. Improved intratumoral nanoparticle extravasation and penetration by mild hyperthermia. *J Control Release*. 2013;167(2):130-137. doi:http://dx.doi.org/10.1016/j.jconrel.2013.01.026.
4. Banno B, Ickenstein LM, Chiu GNC, et al. The functional roles of poly(ethylene glycol)-lipid and lysolipid in the drug retention and release from lysolipid-containing thermosensitive liposomes in vitro and in vivo. *J Pharm Sci*. 2010;99(5):2295-308. doi:10.1002/jps.21988.
5. Landon CD, Park JY, Needham D, Dewhirst MW. Nanoscale Drug Delivery and Hyperthermia: The Materials Design and Preclinical and Clinical Testing of Low Temperature-Sensitive Liposomes Used in Combination with Mild Hyperthermia in the Treatment of Local Cancer. *Open Nanomed J*. 2011;3:38-64.
6. Yarmolenko PS, Zhao Y, Landon C, et al. Comparative effects of thermosensitive doxorubicin-containing liposomes and hyperthermia in human and murine tumours. *Int J Hyperthermia*. 2010;26(5):485-98. doi:10.3109/02656731003789284.
7. Gasselhuber A, Dreher MR, Negussie A, Wood BJ, Rattay F, Haemmerich D. Mathematical spatio-temporal model of drug delivery from low temperature sensitive liposomes during radiofrequency tumour ablation. *Int J Hyperthermia*. 2010;26(August):499-513. doi:10.3109/02656731003623590.
8. Gaber MH, Hong K, Huang SK, Papahadjopoulos D. Thermosensitive sterically stabilized liposomes: formulation and in vitro studies on mechanism of doxorubicin release by bovine serum and human plasma. *Pharm Res*. 1995;12(10):1407-1416. doi:10.1023/A:1016206631006.
9. Needham D, Park J, Wright A, Tong J. Materials Characterization of the Low Temperature Sensitive Liposome (LTSL): Effects of Lipid Composition (Lysolipid and DSPE-PEG2000) on the Thermal Transition and Release of Doxorubicin. *Faraday Discuss*. 2012;515-534. doi:10.1039/c2fd2011a.
10. Li L, ten Hagen TLM, Schipper D, et al. Triggered content release from optimized stealth thermosensitive liposomes using mild hyperthermia. *J Control Release*. 2010;143(2):274-279. doi:http://dx.doi.org/10.1016/j.jconrel.2010.01.006.
11. Needham D, Anyarambhatla G, Kong G, Dewhirst MW. A new temperature-sensitive liposome for use with mild hyperthermia: characterization and testing in a human tumor xenograft model. *Cancer Res*. 2000;60(5):1197-1201.
12. Li L, ten Hagen TLM, Hossann M, et al. Mild hyperthermia triggered doxorubicin release from optimized stealth thermosensitive liposomes improves intratumoral drug delivery and efficacy. *J Control Release*. 2013;168(2):142-150. doi:http://dx.doi.org/10.1016/j.jconrel.2013.03.011.
13. Haran G, Cohen R, Bar LK, Barenholz Y. Erratum: Transmembrane ammonium sulfate gradients in liposomes produce efficient and stable entrapment of amphipathic weak bases (*Biochim. Biophys. Acta* 1151 (1993) 201-215 (BBAMEM 76069)). *Biochim Biophys Acta - Bio-membr*. 1994;1190:197. doi:10.1016/0005-2736(94)90054-X.

14. Mayer LD, Bally MB, Cullis PR. Uptake of adriamycin into large unilamellar vesicles in response to a pH gradient. *Biochim Biophys Acta*. 1986;857(1):123-126. doi:10.1016/0005-2736(86)90105-7.
15. Bartlett GR. Phosphorus assay in column chromatography. *J Biol Chem*. 1959;234(3):466-468.
16. Smet M De, Heijman E, Langereis S, Hijnen NM, Gr  ll H. Magnetic resonance imaging of high intensity focused ultrasound mediated drug delivery from temperature-sensitive liposomes : An in vivo proof-of-concept study. *J Control Release*. 2011;150(1):102-110. doi:10.1016/j.jconrel.2010.10.036.
17. Baurain R, Deprez-De Campeneere D, Trouet A. Determination of daunorubicin, doxorubicin and their fluorescent metabolites by high-pressure liquid chromatography: Plasma levels in DBA2 mice. *Cancer Chemother Pharmacol*. 1979;2:11-14. doi:10.1007/BF00253098.
18. van der Vijgh WJ, Maessen PA, Pinedo HM. Comparative metabolism and pharmacokinetics of doxorubicin and 4'-epidoxorubicin in plasma, heart and tumor of tumor-bearing mice. *Cancer Chemother Pharmacol*. 1990;26:9-12. doi:10.1007/BF02940286.
19. Palmer GM, Fontanella AN, Shan S, et al. In vivo optical molecular imaging and analysis in mice using dorsal window chamber models applied to hypoxia, vasculature and fluorescent reporters. *Nat Protoc*. 2011;6(9):1355-1366. doi:10.1038/nprot.2011.349.
20. Hauck L, Bigner D, Carolina N. Local Antibody Hyperthermia Improves Uptake Xenograft of a Chimeric Monoclonal in a Subcutaneous. *Clin Cancer Res*. 1997;3(January):63-70.
21. Needham D, Dewhirst MW. The development and testing of a new temperature-sensitive drug delivery system for the treatment of solid tumors. *Adv Drug Deliv Rev*. 2001;53(3):285-305. doi:http://dx.doi.org/10.1016/S0169-409X(01)00233-2.
22. Needham D, Park J-YJ, Wright AM, Tong J. Materials characterization of the low temperature sensitive liposome (LTSL): effects of the lipid composition (lysolipid and DSPE-PEG2000) on the thermal transition and release of doxorubicin. *Faraday Discuss*. 2013;161(0):515-534. doi:10.1039/c2fd2011a.
23. Manzoor AA, Lindner LH, Landon CD, et al. Overcoming limitations in nanoparticle drug delivery: triggered, intravascular release to improve drug penetration into tumors. *Cancer Res*. 2012;72(21):5566-5575.
24. de Smet M, Hijnen NM, Langereis S, et al. Magnetic resonance guided high-intensity focused ultrasound mediated hyperthermia improves the intratumoral distribution of temperature-sensitive liposomal doxorubicin. *Invest Radiol*. 2013;48(6):395-405. doi:10.1097/RLI.0b013e3182806940.
25. Drummond DC, Meyer O, Hong K, Kirpotin DB, Papahadjopoulos D. Optimizing liposomes for delivery of chemotherapeutic agents to solid tumors. *Pharmacol Rev*. 1999;51(4):691-743. doi:VL - 51.
26. Devine D V, Wong K, Serrano K, Chonn A, Cullis PR. Liposome-complement interactions in rat serum: implications for liposome survival studies. *Biochim Biophys Acta*. 1994;1191(1):43-51. doi:10.1016/0005-2736(94)90231-3.
27. Zisman N, Johnstone, S, Tsang, A, Bermudes, D, Mayer, L and Tardi, P. NDS, Zisman N, Dos Santos N, et al. Optimizing Liposomal Cisplatin Efficacy through Membrane Composition Manipulations. *Chemother Res Pract*. 2011;2011:7. doi:10.1155/2011/213848.
28. Hossann M, Syunyaeva Z, Schmidt R, et al. Proteins and cholesterol lipid vesicles are mediators of drug release from thermosensitive liposomes. *J Control Release*. 2012;162(2):400-406. doi:http://dx.doi.org/10.1016/j.jconrel.2012.06.032.

29. Guo LS, Hamilton RL, Goerke J, Weinstein JN, Havel RJ. Interaction of unilamellar liposomes with serum lipoproteins and apolipoproteins. *J Lipid Res.* 1980;21(8):993-1003.
30. Al-Jamal WT, Al-Ahmady ZS, Kostarelos K. Pharmacokinetics & tissue distribution of temperature-sensitive liposomal doxorubicin in tumor-bearing mice triggered with mild hyperthermia. *Biomaterials.* 2012;33(18):4608-17. doi:10.1016/j.biomaterials.2012.03.018.
31. Roizin-Towle L, Pirro JP. The response of human and rodent cells to hyperthermia. *Int J Radiat Oncol Biol Phys.* 1991;20(4):751-756. doi:10.1016/0360-3016(91)90018-Y.
32. Vaupel P. Pathophysiological mechanisms of hyperthermia in cancer therapy. In: *Biological Basis of Oncologic Thermotherapy.* Springer; 1990:73-134.
33. Song CW. Effect of local hyperthermia on blood flow and microenvironment: A review. *Cancer Res.* 1984;44(10 Suppl):4721s-4730s. Available at: <http://www.ncbi.nlm.nih.gov/pubmed/6467226>. Accessed May 26, 2013.
34. Phase 3 Study of ThermoDox With Radiofrequency Ablation (RFA) in Treatment of Hepatocellular Carcinoma (HCC). Available at: <https://clinicaltrials.gov/ct2/show/NCT00617981>.
35. Celsion. Celsion Announces Results of Phase III HEAT Study of ThermoDox® in Primary Liver Cancer. 2013. Available at: <http://investor.celsion.com/releasedetail.cfm?releaseid=737033>.
36. Celsion. Celsion Corporation Announces Updated Overall Survival Data from HEAT Study of ThermoDox® in Primary Liver Cancer Data Continue to Show a Statistically Significant Improvement in Overall Survival, Translating to a Greater Than Two-Year Survival Benefit. 2015. Available at: <http://investor.celsion.com/releasedetail.cfm?ReleaseID=926288>. Accessed September 30, 2015.
37. Celsion. Celsion Corporation's ThermoDox® HEAT Study Findings Reviewed at the International Liver Cancer Association (ILCA) 2013 Annual Conference in Washington, D.C. on September 14, 2013. 2013. Available at: <http://investor.celsion.com/releasedetail.cfm?ReleaseID=790781>.
38. Study of ThermoDox With Standardized Radiofrequency Ablation (RFA) for Treatment of Hepatocellular Carcinoma (HCC) (OPTIMA). Available at: <https://www.clinicaltrials.gov/ct2/show/NCT02112656>.
39. El-Kareh AW, Secomb TW. Two-mechanism peak concentration model for cellular pharmacodynamics of Doxorubicin. *Neoplasia.* 2005;7(7):705-713. doi:10.1593/neo.05118.
40. Bates D a, Fung H, Mackillop WJ. Adriamycin uptake, intracellular binding and cytotoxicity in Chinese hamster ovary cells. *Cancer Lett.* 1985;28:213-221. doi:10.1016/0304-3835(85)90077-1.

CHAPTER 3

Investigation of particle accumulation, chemosensitivity and thermosensitivity for effective solid tumor therapy using thermosensitive liposomes and hyperthermia

Wouter J.M. Lokerse

Michiel Bolkestein

Timo L.M. ten Hagen

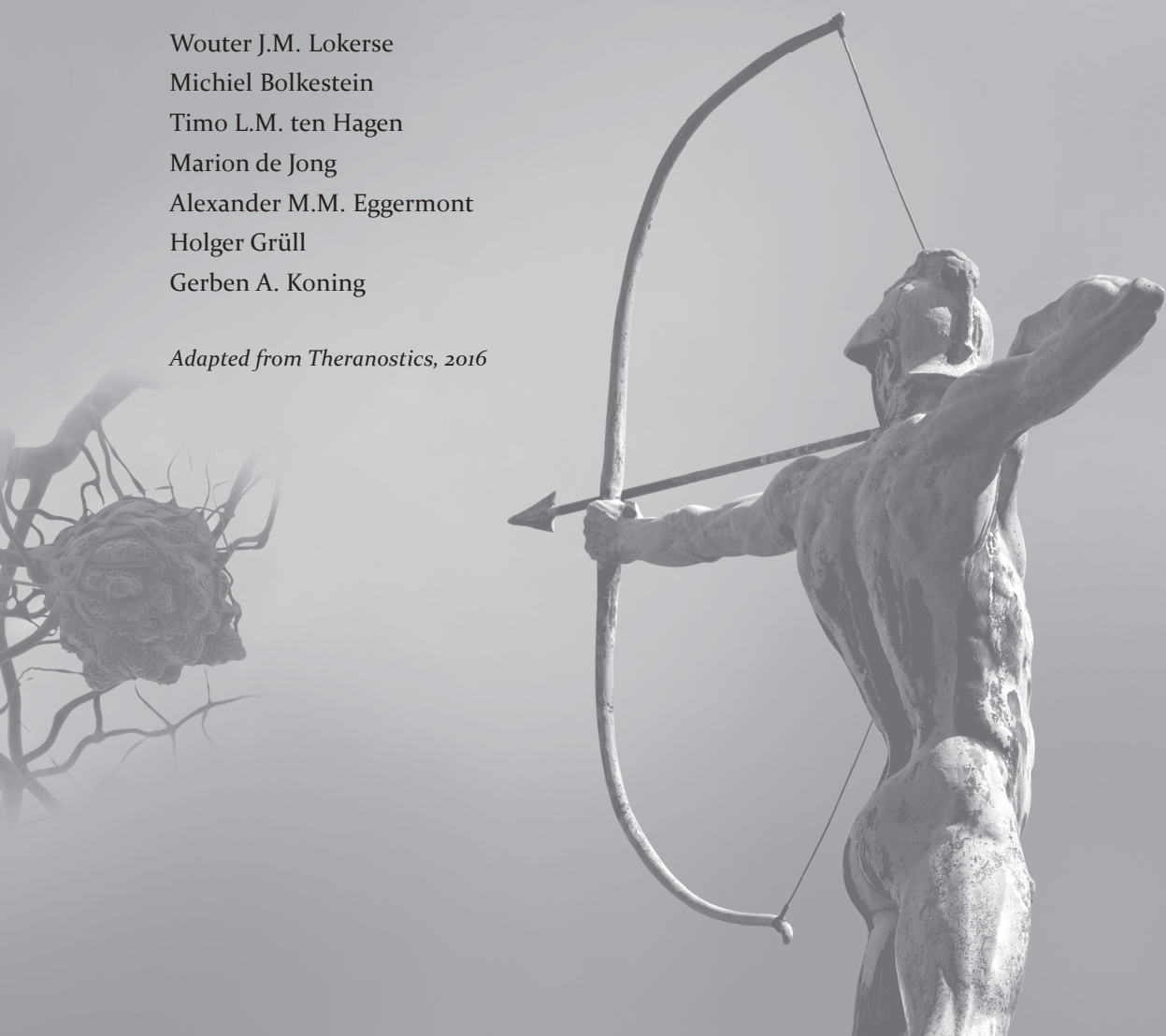
Marion de Jong

Alexander M.M. Eggermont

Holger Gröll

Gerben A. Koning

Adapted from Theranostics, 2016



ABSTRACT

Doxorubicin (Dox) loaded thermosensitive liposomes (TSLs) have shown promising results for hyperthermia-induced local drug delivery to solid tumors. Typically, the tumor is heated to hyperthermic temperatures (41-42 °C), which induced intravascular drug release from TSLs within the tumor tissue leading to high local drug concentrations (*1-step delivery protocol*). Next to providing a trigger for drug release, hyperthermia (HT) has been shown to be cytotoxic to tumor tissue, to enhance chemosensitivity and to increase particle extravasation from the vasculature into the tumor interstitial space. The latter can be exploited for a *2-step delivery protocol*, where HT is applied prior to i.v. TSL injection to enhance tumor uptake, and after 4 hours waiting time for a second time to induce drug release. In this study, we compare the 1- and 2-step delivery protocols and investigate which factors are of importance for a therapeutic response. In murine BL6 melanoma and BFS-1 sarcoma cell lines, HT induced an enhanced Dox uptake in 2D and 3D models, resulting in enhanced chemosensitivity. In vivo, therapeutic efficacy studies were performed for both tumor models, showing a therapeutic response for only the *1-step delivery protocol*. SPECT/CT imaging allowed quantification of the liposomal accumulation in both tumor models at physiological temperatures and after a HT treatment. A simple two compartment model was used to derive respective rates for liposomal uptake, washout and retention, showing that the BL6 model has a two-fold higher liposomal uptake compared to the BFS-1 tumor. HT increases uptake and retention of liposomes in both tumors models by the same factor of 1.66 maintaining the absolute differences between the two models. Histology showed that HT induced apoptosis, blood vessel integrity and interstitial structures are important factors for TSL accumulation in the investigated tumor types. However, modeling data indicated that the intraliposomal Dox fraction did not reach therapeutic relevant concentrations in the tumor tissue in a *2-step delivery protocol* due to the leaking of the drug from its liposomal carrier providing an explanation for the observed lack of efficacy.

INTRODUCTION

Classical chemotherapy for treatment of solid tumors typically employs cytotoxic drugs with low molecular weight that have sizes below 1 nm. The latter allows the drugs to efficiently extravasate upon injection from the vascular compartment into the tumor tissue in order to reach their targets. However, as extravasation is not restricted to the tumor tissue, toxicity imposed on healthy tissues is limiting the therapeutic window. One approach to limit off-target toxicity is the encapsulation of cytotoxic drugs into nanoparticles, such as liposomes with sizes in the range of 50-200 nm, which reduces side effects observed for free drugs. In contrast to healthy tissues, tumors exhibit a poorly organized vascular system [1, 2] with endothelial gaps [3, 4] that allow extravasation and accumulation of nanoparticles up to several hundred nanometers [1, 5]. In addition, as tumors often lack a functional lymphatic system, which impedes efficient clearance of nanoparticles, substantial retention of long circulating nanoparticles is observed [6, 7]. This enhanced permeability and retention (EPR) effect was first described for macromolecules by Matsumura and Maeda [8] and is a prerequisite for liposomal drug targeting. Today, several liposomal drug formulations are clinically approved, mostly due to their improved toxicity profile [7]. One example is Doxil®, a long circulation liposomal formulation of Doxorubicin (Dox) [9, 10]. While liposomal encapsulation reduces off-site toxicity, it unfortunately reduces bioavailability of the parent drug. Drug release from the liposomal carrier is slow as it is based on passive diffusion of the drug across the liposomal lipid bilayer, which strongly reduces peak concentrations [11]. An alternative approach is heat-triggered drug delivery using a drug that is encapsulated in the aqueous core of a temperature sensitive liposome (TSL), as first proposed by Yatvin and Weinstein [12]. A TSL retains the drug at body temperature, but rapidly release their payload at mild hyperthermic temperatures (40-43 °C). Heating the targeted tissue to these temperatures, for example using radiofrequency or high intensity focused ultrasound, leads to rapid intravascular release with subsequent substantial drug deposition in the tumor, which is investigated in numerous preclinical [13-17], yet also clinical studies [18, 19].

Next to providing a trigger for drug release, hyperthermia (HT) exposure can induce multiple other changes on cellular as well as tissue level [20, 21]. HT can cause direct cytotoxicity *in vitro* [22] and *in vivo*, which depends on the absolute temperature and exposure time, but also on the type of cell or tissue [23, 24]. Secondly, HT can increase chemosensitivity [25, 26] due to a synergistic effect between HT- and drug-induced cytotoxicity or due to an increased drug uptake as HT enhances cell membrane permeability [27, 28]. On tissue level, preclinical studies have shown that HT increased liposomal uptake in tumors [29-33]. However, clinical trials using Doxil® in combination with HT showed variable therapeutic outcomes, highlighting the clinical need for a liposomal

formulations that could more effectively release the drug [34, 35]. The latter inspired the design a 2-step drug delivery scheme, where first HT is applied to enhance the EPR effect followed by injection of TSLs. After accumulation of TSLs in the tumor, drug release is triggered with a second application of HT to ensure bioavailability of the drug.

In a previous study, Li et al. performed a comparative study with Dox loaded TSL using the aforementioned 2-step drug delivery scheme versus a 1-step intravascular HT-drug delivery scheme in a murine BLM melanoma model [36]. The conclusion of that study was that a 1-step treatment was more efficacious in treating a solid tumor than the 2-step approach. Here we provide a follow-up study, investigating 1-step and 2-step HT TSL based treatments in terms of *in vitro* cytotoxicity, drug uptake by cells, therapeutic efficacy and quantitative TSL uptake by B16 melanoma and BFS-1 sarcoma tumors. Furthermore, extensive *ex vivo* investigation provide data giving more insights into microenvironmental factors that could play a role in TSL accumulation for B16 and BFS-1 tumors and the influence of HT on these factors.

MATERIALS & METHODS

Materials

1,2-distearoyl-*sn*-glycero-3-phosphocholine (DSPC), 1,2-dipalmitoyl-*sn*-glycero-3-phosphocholine (DPPC) and 1,2-distearoyl-*sn*-glycero-3-phosphoethanolamine-N-(amino(polyethylene glycol)-2000) (DSPE-PEG₂₀₀₀) were purchased from Lipoid (Ludwigshafen, Germany). DSPE-diethylenetriaminepentaacetic acid (DTPA) was obtained from Avanti Polar Lipids Inc. (Alabaster, AL). Doxorubicin-hydrochloride solution (2 mg/ml) was ordered from Accord Healthcare. 4-(2-hydroxyethyl)-1-piperazineethanesulfonic acid (HEPES), (NH₄)₂SO₄, DMEM culture medium, fetal bovine serum (FBS), sulforhodamine B (SRB), poly(2-hydroxyethylmethacrylate; HEMA), 2-Amino-2-hydroxymethyl-propane-1,3-diol (Tris), NaCl, glycerol, Mayer's hematoxylin, eosin Y, Martius yellow, crystal scarlet and methyl blue were from Sigma Aldrich (St. Louis, MO). Nonyl phenoxy polyethoxyethanol (NP40) was purchased from ICN Biomedicals (Irvine, CA). Penicillin-streptomycin (Pen-Strep) solution was from Lonza (Breda, Netherlands). PD-10 desalting columns were bought from GE Healthcare Life Sciences (Buckinghamshire, UK). Entellan and rabbit-anti mouse Collagen IV antibody were from EMD Millipore (Billerica, MA). CD31 antibody (rat anti-mouse) was bought from Abcam (Cambridge, UK) and AlexaFluor 594 (goat anti-rat) and AlexaFluor 488 (goat anti-rabbit) from Invitrogen (Carlsbad, CA). Matrigel was acquired from BD (San Jose, CA). Cryo compound was from Klinipath (Duiven, Netherlands). Fluoromount-G was provided by Southern Biotech (Birmingham, AL). Cell death detection kit was

obtained from Roche (Woerden, Netherlands). Weigert's hematoxylin was purchased from Boom Chemicals (Meppel, Netherlands).

Liposome preparation

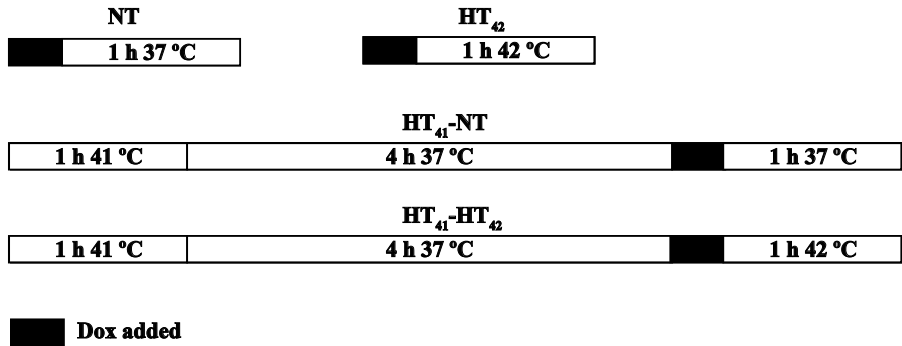
DPPC:DSPC:DSPE-PEG₂₀₀₀ at a molar ratio of 70:25:5 were dissolved in 9:1 (vol:vol) chloroform/methanol. Solvent was evaporated using a rotary evaporator and the resulting lipid film was flushed under a stream of nitrogen. The lipid film was hydrated with a 250 mM solution of (NH₄)₂SO₄ buffer pH 5.5 and extruded five times through 200 nm, 100 nm, 80 nm and 50 nm polycarbonate membrane filters. A pH gradient was established using a PD-10 column and eluting the liposomes with a pH 7.4 HEPES buffered saline (10 mM HEPES, 135 mM NaCl). Phosphate concentration was determined by ammonium molybdate assay [37]. Dox was loaded into the liposomes by mixing Dox and lipid at a ratio of 0.15:1 (mol:mol) and incubating it for 1 h at 39 °C in a thermoshaker. Liposomes were concentrated by ultracentrifugation (193000 *g*, 2 h, 4 °C) and resuspended in 10 mM HEPES buffered saline pH 7.4 yielding the final formulation of Dox-loaded TSLs (TSL_{Dox}).

Radiolabeled liposome preparation

For radiolabeled TSLs (¹¹¹In-TSL), 0.1 mol% DSPE-DTPA was added to the formulation described above and produced in a similar fashion as the regular TSLs, with the exception that the liposomes were not loaded with Dox. 1 μmol TSLs was incubated with 30 MBq ¹¹¹In for 15 min at room temperature after the pH was set at 5.0 with 2.5 M sodium acetate. After incubation labeling efficiency was determined by ITLC-SG (Varian Inc.) and the final volume was adjusted to 200 μL with HEPES buffered saline (10 mM HEPES, 135 mM NaCl, pH 7.4).

Cellular toxicity assay

BL6 or BFS-1 cells were seeded in 96-well plates and allowed to grow till 50% confluency in DMEM medium enriched with 10% FBS and 1% Pen-Strep. The medium was removed and fresh medium with a desired amount of free Dox or TSL_{Dox} was brought onto the cells and incubated according to Scheme 1. NT: incubation with Dox for 1 h at 37°C; HT₄₂: incubation with Dox for 1 h at 42°C; HT₄₁-NT: Preheating cells 1 h at 41°C, 4 h recovery at 37°C and a 1 h incubation with Dox at 37°C; HT₄₁-HT₄₂: Preheating cells for 1 h at 41°C, 4 h recovery at 37°C and a 1 h incubation Dox at 42°C. For a TSL_{Dox} treatments on cells, 10 μM Dox was used. To apply HT, plates were put into a water bath set at the required temperature. After incubation, the Dox containing medium was removed and cells were given fresh medium for 24 h or 48 h incubation at 37°C. Cells were fixed using 10% (w:v) trichloroacetic acid (TCA). After fixation, the plates were washed with water and 0.5% SRB solution was added to stain the fixed cells for 20 min. When staining was



Scheme 1. Overview of different *in vitro* Dox uptake treatments. Dox exposure took place at 37°C (NT) or 42°C (HT₄₂). In two additional groups, cells were preheated for 1 h at 41 °C (HT₄₁) with a 4 h recovery at 37°C before Dox uptake under NT or HT₄₂ conditions (HT₄₁-NT and HT₄₁-HT₄₂, respectively).

completed, cells were washed with 1% acetic acid and left to dry. 10 mM Tris was added to resuspend the SRB and absorbance was measured at 590 nm by spectrophotometry (Wallac Victor 2 Counter).

Cellular Doxorubicin uptake in 2D and 3D models

BL6 or BFS-1 cells were seeded into 75 cm² flasks and grown under similar conditions as mentioned above until 80% confluency was reached. The cells were subjected to 40 μM Dox under four different treatment conditions as stated in Scheme 1. Exposing cells to elevated temperatures was done by submerging the 75 cm² culture flask into a water bath. After incubation, the cells were washed with ice cold PBS, scraped from the flask and centrifuged at 200 *g* at 4°C. The pellets were resuspended in 150 μL lysis buffer (20 mM Tris, 150 mM NaCl, 0.2% NP40, 10% glycerol, pH 7.4), followed by 30 min incubation on ice and centrifugation at 14,000 *g*. The pellets were resuspended and homogenized in 500 μL PBS by brief probe sonication and Dox concentration was measured by fluorometry at 485 nm excitation and 580 nm emission (Wallac Victor 2 Counter). Tumor spheroids were made according to a previously described method [38]. In short, conical shaped 96-well plates were coated with poly-HEMA and 1 x 10⁵ cells which were centrifuged at 1,000 x *g* for 10 min in the presence of 2.5% Matrigel and incubated overnight at 37°C. After incubation, spheroids were handpicked and exposed to identical treatments as in the 2D model in a thermoshaker (no shaking). After incubation, the spheroids were washed in PBS, embedded into Fluoromount-G and imaged by confocal microscopy (Zeiss LSM 510 Meta; Oberkochen, Germany). A 5 μm Z-stack was made over the surface of the spheroid to determine total Dox fluorescence. For each optical slice, the amount of saturated Dox fluorescence pixels were counted. The sum of saturated pixels of all tumor slices was used as an indicator for Dox uptake. For cryo-sectioning,

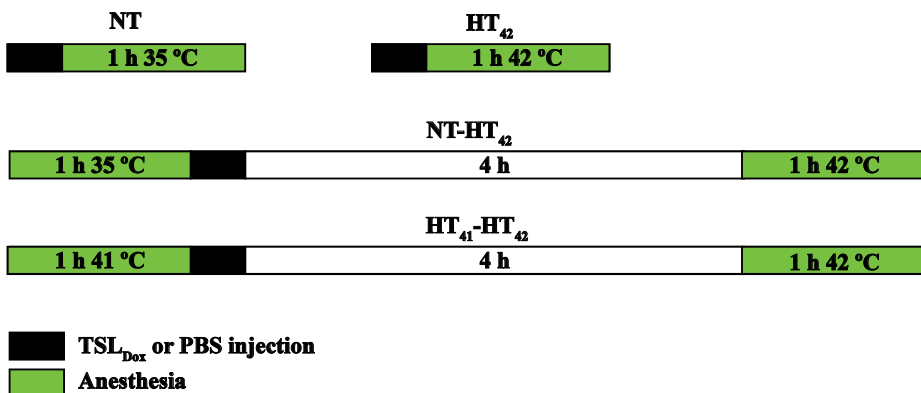
spheroids were embedded into Cryo Compound and snap frozen in liquid nitrogen. 10 μm slices were made using a Cryostat (Leica CMI850 UV; Wetzlar, Germany), and afterwards embedded into Fluoromount-G and imaged using fluorescence microscopy (Zeiss Axiovert 100M; Hamamatsu Photonics C4742-98 camera controller).

B16 and BFS-1 tumor generation

Murine B16 melanoma or BFS-1 sarcoma cells (1×10^6) were subcutaneously injected into the flank of C57BL6 mice (Harlan) to grow bulk tumors. After reaching volumes of approx. 700 mm^3 , animals were sacrificed and tumor pieces were transplanted to the animals of the therapeutic studies. All animal experiments were approved by the Erasmus MC animal research committee, Rotterdam, The Netherlands.

Therapeutic efficacy studies in a B16 and BFS-1 model

1 mm^3 B16 or BFS-1 tumor pieces were transplanted subcutaneously onto the hind limb of C57BL6 mice and allowed to grow to 200 mm^3 after which treatments were initiated as shown in Scheme 2. NT: 1-step with 100 μL i.v. PBS injection and 1 h anesthesia at body temperature; HT₄₂: 1-step with 100 μL i.v. PBS injection and 1 h anesthesia with heated tumor at 42 °C; TSL_{Dox}-NT: 1-step with 100 μL 5 mg/kg TSL_{Dox} i.v. injection and 1 h anesthesia at body temperature; TSL_{Dox}-HT₄₂: 1-step with 100 μL 5 mg/kg TSL_{Dox} i.v. injection and 1 h anesthesia with heated tumor at 42 °C; HT₄₁-HT₄₂: 2-step with 1 h preheating tumor at 41 °C under anesthesia, 100 μL i.v. PBS injection, 4 h waiting period and 1 h anesthesia with heated tumor at 42 °C; TSL_{Dox}-NT-HT₄₂: 2-step with 1 h anesthesia at body temperature, 100 μL 5 mg/kg TSL_{Dox} i.v. injection, 4 h waiting period and 1 h anesthesia with heated tumor at 42 °C; TSL_{Dox}-HT₄₁-HT₄₂: 2-step with 1



Scheme 2. Overview of 1-step and 2-step treatments *in vivo*. For 1-step, i.v. TSL_{Dox} administration was conducted at body temperature (NT) or when the tumor was brought to 42 °C (HT₄₂). 2-step treatments were composed of keeping the mouse under anesthesia at body temperature for 1 h (NT-HT₄₂) or preheating the tumor at 41 °C for 1 h (HT₄₁-HT₄₂), prior to TSL_{Dox} injection, 4h rest and a second tumor heating at 42 °C.

h preheating tumor at 41°C under anesthesia, 100 µL 5 mg/kg TSL_{Dox} i.v. injection, 4 h waiting period and 1 h anesthesia with heated tumor at 42 °C. In the 1-step treatment protocol, the tumor was submerged into a 42.5 °C water bath for heating to 42 °C for 10 min, followed by an i.v. injection of TSL (5 mg/kg Dox) and further heating for another hour. The 2-step treatment procedure included heating of the tumor to 41 °C for one hour and an i.v. injection of TSL (5 mg/kg Dox) 10 min after heating. Afterwards, the animal was allowed to rest for 4 h, followed by a second HT treatment for 1 h at 42 °C. In control groups normothermic (NT; 35 °C) conditions were used, where the animal was put under anesthesia for 1 h and kept at 35 °C on a 37 °C heating plate while covering the animal with tin foil. During both HT and NT experiments, the tumor bearing limb, with exception of the tumor itself, was coated in vaseline to prevent possible skin burns. Body temperatures of the mice were measured using a rectal probe.

SPECT/CT imaging of TSL accumulation in a B16 and BFS-1 model

1×10^6 cells were subcutaneously injected on the hind limb of C57BL6 mice and tumors were allowed to grow to volumes of 200 mm³. Tumors were either heated for one hour at 41 °C prior to injection or kept at 35 °C in a similar fashion as for the therapeutic study. ¹¹¹In-TSL were i.v. injected (200 µL per mouse with an average activity of 33 ± 2 MBq ¹¹¹In) and scans were made 4 h, 8 h, 24 h and 48 h after injection. Scans were acquired using the nanoSPECT/CT (Mediso Medical Imaging Systems) with the following settings for the SPECT scans: 20 projections, 60 seconds/projection, and a quality factor of 0.8. APTI apertures were used with 1.4 mm diameter pinholes (FOV 24 + 16 mm). CT scans were acquired with 240 projections, 45 kVp tube voltage and 500 ms exposure. Data analysis was performed using InVivoScope/VivoQuant software (inviCRO, Boston, MA), where three-dimensional regions of interest were drawn over the tumor to calculate uptake of ¹¹¹In-TSL at the selected time points. After the last scan, the animals were sacrificed and tumors and organs were harvested, weighed and radioactivity was determined using a γ-counter to calculate percentage injected dose per gram (%ID/g). All data were corrected for radioactive decay.

Pharmacokinetic modelling

The blood kinetics and pharmacokinetic parameters of the TSL_{Dox} formulation were determined in an earlier study (Figure 1) [39]. Results from that study showed that the blood half-life of liposomal carrier $C_{lip}(t)$ can be described with a mono-exponential function:

$$C_{lip}(t) = C_{lip}(t = 0) \cdot \text{Exp}(-\ln 2 / t_{1/2, \text{TSL}} \cdot t)$$

Eq.1

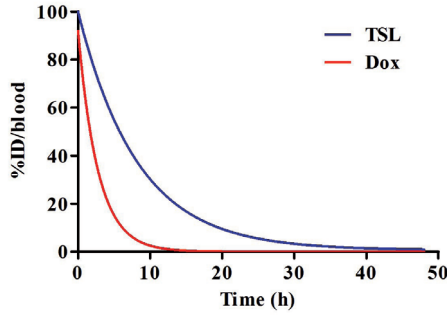


Figure 1. Blood kinetics of TSL and Dox from injected TSL-Dox in C57BL/6 mice. Figure is based on previously shown results by our group [39].

with $C_{lip}(0)=100\%ID$ at time point of injection and $t_{1/2,TSL} = 5.6 \pm 0.4$ h being the circulation half-life of the liposomes. Upon injection, a fraction of Dox is instantaneous released ($Burst = 8 \pm 3$ %) followed by a slow leakage of Dox from the liposomal carrier with a half-life of $t_{1/2,leak} = 2.7 \pm 0.3$ h. The concentration of intraliposomal dox $C_{Dox,TSL}(t)$ can be described with the following equation:

$$\frac{\partial C_{TSL,tumor}(t)}{\partial t} = k_{in} \cdot C_{lip}(t) - k_{out} \cdot C_{TSL,tumor}(t) + k_{ret} \quad \text{Eq. 2}$$

The concentration of (radiolabeled) liposomes in the tumor, $C_{TSL,tumor}(t)$, can be described with a simple two compartment model:

$$\frac{\partial C_{TSL,tumor}(t)}{\partial t} = k_{in} \cdot C_{lip}(t) - k_{out} \cdot C_{TSL,tumor}(t) + k_{ret} \quad \text{Eq.3}$$

where k_{in} , k_{out} and k_{ret} describe the rates of uptake, washout and retention of TSL in the tumor compartment.

Concentration of intraliposomal Dox within the tumor is subsequently numerically calculated assuming the same burst and leakage of Dox from the liposomal carrier as found for TSL-Dox in the blood compartment. Numerical integration of Eq. 3 and fitting of the SPECT data was performed using Mathematica® (version 10.2, Wolfram Research).

Histology

After the SPECT/CT experiments, the excised tumors were snap frozen in liquid nitrogen. 5 μm slices were cut and tumors were stained for vessels with an anti-CD31 antibody and AlexaFluor 594 or collagen with anti-collagen IV antibody and AlexaFluor 488. The TUNEL staining was performed with a cell death detection kit. The CD31 and TUNEL

stains were quantified using ImageJ (version 1.48) software and by setting a manual threshold. A second set of frozen slices was stained with Maier's hematoxylin and Eosin (H&E) or by Weigert's hematoxylin, Martius yellow, crystal scarlet and methyl blue (MSB), followed by mounting in Entellan. The slices were imaged for fluorescence by confocal microscopy (CD31, collagen IV & TUNEL) or bright field microscopy (Leica DM 4000B) for H&E and MSB stained sections.

Statistics

All statistical tests were carried out using Graphpad Prism 5 software. All figures were subjected to unpaired two tailed t-test or one-way ANOVA Bonferroni test with significant difference at $p < 0.05$.

RESULTS

Preparation of TSL_{Dox}

Loading of TSL with the formulation DPPC:DSPC:DSPE-PEG₂₀₀₀ at a molar ratio of 70:25:5 with Dox was achieved with 100% efficacy. Dynamic light scattering of the resulting TSL_{Dox} indicated an average hydrodynamic diameter of 83 ± 3 nm and a zeta-potential of -7.9 ± 0.9 mV. Stability at 37 °C and release kinetics at 42 °C were tested in culture medium (10% FBS and 1% Pen-Strep) and were found to be similar to results obtained with 100% FBS as described in our previous work (Figure 2) [39].

Cytotoxic assays on B16 melanoma and BFS-1 sarcoma cells

In an *in vitro* study, murine B16 melanoma and BFS-1 sarcoma cells were exposed to various Dox concentrations for 1 h under the conditions depicted in Scheme 1. Both cell lines showed an increased sensitivity to Dox when the drug exposure was performed at

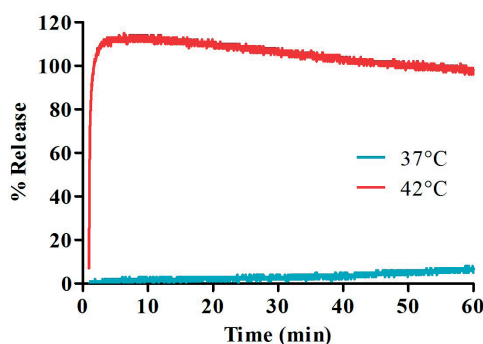


Figure 2. Dox release from TSL at 37 °C and 42 °C in DMEM culture medium with 10% FBS and 1% Pen-Strep using fluorescence readout. Each curve represents an average of three measurements.

hyperthermic temperatures (Figure 3). For B16 (Figure 3A, B) and BFS-1 (Figure 3C, D), the Dox sensitivity increased 8-fold. Additional pre-heating (HT_{41} - HT_{42}) did not result in a further increase in Dox sensitivity for B16. However, the 18-fold increase for BFS-1 was significantly higher than the single HT treatment. In this case direct HT-induced cytotoxicity could have played a predominant role (Figure 4). B16 and BFS-1 cells were furthermore tested for survival after incubation with TSL (empty), 10 μ M TSL_{Dox} or 10 μ M

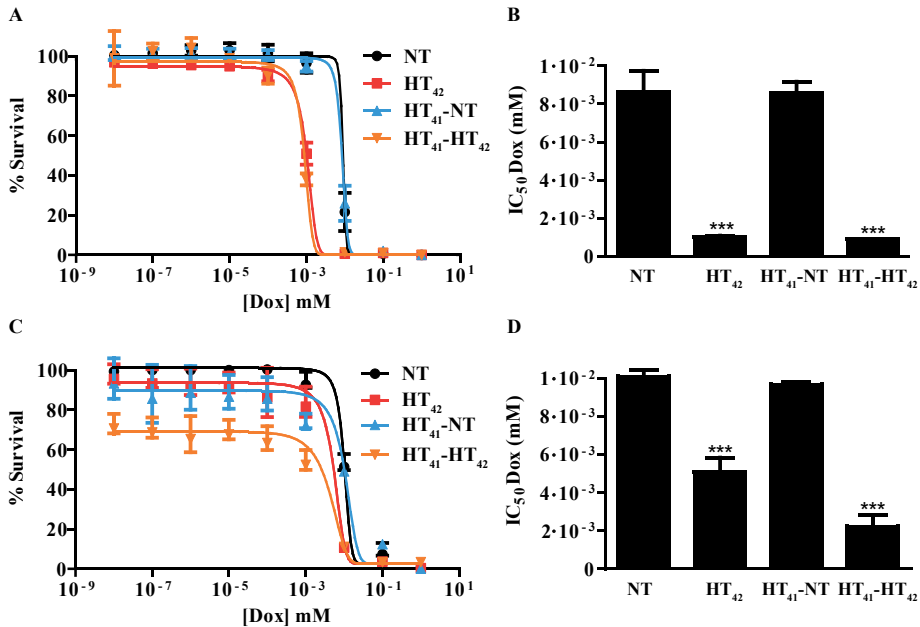


Figure 3. Dox cytotoxicity assay and IC_{50} values for B16 (A, B) and BFS-1 cells (C, D) 48h after treatment by different hyperthermia protocols. $n = 3$ for each data set. Curves were fit by non-linear regression and statistical analysis by one-way ANOVA Bonferroni test. The significance scores of all treatments versus NT groups are indicated with asterisks. * = $p < 0.05$, ** = $p < 0.01$, *** = $p < 0.005$.

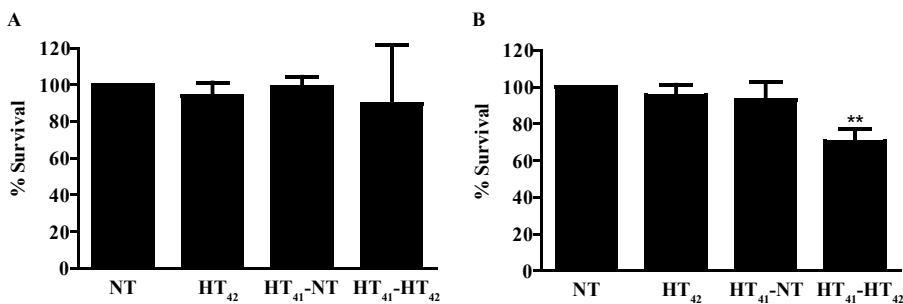


Figure 4. Analysis on HT induced cytotoxicity on B16 (A) and BFS-1 cells (B) in the experimental groups of Figure 1. Survival of experimental groups is normalized versus the NT group. $n = 3$ per group and one-way ANOVA Bonferroni test was used for statistical analysis of the data. * = $p < 0.05$, ** = $p < 0.01$, *** = $p < 0.005$.

free Dox under normothermic (NT; 37 °C) and HT₄₂ conditions for 1 h. After the treatment, the cells were kept in culture medium for 24 h or 48 h. At 37 °C, TSL_{Dox} induced little toxicity to the cells, while at 42 °C the release of Dox was sufficient to cause high cell death (Figure 5). The TSL by itself had no inhibitory effect on cell growth, while HT did show some direct cytotoxicity, which was only significant for B16 24 h after incubation with $72 \pm 11\%$ viable cells compared to the NT group (Figure 5A). The addition of 10 μ M TSL_{Dox} to a 1 h incubation with HT₄₂ resulted in an immediate cytotoxic effect 24 h after the incubation (Figure 5A) with $25 \pm 6\%$ for B16 and $57 \pm 7\%$ for BFS-1. This cytotoxic effect became even more apparent 48 h after incubation, showing an almost complete cell death for both cell types (Figure 5B). The TSL_{Dox} HT₄₂ group showed similar results as where 10 μ M free Dox was used (Dox HT₄₂), suggesting a total Dox release from TSL_{Dox} in these experimental conditions. A cytotoxicity assay using a 2-step heating protocol was not performed, as the main cytotoxic effect was caused by the increased uptake of free or released Dox during HT₄₂.

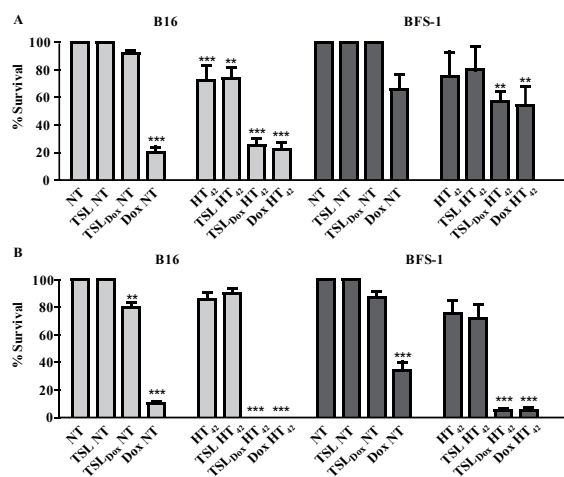


Figure 5. Cytotoxicity assay on B16 and BFS-1 cells 24 h (A) and 48 h (B) after a 1 h incubation with 10 μ M TSL_{Dox} or free Dox under NT (37 °C) or HT₄₂ (42 °C) conditions. $n = 3$ for each data set. Statistical analysis was carried out using one way ANOVA Bonferroni test comparing the treatment groups with the NT group separately at 24h and 48h. The significance scores of all treatments versus NT groups are indicated with asterisks. * = $p < 0.05$, ** = $p < 0.01$, *** = $p < 0.005$.

***In vitro* Doxorubicin uptake in 2D and 3D models**

Next, the effect of HT on Dox uptake was studied in B16 and BFS-1 cells. Both cell lines exhibited a linear uptake of Dox over time at body temperature (Figure 6A,B). Incubation of both cell lines with Dox at HT₄₂ significantly increased Dox uptake 9-fold for B16 (Figure 6A) and 6-fold for BFS-1 cells (Figure 6B). Groups were added where the cells were preheated at 41 °C for 1 h followed by 4 h at 37 °C to mimic a 2-step approach therapy. Preheating of the cells before incubation with Dox at NT (HT₄₁-NT) or HT₄₂

(HT₄₁-HT₄₂) conditions did not result in a significant difference compared to Dox uptake without preheating. Next, we used multicellular spheroids of BFS-I cells to determine the Dox uptake as well as spatial distribution under the different temperature protocols in a 3D model. After performing similar incubation protocols as described before, the BFS-I spheroids showed a similar pattern in Dox uptake than BFS-I cells in the 2D standard culture conditions (Figure 6C). When the Dox fluorescence intensity was quantified (Figure 6D), HT₄₂ and HT₄₁-HT₄₂ presented significantly more Dox positive areas than NT spheroids with a 6-fold and 10-fold increase in the summation of saturated Dox fluorescence pixels, respectively. HT₄₁-NT treatment did not result in a significantly enhanced uptake. Dox did not penetrate farther than the first few cell layers into the spheroid, despite the heating protocol used (Figure 6E). BL6 cells did not form spheroids and could therefore not be studied in the 3D Dox uptake model.

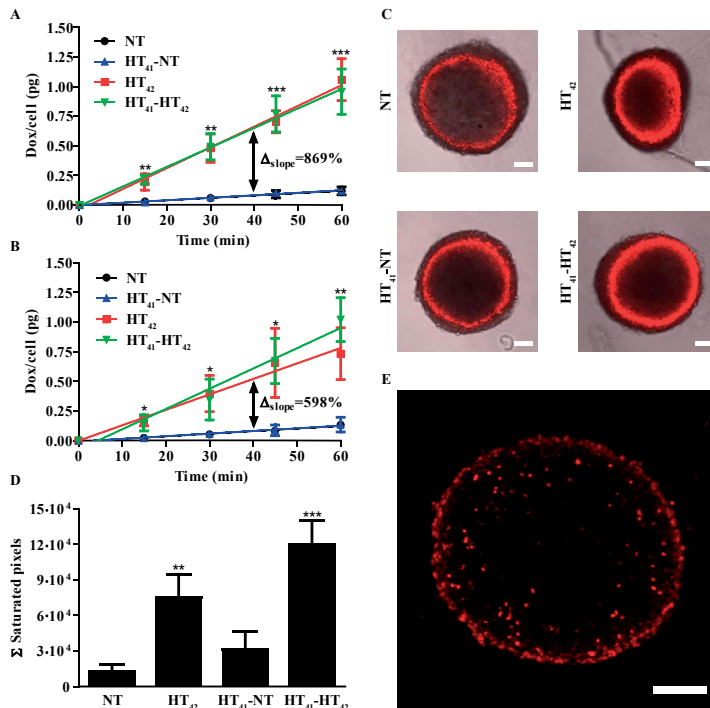


Figure 6. Two-dimensional Dox uptake in BL6 (A) and BFS-I (B) cell cultures and BFS-I spheroids (C-E). Cells or spheroids were exposed to 40 μM Dox for 1 h at 37 °C (NT), 42 °C (HT₄₂), or preheated at 41 °C followed by 4 h at 37 °C before a 1 h exposure to 40 μM Dox at NT (HT₄₁-NT) or HT₄₂ (HT₄₁-HT₄₂). Optical slices of 5 μm made by confocal microscopy of the spheroid (C) were summed up to determine the Σ saturated pixels (red) per spheroid (D). Cryosections of 10 μm (E) of the BFS-I spheroids show spatial distribution of Dox fluorescence (red). All data sets are composed of an n = 3 experiment and compared by one way ANOVA Bonferroni test, * = p < 0.05, ** = p < 0.01, *** = p < 0.005. Asterisks show significance compared to NT groups. Scale bars represent 100 μm.

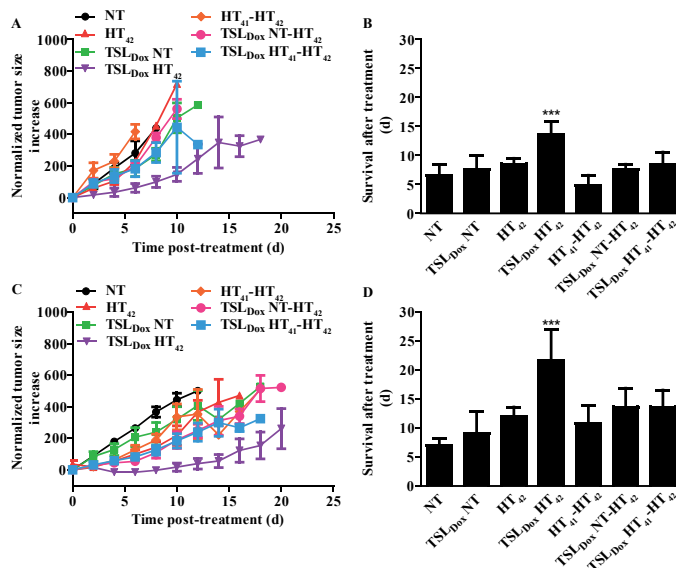


Figure 7. Therapeutic efficacy study in C57BL/6 mice with s.c. BL6 or BFS-1 tumors. After treatment, results for BL6 tumors were plotted for growth (A) and survival (B). Survival (B) was based on a size cutoff at 300% tumor size increase. Error bars in growth curve (A) represent SEM and one way ANOVA Bonferroni test was used to determine differences of survival in B (* = $p < 0.05$, ** = $p < 0.01$, *** = $p < 0.005$). Asterisks above bars show significance versus NT. BFS-1 is presented similarly in C and D. $n = 4$ for NT, TSL_{Dox} NT and HT₄₂ groups; $n = 5$ for all other groups.

1-step & 2-step therapeutic study

A therapeutic study with BL6 (Figure 7A, B) and BFS-1 (Figure 7C, D) tumors were subjected to 1-step or 2-step therapies (Scheme 2). We chose 41 °C as preheating temperature since it has been shown that an intratumoral increase of TSL_{Dox} accumulation can be established [31] without risking significant vascular damage [40]. In both BL6 and BFS-1 tumors, TSL_{Dox} with HT₄₂ significantly outperformed all other treatments with an average improvement of survival of 7.1 ± 1.4 days for BL6 and 14.6 ± 2.8 days for BFS-1 when compared to the NT group. The body temperature differed significantly between NT and HT₄₂ treated mice (Figure 8). Nevertheless, it remained at a physiological level with 35.0 ± 0.4 °C and 36.9 ± 1.1 °C, respectively.

Quantitative SPECT/CT imaging of TSL accumulation in solid tumors

A SPECT/CT study with ¹¹¹In-TSL (labeling efficiency > 99%) was carried out to visualize the particle uptake in BL6 and BFS-1 tumor bearing mice, comparing NT conditions versus tumor preheating for 1 h at 41°C prior to injection (HT₄₁). SPECT imaging over time showed that the majority of the injected ¹¹¹In-TSL were cleared by liver and spleen (Figure 9A, B) with tumor uptake over time. For all tumors, a maximum uptake was observed approx. 4 h post injection followed by a slight reduction over time leveling

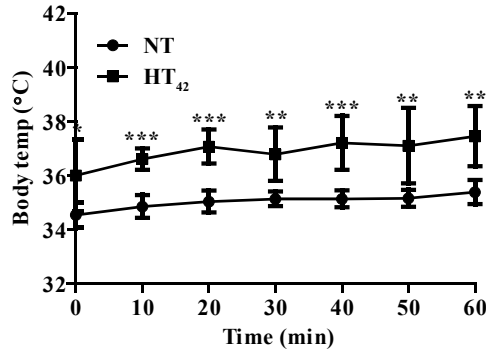


Figure 8. Body temperature readings of mice under anesthesia, on a 37 °C heating plate, covered with tin foil (NT), or mice under anesthesia with the tumor bearing limb submerged in a 42.5 °C water bath (HT₄₂). n = 6 per group. Temperature readings were performed rectally with a probe thermometer every ten minutes. For every time point, statistical analysis was performed by unpaired two-tailed t-test. * = $p < 0.05$, ** = $p < 0.01$, *** = $p < 0.005$.

off at 48 h post injection. Under NT conditions, plateau values of 3.2 ± 0.5 and 1 ± 0.3 %ID/cc were reached for B16 and BFS1 tumors respectively. Applying HT₄₁ before injection increased uptake in both tumors, leading to higher maximum as well as plateau concentrations (B16: 6.2 ± 1.5 %ID/cc, BFS1: 3.3 ± 2.8 %ID/cc at 48 h p.i.) (Figure 9A-D). Biodistribution studies at $t = 48$ h p.i. were consistent with data derived from SPECT showing an uptake of ¹¹¹In-TSL in B16 tumors 2.8 ± 0.5 %ID/g compared to a considerable lower uptake of 0.9 ± 0.2 %ID/g in BFS-1 tumors for NT experiments (Figure 9E,F). Applying HT₄₁ before injection resulted in a significantly increased ¹¹¹In-TSL accumulation measured after 48 h in B16 tumors (5.0 ± 1.0 %ID/g; Figure 9C, E) and BFS-1 tumors (2.6 ± 1.0 %ID/g; Figure 9D, F). SPECT data were used to fit the liposomal tumor uptake according to a simple two compartment model, deriving the rates for uptake, washout and retention, k_{in} , k_{out} , k_{ret} , in the two different tumors under NT and HT₄₁ conditions (Table I). Taking the earlier determined pharmacokinetic properties of the here used TSL_{Dox} formulation into account (Figure 1), the model also allowed to calculate the concentration of intraliposomal Dox present in the tumors as a function of time (Figure 9C,D). Maximum concentrations of intraliposomal Dox were reached approx. 2 hours p.i.. In contrast to the liposomal concentrations, intraliposomal Dox concentrations decreased to zero 15-20 hours p.i. due to the leakage from the liposomal carrier.

Table I. Pharmacokinetic parameters describing the tumor uptake and retention in B16 and BFS-1 tumors.

Tumor	Condition	$k_{in}/(1/h)$	$k_{out}/(1/h)$	$k_{ret}/(1/h)$
B16	NT	0.0157 ± 0.004	0.39 ± 0.16	1.4 ± 0.63
	HT₄₁	0.0233 ± 0.007	0.36 ± 0.22	2.5 ± 1.64
BFS-1	NT	0.0074 ± 0.003	0.69 ± 0.34	0.7 ± 0.38
	HT₄₁	0.0127 ± 0.001	0.36 ± 0.07	1.2 ± 0.24

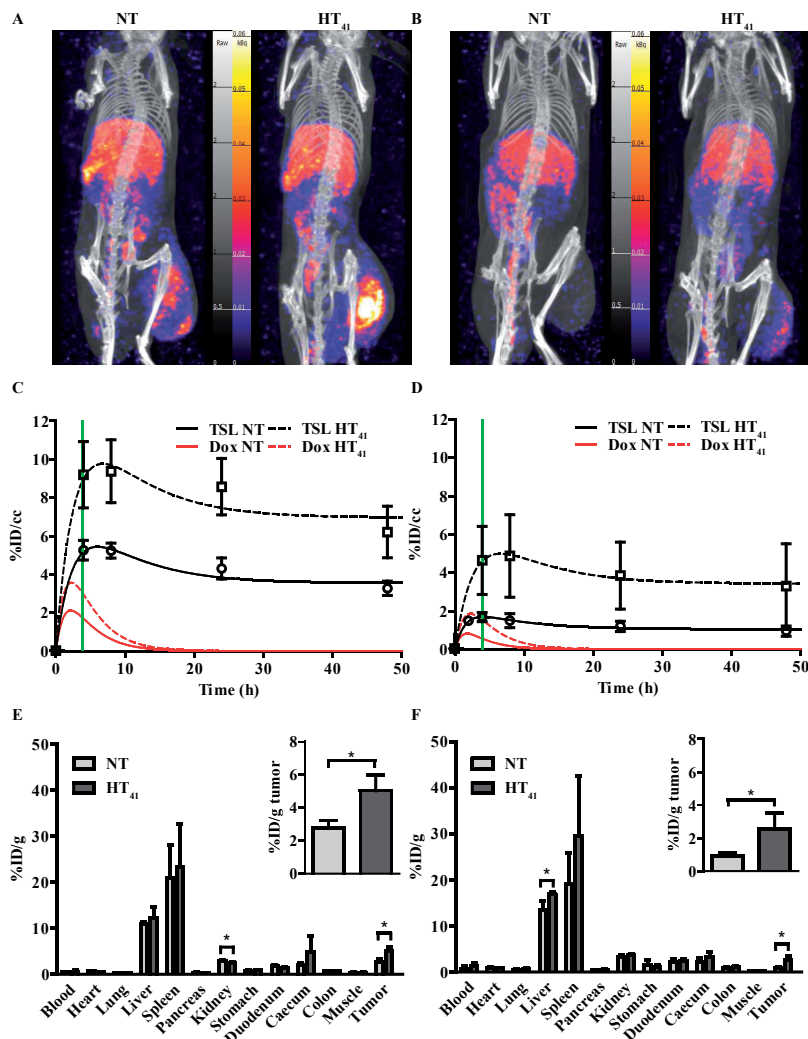


Figure 9. SPECT-CT study on ^{111}In -TSL distribution in BL6 (A, C, E) and BFS-1 (B, D, F) tumor bearing mice. After i.v. administration, scans were made at 4 h, 8 h, 24 h and 48 h for all groups. BL6 (A, C) and BFS-1 (B, D) tumors showed ^{111}In -TSL accumulation after i.v. administration at NT, which could be significantly enhanced (unpaired two-tailed t-test; $p < 0.05$) by pre-heating the tumor for 1 h at 41 °C prior to ^{111}In -TSL administration (HT₄₁). The green line shows the 4 h time point where a second HT treatment would have taken place in case of a 2-step therapy. Biodistribution of ^{111}In -TSL was done by γ -counting on excised organs and tumors (E, F) 48h hours after injection. Every group consisted of three animals ($n = 3$).

The uptake as well as the retention rate of liposomes in BL6 tumors was ca. 2 times higher compared to BFS-1 tumors, while washout was comparable for both tumors. Notably, HT₄₁ induced in both tumors a comparable effect with increasing the k_{in} , and k_{ret} by a factor of ca. 1.66 ± 0.13 leading to a more rapid and higher uptake of liposomes and consequently a high Dox peak concentration.

Histology

After the SPECT-CT study, the tumors were used for H&E, MSB, TUNEL, CD31 and collagen IV staining (Figure 10 & 11). H&E staining indicated that B16 tumors have less strong cellular interactions as can be seen by the gaps in the tissue (Figure 10A), whereas BFS-1 has a much more compact morphology. Furthermore, the H&E (Figure 10A, arrows) suggests that the B16 tumors are more apoptotic. Yet after HT₄₁, apoptotic areas could be seen in both tumor types. MSB staining showed that B16 tumors have a very low presence of extracellular fibers (Figure 10B), whereas BFS-1 showed a more mature extracellular matrix (Figure 10C). Quantitative TUNEL staining (Figure 11A) showed high apoptosis of $14.4 \pm 10.0\%$ for B16 when compared to BFS-1 with $0.4 \pm 0.1\%$. HT₄₁ caused an increase of apoptosis, showing $24.5 \pm 13.2\%$ for B16 and $1.2 \pm 0.4\%$ for BFS-1, which was a significant increase for the latter. The vessel staining using CD31 indicated a comparable mean vessel density for both tumor models (Figure 11B). The quantitative collagen IV staining confirmed the result of the MSB staining with $3.6 \pm 0.3\%$ for B16 and $14.8 \pm 1.2\%$ mean density for BFS-1 (Figure 11C). The B16 vessels were relatively large with collagen almost solely associated with the vessels (Figure 11D), whereas BFS-1 vessels were smaller and the interstitium consisted of more extracellular collagen matrix (Figure 11E).

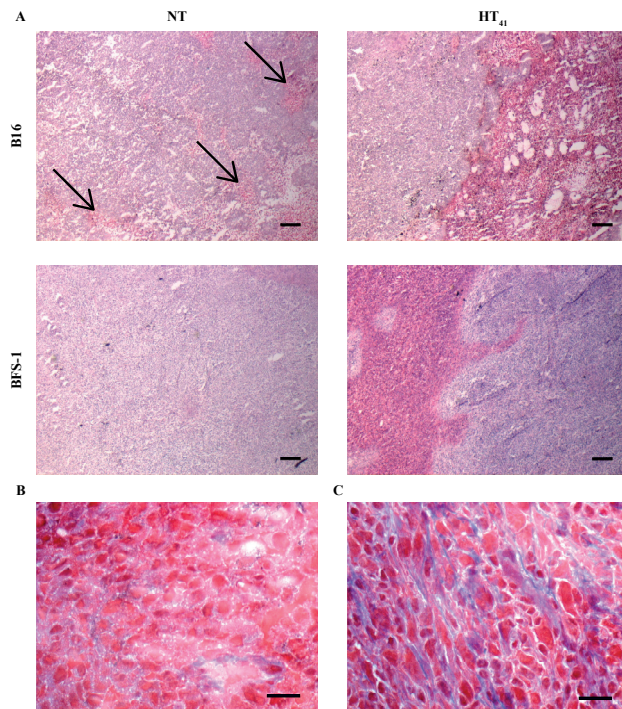


Figure 10. 5 μm H&E stained sections of B16 and BFS-1 tumors 48 h after NT or HT₄₁ (A). Black arrows indicate apoptotic areas. MSB stained B16 (B) and BFS-1 (C) collagen in blue. Scale bars represent 200 μm in A and 20 μm in B and C.

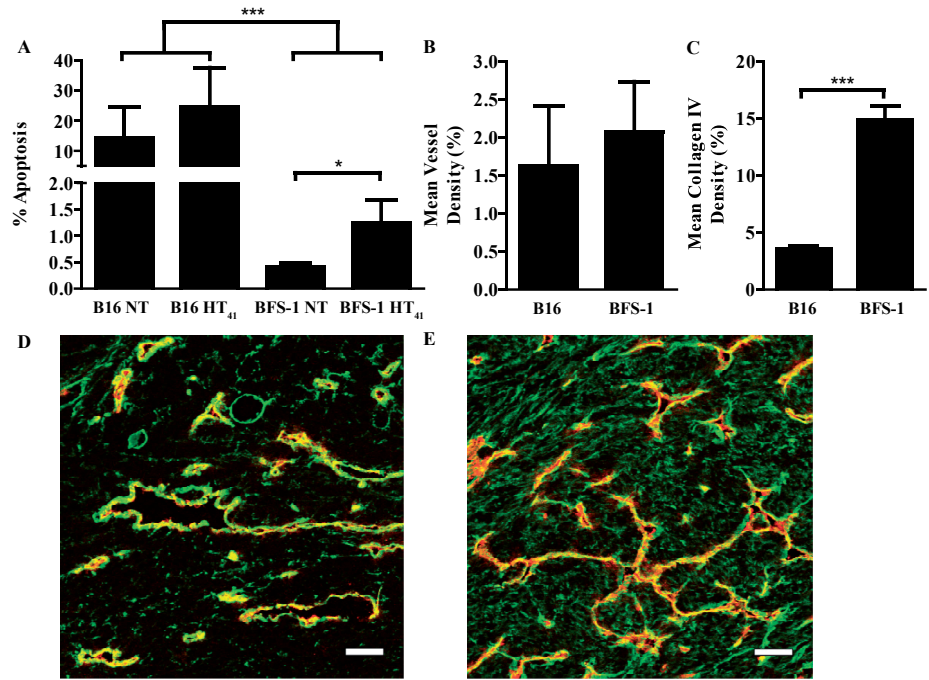


Figure II. Quantification of cryo-section staining with TUNEL (A), CD31 (B) and collagen IV (C) was analyzed by unpaired two tailed t-test (* = $p < 0.05$). B16 (D) and BFS-1 (E) blood vessels colored red for CD31. Collagen IV stained in green. Scale bar shows 50 μ m. $n = 3$ for all groups.

DISCUSSION

In the field of nanomedicine, substantial research has been performed throughout the last decades on HT-triggered drug release from TSLs for treatment of solid tumors. In this context, mainly 1-step intravascular drug delivery schemes were employed, where tumors are heated to hyperthermic temperatures and drug loaded TSL are injected at the start of the HT treatment. In a previous study conducted by Li et al [36], a 2-step treatment scheme was investigated as a possible alternative in a BLM melanoma xenograft, where first HT₄₁ is applied to enhance vascular permeability, then a TSL_{DOX} formulation was injected that subsequently accumulated in the tumor, followed by a second HT₄₂ step to release the drug from its carrier in order to ensure bioavailability. The aforementioned study showed in contrast to the 1-step therapy, that the 2-step approach was not effective in causing a therapeutic response. In our experimental design we chose for a B16 melanoma and BFS-1 sarcoma cell line because tumors from these cell lines have been previously reported to show high and low EPR-mediated uptake of TSL, respectively [31]. We tested how these tumors respond to a 1-step versus 2-step therapy, expanded the knowledge on how the tumor models responded to single versus multiple HT treatments

in combination with local chemotherapy and provide extensive information on what factors can cause the differences in TSL accumulation between these tumors and which of these factors could be influenced by HT to increase TSL accumulation.

BL6 and BFS-1 cells showed a significant increase in Dox sensitivity when the drug exposure happened during HT₄₂. The reduced IC₅₀ with HT correlated with the increase Dox uptake by the cells discussed hereafter. Previously published data on this correlation showed that the outcome of these experiments depend on cell type and specific experimental conditions, e.g. exact temperature and duration of HT exposure [27, 41-43]. Testing TSL_{Dox} on these cells showed that at 37 °C the cytotoxic effect is minimal, whereas at 42 °C, the TSL_{Dox} released all drug and therefore cytotoxicity was comparable to free Dox. The small cytotoxic effect at 37°C could be caused by cellular uptake of TSL_{Dox} or by Dox leaking from the liposomes into culture medium (Figure 2). Next, we investigated the presence of a synergistic effect of Dox and HT for different heating schemes in a 2D and 3D cellular model. In a 2D model, it was shown that HT₄₂ induces a faster cellular uptake of Dox leading to a 6-9 times higher rate of uptake in BL6 and BFS-1 cells than at 37 °C. Preheating the cells for 1 h with HT₄₁ followed by incubation for 4 h at 37 °C before adding Dox did not show any improvement of Dox uptake, indicating that HT-induced effects at 41 °C were reversible in nature and could only improve drug uptake during the heating and not thereafter. As the Dox uptake is caused by passive diffusion across the cell membrane, increase of cellular membrane fluidity and permeability during HT is the most likely explanation, since these effects are temporal in nature and fully reversible [27, 28]. Other studies have shown that preheating to slightly higher temperatures of 43-45.5 °C lead to a reduced Dox uptake most likely due to a more permanent and irreversible temperature of thermal dose induced damage [41, 44]. However, HT₄₁ used for preheating in this study did not induce this effect as has also been reported by others [45]. Spheroids mimic a solid tumor in terms of cell physiology, presence of extracellular matrix and an apoptotic core [46]. For this reason, we employed this model to investigate whether Dox penetration depth into a dense structure of cells is influenced by different heating conditions [47, 48]. BFS-1 spheroids showed a similar response in Dox uptake as the 2D model when different HT protocols were applied. However, it also showed that if cells are closely packed, the drug does not penetrate deep into the structure beyond the first few layers of cells. Neither the spatial distribution nor the penetration depth could be improved by HT in tumor spheroids. A comparative study using BL6 cells was not possible since BL6 cells did not form spheroids. The latter might be caused by the lack of a substantial cell-cell adherence, which was also observed in *ex vivo* examination of BL6 tumors described later in this section.

At this stage we have only shown the potential of local chemotherapy and HT *in vitro*. However, the described features are only a small part of the factors that have to be considered for drug delivery to solid tumors. Therefore, we performed a therapeutic study

as well as *in vivo* imaging and extensive *ex vivo* investigation on B16 and BFS-1 tumors to better understand the factors that could have played a role in various therapeutic responses. For both tumor types, a 1-step approach where TSL_{Dox} is i.v. administered during HT₄₂ gave a significant therapeutic response, whereas a 2-step approach which relied on TSL_{Dox} accumulation in a preheated (HT₄₁) tumor followed by a second HT₄₂ step to induce drug release did not show a therapeutic effect. The SPECT/CT imaging in this case was particularly valuable to follow the TSL accumulation in B16 and BFS-1 tumors. The SPECT data were used for fitting a two compartment model which describes tumor uptake of the liposomal carrier as well as the intraliposomal Dox concentration in the tumor taking the blood kinetic and pharmacokinetic parameters of TSL_{Dox} into account [39]. For both tumors and regardless of applying HT₄₁ beforehand, the maximum concentration of liposomes was reached approx. 4 h p.i., when the second HT₄₂ step was applied. The B16 tumors showed a significant higher liposomal uptake compared to the BFS-1 tumor with ca. two fold higher k_{in} and k_{ret} parameters reflecting a higher intrinsic EPR effect for the B16 model. Interestingly, 1 hour of HT₄₁ induced the same effect in both tumors leading to a 1.66 times increase in k_{in} and k_{ret} and thus maintaining the two fold higher uptake of TSLs in B16 compared to BFSI tumors.

However, calculations suggested that maximum intraliposomal Dox concentrations were already reached 2 h p.i., and declining to zero within 20 h due to leakage from the TSLs. These data imply that a more favorable time point for the second HT₄₂ step is ca. 2-3 h p.i. [36]. Based on our calculations, the intraliposomal Dox reached concentrations of 1.7 % ID/cc for B16 and 0.6 % ID/cc Dox for BFS-1 at the moment of the second HT₄₂ step (i.e. after 4 h) at normal temperature conditions, and 3.0 % ID/cc and 1.5 % ID/cc Dox with a preceding HT₄₁ treatment. These concentrations are lower compared to typical values found for a 1-step delivery approach [49], which provides an explanation for the lack of a significant therapeutic response in a 2-step drug delivery protocol.

Finally, we performed histological analysis of excised tumors and investigated factors that may cause the differences in TSL uptake and the intrinsically higher EPR effect found in B16 and BFS-1 tumors. B16 tumors grew more aggressively than BFS-1, reaching volumes of 200 mm³ in 7-14 and 14-21 days after inoculation, respectively. Especially in preclinical models, fast growing tumors show higher structural and functional abnormalities of the vasculature, thereby increasing the odds for a high EPR effect [1, 50, 51]. The mean vessel density was similar for B16 and BFS-1, however the morphology of B16 vessels appeared more tortuous and overall larger in size. Next to the growth rate and vascular properties, we also observed noticeable differences in cell packing and organization, which is important for the penetration depth of extravasated compounds into the tumor interstitium [47, 52, 53]. H&E staining showed less dense cellular packing with gaps in the B16 tumor tissue, whereas BFS-1 showed a higher density and no gaps. Therefore, the finding that BFS-1 cells could form spheroids while B16 cells did

not, might be indicative for cell packing and organization in an actual tumor. *In vivo*, cell packing density and organization is, among other reasons, depends on the presence of a well-defined extracellular matrix. Analysis on the extracellular matrix by MSB staining and quantitative collagen IV immunostaining showed that B16 tumors have an almost completely absent extracellular matrix, whereas BFS-1 tumors had a more mature extracellular matrix. These findings suggest that the immature interstitium of the B16 tumor could have played a role in facilitating a higher EPR, confirming previously published results [54]. Histological analysis and quantitative TUNEL staining also indicated a much higher amount of apoptosis in the B16 tumors than in the BFS-1 tumors, which is typically associated with a more pronounced EPR effect [55, 56]. The HT₄₁ induced increase of apoptosis was significant for the sectioned BFS-1 tumors. While our study is in line with earlier findings showing that HT increases vascular permeability and promotes extravasation of nanoparticles [29-31], our histology data also suggest that substantial HT₄₁ induced apoptosis can further aid EPR.

In summary, we have shown that HT can aid in drug delivery by making cells more susceptible for Dox uptake, increasing the EPR-mediated uptake of liposomal drugs and by providing a trigger for drug release from TSL_{Dox}. All above factors play a pivotal role in the here employed 2-step delivery scheme. However, the actual amount of Dox delivered in a 2-step approach is determined by liposomal uptake and stability of the formulation and can therefore never exceed the liposomal uptake (in %ID/g). This study has shown that preheated B16 and BFS-1 tumors accumulated a maximum of 9.8 %ID/cc and 5.0 %ID/cc of the injected TSL dose, while the intraliposomal Dox concentration only reached 3 and 1.5 %ID/cc at 4 hours p.i. respectively. These Dox concentrations appeared insufficient to induce a noticeable therapeutic response. The 1-step intravascular drug release seems to be advantageous, since the injected TSL_{Dox} provide a high plasma concentration of Dox exposing the tumor to a high *area under the curve* over the time span of HT. Furthermore, the HT induced increase in Dox uptake by tumor cells may lead in both delivery schemes to a higher intracellular concentration.

REFERENCES

1. Jain RK. Normalization of Tumor Vasculature: An Emerging Concept in Antiangiogenic Therapy. *Science*. 2005; 307: 58-62.
2. Nagy JA, Chang SH, Dvorak AM, Dvorak HF. Why are tumour blood vessels abnormal and why is it important to know? *Br J Cancer*. 2009; 100: 865-9.
3. Hobbs SK, Monsky WL, Yuan F, Roberts WG, Griffith L, Torchilin VP, et al. Regulation of transport pathways in tumor vessels: role of tumor type and microenvironment. *Proc Natl Acad Sci U S A*. 1998; 95: 4607-12.
4. Hashizume H, Baluk P, Morikawa S, McLean JW, Thurston G, Roberge S, et al. Openings between defective endothelial cells explain tumor vessel leakiness. *Am J Pathol*. 2000; 156: 1363-80.
5. Kobayashi H, Watanabe R, Choyke PL. Improving conventional enhanced permeability and retention (EPR) effects; what is the appropriate target? *Theranostics*. 2013; 4: 81-9.
6. Allen TM, Cullis PR. Drug delivery systems: entering the mainstream. *Science*. 2004; 303: 1818-22.
7. Allen TM, Cullis PR. Liposomal drug delivery systems: from concept to clinical applications. *Adv Drug Deliv Rev*. 2013; 65: 36-48.
8. Matsumura Y, Maeda H. A new concept for macromolecular therapeutics in cancer chemotherapy: mechanism of tumorotropic accumulation of proteins and the antitumor agent smancs. *Cancer Res*. 1986; 46: 6387-92.
9. Gabizon A, Catane R, Uziely B, Kaufman B, Safra T, Cohen R, et al. Prolonged circulation time and enhanced accumulation in malignant exudates of doxorubicin encapsulated in polyethylene-glycol coated liposomes. *Cancer Res*. 1994; 54: 987-92.
10. Gabizon A, Shmeeda H, Barenholz Y. Pharmacokinetics of pegylated liposomal doxorubicin - Review of animal and human studies. *Clin Pharmacokinet*. 2003; 42: 419-36.
11. Laginha KM, Verwoert S, Charrois GJR, Allen TM. Determination of doxorubicin levels in whole tumor and tumor nuclei in murine breast cancer tumors. *Clinical Cancer Research*. 2005; 11: 6944-9.
12. Yatvin MB, Weinstein JN, Dennis WH, Blumenthal R. Design of liposomes for enhanced local release of drugs by hyperthermia. *Science*. 1978; 202: 1290-3.
13. Needham D, Anyarambhatla G, Kong G, Dewhirst MW. A new temperature-sensitive liposome for use with mild hyperthermia: characterization and testing in a human tumor xenograft model. *Cancer Res*. 2000; 60: 1197-201.
14. Li L, ten Hagen TL, Hossann M, Suss R, van Rhooen GC, Eggermont AM, et al. Mild hyperthermia triggered doxorubicin release from optimized stealth thermosensitive liposomes improves intratumoral drug delivery and efficacy. *J Control Release*. 2013; 168: 142-50.
15. de Smet M, Langereis S, van den Bosch S, Grull H. Temperature-sensitive liposomes for doxorubicin delivery under MRI guidance. *J Control Release*. 2010; 143: 120-7.
16. Lindner LH, Eichhorn ME, Eibl H, Teichert N, Schmitt-Sody M, Issels RD, et al. Novel temperature-sensitive liposomes with prolonged circulation time. *Clin Cancer Res*. 2004; 10: 2168-78.
17. de Smet M, Heijman E, Langereis S, Hijnen NM, Grull H. Magnetic resonance imaging of high intensity focused ultrasound mediated drug delivery from temperature-sensitive liposomes: an in vivo proof-of-concept study. *J Control Release*. 2011; 150: 102-10.

18. Celsion. Phase 3 Study of ThermoDox With Radiofrequency Ablation (RFA) in Treatment of Hepatocellular Carcinoma (HCC). ClinicalTrialsgov NCT00617981; 2008.
19. Celsion. Study of ThermoDox With Standardized Radiofrequency Ablation (RFA) for treatment of Hepatocellular Carcinoma (HCC) (OPTIMA). ClinicalTrialsgov NCT02112656; 2014.
20. Overgaart J. Effect of hyperthermia on malignant cells in vivo: A review and a hypothesis. *Cancer*. 1977; 39: 2637-46.
21. Song CW. Effect of Local Hyperthermia on Blood-Flow and Microenvironment - a Review. *Cancer Research*. 1984; 44: 4721-30.
22. Calabro A, Singletary SE, Tucker S, Boddie A, Spitzer G, Cavaliere R. In vitro thermo-chemo-sensitivity screening of spontaneous human tumors: significant potentiation for cisplatin but not adriamycin. *Int J Cancer*. 1989; 43: 385-90.
23. Sakaguchi Y, Stephens LC, Makino M, Kaneko T, Strebel FR, Danhauser LL, et al. Apoptosis in tumors and normal tissues induced by whole body hyperthermia in rats. *Cancer Res*. 1995; 55: 5459-64.
24. Yarmolenko PS, Moon EJ, Landon C, Manzoora A, Hochman DW, Viglianti BL, et al. Thresholds for thermal damage to normal tissues: an update. *Int J Hyperthermia*. 2011; 27: 320-43.
25. Hildebrandt B, Wust P, Ahlers O, Dieing A, Sreenivasa G, Kerner T, et al. The cellular and molecular basis of hyperthermia. *Crit Rev Oncol Hematol*. 2002; 43: 33-56.
26. Issels RD, Lindner LH, Verweij J, Wust P, Reichardt P, Schem BC, et al. Neo-adjuvant chemotherapy alone or with regional hyperthermia for localised high-risk soft-tissue sarcoma: a randomised phase 3 multicentre study. *Lancet Oncol*. 2010; 11: 561-70.
27. Bates DA, Mackillop WJ. Hyperthermia, adriamycin transport, and cytotoxicity in drug-sensitive and -resistant Chinese hamster ovary cells. *Cancer Res*. 1986; 46: 5477-81.
28. Kawai H, Minamiya Y, Kitamura M, Matsuzaki I, Hashimoto M, Suzuki H, et al. Direct measurement of doxorubicin concentration in the intact, living single cancer cell during hyperthermia. *Cancer*. 1997; 79: 214-9.
29. Huang SK, Stauffer PR, Hong K, Guo JW, Phillips TL, Huang A, et al. Liposomes and hyperthermia in mice: increased tumor uptake and therapeutic efficacy of doxorubicin in sterically stabilized liposomes. *Cancer Res*. 1994; 54: 2186-91.
30. Kong G, Braun RD, Dewhirst MW. Characterization of the effect of hyperthermia on nanoparticle extravasation from tumor vasculature. *Cancer Res*. 2001; 61: 3027-32.
31. Li L, ten Hagen TLM, Bolkestein M, Gasselhuber A, Yatvin J, van Rhoon GC, et al. Improved intratumoral nanoparticle extravasation and penetration by mild hyperthermia. *Journal of Controlled Release*. 2013; 167: 130-7.
32. de Smet M, Langereis S, van den Bosch S, Bitter K, Hijnen NM, Heijman E, et al. SPECT/CT imaging of temperature-sensitive liposomes for MR-image guided drug delivery with high intensity focused ultrasound. *J Control Release*. 2013; 169: 82-90.
33. Matteucci ML, Anyambhatla G, Rosner G, Azuma C, Fisher PE, Dewhirst MW, et al. Hyperthermia increases accumulation of technetium-99m-labeled liposomes in feline sarcomas. *Clin Cancer Res*. 2000; 6: 3748-55.
34. Alvarez Secord A, Jones EL, Hahn CA, Petros WP, Yu D, Havrilesky LJ, et al. Phase I/II trial of intravenous Doxil and whole abdomen hyperthermia in patients with refractory ovarian cancer. *Int J Hyperthermia*. 2005; 21: 333-47.
35. Vujaskovic Z, Kim DW, Jones E, Lan L, McCall L, Dewhirst MW, et al. A phase I/II study of neoadjuvant liposomal doxorubicin, paclitaxel, and hyperthermia in locally advanced breast cancer. *Int J Hyperthermia*. 2010; 26: 514-21.

36. Li L, ten Hagen TL, Haeri A, Soullie T, Scholten C, Seynhaeve AL, et al. A novel two-step mild hyperthermia for advanced liposomal chemotherapy. *J Control Release*. 2014; 174: 202-8.
37. Bartlett GR. Phosphorus Assay in Column Chromatography. *Journal of Biological Chemistry*. 1959; 234: 466-8.
38. Nagelkerke A, Bussink J, Sweep FC, Span PN. Generation of multicellular tumor spheroids of breast cancer cells: how to go three-dimensional. *Anal Biochem*. 2013; 437: 17-9.
39. Lokerse WJM, Kneepkens ECM, ten Hagen TLM, Eggermont AMM, Grull H, Koning GA. In depth study on thermosensitive liposomes: Optimizing formulations for tumor specific therapy and in vitro to in vivo relations. *Biomaterials*. 2016; <http://dx.doi.org/10.1016/j.biomaterials.2015.12.023>.
40. Eddy HA. Alterations in tumor microvasculature during hyperthermia. *Radiology*. 1980; 137: 515-21.
41. Hahn GM, Strande DP. Cytotoxic effects of hyperthermia and adriamycin on Chinese hamster cells. *J Natl Cancer Inst*. 1976; 57: 1063-7.
42. Herman TS. Temperature dependence of adriamycin, cis-diamminedichloroplatinum, bleomycin, and 1,3-bis(2-chloroethyl)-1-nitrosourea cytotoxicity in vitro. *Cancer Res*. 1983; 43: 517-20.
43. Nagaoka S, Kawasaki S, Sasaki K, Nakanishi T. Intracellular uptake, retention and cytotoxic effect of adriamycin combined with hyperthermia in vitro. *Jpn J Cancer Res*. 1986; 77: 205-11.
44. Rice GC, Hahn GM. Modulation of adriamycin transport by hyperthermia as measured by fluorescence-activated cell sorting. *Cancer Chemother Pharmacol*. 1987; 20: 183-7.
45. Moriyama-Gonda N, Igawa M, Shiina H, Wada Y. Heat-induced membrane damage combined with adriamycin on prostate carcinoma PC-3 cells: correlation of cytotoxicity, permeability and P-glycoprotein or metallothionein expression. *Br J Urol*. 1998; 82: 552-9.
46. Hirschhaeuser F, Menne H, Dittfeld C, West J, Mueller-Klieser W, Kunz-Schughart LA. Multicellular tumor spheroids: an underestimated tool is catching up again. *J Biotechnol*. 2010; 148: 3-15.
47. Mikhail AS, Eetezadi S, Ekdawi SN, Stewart J, Allen C. Image-based analysis of the size- and time-dependent penetration of polymeric micelles in multicellular tumor spheroids and tumor xenografts. *Int J Pharm*. 2014; 464: 168-77.
48. Kim TH, Mount CW, Gombotz WR, Pun SH. The delivery of doxorubicin to 3-D multicellular spheroids and tumors in a murine xenograft model using tumor-penetrating triblock polymeric micelles. *Biomaterials*. 2010; 31: 7386-97.
49. Hijnen N, Langereis S, Grull H. Magnetic resonance guided high-intensity focused ultrasound for image-guided temperature-induced drug delivery. *Advanced Drug Delivery Reviews*. 2014; 72: 65-81.
50. Dvorak HF, Nagy JA, Dvorak JT, Dvorak AM. Identification and characterization of the blood vessels of solid tumors that are leaky to circulating macromolecules. *Am J Pathol*. 1988; 133: 95-109.
51. Lammers T, Kiessling F, Hennink WE, Storm G. Drug targeting to tumors: principles, pitfalls and (pre-) clinical progress. *J Control Release*. 2012; 161: 175-87.
52. McGuire S, Yuan F. Improving interstitial transport of macromolecules through reduction in cell volume fraction in tumor tissues. *Nanomedicine*. 2012; 8: 1088-95.
53. Minchinton AI, Tannock IF. Drug penetration in solid tumours. *Nat Rev Cancer*. 2006; 6: 583-92.

54. Netti PA, Berk DA, Swartz MA, Grodzinsky AJ, Jain RK. Role of extracellular matrix assembly in interstitial transport in solid tumors. *Cancer Res.* 2000; 60: 2497-503.
55. Jang SH, Wientjes MG, Au JL. Enhancement of paclitaxel delivery to solid tumors by apoptosis-inducing pretreatment: effect of treatment schedule. *J Pharmacol Exp Ther.* 2001; 296: 1035-42.
56. Heneweer C, Holland JP, Divilov V, Carlin S, Lewis JS. Magnitude of Enhanced Permeability and Retention Effect in Tumors with Different Phenotypes: Zr-89-Albumin as a Model System. *J Nucl Med.* 2011; 52: 625-33.

CHAPTER 4

Comparing the therapeutic potential of thermosensitive liposomes and hyperthermia in two distinct subtypes of breast cancer

Wouter J.M. Lokerse

Michiel Bolkestein

Simone U. Dalm

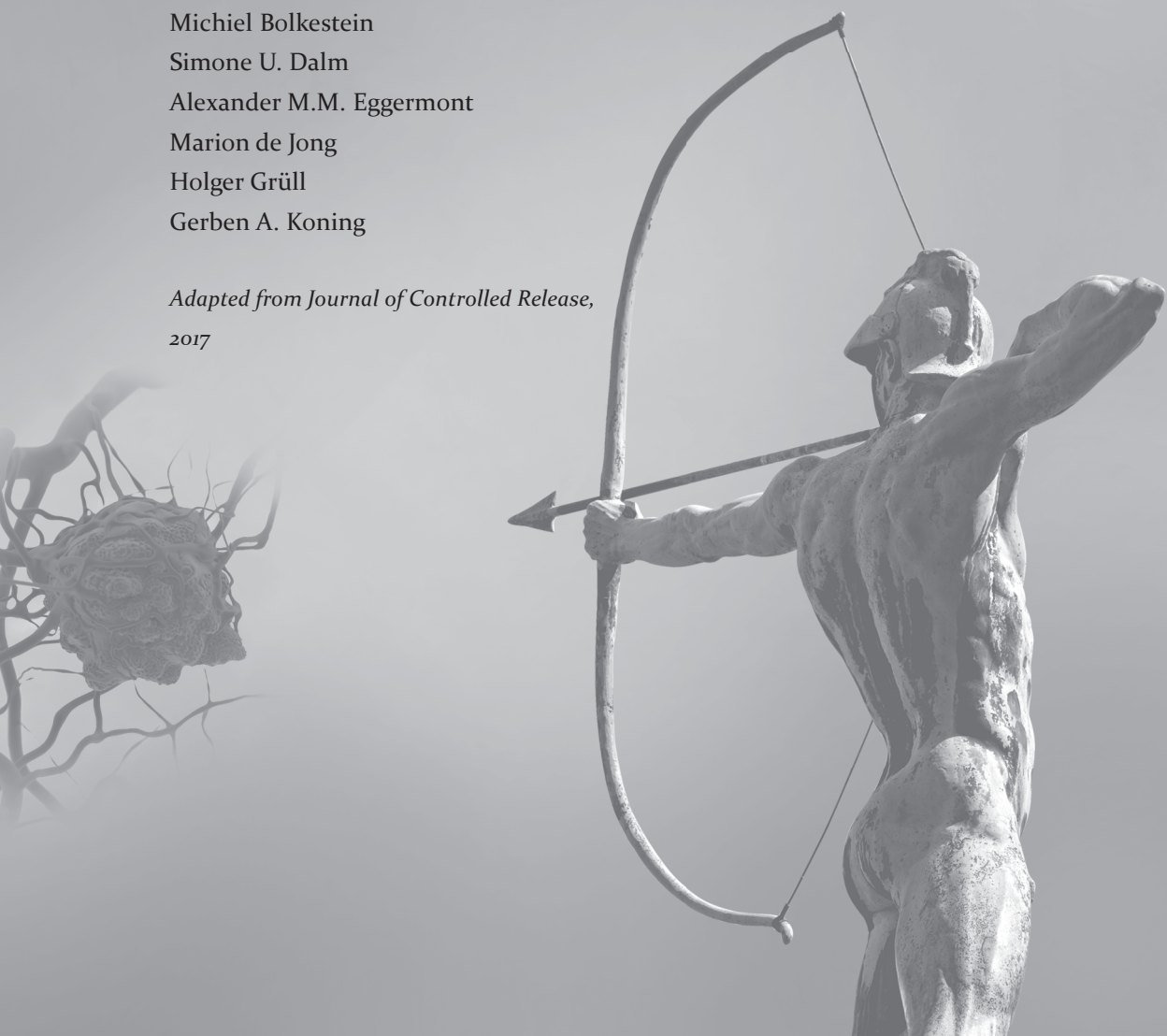
Alexander M.M. Eggermont

Marion de Jong

Holger Gröll

Gerben A. Koning

Adapted from Journal of Controlled Release,
2017



ABSTRACT

Local drug delivery of Doxorubicin (Dox) with thermosensitive liposomes (TSL) and hyperthermia (HT) has shown preclinically to achieve high local drug concentrations with good therapeutic efficacy. Currently, this is clinically studied for treatment of chest wall recurrence of breast cancer, however with various outcomes. This study examines the potency of neoadjuvant TSL HT combination therapy in two orthotopic mouse models of human breast cancer, MDA-MB-231 and T-47D, which morphologically correlate to mesenchymal and epithelial phenotypes, respectively. Both cell lines showed improved *in vitro* chemosensitivity and Dox uptake at HT. Dox-loaded TSL (TSL_{Dox}) was stable 0 mm in FBS, BALB/c-nu plasma and human plasma, although release of the drug at HT was incomplete for the latter two. Combination treatment with TSL_{Dox} and HT *in vivo* was significantly more effective against MDA-MB-231 tumors, whereas T-47D tumors showed no significant therapeutic response. *Ex vivo* investigation revealed a higher mean vessel density and poorly differentiated extracellular matrix (ECM) in MDA-MB-231 tumors relative to T-47D tumors. Although *in vitro* results of the TSL_{Dox} and HT treatment were favorable for both cell types, the therapeutic efficacy *in vivo* was remarkably different. The well-differentiated and slowly-growing T-47D tumors may provide a microenvironment that limits drug delivery to the target cell and therefore renders the therapy ineffective. Mesenchymal and invasive MDA-MB-231 tumors display higher vascularization and less mature ECM, significantly enhancing tumor response to TSL_{Dox} and HT treatment. These results yield insight into the efficacy of TSL treatment within different tumor microenvironments, and further advance our understanding of factors that contribute to heterogeneous therapeutic outcomes in clinical trials.

INTRODUCTION

According to estimates made by the American Cancer Society, approximately 250,000 new patients are diagnosed each year in the US with invasive breast cancer and despite all medical progress, this disease will be responsible for about 40,000 deaths in the US in 2016 [1]. Chemotherapy is the standard of care for invasive breast cancer and can be applied as (neo)adjuvant therapy in addition to surgery or mastectomy for stage I-III tumors or for metastasized breast cancer (stage IV). Doxorubicin (Dox) is a drug that is used in many chemotherapy regimens as a single agent, in combination with other chemotherapeutic drugs, or as adjuvant for antibody-based therapies that target the estrogen receptor (ER), progesterone receptor (PR) or human epidermal growth factor receptor 2 (HER2). When a breast tumor lacks the expression of any of these three receptors, it is diagnosed as a triple negative breast cancer (TNBC). Depending on the stage of its diagnosis, TNBC can be particularly aggressive and is more likely to recur after local treatments compared to other subtypes of breast cancer. Lacking any response to receptor-targeted therapies, chemotherapy remains the only efficacious form of treatment [2]. However, severe side effects have been observed after treatment with Dox, including cardiac toxicity, nausea and hair loss, among others [3]. These side effects can be largely reduced by incorporation of the drug in long-circulating nanoparticles such as liposomes. Due to their size of approximately 100 nm, the liposomes do not extravasate into healthy tissue, but passively accumulate in neoplastic tissue where the drug slowly diffuses out of its carrier. In fact, the use of liposomal Dox (Doxil®) has resulted in a similar therapeutic efficacy as free Dox, yet has greatly reduced the above-mentioned side effects [4, 5], therefore becoming a preferred first-line single agent for stage IV TNBC [2]. However, further research has indicated that the parental drug Dox is actually retained too effectively inside the liposomes, which reduces its bioavailability and therefore strategies to exploit the full therapeutic potential of these drug delivery systems are warranted [6]. One solution is the development of thermosensitive liposomes (TSLs), which stably encapsulate the drug at body temperature and therefore reduce the side effects associated with free Dox, but enable fast Dox release when exposed to mild hyperthermia (40-42°C; HT) [7]. This approach requires heating of the tumor area and has been shown in numerous preclinical studies to lead to higher accumulation of Dox compared to standard treatments, as well as improved tumor control [8-11]. The above-mentioned temperature-induced drug delivery may be particularly applicable for (neo) adjuvant treatment of local breast cancer or in case of local recurrence of breast cancer at the chest wall. Application to breast cancer has been performed in several subcutaneous murine models showing enhanced intratumoral Dox levels and therapeutic response [12, 13]. Recently, a first clinical study was performed with a lysolipid-containing TSL (LTSL) formulation of Dox (ThermoDox®) in combination with HT for treatment of

breast cancer recurrence at the chest wall showing a local response rate of 50% [14-16]. Though these results are promising, treatment response remains very heterogeneous and requires more investigation to further improve response rates.

Here, we present a study on the therapeutic efficacy of Dox-loaded, lysolipid-lacking TSLs for breast cancer. Removal of lysolipid from a thermosensitive formulation establishes a drug release by membrane defects in the liposome [17] instead of through pores established by the lysolipid (LTSL) [18]. Although our lysolipid-lacking TSL (hereafter abbreviated as “TSL”) has shown to slightly improve therapeutic outcome over LTSL [19], we focused in this study on tumor type comparison and relation to significant therapeutic response. For this comparison, ductal breast cancer orthotopic xenografts based on cell lines T-47D and MDA-MB-231 were selected. MDA-MB-231 is a TNBC, for which chemotherapy would be the standard of care, whereas T-47D expresses estrogen and progesterone growth receptors, rendering it susceptible to hormone therapy despite resistance remaining a problem in e.g. tamoxifen-based therapies [2, 20]. T-47D cells belong to the luminal A class of breast cancer, which are well differentiated, epithelioid and relatively poorly invasive, therefore conferring a good prognosis [21]. MDA-MB-231 belongs to the basal/claudin-low class, is poorly differentiated and mesenchymal in nature, making it highly invasive, and resulting in a poor prognosis [22, 23]. Investigating these extremes in breast cancer differentiation may provide new insights into the efficacy of preoperative TSL and HT based therapy among breast cancer subtypes.

MATERIALS & METHODS

TSL preparation

1,2-dipalmitoyl-*sn*-glycero-3-phosphocholine (DPPC; Lipoid; Ludwigshafen, Germany) 1,2-distearoyl-*sn*-glycero-3-phosphocholine (DSPC; Lipoid), and 1,2-distearoyl-*sn*-glycero-3-phosphoethanolamine-N-(amino(polyethylene glycol)-2000) (DSPE-PEG₂₀₀₀; Lipoid) were dissolved in 9:1 (v:v) chloroform:methanol at a molar ratio of 70:25:5. The solvent was gradually evaporated by a rotary evaporator (Büchi; Flawil, Switzerland) and the resulting lipid was dried by nitrogen flushing. The lipid film was hydrated in (NH₄)₂SO₄ (250 mM, pH 5.3) to form liposomes which were extruded through 5x 200 nm, 5x 100 nm, 5x 80 nm and 5x 50 nm polycarbonate filters with a thermobarrel extruder (Northern Lipids; Burnaby, Canada). The liposomes were run over a PD-10 column (GE Healthcare Life Sciences; Eindhoven, Netherlands) and eluted with HEPES (10 mM) buffered NaCl (135 mM, pH 7.4). The phosphorus concentration of the sample was determined by ammonium molybdate spectrophotometry (Bartlett assay [24]) and liposomes were loaded with Dox (Actavis; Dublin, Ireland) by a (NH₄)₂SO₄ gradient as described before [25] at a 0.15:1 (mol:mol) Dox:lipid ratio, which was incubated for 1 h

at 39°C at 300 rpm in a thermoshaker. This $(\text{NH}_4)_2\text{SO}_4$ loading gave more stable TSLs at body temperature than the commonly used citrate loading [25], which has been used for LTSL [26]. Liposomes were concentrated by ultracentrifugation and the final product was tested for size, polydispersity and zeta-potential in HEPES buffer (10mM) at a lipid concentration of 0.3 mM using a Zetasizer (Malvern Instruments; Worcestershire, UK).

***In vitro* Doxorubicin cytotoxicity assay**

T-47D and MDA-MB-231 breast cancer cell lines were kindly provided by Dr. John Martens (Medical Oncology, Erasmus MC, Rotterdam, Netherlands). For chemosensitivity assays, cells were seeded in a 96-well plate and grown until 50% confluency, followed by addition of Dox and incubation at normothermic (37°C; NT) or hyperthermic (42°C; HT) temperature for 1 h. After incubation, the Dox-containing medium was removed and cells were washed with phosphate-buffered saline (PBS; Sigma-Aldrich; St Louis, Missouri). For investigation of the long-term effects of Dox incubation, fresh culture medium (RPMI medium + 10% FBS + 1% Penicillin/ Streptomycin; Sigma-Aldrich) was added periodically. After a period of incubation (24-72 h), the cells were fixed in 10% (w:v) trichloroacetic acid (Sigma-Aldrich) for 4 h at 4°C. Following fixation, the plates were washed with running tap water and cells were stained with 0.5% (w:v) sulforhodamine B (Sigma-Aldrich) for 20 min at room temperature. The plates were washed with 1% (v:v) acetic acid (Sigma-Aldrich) and left to dry, after which the stain was resuspended and homogenized by adding 10 mM Tris (Sigma-Aldrich). Absorbance was measured at 590 nm using a Wallac Victor 2 plate reader (Perkin Elmer; Waltham, Massachusetts). In case of a NT experiment, the Dox incubation on the cells took place in an incubator set to 37°C, whereas a HT experiment was carried out by vacuum sealing the culture plate and submerging it into a water bath set to 42°C. Cellular cytotoxicity and the following Dox uptake curves were only generated with free drug as previous studies showed that drug fully released from TSLs in culture media within seconds [27] and this study focused on an intravascular release approach in a heated tumor and thus bioavailable free drug to the tumor cell.

***In vitro* Doxorubicin uptake studies**

Cells were grown until 80% confluency in a T75 culture flask and exposed to 40 μM Dox for 1 h, after which the cells were washed with ice-cold PBS. 40 mM was chosen as concentration Dox for an adequate fluorescent signal at the time of measurement. The cells were scraped from the flask in ice-cold PBS and centrifuged at 200 g at 4°C for 10 min. 150 μL lysis buffer (20 mM Tris, 150 mM NaCl, 0.2% NP40, 10% glycerol, pH 7.4; Sigma-Aldrich) was used to resuspend the pellet and the resulting suspension was incubated on ice for 30 min. The lysates were centrifuged at 14,000 g for 15 min and pellets homogenized in 500 μL PBS by vortexing and 1 min probe sonication. Dox

concentration was measured at 485 nm excitation and 580 nm emission by a Wallac Victor 2 plate reader. One additional T75 culture flask was seeded with cells in parallel to the flasks used for Dox uptake experiments in order to determine cell number at the time of the experiment.

TSL stability and release assays by fluorometry

2950 μL freshly isolated BALB/c-nu plasma, human plasma or FBS was put into a quartz cuvette and placed into a F-4500 fluorometer (Hitachi; Tokyo, Japan) and heated to 37°C or 42°C by an externally connected water bath. After 1 min measurement, 50 μL of a 5 mM (phosphate) TSL solution was introduced into the heated plasma via a piece of surgical tubing and measurement continued for 1 h. The percentage of released Dox was calculated by: $\% \text{ Dox}_{\text{release}} = ((\text{Dox}_n - \text{Dox}_{\text{base}}) / (\text{Dox}_{\text{total}} - \text{Dox}_{\text{base}})) \times 100\%$ where Dox_n = signal at time point n, Dox_{base} = base signal of sample with no release and $\text{Dox}_{\text{total}}$ = maximum Dox release after adding 50 μL 10% Triton X-100 (Sigma-Aldrich).

***In vivo* orthotopic breast cancer model**

The establishment of T-47D and MDA-MB-231 orthotopic tumor models and subsequent treatments of tumor-bearing animals has been judged and approved by the Erasmus MC animal research committee, Rotterdam, the Netherlands. 10 week old BALB/c nude mice were ordered from Janvier Labs (Nijmegen, Netherlands) and were given an *ad libitum* supply of β -estradiol (Sigma Aldrich) enriched drinking water, which was prepared by adding 1 mL of a 4 mg/mL β -estradiol solution in ethanol to 1 L of drinking water. $8 \cdot 10^6$ cells were mixed 1:1 (v:v) with Matrigel (BD Biosciences; East Rutherford, New Jersey) and injected into the mammary fat pad. Drinking water was refreshed twice a week.

Treatment of orthotopic breast cancer with TSL and HT

When tumors reached 200 mm³, mice were treated by a single 5 mg/kg free Dox or TSL_{Dox} dose which was i.v. administered via the tail vein. The equal dosing of free and liposomal drug at 5 mg/kg was chosen in order to show the benefit of TSL_{Dox} therapy over free Dox without risking severe side effects and adequately compare the results to the outcome of our previously published results [25, 27]. For NT experiments, mice were put under anaesthesia on a heating pad, and covered with aluminium foil for 1 h after injection. For HT experiments, mice were put under anaesthesia and tumors were submerged into a water bath to reach an intratumoral temperature of 42°C which was maintained for 1 h after injection. The intratumoral temperature was expected to be similar to previous findings where tumors inoculated on the hind limb were heated by a water bath set at 42.5°C [25]. Injections took place after 10min of tumor heating. Skin exposed to HT was protected by covering a 1 cm radius surrounding the tumor with vaseline as a precaution to prevent possible skin damage. After treatment, every other day, mice were weighed

and tumors measured by a calliper and volumes calculated (volume = length x width x height x 0.4). Statistical comparison between treatment groups was done using tumor volume doubling time and Kaplan-Meier plots were generated accordingly. Tumor size analysis was normalized to the starting size of 200 mm³ and MDA-MB-231 inoculated animals were sacrificed when tumors reached 18 mm in one dimension or 15 mm in all dimensions while T-47D inoculated animals were sacrificed when tumor volume doubled (100% size increase). For statistical analysis, the tumor doubling time was used as a measure for therapeutic efficacy.

Ex vivo staining and analysis of excised tumors

Tumors were excised from sacrificed mice, snap frozen in liquid nitrogen and sliced into 5 µm sections. The sections were stained by Martius Scarlet Blue (MSB), for TUNEL, CD31, collagen IV and fibrillin I. For MSB staining, slides were fixed in Bouin's fixative (4% formalin: saturated picric acid : glacial acetic acid; 25:70:5; Sigma-Aldrich) for 1 h at 60°C, followed by staining with Weigert's hematoxylin (Boom; Meppel, Netherlands), Martius yellow, crystal scarlet and methyl blue (Sigma-Aldrich). Stained slides were mounted with Entellan (EMD Millipore; Billerica, Massachusetts) and smaller regions were imaged using a DM 4000B microscope (Leica; Wetzlar, Germany) and analysed by Leica QWin Y2.8 software (Leica Microsystems Imaging Solutions Ltd; Cambridge, UK). A cell death detection kit (Roche; Basel, Switzerland) was used for TUNEL staining on paraformaldehyde fixed slides. Immunologic stains for CD31 and fibrillin I were done on acetone fixed slides with primary rat anti-mouse CD31 (BD Pharmingen; San Diego, California) and rabbit anti-mouse fibrillin I (Abcam; Cambridge, UK), followed by secondary goat anti-rat AlexaFluor594 and goat anti-rabbit AlexaFluor488 (Thermo Fisher; Waltham, Massachusetts), respectively. Collagen IV staining was performed with a primary rabbit anti-mouse collagen IV antibody (EMD Millipore; Billerica, MA) and a secondary goat anti-rabbit AlexaFluor488 antibody. Slides were mounted with DAPI (Molecular Probes; Eugene, Oregon) enriched Fluoromount-G (Southern Biotech; Birmingham, Alabama). Confocal and widefield fluorescence microscopy was performed on a LSM 510 Meta (Zeiss; Oberkochen, Germany) and Axiovert 100M microscope (Zeiss) with Hamamatsu Photonics C4742-98 camera controller, respectively. Tile scans generated from the confocal microscope yielded whole-tumor images that were subsequently processed in ImageJ (version 1.48). Whole-tumor ROIs were drawn, excluding artifacts such as tissue folds, and CD31, collagen IV and fibrillin I signal were quantified as % positive pixels. A fixed, manually set threshold was implemented for each individual stain and maintained for all replicates. The mean and standard deviation were determined for each tumor type (N = 5), whereby one section was analyzed per tumor.

Statistical analysis

All statistical tests were performed in Graphpad Prism 6.07. For the comparative *in vitro* cytotoxicity (Figure 1A-D), cellular Dox uptake (Figure 1E and F), *in vitro* Dox release (Figure 3 and Additional file 1: Table S1) and *in vivo* tumor growth analysis (Additional file 1: Figure S1) an unpaired two-tailed t-test was applied to determine statistical significance between groups. One-way ANOVA Bonferroni tests were done to determine statistical significance between different TSL treatment groups of the *in vitro* cytotoxicity experiment (Figure 2) and of the *in vivo* therapeutic study (Figure 4A and B), with the only exception of the T-47D model which was only composed of PBS NT and a TSL_{Dox} HT groups (Figure 4C and D) and therefore analyzed by an unpaired two-tailed t-test. Statistical analysis of histological sections (Figure 5) was done by Mann-Whitney test.

RESULTS

In vitro cytotoxicity and Dox uptake in breast cancer cell lines under NT and HT conditions

MDA-MB-231 and T-47D cells were tested for Dox sensitivity and the drug showed a comparable growth inhibitory effect in both cell lines. These cell lines exhibited IC₅₀ values of $9.6 \cdot 10^{-3} \pm 0.2 \cdot 10^{-3}$ and $2.5 \cdot 10^{-2} \pm 1.3 \cdot 10^{-2}$ mM Dox (Figure 1A-D), respectively, 72 h after a 1 h Dox incubation at NT (37°C). The Dox sensitivity of the cell lines was enhanced by HT, where MDA-MB-231 cells showed an IC₅₀ of $1.5 \cdot 10^{-3} \pm 0.6 \cdot 10^{-3}$ mM Dox (significant versus NT) and T-47D showed an IC₅₀ of $6.8 \cdot 10^{-3} \pm 2.1 \cdot 10^{-3}$ mM (not significant versus NT because of large variation in NT group) at HT conditions. Next, the Dox uptake by these cells at NT and HT was tested (Figure 1E, F). When the cells were exposed to 40 µM Dox for 1 h, MDA-MB-231 and T-47D cells showed 0.06 ± 0.03 and 0.14 ± 0.03 pg Dox/cell uptake, respectively. At HT conditions, the Dox uptake significantly increased for both cell lines with 0.25 ± 0.03 pg Dox/cell for MDA-MB-231 and 0.44 ± 0.05 pg Dox/cell for T-47D.

Before TSLs were tested on cells, they were analyzed for size, polydispersity, zeta-potential and Dox loading efficiency. The liposomes had a hydrodynamic diameter of 77 ± 3 nm, a polydispersity index of 0.036 ± 0.006 and a zeta-potential of -12 ± 1 mV. Dox loading was established with 100% efficacy (0.15:1 Dox:lipid ratio was maintained after Dox loading). The transition temperature (T_m) of this Dox-loaded formulation was 44.4 ± 0.3 °C (obtained by differential scanning calorimetry), as described previously [25]. The presence of Dox in the formulation seemed to lower the T_m with ± 1 °C when compared to similar TSL formulations that did not contain Dox [17]. When cells were exposed to 10 µM free Dox or TSL_{Dox} for 1 h, a limited cytotoxic effect was observed 24 h after the experiment (Figure 2A), which was only significant for MDA-MB-231 with $81 \pm 9\%$ surviving cells.

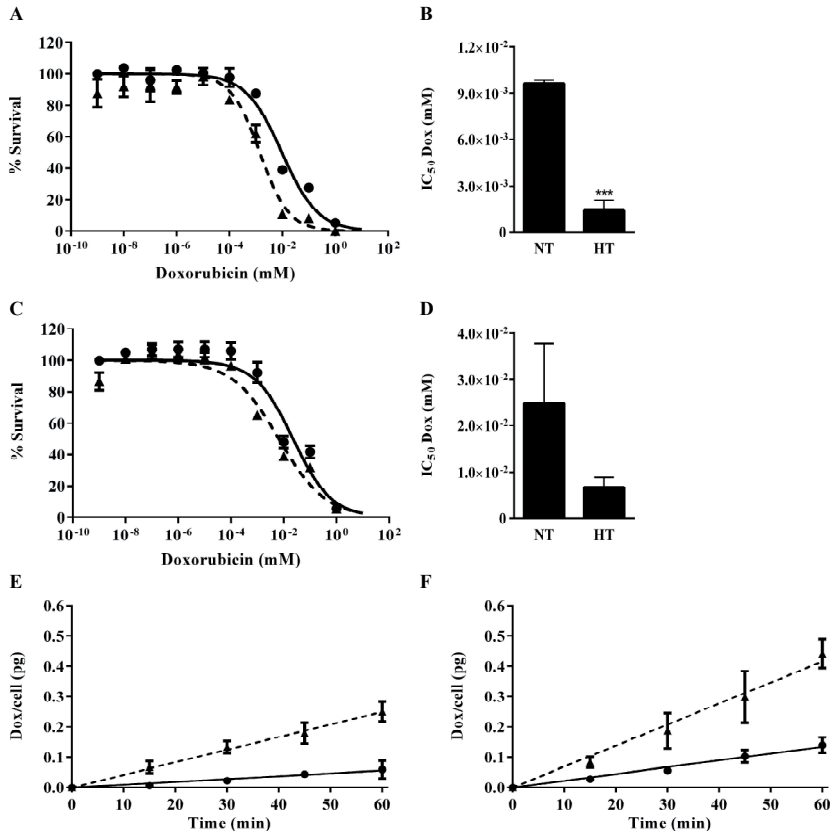


Figure 1. *In vitro* chemosensitivity and Dox uptake at NT (37°C; □) or HT (42°C; ▢). MDA-MB-231 (A, B) and T-47D (C, D) cell lines showed increased Dox sensitivity at HT, which was significant for the former. Dox uptake was significantly improved under HT conditions for both MDA-MB-231 (E) and T-47D (F). 40 μ M Dox was used for the drug uptake experiment (E, F). N = 3 for all experimental groups and unpaired two-tailed t-test was used for statistical analysis. *** = $p < 0.005$.

A simultaneous HT and Dox incubation caused a significant cytotoxic effect with free and TSL_{Dox} for both cell lines after 24 h. However, 72 h after incubation, the cytotoxic effects of the different treatments became more pronounced (Figure 2B). Dox exposure at NT resulted in $67 \pm 16\%$ and $38 \pm 7\%$ cell survival for MDA-MB-231 and T-47D, respectively. Similarly, 72 h after exposure, the HT TSL_{Dox} groups showed a relatively high cytotoxic effect with $11 \pm 7\%$ cell survival for MD-MB-231 and $23 \pm 3\%$ for T-47D. The T-47D cell line also showed significant cytotoxic effects in the NT TSL_{Dox} ($71 \pm 6\%$ cell survival), and HT (empty) TSL groups ($81 \pm 5\%$ cell survival).

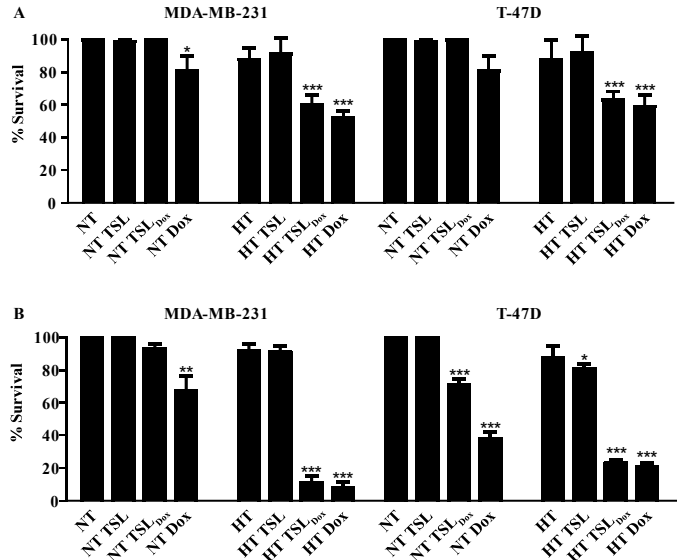


Figure 2. Chemosensitivity assay 24 h (A) or 72 h (B) after a 1 h incubation with empty 67 μ M TSL (as determined by PO_4 quantification), 10 μ M TSL_{Dox} or 10 μ M free Dox at NT (37°C) or HT (42°C). N = 3 for all experimental groups. Statistical differences were determined by one-way ANOVA Bonferroni test. * = $p < 0.05$, ** = $p < 0.01$, *** = $p < 0.005$.

Validation of Dox retention and release in BALB/c-nu mouse plasma

Fresh plasma was collected from BALB/c-nu mice to validate the stability and release of TSL_{Dox} prior to animal experimentation. TSL_{Dox} was stable at 37°C, showing $2 \pm 1\%$ Dox release in 1 h (Figure 3A). A rapid release, which reached a maximum of $69 \pm 7\%$, was established after TSL_{Dox} was exposed to HT for 1 h. This was considerably lower than Dox

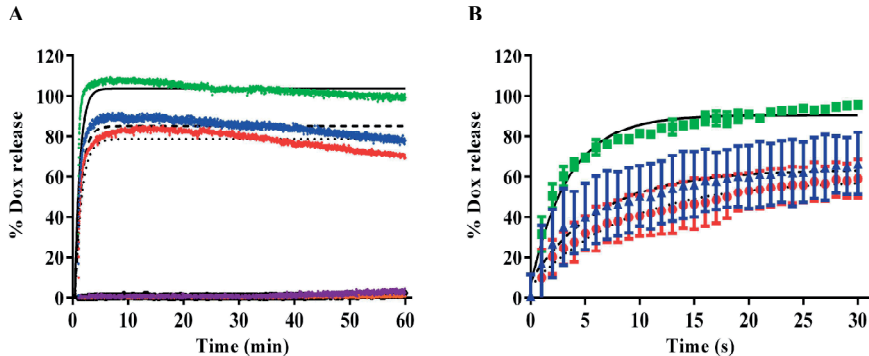


Figure 3. 1 h Dox release from TSL_{Dox} (A) at 37°C in FBS (purple), fresh BALB/c plasma (orange) or human plasma (brown); or at 42°C in the same media (green, red and blue, respectively) with a magnification of the first 30 s of release (B). N = 3 for all experimental groups. An exponential one-phase association curve was fitted through the 42°C release data sets obtained in FBS (solid line), BALB/c plasma (dotted line) and human plasma (dashed line). K-value and plateau value were used as parameters to determine statistical differences between release curves (Table 1).

release in FBS in terms of speed and completeness of release (Figure 3A, B). However, the Dox retention at NT and release at HT in BALB/c-nu plasma did closely resemble that of human plasma.

Table 1. Doxorubicin release characteristics from thermosensitive liposomes in serum or plasma from different species. Plateau_{1h} and K_{30s} parameters calculated from the exponential fits in Figures 3A and 3B, respectively. The parameters were statistically compared by one-way ANOVA Bonferroni test. Asterisks indicate statistically significant differences compared to FBS (* = $p < 0.05$, ** = $p < 0.01$).

	K_{30s} (% Dox release/ sec)	Plateau_{1h} (Max % Dox release)
FBS	0.29 ± 0.03	104 ± 1
BALB/c plasma	$0.11 \pm 0.05^{**}$	$79 \pm 8^{**}$
Human plasma	0.17 ± 0.05	$85 \pm 6^*$

Therapeutic study of TSL in orthotopic breast cancer

After inoculation, MDA-MB-231 and T-47D showed significantly different tumor growth rates. MDA-MB-231 tumors reached 200 mm^3 at $38 \pm 9 \text{ d}$ after inoculation, while T-47D inoculated mice showed a 200 mm^3 tumor after $113 \pm 20 \text{ d}$ (Figure 4). The MDA-MB-231 tumors showed a significant therapeutic response to TSL_{Dox} and HT, exhibiting $25 \pm 4 \text{ d}$ until tumor doubling was reached versus $15 \pm 1 \text{ d}$ for the PBS NT group (Figure 5A, B). All control treatments did not lead to any significant therapeutic response. T-47D tumors responded heterogeneously to TSL_{Dox} and HT therapy, which resulted in no significant difference in tumor growth delay compared to the NT group. In this tumor model, the PBS NT group had an average tumor doubling time of $34 \pm 16 \text{ d}$ after therapy, while for the TSL_{Dox} HT group this was $51 \pm 25 \text{ d}$ (Figure 5C, D). Because of the relatively slow tumor growth for T-47D and the lack of a significant response for the TSL_{Dox} HT group, additional control groups were omitted.

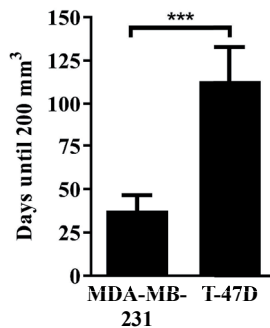


Figure 4. Orthotopic tumor growth MDA-MB-231 and T-47D tumors in BALB/c-nu mice ($N = 14$ for both groups). T-47D tumors grew significantly slower than MDA-MB-231 tumors (two-tailed unpaired t-test; *** = $p < 0.005$). When tumors reached 200 mm^3 , they were treated with one of the treatments described in the therapeutic study.

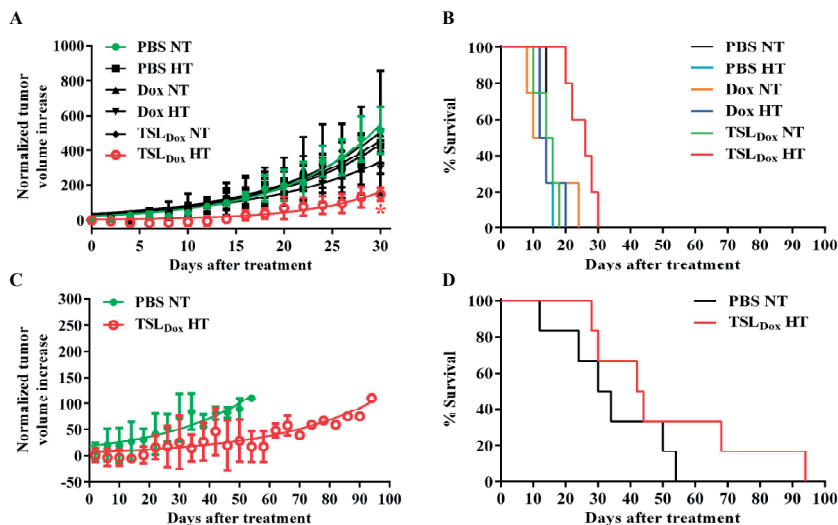


Figure 5. Therapeutic efficacy using TSL-Dox on orthotopic MDA-MB-231 and T-47D tumors. MDA-MB-231 average growth curves normalized against the start of therapy at a tumor size of 200 mm³ (A) and a Kaplan-Meier plot for tumor doubling time (B) show that PBS HT, TSL-Dox NT and control groups with free Dox did not show a significant difference compared to PBS NT (N = 4 for all groups). TSL-Dox HT (N = 5) did elicit a significant therapeutic effect based on one-way ANOVA Bonferroni test (* = $p < 0.05$). A similar growth curve (C) and Kaplan-Meier plot (D) for T-47D tumors indicate no significant tumor growth inhibition for TSL-Dox HT versus PBS NT (N=6 for both groups). Additional control groups similar to the therapeutic efficacy study on MDA-MB-231 were omitted due to the slow growth of the T-47D tumors and the lack of statistical significance of the TSL-Dox HT treatment in this tumor model.

Ex vivo investigation

MDA-MB-231 and T-47D tumors were examined for overall tissue morphology, apoptosis, vascularization and fibrillin I/collagen IV density. The MSB stained sections show that MDA-MB-231 tumors possess a relatively poorly organized extracellular matrix (ECM) with fibers randomly distributed, while T-47D tumors show a more organized structure of dense ECM with thick fibers (Figure 6A, B). Fluorescence microscopy analysis also revealed a random distribution of vessels and extracellular fibers for MDA-MB-231 tumors, whereas blood vessels of T-47D tumors were often found in close proximity to the dense extracellular fibers (Figure 6C, D; Figure 7). Quantitative tile scan analysis of fluorescently stained sections revealed that both tumor types did not differ in viability (Figure 6E). However, MDA-MB-231 tumors had a higher degree of vascularization with 5.7 ± 0.8 % mean vessel density versus 2.3 ± 1.4 % for T-47D. Furthermore, the mean fibrillin I density was also significantly lower for MDA-MB-231 tumors with 3.7 ± 1.2 % relative to 6.8 ± 3.0 % for T-47D (Figure 6F, G; Figure 7). MDA-MB-231 and T-47D tumors showed similar levels of collagen IV expression (Figure 6H).

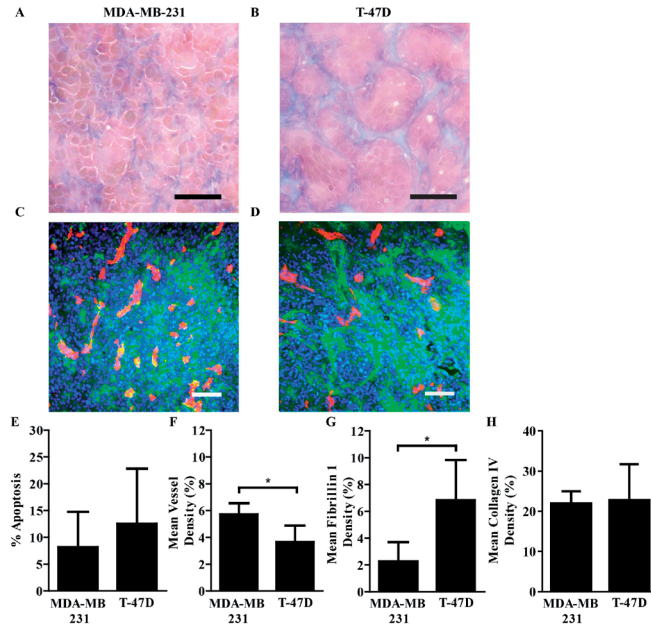


Figure 6. Histological analysis of MDA-MB-231 and T-47D tumors. MSB staining indicated differences in overall tissue make up regarding extracellular matrix distribution (blue) for MDA-MB-231 (A) and T-47D (B). MDA-MB-231 (C) and T-47D (D) sections were immunostained for CD31 (red), fibrillin I (green) and nuclei were stained by DAPI (blue) and imaged by widefield fluorescence microscopy. Quantification of tile scans (obtained by confocal fluorescence microscopy; Supplemental Fig 2) of both tumor types was done on TUNEL (E), CD31 (F), fibrillin I (G) and collagen IV (H) stained sections. Scale bars for MSB sections (A, B) represent 20 μ m. Scale bars for immunostained sections (C, D) represent 100 μ m. For quantitative analysis (E-G), 5 sections were used for each group (N = 5), with exception for the collagen IV staining (N = 3). Groups were statistically compared by Mann-Whitney test. * = $p < 0.05$. Contrast and brightness were enhanced in A-D for publication purposes only.

DISCUSSION

It has been shown in numerous cases that the heterogeneity of breast cancer subtypes results in varying chemotherapy response rates [28-31]. This warrants the evaluation of therapies across various tumor subtypes towards patient-specific treatment planning. In many of the preclinical cancer models employed, a rapidly growing, invasive tumor is often chosen. However, a debate continues as to whether these preclinical models sufficiently recapitulate the disease in a clinical setting [32], as they often lack an appropriate tumor microenvironment. By using an orthotopic xenograft, the tumor develops within a more native microenvironment, resulting in a more clinically translatable model [33, 34]. T-47D and MDA-MB-231 reflect two distinct breast cancer subtypes varying in invasiveness and tumor morphology. Epithelial T-47D is less aggressively growing than mesenchymal MDA-MB-231 and possesses a cell morphology much like cells found in the healthy ducts of the breast [35]. Relatively high expression of E-cadherin and claudins confer good cell-cell adhesion for T-47D cells [36, 37] and the low invasiveness

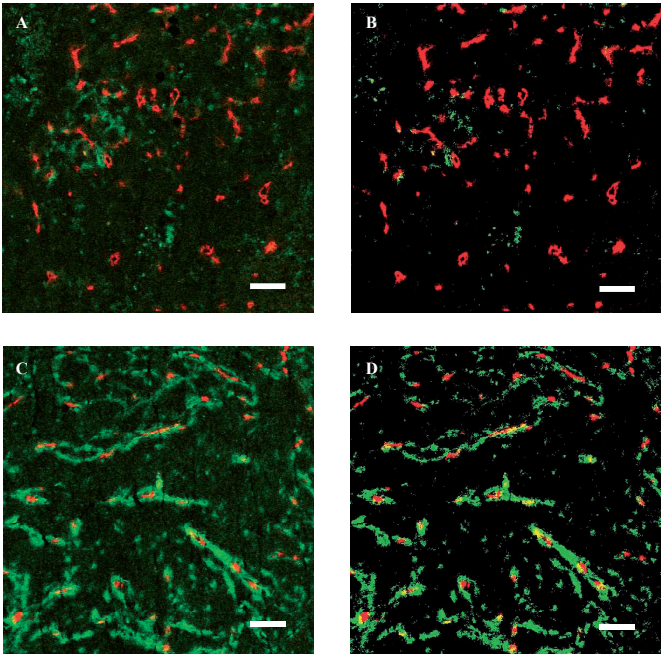


Figure 7. Representative histology images of MDA-MB-231 (A, B) and T-47D (C, D) tumors. CD31 is marked in red and fibrillin in green. The original images (A and C) were subjected to a constant threshold (B and D) and the positive pixel count of the whole section was used as a measure for CD31 and fibrillin expression. Scale bar indicates 50 μm . The given pictures are a magnification of the whole section tile scans used for the quantitative analysis.

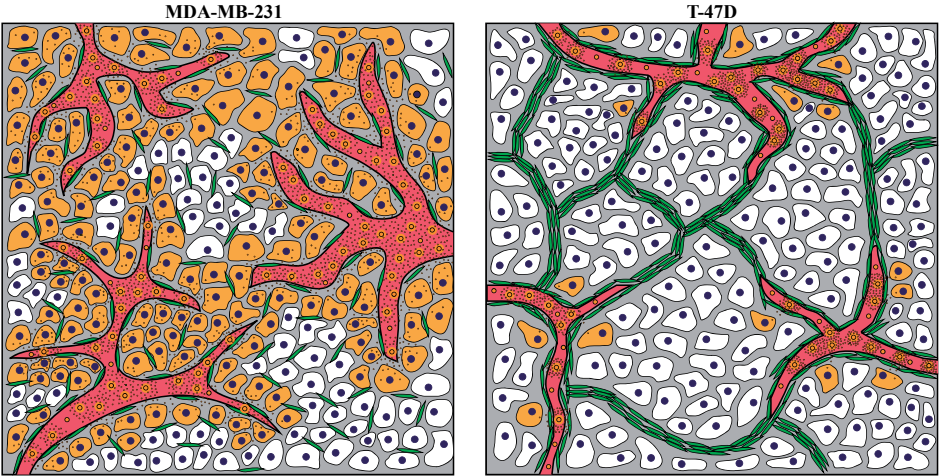


Figure 8. Schematic representation of hypothesized Dox delivery by TSL (represented by orange intravascular particles) and HT in MDA-MB-231 and T-47D tumors. MDA-MB-231 tumors show a relatively high Dox uptake (orange cells), due to greater tissue perfusion (vessels in red) and a lower presence of mature extracellular fibers (green), which enables an increased Dox extravasation into the tumor interstitium. T-47D tumors are less likely to take up high

is usually paired with a well-defined ECM, reducing the chance of metastasis [38]. MDA-MB-231 on the other hand, has lower E-cadherin and claudin expression and a more disorganized ECM, resulting in poor cell-cell adhesion and greater metastatic potential. Therefore, these cell lines represent two very different types of breast cancer and are used herein to investigate their response to local drug delivery of Dox using TSL_{Dox} in combination with HT.

Hyperthermia-triggered local drug delivery using TSL_{Dox} has shown considerable success in solid tumor treatment over the last decades [39], with the LTSL formulation currently being tested in clinical trials [14, 15]. In earlier work, we have shown that Dox can be effectively released from TSLs in physiological media and that HT can increase Dox uptake in cells, leading to a higher cytotoxic effect for B16 melanoma and BFS-1 sarcoma cell lines [27]. In the present study, a similar effect was observed for T-47D and MDA-MB-231 breast cancer cells. Nevertheless, for the epithelial T-47D cell line, there was higher variability between experiments leading to higher standard deviations relative to mesenchymal MDA-MB-231 since the former grows inconsistent, slowly and clustered while the latter grows consistent, rapidly and as a robust monolayer [35, 40]. Incubation of these cells with TSL_{Dox} at HT was equally effective as free Dox *in vitro*, indicative of the complete release of the drug from its temperature-sensitive carrier and its bioavailability to the cells. Similar work in this field has shown that drug release and stability assays are heavily dependent on the media (buffer, serum, plasma) and the dilution in which they are performed, and it is still relatively unknown why drug release varies between different plasma/ sera of different sources [41, 42]. Therefore, we conducted Dox release assays from TSL_{Dox} in freshly isolated BALB/c and human plasma to give a better indication of drug release that may occur in the (pre)clinical setting. Dox release in these media was slightly slower and incomplete when compared to the typically used medium consisting of FBS. BALB/c and human plasma showed identical Dox release curves, suggesting comparable release and stability of TSL_{Dox} in the systemic circulation of both species, though extrapolation from *in vitro* to *in vivo* behavior is cautioned [25] and may be further subject to differences as a function of the chosen *in vivo* model [42, 43].

The growth of the invasive MDA-MB-231 orthotopic tumor model was found to be significantly faster than the growth of T-47D tumors in immunodeficient BALB/c mice. TSL_{Dox} with HT could significantly reduce tumor growth for MDA-MB-231, but the relative therapeutic response of T-47D tumors was not statistically significant. Differential chemosensitivity is a common observation among cancer subtypes. T-47D, being a luminal breast cancer [44], exhibiting low proliferation [45] and enhanced ER/PR expression [46], is likely less chemosensitive than MDA-MB-231. Surprisingly, local drug delivery by TSL and HT failed to elicit a statistically significant therapeutic response, despite the therapy proving successful in a variety of tumor types [12, 27]. The considerable variation

in response in the T-47D model (i.e. high SD) and limited tumor growth rate narrowed our study to that of one treatment and one control group (i.e. TSL_{Dox} HT and PBS NT). As the results of the TSL_{Dox} HT therapy did not show statistically significant superiority over PBS NT, the remaining control groups in addition to PBS NT were omitted. However, a statistically significant difference may have been achieved by adding more animals to the experimental groups. This is particularly pertinent given that only two animals remained in the study at 50-100 d post-treatment. Alternatively, repeated treatment cycles may have proven to be a more effective therapeutic strategy against slowly progressing tumors, as performed in the LTSL clinical trial [16]. Nevertheless, the differences in the MDA-MB-231 and T-47D tumor microenvironments may provide important insights into the disparate therapeutic responses between these tumor types. The MSB staining showed a highly organized ECM with dense fibers that seemingly divided T-47D tumors into sub-compartments, whereas MDA-MB-231 tumors showed relatively less dense fibers and were more randomly distributed in their composition. Furthermore, T-47D tumors also had a higher fibrillin-I density; however, this was not the case for all ECM components as there was no difference observed in collagen IV density between both tumor types. This compartmentalized tumor morphology, irrespective of overall stromal content, has previously been related to lower chemosensitivity [47]. Further investigation of the tumor vascular network between models was performed as a measure of the efficacy of our drug delivery approach. We observed that blood vessels of T-47D tumors could often be found in the vicinity of the extracellular fibers, analogous to a basal membrane that in healthy breast separates the blood capillary from the epithelial ducts [48]. Conversely, MDA-MB-231 tumors showed no distinct organization of blood vessels within the ECM, which corresponds with its mesenchymal and invasive characteristics [49]. We hypothesize that the basal membrane-like features in T-47D tumors may have reduced Dox delivery to the tumor cellular compartment (Figure 8), as previous results have shown lower vascular permeability and lower degradation of the endothelial ECM by T-47D cells when compared to MDA-MB-231 [50-52]. Furthermore, the poorly vascularized nature of T-47D tumors relative to MDA-MB-231 tumors limits the overall delivery of Dox to the tumor, as tumor perfusion is one of the key factors in temperature-induced drug delivery [27]. Our study has limitations. Firstly, the therapeutic study for the T-47D tumor type lacks additional control groups next to PBS NT. These groups were omitted since tumor progression was slow and there was no significant delay in tumor growth by treatment with TSL_{Dox} and HT. Adding extra animals or altering treatment regimens in the T-47D therapeutic study might have given a more significant tumor growth delay. Secondly, a comparative Dox uptake study between MDA-MB-231 and T-47D tumors could have provided a relation between therapeutic response and achieved Dox uptake in the tumor. Also on a microscopic scale, in tumor sections, this would be interesting to investigate, although low Dox levels in sections can be difficult to detect because of

the relatively weak fluorescence of Dox when compared to commonly used fluorophores used for histology. As suggested above, the organization of the ECM in a tumor can provide an important barrier for effective targeting of therapeutic compounds towards the tumor cell, which results in more therapy resistance [53, 54]. However, other factors like tumor cell density [55, 56], hypoxia [57, 58], high interstitial fluid pressure [59], low pH in tumor interstitial space [60] and tumor cell – stroma molecular signaling [61, 62] can also induce lower therapeutic response. In addition, the amount of therapeutic agent accumulating in the tumor cannot always be directly correlated to therapeutic response [63]. Because of these reasons, it is still not entirely certain if a drug uptake study would answer the lack of therapeutic response for the T-47D tumors. The T-47D tumors are clearly different in growth rate and microenvironment factors than tumors which we have observed previously [27]. Although we hypothesize that the ECM has played a dominant role in preventing effective drug accumulation in T-47D tumors, the other above-mentioned factors also have to be carefully investigated in future studies in order to create an understanding on which cancers are suitable for TSL-based therapy.

Local drug delivery by TSL and HT to solid tumors is a rapidly growing field, likely resulting in a rapid increase of clinical trials in the years to come. Therefore, it is important to investigate the heterogeneity in therapeutic response that has been observed in clinical trials thus far. (L)TSL and HT therapy has been shown to outperform free drug and non-TSL based therapies in previous reports [8, 64]. However, as cancer treatment adapts towards a more personalized approach, a greater understanding of the possibilities and limitations of TSL and HT based treatments for specific tumor (sub)types is important. By comparing the therapeutic potential of TSL and HT in MDA-MB-231 and T-47D tumors, we show that this treatment strategy remains promising for breast cancer, but that well-differentiated and slowly proliferating tumors may prove more challenging for TSL based treatments. Our study shows that a single treatment is insufficient to achieve statistically significant tumor growth inhibition in the T-47D tumor model. For slow growing, well-differentiated and poorly perfused tumors, a multiple-dose regimen for local drug delivery should be further investigated.

REFERENCES

1. American Breast Cancer Society, Breast Cancer Key Statistics, (2016).
2. R.W. Carlson, D.C. Allred, B.O. Anderson, H.J. Burstein, W.B. Carter, S.B. Edge, J.K. Erban, W.B. Farrar, L.J. Goldstein, W.J. Gradishar, D.F. Hayes, C.A. Hudis, M. Jahanzeb, K. Kiel, B.M. Ljung, P.K. Marcom, I.A. Mayer, B. McCormick, L.M. Nabell, L.J. Pierce, E.C. Reed, M.L. Smith, G. Somlo, R.L. Theriault, N.S. Topham, J.H. Ward, E.P. Winer, A.C. Wolff, Breast cancer. Clinical practice guidelines in oncology, Journal of the National Comprehensive Cancer Network : JNCCN, 7 (2009) 122-192.
3. A.M. Griffin, P.N. Butow, A.S. Coates, A.M. Childs, P.M. Ellis, S.M. Dunn, M.H. Tattersall, On the receiving end. V: Patient perceptions of the side effects of cancer chemotherapy in 1993, Annals of oncology : official journal of the European Society for Medical Oncology, 7 (1996) 189-195.
4. M.E. O'Brien, N. Wigler, M. Inbar, R. Rosso, E. Grischke, A. Santoro, R. Catane, D.G. Kieback, P. Tomczak, S.P. Ackland, F. Orlandi, L. Mellars, L. Alland, C. Tendler, Reduced cardiotoxicity and comparable efficacy in a phase III trial of pegylated liposomal doxorubicin HCl (CAELYX/Doxil) versus conventional doxorubicin for first-line treatment of metastatic breast cancer, Annals of oncology : official journal of the European Society for Medical Oncology, 15 (2004) 440-449.
5. J.W. Park, Liposome-based drug delivery in breast cancer treatment, Breast cancer research : BCR, 4 (2002) 95-99.
6. K.M. Laginha, S. Verwoert, G.J. Charrois, T.M. Allen, Determination of doxorubicin levels in whole tumor and tumor nuclei in murine breast cancer tumors, Clinical cancer research : an official journal of the American Association for Cancer Research, 11 (2005) 6944-6949.
7. M.H. Gaber, N.Z. Wu, K. Hong, S.K. Huang, M.W. Dewhirst, D. Papahadjopoulos, Thermo-sensitive liposomes: extravasation and release of contents in tumor microvascular networks, International journal of radiation oncology, biology, physics, 36 (1996) 1177-1187.
8. G. Kong, G. Anyarambhatla, W.P. Petros, R.D. Braun, O.M. Colvin, D. Needham, M.W. Dewhirst, Efficacy of liposomes and hyperthermia in a human tumor xenograft model: importance of triggered drug release, Cancer research, 60 (2000) 6950-6957.
9. D. Needham, G. Anyarambhatla, G. Kong, M.W. Dewhirst, A new temperature-sensitive liposome for use with mild hyperthermia: characterization and testing in a human tumor xenograft model, Cancer research, 60 (2000) 1197-1201.
10. A.A. Manzoor, L.H. Lindner, C.D. Landon, J.Y. Park, A.J. Simnick, M.R. Dreher, S. Das, G. Hanna, W. Park, A. Chilkoti, G.A. Koning, T.L. ten Hagen, D. Needham, M.W. Dewhirst, Overcoming limitations in nanoparticle drug delivery: triggered, intravascular release to improve drug penetration into tumors, Cancer research, 72 (2012) 5566-5575.
11. J.P. May, M.J. Ernsting, E. Undzys, S.D. Li, Thermosensitive liposomes for the delivery of gemcitabine and oxaliplatin to tumors, Molecular pharmaceutics, 10 (2013) 4499-4508.
12. P.S. Yarmolenko, Y. Zhao, C. Landon, I. Spasojevic, F. Yuan, D. Needham, B.L. Viglianti, M.W. Dewhirst, Comparative effects of thermosensitive doxorubicin-containing liposomes and hyperthermia in human and murine tumours, International journal of hyperthermia : the official journal of European Society for Hyperthermic Oncology, North American Hyperthermia Group, 26 (2010) 485-498.

13. T. Tagami, M.J. Ernsting, S.D. Li, Efficient tumor regression by a single and low dose treatment with a novel and enhanced formulation of thermosensitive liposomal doxorubicin, *Journal of controlled release : official journal of the Controlled Release Society*, 152 (2011) 303-309.
14. Celsion, http://celsion.com/docs/technology_thermodox.
15. Celsion, Phase 1/2 Study of ThermoDox With Approved Hyperthermia in Treatment of Breast Cancer Recurrence at the Chest Wall (DIGNITY),, *ClinicalTrials.gov*, (2009).
16. T.M. Zagar, Z. Vujaskovic, S. Formenti, H. Rugo, F. Muggia, B. O'Connor, R. Myerson, P. Stauffer, I.C. Hsu, C. Diederich, W. Straube, M.K. Boss, A. Boico, O. Craciunescu, P. Maccarini, D. Needham, N. Borys, K.L. Blackwell, M.W. Dewhirst, Two phase I dose-escalation/ pharmacokinetics studies of low temperature liposomal doxorubicin (LTLTD) and mild local hyperthermia in heavily pretreated patients with local regionally recurrent breast cancer, *International journal of hyperthermia : the official journal of European Society for Hyperthermic Oncology, North American Hyperthermia Group*, 30 (2014) 285-294.
17. T. Lu, T.L. Ten Hagen, Inhomogeneous crystal grain formation in DPPC-DSPC based thermosensitive liposomes determines content release kinetics, *Journal of controlled release : official journal of the Controlled Release Society*, 247 (2017) 64-72.
18. C.D. Landon, J.Y. Park, D. Needham, M.W. Dewhirst, Nanoscale Drug Delivery and Hyperthermia: The Materials Design and Preclinical and Clinical Testing of Low Temperature-Sensitive Liposomes Used in Combination with Mild Hyperthermia in the Treatment of Local Cancer, *The open nanomedicine journal*, 3 (2011) 38-64.
19. L. Li, T.L. ten Hagen, M. Hossann, R. Suss, G.C. van Rhoon, A.M. Eggermont, D. Haemmerich, G.A. Koning, Mild hyperthermia triggered doxorubicin release from optimized stealth thermosensitive liposomes improves intratumoral drug delivery and efficacy, *Journal of controlled release : official journal of the Controlled Release Society*, 168 (2013) 142-150.
20. E.A. Musgrove, R.L. Sutherland, Biological determinants of endocrine resistance in breast cancer, *Nature reviews. Cancer*, 9 (2009) 631-643.
21. K. Polyak, R.A. Weinberg, Transitions between epithelial and mesenchymal states: acquisition of malignant and stem cell traits, *Nature reviews. Cancer*, 9 (2009) 265-273.
22. A. Prat, J.S. Parker, O. Karginova, C. Fan, C. Livasy, J.I. Herschkowitz, X. He, C.M. Perou, Phenotypic and molecular characterization of the claudin-low intrinsic subtype of breast cancer, *Breast cancer research : BCR*, 12 (2010) R68.
23. B. Weigelt, J.S. Reis-Filho, Histological and molecular types of breast cancer: is there a unifying taxonomy?, *Nature reviews. Clinical oncology*, 6 (2009) 718-730.
24. G.R. Bartlett, Phosphorus assay in column chromatography, *The Journal of biological chemistry*, 234 (1959) 466-468.
25. W.J. Lokerse, E.C. Kneepkens, T.L. ten Hagen, A.M. Eggermont, H. Grull, G.A. Koning, In depth study on thermosensitive liposomes: Optimizing formulations for tumor specific therapy and in vitro to in vivo relations, *Biomaterials*, 82 (2016) 138-150.
26. D. Needham, J.Y. Park, A.M. Wright, J. Tong, Materials characterization of the low temperature sensitive liposome (LTSL): effects of the lipid composition (lysolipid and DSPE-PEG2000) on the thermal transition and release of doxorubicin, *Faraday discussions*, 161 (2013) 515-534; discussion 563-589.
27. W.J. Lokerse, M. Bolkestein, T.L. Ten Hagen, M. de Jong, A.M. Eggermont, H. Grull, G.A. Koning, Investigation of Particle Accumulation, Chemosensitivity and Thermosensitivity for Effective Solid Tumor Therapy Using Thermosensitive Liposomes and Hyperthermia, *Theranostics*, 6 (2016) 1717-1731.

28. M.A. Troester, K.A. Hoadley, T. Sorlie, B.S. Herbert, A.L. Borresen-Dale, P.E. Lonning, J.W. Shay, W.K. Kaufmann, C.M. Perou, Cell-type-specific responses to chemotherapeutics in breast cancer, *Cancer research*, 64 (2004) 4218-4226.
29. L.A. Carey, E.C. Dees, L. Sawyer, L. Gatti, D.T. Moore, F. Collichio, D.W. Ollila, C.I. Sartor, M.L. Graham, C.M. Perou, The triple negative paradox: primary tumor chemosensitivity of breast cancer subtypes, *Clinical cancer research : an official journal of the American Association for Cancer Research*, 13 (2007) 2329-2334.
30. A.R. Razzak, N.U. Lin, E.P. Winer, Heterogeneity of breast cancer and implications of adjuvant chemotherapy, *Breast cancer (Tokyo, Japan)*, 15 (2008) 31-34.
31. A. Prat, C. Fan, A. Fernandez, K.A. Hoadley, R. Martinello, M. Vidal, M. Viladot, E. Pineda, A. Arance, M. Munoz, L. Pare, M.C. Cheang, B. Adamo, C.M. Perou, Response and survival of breast cancer intrinsic subtypes following multi-agent neoadjuvant chemotherapy, *BMC medicine*, 13 (2015) 303.
32. S.E. Gould, M.R. Junttila, F.J. de Sauvage, Translational value of mouse models in oncology drug development, *Nature medicine*, 21 (2015) 431-439.
33. J.J. Killian, R. Radinsky, I.J. Fidler, Orthotopic models are necessary to predict therapy of transplantable tumors in mice, *Cancer metastasis reviews*, 17 (1998) 279-284.
34. J.M. Fleming, T.C. Miller, M.J. Meyer, E. Ginsburg, B.K. Vonderhaar, Local regulation of human breast xenograft models, *Journal of cellular physiology*, 224 (2010) 795-806.
35. C.L. Sommers, S.W. Byers, E.W. Thompson, J.A. Torri, E.P. Gelmann, Differentiation state and invasiveness of human breast cancer cell lines, *Breast cancer research and treatment*, 31 (1994) 325-335.
36. D.L. Holliday, V. Speirs, Choosing the right cell line for breast cancer research, *Breast cancer research : BCR*, 13 (2011) 215.
37. S. Lamouille, J. Xu, R. Derynck, Molecular mechanisms of epithelial-mesenchymal transition, *Nature reviews. Molecular cell biology*, 15 (2014) 178-196.
38. D.M. Gilkes, G.L. Semenza, D. Wirtz, Hypoxia and the extracellular matrix: drivers of tumour metastasis, *Nature reviews. Cancer*, 14 (2014) 430-439.
39. B. Kneidl, M. Peller, G. Winter, L.H. Lindner, M. Hossann, Thermosensitive liposomal drug delivery systems: state of the art review, *International Journal of Nanomedicine*, 9 (2014) 4387-4398.
40. C.L. Sommers, E.W. Thompson, J.A. Torri, R. Kemler, E.P. Gelmann, S.W. Byers, Cell adhesion molecule uromodulin expression in human breast cancer cell lines: relationship to morphology and invasive capacities, *Cell growth & differentiation : the molecular biology journal of the American Association for Cancer Research*, 2 (1991) 365-372.
41. M.H. Gaber, K. Hong, S.K. Huang, D. Papahadjopoulos, Thermosensitive sterically stabilized liposomes: formulation and in vitro studies on mechanism of doxorubicin release by bovine serum and human plasma, *Pharmaceutical research*, 12 (1995) 1407-1416.
42. M. Hossann, Z. Syunyaeva, R. Schmidt, A. Zengerle, H. Eibl, R.D. Issels, L.H. Lindner, Proteins and cholesterol lipid vesicles are mediators of drug release from thermosensitive liposomes, *Journal of controlled release : official journal of the Controlled Release Society*, 162 (2012) 400-406.
43. L.H. Lindner, M.E. Eichhorn, H. Eibl, N. Teichert, M. Schmitt-Sody, R.D. Issels, M. Dellian, Novel temperature-sensitive liposomes with prolonged circulation time, *Clinical cancer research : an official journal of the American Association for Cancer Research*, 10 (2004) 2168-2178.

44. R. Rouzier, C.M. Perou, W.F. Symmans, N. Ibrahim, M. Cristofanilli, K. Anderson, K.R. Hess, J. Stec, M. Ayers, P. Wagner, P. Morandi, C. Fan, I. Rabiul, J.S. Ross, G.N. Hortobagyi, L. Pusztai, Breast cancer molecular subtypes respond differently to preoperative chemotherapy, *Clinical cancer research : an official journal of the American Association for Cancer Research*, 11 (2005) 5678-5685.
45. M. Campiglio, G. Somenzi, C. Olgiati, G. Beretta, A. Balsari, N. Zaffaroni, P. Valagussa, S. Menard, Role of proliferation in HER2 status predicted response to doxorubicin, *International journal of cancer*, 105 (2003) 568-573.
46. M. Colleoni, G. Viale, D. Zahrieh, G. Pruneri, O. Gentilini, P. Veronesi, R.D. Gelber, G. Curigliano, R. Torrisi, A. Luini, M. Intra, V. Galimberti, G. Renne, F. Nole, G. Peruzzotti, A. Goldhirsch, Chemotherapy is more effective in patients with breast cancer not expressing steroid hormone receptors: a study of preoperative treatment, *Clinical cancer research : an official journal of the American Association for Cancer Research*, 10 (2004) 6622-6628.
47. J.A. Delgado San Martin, J.I. Hare, J.W. Yates, S.T. Barry, Tumour stromal morphology impacts nanomedicine cytotoxicity in patient-derived xenografts, *Nanomedicine : nanotechnology, biology, and medicine*, 11 (2015) 1247-1252.
48. R. Kalluri, M. Zeisberg, Fibroblasts in cancer, *Nature reviews. Cancer*, 6 (2006) 392-401.
49. P. Schedin, Pregnancy-associated breast cancer and metastasis, *Nature reviews. Cancer*, 6 (2006) 281-291.
50. J.C. Harrell, A.D. Pfefferle, N. Zalles, A. Prat, C. Fan, A. Khramtsov, O.I. Olopade, M.A. Troester, A.C. Dudley, C.M. Perou, Endothelial-like properties of claudin-low breast cancer cells promote tumor vascular permeability and metastasis, *Clinical & experimental metastasis*, 31 (2014) 33-45.
51. E.M. Huuse, S.A. Moestue, E.M. Lindholm, T.F. Bathen, H. Nalwoga, K. Kruger, A. Bofin, G.M. Maelandsmo, L.A. Akslen, O. Engebraaten, I.S. Gribbestad, In vivo MRI and histopathological assessment of tumor microenvironment in luminal-like and basal-like breast cancer xenografts, *Journal of magnetic resonance imaging : JMRI*, 35 (2012) 1098-1107.
52. C. Yee, R.P. Shiu, Degradation of endothelial basement membrane by human breast cancer cell lines, *Cancer research*, 46 (1986) 1835-1839.
53. P.A. Netti, D.A. Berk, M.A. Swartz, A.J. Grodzinsky, R.K. Jain, Role of extracellular matrix assembly in interstitial transport in solid tumors, *Cancer research*, 60 (2000) 2497-2503.
54. A.I. Minchinton, I.F. Tannock, Drug penetration in solid tumours, *Nature reviews. Cancer*, 6 (2006) 583-592.
55. H. Kobayashi, Y. Takemura, T. Ohnuma, Relationship between tumor cell density and drug concentration and the cytotoxic effects of doxorubicin or vincristine: mechanism of inoculum effects, *Cancer chemotherapy and pharmacology*, 31 (1992) 6-10.
56. R.S. Kerbel, B. St Croix, V.A. Florenes, J. Rak, Induction and reversal of cell adhesion-dependent multicellular drug resistance in solid breast tumors, *Human cell*, 9 (1996) 257-264.
57. K.A. Kennedy, Hypoxic cells as specific drug targets for chemotherapy, *Anti-cancer drug design*, 2 (1987) 181-194.
58. K.M. Comerford, T.J. Wallace, J. Karhausen, N.A. Louis, M.C. Montalto, S.P. Colgan, Hypoxia-inducible factor-1-dependent regulation of the multidrug resistance (MDR1) gene, *Cancer research*, 62 (2002) 3387-3394.
59. P.A. Netti, L.M. Hamberg, J.W. Babich, D. Kierstead, W. Graham, G.J. Hunter, G.L. Wolf, A. Fischman, Y. Boucher, R.K. Jain, Enhancement of fluid filtration across tumor vessels: Implica-

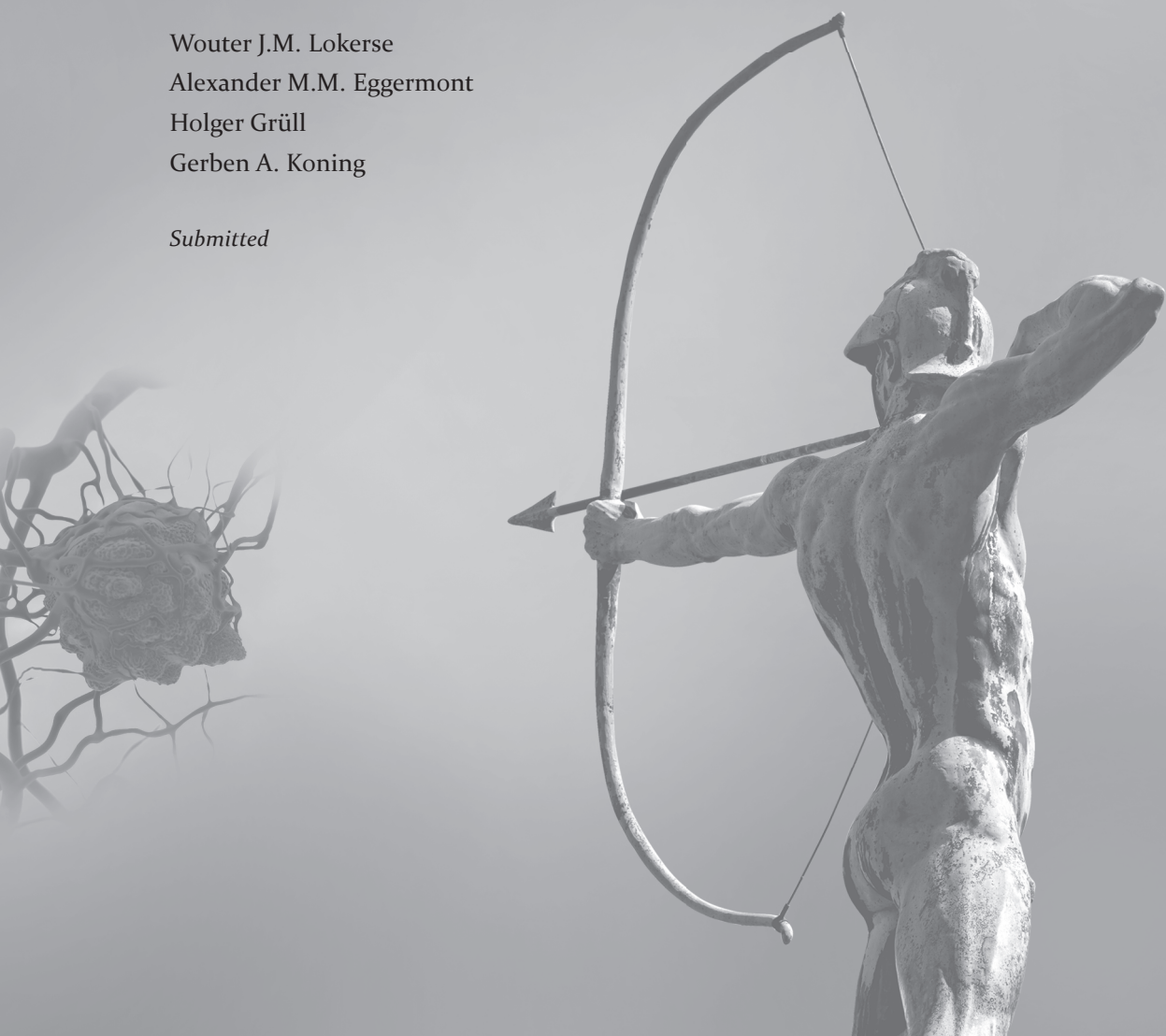
- tion for delivery of macromolecules, *Proceedings of the National Academy of Sciences of the United States of America*, 96 (1999) 3137-3142.
60. L.E. Gerweck, S. Vijayappa, S. Kozin, Tumor pH controls the in vivo efficacy of weak acid and base chemotherapeutics, *Molecular cancer therapeutics*, 5 (2006) 1275-1279.
 61. E.S. Nakasone, H.A. Askautrud, T. Kees, J.H. Park, V. Plaks, A.J. Ewald, M. Fein, M.G. Rasch, Y.X. Tan, J. Qiu, J. Park, P. Sinha, M.J. Bissell, E. Frengen, Z. Werb, M. Egeblad, Imaging tumor-stroma interactions during chemotherapy reveals contributions of the microenvironment to resistance, *Cancer cell*, 21 (2012) 488-503.
 62. O.C. Olson, J.A. Joyce, Microenvironment-mediated resistance to anticancer therapies, *Cell research*, 23 (2013) 179-181.
 63. E. El Emir, U. Qureshi, J.L. Dearling, G.M. Boxer, I. Clatworthy, A.A. Folarin, M.P. Robson, S. Nagl, M.A. Konerding, R.B. Pedley, Predicting response to radioimmunotherapy from the tumor microenvironment of colorectal carcinomas, *Cancer research*, 67 (2007) 11896-11905.
 64. L. Li, T.L. ten Hagen, A. Haeri, T. Soullie, C. Scholten, A.L. Seynhaeve, A.M. Eggermont, G.A. Koning, A novel two-step mild hyperthermia for advanced liposomal chemotherapy, *Journal of controlled release : official journal of the Controlled Release Society*, 174 (2014) 202-208.

CHAPTER 5

Development and validation of an isolated limb infusion model for investigation of drug delivery kinetics to solid tumors by thermosensitive liposomes and hyperthermia

Wouter J.M. Lokerse
Alexander M.M. Eggermont
Holger Gröll
Gerben A. Koning

Submitted



ABSTRACT

The combination of combined administration of thermosensitive liposomes (TSLs) and hyperthermia (HT) has been increasingly shown to be a powerful tool for the treatment of solid tumors. At present, it is hypothesized that the circulation of TSLs through the vasculature of a heated tumor results in the rapid release of the entrapped drug, followed by its uptake and distribution within the tumor microenvironment. However, simple questions on how much of the nanoparticles travel through the heated tumor and how much drug is retained in this tumor upon a passage of a TSL has not been investigated in an experimental setting to date. The present work describes a novel isolated limb infusion (ILI) procedure developed in a rat model of sarcoma. This approach was used to assess the efficacy of Doxorubicin (Dox) delivery by TSL in a heated (42°C) tumor following a single passage of TSL through the tumor vasculature. Analysis of the effluent post-ILI, whole-tumor histological sections, and tissue homogenates revealed that upon a single passage, Dox delivery by TSL at 42°C did not exceed delivery under conventional (i.e. free Dox) or physiological (i.e. TSL at 37°C, or normothermia; NT) conditions. In fact, mathematical modeling demonstrated that at least thirteen passages are required to obtain the intratumoral Dox levels typically achieved using TSL (i.e. ~5 %ID/g). Overall, this work investigates TSL-based determinants for achieving efficacious drug delivery using a model of ILI in tumor-bearing rats and the results bear important implications for TSL disposition *in vivo*.

INTRODUCTION

Liposomes are established delivery vehicles for chemotherapeutic drugs to solid tumors [1, 2]. The encapsulation of drugs into these carriers prolongs their circulation time by preventing rapid renal excretion and extravasation into healthy tissues. Tumor accumulation is obtained via passive uptake of the liposomal carrier, mediated by the enhanced permeability and retention effect [3-6]. The stable encapsulation of the drug inside the liposome ensures high plasma concentrations, but also hampers quick release of the drug from the carrier once it accumulated in the tumor tissue [7-9]. As a result, there has been increasing interest in the development of nanoparticle-based drug delivery systems that rely on an external, non-invasive trigger for intratumoral drug release [10-12]. Among such external triggers, hyperthermia (HT) constitutes a versatile choice as it can render the tumor vasculature more permeable to liposomes [13-15], but can also induce vascular damage [16, 17] or apoptosis [18, 19] in the tumor as a single modality, depending on the dose and the duration of heating [20, 21]. Furthermore, it can enhance chemo- [22] and radiosensitivity [23] of tumors. The first description of thermosensitive liposomes (TSL) by Yatvin and Weinstein et al prompted an increased interest in using this platform for heat-mediated drug delivery to tumors [24, 25]. This resulted in numerous studies describing TSL formulations of which doxorubicin (Dox) has been consistently employed as the incorporated drug (Dox-TSL) [26, 27]. Despite slight variations in TSL design and experimental setup, these studies showed a significant therapeutic response in a variety of pre-clinical tumor models [28, 29]. However, there remains considerable uncertainty in the mechanism(s) governing HT-mediated drug delivery via TSL *in vivo*. Recently, a theoretical framework was presented by Gasselhuber et al, describing the most important parameters for HT-induced drug delivery using TSLs [30, 31]. While some of these parameters can be experimentally assessed [15, 32], others are difficult to determine in a typical experimental session. For example, the amount of TSLs that pass through the heated tumor depends on tumor perfusion and tumor size (vessel quantity and size). Drug release from these TSLs has to be fast enough to ensure adequate accumulation of the drug in the tumor tissue during this transition time. The theoretical framework described above has addressed tumor transition time of TSL versus time to release and how this can affect drug accumulation [30, 31]. However, experimental validation of this computational model, for example using subcutaneously growing tumors, has not been performed to this date. To investigate the efficacy of Dox delivery using TSL, we present a novel isolated limb infusion (ILI) model that may allow evaluation of particle delivery at the single-passage level through the tumor (Figure 1). Using this model, we can establish a controlled inflow of Dox-TSL into the limb bearing a heated tumor. By sampling fractions of the effluent following TSL administration, Dox delivery can be characterized upon immediate exposure at the tumor site, represented by a quantitative measurement

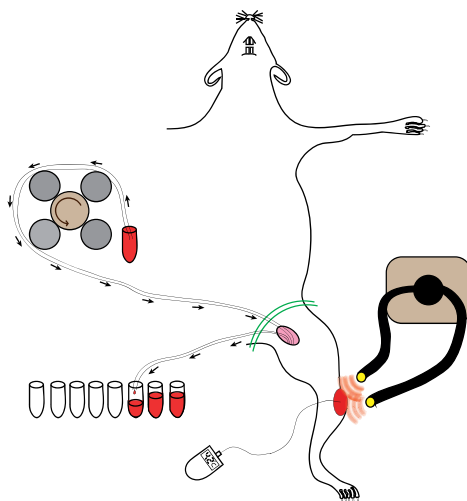


Figure 1. Schematic representation of the ILI setup. The rat is fixed on a stage and a cannula is placed in the femoral artery for the influent and in the femoral vein for the effluent. A groin tourniquet (green) is placed to occlude collateral vessels. A temperature probe is placed into the tumor at 0.5 cm depth, followed by bringing the tumor to 42°C by a goose neck light source. Dox (free or in TSL) is infused by a peristaltic pump and effluent fractions are collected. After the procedure, the rat is sacrificed and tumors dissected and snap frozen in liquid nitrogen.

of systemic Dox levels after a single passage through the tumor-bearing limb. Further insight into the heterogeneity of delivery is revealed via microscopy of whole tissue sections obtained from the excised tumors. Determination of the Dox concentration in the whole tumor provides a quantitative measure of drug deposition, yielding more information on TSL-mediated drug delivery. By investigating the efficacy of drug delivery following a single passage through the tumor, these findings support efforts to optimize delivery platforms that rely on triggered release and/or extended circulation strategies within the vascular compartment.

MATERIALS & METHODS

Materials

1,2-distearoyl-*sn*-glycero-3-phosphocholine (DSPC), 1,2-dipalmitoyl-*sn*-glycero-3-phosphocholine (DPPC) and 1,2-distearoyl-*sn*-glycero-3-phosphoethanolamine-N-(methoxy (polyethylene glycol)-2000) (DSPE-PEG₂₀₀₀) were purchased from Lipoid (Ludwigshafen, Germany). Doxorubicin-hydrochloride solution (2 mg/ml) was obtained from Accord Healthcare (Middlesex, UK). PD-10 columns were purchased from GE-Healthcare Life Sciences (Little Chalfont, UK). Gelofusine was from Braun (Melsungen, Germany). Heparin was obtained from Leo Pharma (Ballerup, Denmark). Normal rat serum was purchased from Millipore (Billerica, Massachusetts, USA). Mouse anti-rat

CD31 antibody and goat anti-mouse AlexaFluor 488 antibody was obtained from Abcam (Cambridge, UK) and Thermo Fisher (Waltham, Massachusetts, USA), respectively. All remaining chemicals were bought from Sigma-Aldrich (St. Louis, Missouri, USA).

Liposome preparation

TSL liposomes consisted of a 70:25:5 DPPC, DSPC and DSPE-PEG₂₀₀₀ molar ratio, respectively, and were prepared by the film hydration and extrusion method. In brief, lipids were dissolved in a 9:1 chloroform:methanol mixture and the solvent was evaporated to create a thin lipid film. The film was hydrated in a 250 mM NH₄SO₄ solution (pH 5.3) to form TSL. The TSL were extruded five times through 200 nm, 100 nm, 80 nm and 50 nm polycarbonate filters and loaded with Dox by a pH gradient at a Dox:lipid molar ratio of 0.15:1. The resulting Dox-TSL were concentrated by ultracentrifugation and resuspended in HEPES-buffered saline (10 mM HEPES, 135 mM NaCl). Size and Zeta-potential were measured in 10 mM HEPES buffer by dynamic light scattering using a Zetasizer (Malvern Instruments, Worcestershire, UK).

***In vitro* drug release and liposome stability by fluorometry**

2950 μ L fresh Brown Norway (BN) rat serum or filtered (400 nm pore size) commercial rat serum (MilliPore; MP) was added to a quartz cuvette and placed into a fluorimeter (Hitachi F-4500; Tokyo, Japan). The sample was heated to 37°C or 42°C by an externally connected water bath. A sample of 50 μ L Dox-TSL (5 mM PO₄) was injected into the sample via surgical tubing during measurement. The sample was scanned for a period of 1 h at 482 nm excitation and 594 nm emission. 10% Triton was added to the sample after the 1 h scan to determine the maximum Dox fluorescent signal (S_{\max}) and percentage release calculated by: % release = $(S_n - S_{\text{base}}) / (S_{\max} - S_{\text{base}}) \times 100\%$. S_n = Dox signal at a given time point. S_{base} = Background signal of Dox-TSL in serum.

***In vivo* BN175 tumor growth**

BN rats were used at 8 weeks old from Charles River Laboratories (Wilmington, Massachusetts, USA) and were given a subcutaneous injection of $1 \cdot 10^6$ BN175 sarcoma cells on the flank to grow tumors. When tumors reached 1 cm³, they were excised and 10 mm³ pieces were used for subcutaneous implantation on the hind limb of recipient BN rats for the subsequent ILI experiment. Tumors were measured using calipers, and tumor volumes determined by the standard formula for ellipsoids: $V = \text{length} \cdot \text{width} \cdot \text{depth} \cdot 0.4$; with dimensions being diameters.

Isolated limb infusion (ILI)

The experiment was conducted as illustrated in Figure 1. Rats bearing a 1 cm³ BN175 tumor on the hind limb were fixed on a heating pad and subjected to isoflurane an-

esthesia. The tumor was punctured in the center with a 25 gauge 5/8th sterile needle at a 5 mm depth, followed by placement of a thermocouple thermometer. The rat was left for 5 min before the start of the ILI procedure to allow blood clotting to close the wound. 50 UI heparin in physiological saline solution were i.v. administered via the penile vein before installing the ILI setup. An incision was made on the inner thigh of the tumor-bearing limb, followed by cannulation of the femoral artery and vein using silastic tubing, and placement of a groin tourniquet. The arterial tube was connected to a peristaltic pump used for inflow of the influent (influent tube: 0.012 inch inner diameter & 0.025 inch outer diameter) at a rate of 0.75 ml/min. The tube connected to the femoral vein provided the effluent (effluent tube: 0.025 inch inner diameter & 0.047 inch outer diameter) of the ILI setup. First, the system was washed two times with 3 mL of 1 UI heparin in 37°C Gelofusine (40 g/L succinylated gelatin), followed by a two times 3 mL wash in filtered commercial rat serum (MP) at 37°C. During the washing step, a goose neck light source was used to bring the tumor to 42°C (HT) or no lamp in case of a body temperature infusion (normothermia; NT). Subsequently, the influent tube was placed in a 0.25 mM free Dox or Dox-TSL solution in filtered commercial rat serum, while the effluent tube was placed in the first of fifteen tubes for collection of 0.5 mL fractions. 1 mL of the solution was introduced, after which the influent tube was placed back into filtered commercial rat serum maintained at 37°C (136 µg Dox total dose, ~0.5 mg/kg total body weight; ~13 mg/kg for the infused leg given the average weight of the hind limb of 10 g). This Dox dosage was chosen since the hind limb of the used rats makes up for approximately 5-10% of the total body weight [33] and we used 5 mg/kg in previously published therapeutic studies [15, 32]. The ILI lasted until the fifteen fractions were collected and were finally stored at -20°C until further use. A heat lamp was used to keep the body temperature on the ventral side of the rat stable during the procedure. At the conclusion of the experiment, the tumors were excised and snap-frozen in liquid nitrogen. Rats were sacrificed by cardiac puncture.

Analysis of Dox concentration in ILI fractions and tumors

Each effluent fraction was added to a 0.5% Triton X-100 solution for a series of seven 1:1 dilutions in a black 96-well plate. Dox concentrations were determined by a fluorimetry plate reader (Wallac Victor 2 Counter) at 485 nm excitation and 580 nm emission wavelengths. Intratumoral Dox analysis was determined by a method highly similar as described by Charrois et al [34]. 200 mg of the excised tumors was ground into small fragments in 200 µL lysis buffer (20 mM Tris, 150 mM NaCl, 0,2% NP40, 10% glycerol, pH 7.4) using a Bio-Gen PRO200 homogenizer (Pro Scientific, Oxford, UK). 50 µL of 10% Triton X-100 and 750 µL 9:1 (v:v) isopropanol/HCl was added and slurries were homogenized on ice. Following overnight storage at 4°C, samples were centrifuged at 15000 g for 20 min and supernatants measured for Dox fluorescence as described above.

Imaging of Dox delivery in ILI-treated tumors

5 μm sections were cut from frozen tumors and imaged for Dox fluorescence using a tile scan on a confocal microscope (Zeiss LSM 510 Meta; Oberkochen, Germany). The sections were left to dry and were fixed in acetone after which vessels were stained by mouse anti-rat CD31 and goat anti-mouse AlexaFluor 488. The CD31-stained slices were also imaged by confocal microscopy in a similar fashion as described above.

Statistics

All statistical tests were performed using Graphpad Prism version 7 software.

RESULTS

TSL stability and release in rat serum

Before starting the ILI experiment, we verified the release and stability of Dox-TSL in commercial rat serum (source: MilliPore; hereafter labeled 'MP') versus serum extracted from BN rats. After 1 h at 37°C, Dox-TSL showed good stability in both rat sera, with $7.9 \pm 1.5\%$ Dox release in MP serum and $1.5 \pm 0.1\%$ in BN serum (Figure 2A; Figure 3A, B). However, a significant difference in release was found as a function of serum origin ($p < 0.01$), as the maximum Dox release at 42°C was $73 \pm 5\%$ in MP serum and $87 \pm 4\%$ in BN serum ($p < 0.05$). The difference in release rate between sera was examined and found to be most significant during the first 30 sec of incubation at 42°C (Figure 2B; Figure 3C, D). Specifically, BN serum revealed $58 \pm 8\%$ Dox release, while release in MP serum was considerably slower with $14 \pm 3\%$ release ($p < 0.01$).

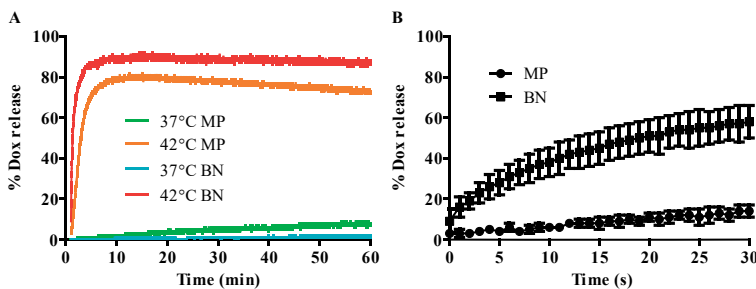


Figure 2. Time-dependent Dox release at 37°C or 42°C in commercial rat serum (source: MilliPore; MP), or serum extracted from BN rats. 1 h time scans show full extent of release (A), while the first 30 sec reveal the rate of release at 42°C (B). Error bars represent SD, and release rates were compared by unpaired two-tailed t-test (Figure 3). N=3 for all groups.

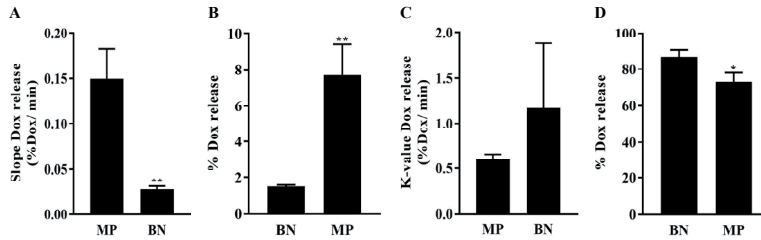


Figure 3. *In vitro* Dox release parameters at 37 °C and 42 °C in commercial rat serum (MP) or freshly isolated rat serum (BN). At 37 °C, a linear Dox leakage pattern was observed with MP serum showing a higher slope (A) and total Dox leakage after 1h of incubation (B). At 42 °C, an exponential Dox release curve was observed (C), where MP serum showed a lower plateau level of Dox release after 1h of incubation (D). For each data set, MP and BN was compared by unpaired two tailed t-test (N=3). * = $p < 0.05$, ** = $p < 0.01$.

Dox quantification of effluent fractions and tumors after ILI

The individual effluent fractions did not show a significant difference in Dox quantity between ILI-treated groups i.e. tumors that were heated (HT) versus tumors that were normothermic (NT). This observation was found irrespective of Dox formulation i.e. using free Dox (Figure 4A) or Dox-TSL (Figure 4B). When the values of all fractions were summed up, it showed that the majority of Dox infused was retrieved in the total effluent. For free Dox at NT, $30 \pm 8\%$ of the infused dose was retained in the tumor-bearing limb, while rats in the HT group yielded a Dox level of $35 \pm 4\%$. For TSL, the amount of Dox retained was significantly lower with $10 \pm 4\%$ at NT and $16 \pm 5\%$ for HT-treated animals. The blood collected from the heart at the end of the experiment showed no presence of Dox in all groups, indicating no leakage passed the groin tourniquet. Measurement of Dox content from excised tumors showed no difference in uptake between free and liposomal Dox, or between NT and HT conditions (Figure 5A). Dox-infused tumors at NT contained $0.14 \pm 0.17\%$ ID/g tumor versus $0.36 \pm 0.37\%$ ID/g under HT conditions. For infusions of TSL at NT and HT, the tumors contained 0.17 ± 0.03 and $0.28 \pm 0.19\%$ ID/g tumor, respectively.

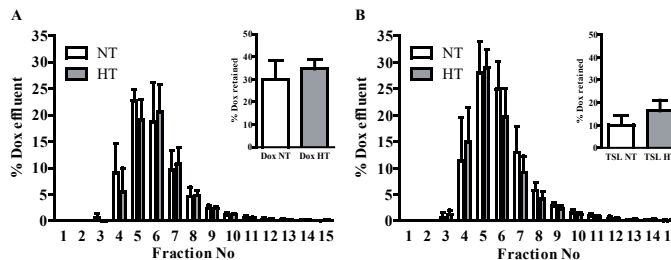


Figure 4. Analysis of ILI fractions with free Dox (A) and Dox-TSL (B) under NT and HT conditions. Inserts show the percentage that was retained in the rat calculated from the total amount of Dox in the entire effluent. N=5 for each group and error bars represent SD. Dox retention between free Dox and Dox-TSL and between NT and HT (inserts) was compared by one-way ANOVA Bonferroni test.

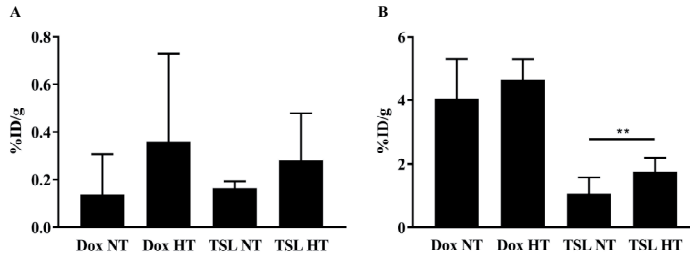


Figure 5. Dox uptake in tumors (A) and residual Dox uptake in the infused leg (B) after ILI treatment. The amount of Dox retained in the leg was obtained by subtracting the Dox quantity in the total effluent and total intratumoral Dox level from the infused dose. Two-way ANOVA Bonferroni test was conducted to analyze differences between groups. N=5 for all groups and error bars represent SD. Asterisks represent the statistical difference between free Dox and Dox-TSL groups by one-way ANOVA Bonferroni test (** = $p < 0.01$).

The Dox amount retained in the leg after ILI (Figure 5B) was significantly higher for legs infused with free Dox (4.05 ± 1.26 % ID/g for NT and 4.65 ± 0.65 % ID/g for HT) than for TSL infused legs (1.07 ± 0.51 % ID/g for NT and 1.77 ± 0.43 % ID/g for HT). To verify the presence of Dox in the tumors, cryo-sections were made and imaged by confocal fluorescence microscopy (Figure 6). The tumors were found to be well-vascularized, as shown by CD31 staining (Figure 6A), and Dox signal could be observed throughout the tumor section (Figure 6B).

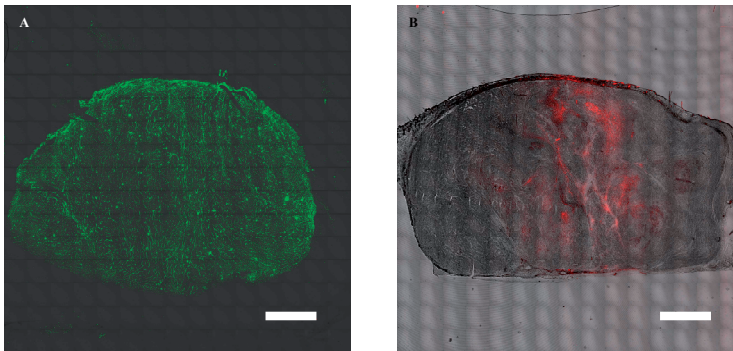


Figure 6. Tile scan of excised cryo-section after ILI. CD31 immunostaining (green) showed that the BNI75 tumor is well- and homogenously vascularized (A). Dox (red) could be visualized in other sections of the tumor (B). Both pictures originated from a Dox-TSL and HT treated tumor. Scale bar represents 2 mm.

Correlation to therapy experiment

If these results would to be used as a predictor for future therapeutic efficacy experiments, several parameter corrections have to be considered. Firstly, we require a correction for the different Dox leakage rates at 37°C between commercial rat serum (MP) used for the ILI, and the isolated, endogenous BN rat plasma. Both curves (MP_{leak} & BN_{leak})

showed a linear correlation with a slightly different slope. The leakage correction factor ($\text{Corr}_{\text{leak}}$) was calculated as follows:

$$\begin{aligned}\text{MP}_{\text{leak}} (\%) &= 100 - \alpha_{\text{MP}} * t \\ \text{BN}_{\text{leak}} (\%) &= 100 - \alpha_{\text{BN}} * t \\ \text{Corr}_{\text{leak}(t)} &= \text{BN}_{\text{leak}(t)} / \text{MP}_{\text{leak}(t)}\end{aligned}$$

Where: α_{MP} : Dox leakage kinetics in MP serum = 0.150 % Dox per minute

α_{BN} : Dox leakage kinetics in BN serum = 0.026 % Dox per minute

t = time in minutes

Next to the different Dox leakage rates at 37°C, there was also a difference in the Dox release from TSL at 42°C. In both data sets ($\text{MP}_{\text{release}}$ & $\text{BN}_{\text{release}}$), an exponential curve could be plotted from which a release correction factor ($\text{Corr}_{\text{release}}$) could be determined:

$$\begin{aligned}\text{MP}_{\text{release}} (\%) &= \text{MAX}_{\text{MP}} * (1 - e^{-\beta_{\text{MP}} * t}) \\ \text{BN}_{\text{release}} (\%) &= \text{MAX}_{\text{BN}} * (1 - e^{-\beta_{\text{BN}} * t}) \\ \text{Corr}_{\text{release}(t)} &= \text{BN}_{\text{release}} / \text{MP}_{\text{release}}\end{aligned}$$

Where: MAX_{MP} : Maximal Dox release in MP serum = 77 %

β_{MP} : Dox release kinetics in MP serum = 0.55 % Dox per minute

MAX_{BN} : Maximal Dox release in BN serum = 88 %

β_{BN} : Dox release kinetics in BN serum = 1.79 % Dox per minute

t = time in minutes

Lastly, a correction was made for the infusion pressure relative to the blood pressure inside the femoral artery. The infusion via the femoral artery was performed using 0.8 m silastic tubing with an inner diameter of 0.0305 cm and a 0.0635 cm outer diameter. The inflow rate by the peristaltic pump was fixed at 0.75 mL/min and influent was kept at 37 °C. With these data, we calculated that the inflow pressure was 30.26 kPa according to the Hagen-Poiseuille equation [35, 36]:

$$\Delta P = 8 \eta L \Phi / \pi r^4$$

Where ΔP : Pressure difference between two ends of tube in Pa

η : Dynamic viscosity in Pa·s = $6.9 \cdot 10^{-4}$ Pa·s for water at 37 °C

L : Length of the tube in m

Φ : Volumetric flow rate in m^3/s

r : Inner radius of tube in m

The reported average blood pressure in the rat femoral artery when the animal is under anesthesia is ± 90 mm Hg (i.e. 12 kPa) [37], which indicates that the infusion pressure of our ILI system is a factor of 2.52 higher. This correlates to a flow rate of 0.28 mL/min, which is a factor 2.68 lower than the flow rate used for in the infusion.

The average amount of Dox accumulated in tumors was 0.28 ± 0.19 % ID/g for TSL infusion at HT. With these data, we assumed a simple exponential formula for intratumoral Dox accumulation and *in vivo* passage number (P):

$$\text{Dox}_{\text{tumor}} = \text{Dox}_{\text{sat}} \cdot (1 - e^{-K \cdot P})$$

Where Dox_{sat} : Saturation for Dox accumulation in tumor in % ID/g

K: HT-induced Dox delivery by TSL-Dox per passage = 0.28 ± 0.19 % ID/g

P: Number of passages

DISCUSSION

Throughout the last decades, much work has been published on TSL and the delivery of Dox to solid tumors. The design of TSL-based therapy constitutes a balance between the need for fast release and full availability of the drug, and high particle stability and circulation time, allowing for TSL particles to pass through the heated tumor an adequate number of times for optimal drug accumulation [32, 38]. The investigation on delivery dynamics using TSLs has currently only been analyzed by mathematical modelling [30, 31]. Using the here presented ILI model, we assessed the delivery of Dox from TSLs to heated solid tumors upon a single passage. In principle, the animal model for the ILI system is similar to that of the isolated limb perfusion (ILP) [39], with the exception that the drug is not continuously pumped through the limb. Furthermore, the tumor was heated to hyperthermic temperatures using a light source, similarly as described recently [40]. In our study, the effluent fractions indicated that the majority of the infused free Dox and Dox-TSL is not retained in the tumor-bearing limb following a single passage. However, free Dox-infused limbs retained significantly more Dox than Dox-TSL infused limbs, with 4.05 ± 1.26 % ID/g versus 1.07 ± 0.51 % ID/g, respectively. These findings confirm the non-specific accumulation of free drug in healthy tissues [41]. Nevertheless, within one passage, HT-induced Dox release from TSLs could not achieve significantly higher intratumoral Dox concentrations compared NT and free Dox infusions.

A recent study by Willerding et al where the same tumor model was used as for our ILI study reported an intratumoral Dox concentration of 23.1 ± 0.4 μg Dox/g tumor tissue using an i.v. administration of 2 mg/kg and 60 min of heating [40]. This would correspond to 4.6 ± 0.1 % ID/g for an average sized (~ 250 g) rat and is also in concordance

with other recently published data using a different tumor model and 90 min of heating [42]. If one would consider this value to be Dox_{sat} in the above-mentioned formula given the long HT duration, the amount of passages required by our ILI system to achieve 98% of Dox_{sat} in the tumor would be 13.7. To the best of our knowledge, this is the first account of empirical data on drug delivery via TSL upon a single passage at the tumor site, and further complements previously reported models [10, 30, 31].

In order to translate these results to therapeutically relevant conditions, there are considerations that must be made (Table I). Firstly, our ILI experiment was conducted using commercial rat serum, which does not fully mimic the composition of the blood compartment *in vivo*. We have previously reported that the leakage of Dox from TSL *in vivo* is much more profound than when evaluated *in vitro*. Furthermore, it was shown that an immediate burst release can take place when the particles come into contact with blood components [32]. As a result, our data reveal that we cannot accurately predict the release of drug from TSL *in vivo* by solely incubating the particles at 42°C. The blood compartment is far more complex in its composition and fluid dynamics [43, 44] and more research is required to determine actual drug release kinetics and release completeness in circulation.

A possible improvement for the described ILI model would be to infuse the limb with pooled rat blood with an anti-coagulant for conditions as close to the (patho)physiological state as possible. In addition, the ILI model does not simulate the traditional pharmacokinetics and biodistribution of TSL, i.e. clearance from the systemic circulation and accumulation of the particles in distant organs. It is well-known that particles can be taken up by liver and spleen within minutes of i.v. injection in rodent models [45, 46]. Therefore, the local and limited manifestation of the ILI model is an important factor to take into account for further therapeutic translation. The flow rate of infusion, compared to that of systemic blood flow, is also an important factor for particle circulation and clearance. Not only is blood flow rate correlated to particle circulation half-life [47], it also influences the retention time of TSLs travelling through the heated tumor via the blood stream. Because the inflow pressure of the ILI was higher than the normal

Table I. Comparison of variables between the Isolated Limb Infusion model and an intravenous administration for therapy.

	Isolated Limb Infusion	I.V. administration for therapy
Drug leakage	Minimal (in commercial serum)	Higher [32]
Particle clearance	Absent	Present
Drug release	Adequate (in commercial serum)	Unknown
Blood flow	30.26 kPa (high)	12 kPa (normal)
Administration	Concentrated bolus	Bolus/ distribution in total blood volume
Dosage	~13 mg Dox/ kg leg weight	2-5 mg Dox/ kg total body weight

femoral arterial blood pressure in rat under anesthesia, it is likely that the observed TSL retention and Dox delivery constitute an under-estimation of levels that would be achieved upon systemic i.v. administration for therapy. Lastly, we have to correct for the administration method and dosage. With the presented ILI model, the TSLs are introduced into the tumor bearing limb as a highly concentrated bolus, increasing the odds for higher drug delivery. In common i.v. injections or infusions, the TSLs reach the target site in a much more diluted fashion, likely giving altered kinetics for Dox delivery. Furthermore, with ~13 mg Dox/ kg leg weight, the administered dose is rather high compared more commonly known dosages (2-5 mg/kg). This could for example cause a 2 mg/kg leg weight ILI to require 89 passages to reach intratumoral Dox accumulation values close to Dox_{sat} .

This study has validated the use of an ILI system for the investigation of quantitative drug delivery kinetics by TSLs in heated solid tumors. Recognizing the limitations of ILI, this model has nonetheless revealed the distinct influence of serum components and haemodynamics on drug release from TSL, abrogating sole dependence on *in vitro* release studies. Furthermore, Dox-TSL demonstrates superior tumor-specific accumulation compared to free Dox as less drug accumulates in the healthy tissues for the former. The ILI model may prove a useful tool for the evaluation of local drug delivery, and can be further extended to alternate forms of delivery. Overall, the evaluation of distinct TSL properties (e.g. release versus stability) in controlled, representative experimental conditions is something that can be investigated in future studies using this model.

REFERENCES

1. T.M. Allen, P.R. Cullis, Liposomal drug delivery systems: from concept to clinical applications, *Advanced drug delivery reviews*, 65 (2013) 36-48.
2. J.I. Hare, T. Lammers, M.B. Ashford, S. Puri, G. Storm, S.T. Barry, Challenges and strategies in anti-cancer nanomedicine development: An industry perspective, *Advanced drug delivery reviews*, 108 (2017) 25-38.
3. A.A. Gabizon, Liposome circulation time and tumor targeting: implications for cancer chemotherapy, *Advanced drug delivery reviews*, 16 (1995) 285-294.
4. Y. Matsumura, H. Maeda, A new concept for macromolecular therapeutics in cancer chemotherapy: mechanism of tumoritropic accumulation of proteins and the antitumor agent smancs, *Cancer research*, 46 (1986) 6387-6392.
5. V. Torchilin, Tumor delivery of macromolecular drugs based on the EPR effect, *Advanced drug delivery reviews*, 63 (2011) 131-135.
6. R.K. Jain, T. Stylianopoulos, Delivering nanomedicine to solid tumors, *Nature reviews. Clinical oncology*, 7 (2010) 653-664.
7. K.M. Laginha, S. Verwoert, G.J. Charrois, T.M. Allen, Determination of doxorubicin levels in whole tumor and tumor nuclei in murine breast cancer tumors, *Clinical cancer research : an official journal of the American Association for Cancer Research*, 11 (2005) 6944-6949.
8. A.L. Seynhaeve, B.M. Dicheva, S. Hoving, G.A. Koning, T.L. ten Hagen, Intact Doxil is taken up intracellularly and released doxorubicin sequesters in the lysosome: evaluated by in vitro/in vivo live cell imaging, *Journal of controlled release : official journal of the Controlled Release Society*, 172 (2013) 330-340.
9. A.L. Seynhaeve, S. Hoving, D. Schipper, C.E. Vermeulen, G. de Wael-Ambagtsheer, S.T. van Tiel, A.M. Eggermont, T.L. Ten Hagen, Tumor necrosis factor alpha mediates homogeneous distribution of liposomes in murine melanoma that contributes to a better tumor response, *Cancer research*, 67 (2007) 9455-9462.
10. A.A. Manzoor, L.H. Lindner, C.D. Landon, J.Y. Park, A.J. Simnick, M.R. Dreher, S. Das, G. Hanna, W. Park, A. Chilkoti, G.A. Koning, T.L. ten Hagen, D. Needham, M.W. Dewhirst, Overcoming limitations in nanoparticle drug delivery: triggered, intravascular release to improve drug penetration into tumors, *Cancer research*, 72 (2012) 5566-5575.
11. S. Mura, J. Nicolas, P. Couvreur, Stimuli-responsive nanocarriers for drug delivery, *Nature materials*, 12 (2013) 991-1003.
12. Y. Wang, D.S. Kohane, External triggering and triggered targeting strategies for drug delivery, 2 (2017) 17020.
13. G. Kong, R.D. Braun, M.W. Dewhirst, Characterization of the effect of hyperthermia on nanoparticle extravasation from tumor vasculature, *Cancer research*, 61 (2001) 3027-3032.
14. L. Li, T.L.M. ten Hagen, M. Bolkestein, A. Gasselhuber, J. Yatvin, G.C. van Rhoon, A.M.M. Eggermont, D. Haemmerich, G.A. Koning, Improved intratumoral nanoparticle extravasation and penetration by mild hyperthermia, *Journal of Controlled Release*, 167 (2013) 130-137.
15. W.J. Lokerse, M. Bolkestein, T.L. Ten Hagen, M. de Jong, A.M. Eggermont, H. Grull, G.A. Koning, Investigation of Particle Accumulation, Chemosensitivity and Thermosensitivity for Effective Solid Tumor Therapy Using Thermosensitive Liposomes and Hyperthermia, *Theranostics*, 6 (2016) 1717-1731.
16. H.A. Eddy, Alterations in tumor microvasculature during hyperthermia, *Radiology*, 137 (1980) 515-521.

17. Y. Nishimura, M. Hiraoka, S. Jo, K. Akuta, Y. Yukawa, Y. Shibamoto, M. Takahashi, M. Abe, Microangiographic and histologic analysis of the effects of hyperthermia on murine tumor vasculature, *International journal of radiation oncology, biology, physics*, 15 (1988) 411-420.
18. Y. Sakaguchi, L.C. Stephens, M. Makino, T. Kaneko, F.R. Strebel, L.L. Danhauser, G.N. Jenkins, J.M.C. Bull, Apoptosis in Tumors and Normal Tissues Induced by Whole Body Hyperthermia in Rats, *Cancer research*, 55 (1995) 5459-5464.
19. K. Ahmed, Y. Tabuchi, T. Kondo, Hyperthermia: an effective strategy to induce apoptosis in cancer cells, *Apoptosis : an international journal on programmed cell death*, 20 (2015) 1411-1419.
20. C.A. Perez, S.A. Sapareto, Thermal dose expression in clinical hyperthermia and correlation with tumor response/control, *Cancer research*, 44 (1984) 4818s-4825s.
21. W.C. Dewey, Arrhenius relationships from the molecule and cell to the clinic, *International journal of hyperthermia : the official journal of European Society for Hyperthermic Oncology, North American Hyperthermia Group*, 25 (2009) 3-20.
22. R.D. Issels, L.H. Lindner, J. Verweij, P. Wust, P. Reichardt, B.C. Schem, S. Abdel-Rahman, S. Daugaard, C. Salat, C.M. Wendtner, Z. Vujaskovic, R. Wessalowski, K.W. Jauch, H.R. Durr, F. Ploner, A. Baur-Melnyk, U. Mansmann, W. Hiddemann, J.Y. Blay, P. Hohenberger, Neoadjuvant chemotherapy alone or with regional hyperthermia for localised high-risk soft-tissue sarcoma: a randomised phase 3 multicentre study, *The Lancet. Oncology*, 11 (2010) 561-570.
23. J. Van Der Zee, M. De Bruijne, J.W. Mens, A. Ameziane, M.P. Broekmeyer-Reurink, T. Drizdal, M. Linthorst, G.C. Van Rhoon, Reirradiation combined with hyperthermia in breast cancer recurrences: overview of experience in Erasmus MC, *International journal of hyperthermia : the official journal of European Society for Hyperthermic Oncology, North American Hyperthermia Group*, 26 (2010) 638-648.
24. J.N. Weinstein, R.L. Magin, M.B. Yatvin, D.S. Zaharko, Liposomes and local hyperthermia: selective delivery of methotrexate to heated tumors, *Science (New York, N.Y.)*, 204 (1979) 188-191.
25. M.B. Yatvin, J.N. Weinstein, W.H. Dennis, R. Blumenthal, Design of liposomes for enhanced local release of drugs by hyperthermia, *Science (New York, N.Y.)*, 202 (1978) 1290-1293.
26. B. Kneidl, M. Peller, G. Winter, L.H. Lindner, M. Hossann, Thermosensitive liposomal drug delivery systems: state of the art review, *International journal of nanomedicine*, 9 (2014) 4387-4398.
27. Z. Al-Ahmady, K. Kostarelos, Chemical Components for the Design of Temperature-Responsive Vesicles as Cancer Therapeutics, *Chemical reviews*, 116 (2016) 3883-3918.
28. P.S. Yarmolenko, Y. Zhao, C. Landon, I. Spasojevic, F. Yuan, D. Needham, B.L. Viglianti, M.W. Dewhirst, Comparative effects of thermosensitive doxorubicin-containing liposomes and hyperthermia in human and murine tumours, *International journal of hyperthermia : the official journal of European Society for Hyperthermic Oncology, North American Hyperthermia Group*, 26 (2010) 485-498.
29. L. Li, T.L. ten Hagen, M. Hossann, R. Suss, G.C. van Rhoon, A.M. Eggermont, D. Haemmerich, G.A. Koning, Mild hyperthermia triggered doxorubicin release from optimized stealth thermosensitive liposomes improves intratumoral drug delivery and efficacy, *Journal of controlled release : official journal of the Controlled Release Society*, 168 (2013) 142-150.
30. A. Gasselhuber, M.R. Dreher, A. Partanen, P.S. Yarmolenko, D. Woods, B.J. Wood, D. Haemmerich, Targeted drug delivery by high intensity focused ultrasound mediated hyperthermia combined with temperature-sensitive liposomes: computational modelling and preliminary

- in vivo validation, *International journal of hyperthermia : the official journal of European Society for Hyperthermic Oncology, North American Hyperthermia Group*, 28 (2012) 337-348.
31. A. Gasselhuber, M.R. Dreher, F. Rattay, B.J. Wood, D. Haemmerich, Comparison of conventional chemotherapy, stealth liposomes and temperature-sensitive liposomes in a mathematical model, *PLoS one*, 7 (2012) e47453.
 32. W.J. Lokerse, E.C. Kneepkens, T.L. ten Hagen, A.M. Eggermont, H. Grull, G.A. Koning, In depth study on thermosensitive liposomes: Optimizing formulations for tumor specific therapy and in vitro to in vivo relations, *Biomaterials*, 82 (2016) 138-150.
 33. R.B. Armstrong, R.O. Phelps, Muscle fiber type composition of the rat hindlimb, *The American journal of anatomy*, 171 (1984) 259-272.
 34. G.J. Charrois, T.M. Allen, Drug release rate influences the pharmacokinetics, biodistribution, therapeutic activity, and toxicity of pegylated liposomal doxorubicin formulations in murine breast cancer, *Biochimica et biophysica acta*, 1663 (2004) 167-177.
 35. R.K. Jain, Determinants of tumor blood flow: a review, *Cancer research*, 48 (1988) 2641-2658.
 36. R.J. Gillies, P.A. Schornack, T.W. Secomb, N. Raghunand, Causes and effects of heterogeneous perfusion in tumors, *Neoplasia (New York, N.Y.)*, 1 (1999) 197-207.
 37. Y. Wang, Y. Cong, J. Li, X. Li, B. Li, S. Qi, Comparison of invasive blood pressure measurements from the caudal ventral artery and the femoral artery in male adult SD and Wistar rats, *PLoS one*, 8 (2013) e60625.
 38. L.H. Lindner, M.E. Eichhorn, H. Eibl, N. Teichert, M. Schmitt-Sody, R.D. Issels, M. Dellian, Novel temperature-sensitive liposomes with prolonged circulation time, *Clinical cancer research : an official journal of the American Association for Cancer Research*, 10 (2004) 2168-2178.
 39. F. Brunstein, I.D. Santos, L.M. Ferreira, S.T. van Tiel, A.M. Eggermont, T.L. Ten Hagen, Histamine combined with melphalan in isolated limb perfusion for the treatment of locally advanced soft tissue sarcomas: preclinical studies in rats, *Acta chirurgica brasileira / Sociedade Brasileira para Desenvolvimento Pesquisa em Cirurgia*, 20 (2005) 275-279.
 40. L. Willerding, S. Limmer, M. Hossann, A. Zengerle, K. Wachholz, T.L. Ten Hagen, G.A. Koning, R. Sroka, L.H. Lindner, M. Peller, Method of hyperthermia and tumor size influence effectiveness of doxorubicin release from thermosensitive liposomes in experimental tumors, *Journal of controlled release : official journal of the Controlled Release Society*, 222 (2016) 47-55.
 41. K.J. Patel, O. Tredan, I.F. Tannock, Distribution of the anticancer drugs doxorubicin, mitoxantrone and topotecan in tumors and normal tissues, *Cancer chemotherapy and pharmacology*, 72 (2013) 127-138.
 42. N. Hijnen, E. Kneepkens, M. de Smet, S. Langereis, E. Heijman, H. Grull, Thermal combination therapies for local drug delivery by magnetic resonance-guided high-intensity focused ultrasound, *Proceedings of the National Academy of Sciences of the United States of America*, 114 (2017) E4802-e4811.
 43. M.A. Dobrovolskaia, P. Aggarwal, J.B. Hall, S.E. McNeil, Preclinical studies to understand nanoparticle interaction with the immune system and its potential effects on nanoparticle biodistribution, *Molecular pharmaceuticals*, 5 (2008) 487-495.
 44. S.M. Moghimi, A.C. Hunter, T.L. Andresen, Factors controlling nanoparticle pharmacokinetics: an integrated analysis and perspective, *Annual review of pharmacology and toxicology*, 52 (2012) 481-503.
 45. T. Ishida, H. Harashima, H. Kiwada, Liposome clearance, *Bioscience reports*, 22 (2002) 197-224.

46. X. Yan, G.L. Scherphof, J.A. Kamps, Liposome opsonization, *Journal of liposome research*, 15 (2005) 109-139.
47. K.M. Tsoi, S.A. MacParland, X.Z. Ma, V.N. Spetzler, J. Echeverri, B. Ouyang, S.M. Fadel, E.A. Sykes, N. Goldaracena, J.M. Kathis, J.B. Conneely, B.A. Alman, M. Selzner, M.A. Ostrowski, O.A. Adeyi, A. Zilman, I.D. McGilvray, W.C. Chan, Mechanism of hard-nanomaterial clearance by the liver, *Nature materials*, 15 (2016) 1212-1221.

CHAPTER 6

Feasibility study on magnetic nanoparticle-entrapping liposomes for localized hyperthermia and image-guided drug delivery to solid tumors

Wouter J.M. Lokerse

Sophie Laurent

Sarah Belaïd

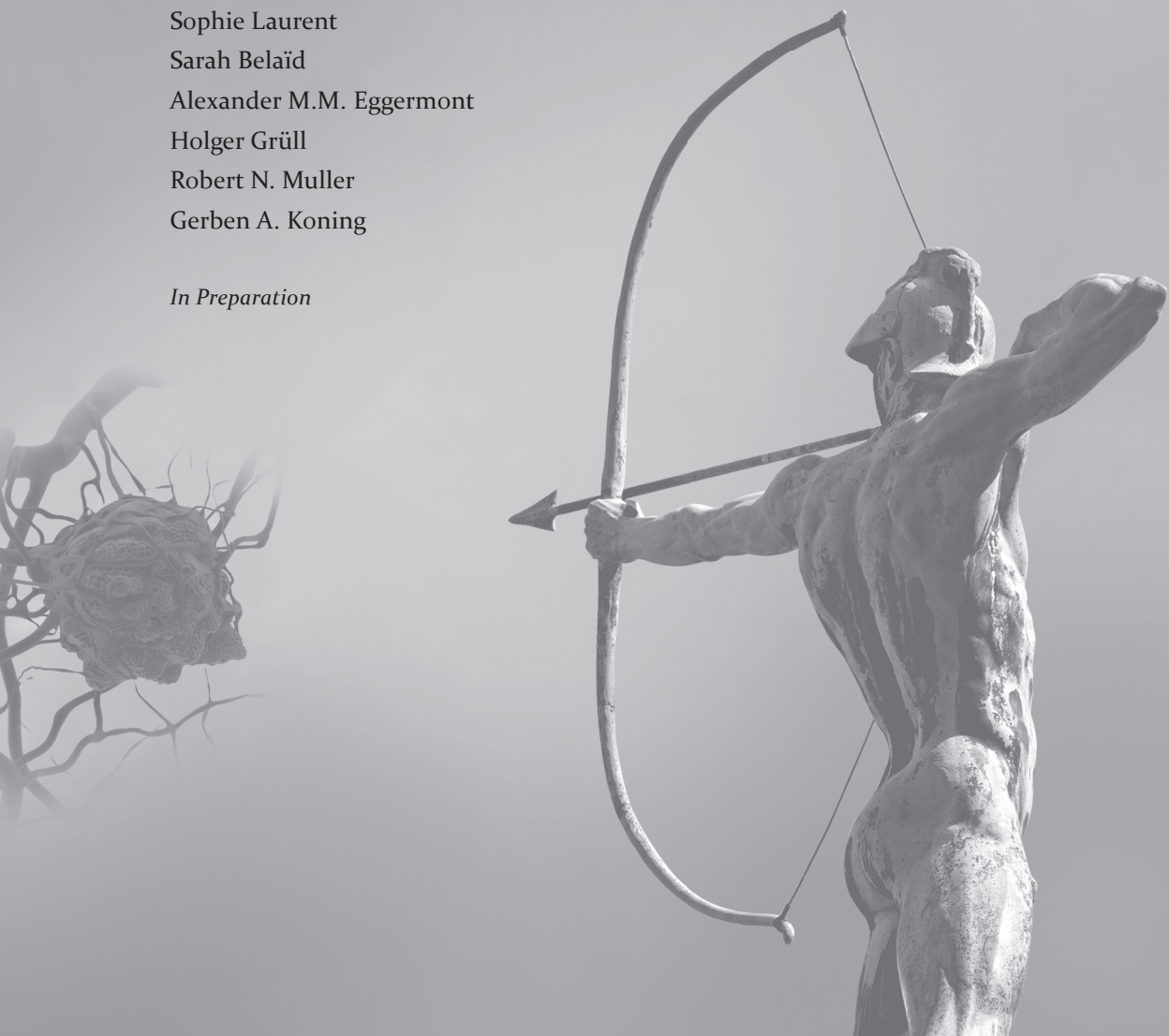
Alexander M.M. Eggermont

Holger Gröll

Robert N. Muller

Gerben A. Koning

In Preparation



ABSTRACT

In this study, the goal was to produce magnetoliposomes (MLs) with either iron oxide nanoparticles entrapped in the lipid bilayer, or encapsulated in the aqueous core of a liposome to establish a nanocarrier that is capable to be imaged by MRI and can release drug by hyperthermia (HT) upon exposure to an alternating magnetic field (AMF). Film hydration, reversed phase evaporation, detergent removal and modified ethanol injection were the liposome preparation techniques used to compare loading efficacy of oleic acid (C18:1) coated magnetic nanoparticles (MNPs) into liposome bilayers. (Cryo-) transmission electron microscopy (TEM) and inductively coupled plasma optical emission spectrometry (ICP-OES) indicated that the film hydration or reversed phase evaporation methods produced mainly MNP agglomerates next to the DSPC:DSPE-PEG₂₀₀₀ (95:5) liposome population. ICP-OES analysis showed that the detergent removal and modified ethanol injection method showed better retention of iron from C18:1 MNPs, but (Cryo-) TEM imaged indicated that these two methods produced detergent-lipid micelles and disc-shaped micelles, respectively. For incorporation of hydrophilic, 3-(triethoxysilyl)propyl succinic anhydride (TEPSA) coated MNPs, we were capable to produce magnetoliposomes using film hydration and reversed phase evaporation with a higher loading efficiency than for C18:1 MNPs. However, the loading efficacy was not high enough to conduct consecutive studies on HT and *in vivo* use.

INTRODUCTION

Mild hyperthermia (HT) in the clinic implies subtle heating of a tissue to 40–43°C. This form of treatment has already shown great potency in enhancing the efficacy of chemo- and/ or radiotherapy [1, 2]. Typically, heating of the target tissue is established using radiofrequency based applicators [3, 4] or emerging alternatives, such as high intensity focused ultrasound [5, 6]. As an alternative, iron oxide (magnetic) nanoparticles (MNPs) have been proposed and investigated for local heating using externally applied alternating magnetic fields (AMF) [7, 8]. Superparamagnetic particles that are sufficiently small to contain only a single magnetic domain heat in an AMF through remagnetisation when the magnetization direction coincides with magnetic the easy axis (Néel relaxation) [7]. However, the amount of heat produced by MNPs of this size is negligible for large volume heating [9]. When superparamagnetic cores are brought in close proximity they are considered multi-domain (superferromagnetism) and have a higher heating potential because of magnetic hysteresis [8, 10]. Here the material is first brought into a saturated state by forcing all the magnetic domains in one direction and it retains this magnetization if the magnetic field would be removed. To release energy/ heat from the material, multiple magnetic domains have to be forced back to the ground state by turning the magnetization direction 180 degrees [7, 11, 12]. Tumors occasionally have a chaotically organized vascular system which allow nanoparticles to extravasate from the blood stream into the tumor interstitium [13, 14], a system which is known as the enhanced permeability and retention (EPR) effect and this has been exploited for drug delivery purposes for decades [15]. The EPR effect could also cause i.v. administered MNPs to accumulate in the tumor and generate heat when an external AMF is applied [16, 17]. However, the accumulation of particles via this mechanism is often heterogeneous and inconsistent [18], which often requires MNPs to be intratumorally administered for sufficient heating potential [19, 20].

Thermosensitive liposomes (TSLs) are particles which encapsulate a chemotherapeutic compound and do not rely on the EPR effect for high drug delivery to solid tumors as TSLs release their contents intravascularly when passing through the blood vessels of a heated tumor [21, 22]. The lipid bilayer of TSLs is composed of lipids that undergo a phase transition at hyperthermic temperatures which facilitates drug release [22, 23]. Heating of the lipid bilayer can be achieved by encapsulation of hydrophilic MNPs in the aqueous lumen [24–26] or by incorporation of hydrophobic MNPs in the lipid bilayer of the liposome. However, the latter is restricted to particles below a cut-off diameter of ~6.5 nm [27–29]. Nevertheless, incorporation of MNPs in a liposomal bilayer might hold several advantages over MNPs entrapped in the aqueous lumen of the liposome. Firstly, MNPs encapsulated in the lumen of the liposome require heating of the entire bulk fluid of the lumen in order to induce a phase transition of the lipid bilayer, whereas the bilayer

incorporated MNPs generate heat much more locally and do not require bulk fluid heating. Furthermore, MNP oscillation while exposed to the AMF might also induce physical stress to the lipid bilayer, thereby facilitating drug release [30].

In this study, we have tested the feasibility of incorporating oleic acid (C18:1) coated MNPs into the liposome bilayer for direct heating. As a second approach, we investigated the loading of hydrophilic triethoxysilylpropyl succinic anhydride (TEPSA) coated MNPs into the aqueous core of the liposome. Samples were characterized with (cryo-) transmission electron microscopy (TEM) and inductively coupled plasma optical emission spectrometry (ICP-OES) to observe the liposome structure, loading of MNPs and to quantify iron content.

MATERIALS AND METHODS

Materials

1,2-distearoyl-*sn*-glycero-3-phosphocholine (DSPC) and 1,2-distearoyl-*sn*-glycero-3-phosphoethanolamine-N-[methoxy(polyethylene glycol)-2000] (DSPE-PEG₂₀₀₀) were purchased from Lipoid (Ludwigshafen, Germany). Octyl β -D-glucopyranoside (OG) was purchased from Sigma (St Louis, Missouri). Float-A-Lyzer (8-10kDa) was purchased from Spectrum Labs (Los Angeles, California). Sepharose CL-4B was obtained from GE-healthcare (Freiburg, Germany). C18:1 and triethoxysilylpropyl succinic anhydride (TEPSA) coated MNPs were obtained as described before [31, 32]. Crystal diameter (core plus amorphous layer) of the C18:1 coated MNPs was on average 5 nm and for TEPSA coated particles 10 nm.

Preparation of magnetoliposomes using film hydration

200 μ mol of lipid (95:5-DSPC:DSPE-PEG₂₀₀₀) was dissolved in chloroform: methanol (9:1) and 5 μ mol (Fe) of C18:1 MNPs (dispersed in chloroform) were added. The organic solvent was evaporated until a lipid/ MNP film was produced. The lipid film was further dried in a steady nitrogen stream to remove any remaining solvent. Subsequently, the film was hydrated with HEPES buffered saline pH 7.4 (10 mM HEPES, 135 mM NaCl) followed by magnetic separation of MNP agglomerates from the liposome fraction by an externally placed neodymium magnet. The liposomes were extruded through two times 400, three times 200, three times 100 and two times 80 nm polycarbonate filters. Liposome hydrodynamic diameter and polydispersity index (PDI) were determined by dynamic light scattering (DLS) using a Zetasizer (Malvern Instruments, Malvern, UK). When TEPSA-MNPs were used, 8 μ mol (Fe) was included into the hydration volume and unincorporated MNPs were separated from MLs by an 18 x 1.5 cm sepharose CL-4B column. MNP loading efficacy was determined by ICP-OES.

Preparation of magnetoliposomes using reversed phase evaporation

200 μmol of lipid (95:5-DSPC:DSPE-PEG₂₀₀₀) was dissolved in 24 mL chloroform/di-isopropylether (1:1) and 5 μmol (Fe) of C18:1-MNPs (dispersed in chloroform) was added. 8mL HEPES buffered saline pH 7.4 was added and the solution was (probe) sonicated briefly to obtain a brown colored emulsion. The organic solvents were gradually removed using a rotation evaporator for approximately 1 hour. During the evaporation, first a gel state formed which later collapsed into a liposome solution in the remaining aqueous phase. The following extrusion and purification procedures were similar as for film hydration. MNP loading efficacy was determined by ICP-OES.

Preparation of magnetoliposomes using detergent removal

200 μmol of lipid (95:5-DSPC:DSPE-PEG₂₀₀₀) was dissolved in chloroform: methanol (9:1) and 5 μmol (Fe) of C18:1-MNPs (dispersed in chloroform) was added. A lipid/MNP film was made similar to the film hydration method, which was hydrated in a 35 mM OG solution in HEPES buffered saline pH 7.4. This solution was introduced into a Float-A-Lyzer (8-10 kDa) and dialysis was performed under gentle stirring against 2L of HEPES buffered saline pH 7.4 five times for 1 hour and once overnight at 65°C. Liposome size and PDI were determined using DLS and MNP loading efficacy was determined by ICP-OES.

Preparation of magnetoliposomes by modified ethanol injection

The method is similar as described in previous publications by Maitani and colleagues [33, 34]. In short, 200 μmol of lipid (95:5-DSPC:DSPE-PEG₂₀₀₀) was dissolved in 7.5 mL 60°C ethanol and 5 μmol (Fe) of C18:1-MNPs (dispersed in chloroform) were added. Under rapid stirring, 25 mL of 60°C HEPES buffered saline pH 7.4 was added. The ethanol and chloroform was gradually removed, using a rotation evaporator. Liposome size and pdi were determined using DLS and MNP loading efficacy was determined by ICP-OES.

Electron microscopy

Cryo-TEM was performed similar as described in Lokerse et al [35]. All TEM images were obtained using a Microscope Leo960E operating at an accelerating voltage of 60kV (Oregon, USA). The sample was prepared by placing a drop of diluted iron oxide nanoparticle suspension on a carbon-coated copper grid, followed by drying at room temperature.

Statistics

All statistical tests were performed using Graphpad Prism version 7 software.

RESULTS

Preparation of liposomes loaded with MNPs inside bilayers by film hydration

Direct extrusion after hydration of a lipid/ C18:1 MNP film caused membrane obstruction and therefore large MNP agglomerates had to be removed from the sample by magnetic separation prior to extrusion. Extrusion two times through a 400 nm filter and three times through a 200 nm filter resulted in a liposome batch with a $0.57 \pm 0.14 \cdot 10^{-4}$ Fe/PO₄ ratio (Table I; encapsulation efficiency 0.23 ± 0.06 %). Cryo-TEM analysis of these samples indicated that there were very few C18:1 MNPs that interacted with a liposome membrane (Figure 1A) and that the majority of these particles agglomerated (Figure 2A and 2C).

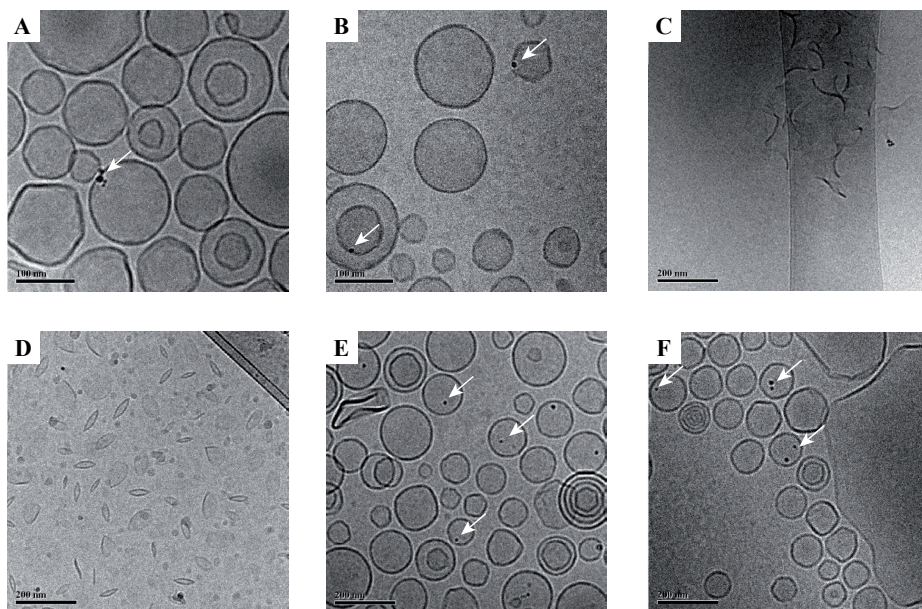


Figure 1. Cryo-TEM imaging of differently prepared magnetoliposomes. Oleic acid coated MNPs (white arrows) incorporated minimally into liposomal bilayers when film hydration (A) or reversed phase evaporation (B) was used. Detergent removal samples (C) did not show any nanoparticle structures in the sample, only seemingly filament-like membrane-detergent intermediates. The modified ethanol injection method (D) produced disc-shaped micelles and MNPs could not be observed in the sample. TEPSA coated MNPs were incorporated more effectively in the aqueous core of the liposomes (white arrows) when film hydration or reversed phase evaporation was used. Scale bar indicates 100 nm for A and B and 200 nm for C-F.

Preparation of liposomes loaded with MNPs inside bilayers by reversed phase evaporation

For reversed phase evaporation, the same extrusion and purification strategy was applied as for the film hydration method described above. After magnetic separation and

extrusion through 400 and 200 nm filters, the Fe/PO₄ ratio was with $1.07 \pm 0.46 \cdot 10^{-4}$ (Table 1; encapsulation efficiency 0.43 ± 0.18 %) only slightly higher than for batches prepared by film hydration. However, similar MNP agglomeration and low liposome bilayer encapsulation was observed after additional extrusion through 100 and 80 nm filters (Figure 1B, 2B and 2D).

Table 1. Size and loading characteristics of different liposome preparation techniques determined by DLS and ICP-OES. For TEPSA-MNPs, only the film hydration and reversed phase evaporation technique were performed (T). For film hydration and reversed phase evaporation using C18:1 MNPs, samples were subjected to magnetic separation to remove large MNP agglomerates and extruded through 400 and 200 nm filters. The TEPSA magnetoliposome samples were extruded through the same filters and unencapsulated MNPs were removed by size exclusion chromatography. N=3 samples for each preparation method.

	Hydrodynamic diameter (nm)	Polydispersity index	Fe/ PO ₄ (mol/ mol)
Film Hydration	185 ± 9	0.09 ± 0.03	$0.57 \pm 0.14 \cdot 10^{-4}$
Reversed Phase Evaporation	173 ± 20	0.13 ± 0.07	$1.07 \pm 0.46 \cdot 10^{-4}$
Detergent Removal	100 ± 20	0.24 ± 0.01	$1.43 \pm 0.04 \cdot 10^{-4}$
Modified Ethanol Injection	65 ± 3	0.06 ± 0.01	$0.77 \pm 0.43 \cdot 10^{-4}$
Film Hydration (T)	183 ± 7	0.08 ± 0.02	$0.88 \pm 0.29 \cdot 10^{-4}$
Reversed Phase Evaporation (T)	175 ± 6	0.12 ± 0.03	$0.57 \pm 0.20 \cdot 10^{-4}$

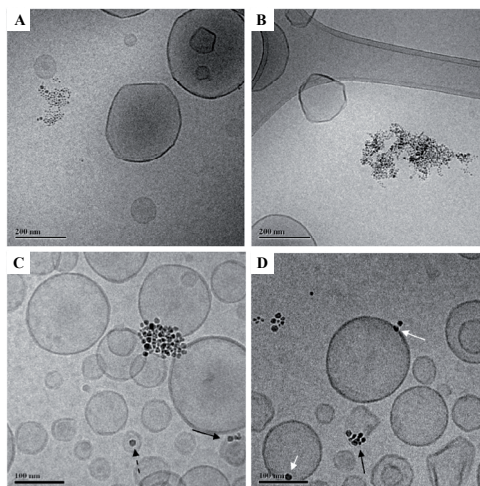


Figure 2. Cryo-TEM images of MNP agglomeration using the film hydration method (A, C) or reversed phase evaporation (B, D). Samples were subjected to magnetic separation for large MNP agglomerate removal and extruded. Small agglomerates could still be observed after magnetic separation (A, B). At a low incidence, some MNPs appear inside liposomes (C; dashed arrow), possibly interact with the liposomal bilayer (C, D; solid arrow) or are found in the liposomal bilayer (D; solid white arrow).

Preparation of liposomes loaded with MNPs inside bilayers by detergent removal

Hydration of a lipid/ C18:1 MNP film in a concentrated Triton X-100 solution seemed to result in a lowering of MNP agglomeration as could be observed by magnetic separation and (Figure 3). Because Triton X-100 has a low critical micelle concentration and is difficult to dialyze out of a mixed micelle population, OG was selected as the detergent of choice for the liposome generation by detergent removal. ICP-OES measurements on these OG hydrated lipid/ C18:1 MNP films showed a Fe/PO_4 ratio of $1.43 \pm 0.04 \cdot 10^{-4}$ after magnetic separation (Table I; encapsulation efficiency $0.57 \pm 0.02 \%$), which was another slight improvement compared to the two previously described methods. Removal of the OG by dialysis was not successful and intermediate lipid-OG structures were observed by Cryo-TEM (Figure 1C). However, TEM analysis occasionally showed small MNP clusters encapsulated in micelle-like structures (Figure 4A and 4B)

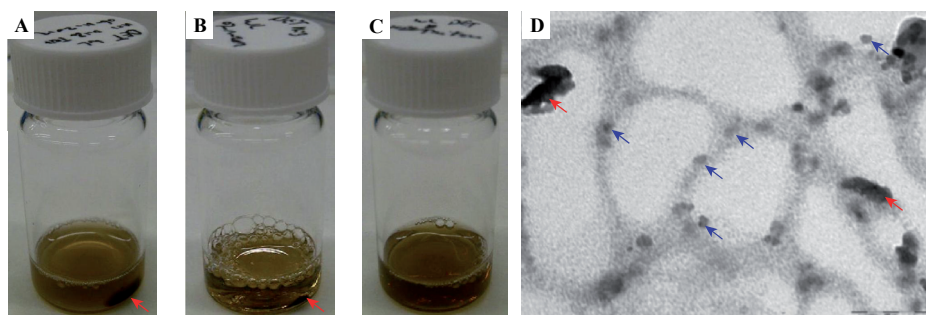


Figure 3. Results of lipid/ C18:1 MNP film hydration with Triton X-100. When the concentration of Triton X-100 for hydration of the lipid film was increased from 0.1 (A), to 1 (B) and to 10 w/v % (C), a decrease in MNP agglomeration could be observed after magnetic separation (red arrows in A and B). TEM recordings (D) of a 10% Triton X-100 hydrated lipid/ C18:1 MNP film show a detergent-lipid mesh with individual MNPs (blue arrows) and small MNP agglomerates (red arrows) embedded inside.

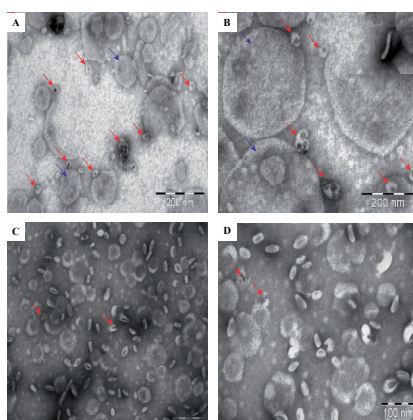


Figure 4. TEM images of MNPs in detergent removal (A and B) and modified ethanol injection samples (C and D). Red arrows indicate the MNPs. Scale bars in A-C represent 200 nm and 100 nm in D.

Preparation of liposomes loaded with MNPs inside bilayers by modified ethanol injection

The modified ethanol injection method used in these studies produced particles with a hydrodynamic diameter of 65 ± 3 nm, but was considerably smaller than the average liposome (± 100 nm). Despite that after magnetic separation the sample had a Fe/PO₄ ratio of $0.77 \pm 0.43 \cdot 10^{-4}$ (Table 1; encapsulation efficiency 0.31 ± 0.17 %), very few C18:1 MNPs could be observed in the cryo-TEM images (Figure 1D). Furthermore, the particles observed in these images were disc-shaped lipid micelles. TEM analysis showed some MNPs which were embedded within these micelles (Figure 4C and 4D; red arrows).

Preparation of liposomes loaded with MNPs inside the aqueous core

To obtain liposomes with hydrophilic, TEPSA coated MNPs inside the liposome aqueous core, we applied film hydration and reversed phase evaporation as preparation methods. After extrusion (two times 400, three times 200, three times 100 and two times 80 nm) and removal of unencapsulated MNPs by size exclusion chromatography, film hydration liposome samples had a Fe/PO₄ ratio of $0.88 \pm 0.29 \cdot 10^{-4}$ and reversed phase evaporation liposomes a Fe/PO₄ ratio of $0.57 \pm 0.20 \cdot 10^{-4}$ (Table 1; encapsulation efficiency 0.22 ± 0.07 % and 0.14 ± 0.05 %, respectively). However, the amount of MNPs that were loaded into liposomes was not higher than two per liposome (Figure 1E and 1F), which makes the loading efficacy too low for conducting any follow up experiments.

DISCUSSION

In this study, we assessed the feasibility of producing MLs with MNPs incorporated into the liposome bilayer or the aqueous core. Several liposome preparation techniques and surface modifications to the MNPs have been applied in order to produce MLs with a high MNP loading efficacy. However, the latter could not be achieved in this study. Several recently published articles give a possible explanation on the obtained results [36-39].

Amstad and coworkers are one of the few research groups that have described the successful encapsulation of MNPs in a liposome bilayer [37]. In these studies, palmityl-nitroDOPA was used as a MNP surface modification, which resulted in a ~30% loading efficacy of these particles into liposomes. Palmityl-nitroDOPA was compared to C18:1 as a MNP surface modification and for the latter, agglomeration was similar as observed in this study. Amstad and colleagues emphasized that C18:1 is a reversibly adsorbing dispersant, which makes MNPs with this surface modification more likely agglomerate [36, 37]. Others have also shown that oleic acid stabilized MNPs are more likely to be encapsulated in the hydrophobic core of a lipid micelle, rather than to be embedded

in a liposome membrane [38, 39]. We hypothesize that the mono-unsaturation and the length of the oleic acid carbon chain might hamper effective loading of MNPs in liposome bilayers (Table 2). Another illustrative observation is that in the methods mentioned above that generated micelles, slightly higher iron levels could be detected, thereby confirming the high affinity for these hydrophobic MNPs with micelles over liposomes [39, 40]. Removal of OG by dialysis in the detergent removal protocol was not fully established, which was likely the cause of the lipids used in this study (DSPC:DSPE-PEG₂₀₀₀). In most studies describing liposome preparation by detergent removal, Egg-PC is used [41, 42]. Egg-PC is a mixture of lipids with one or more double bonds, which might create a micelle which is more prone to release detergent monomers which are consecutively removed by dialysis. However, increased MNP aggregation after dialysis was observed and indicated that the amount of detergent in the dialysis bag decreased to a certain extent over time. The modified ethanol injection method, although used with a highly similar lipid concentration and ethanol : aqueous phase ratio produced disc-shaped micelles instead of liposomes as described by Maitani et al [33, 34]. We suggest that the addition of DSPE-PEG₂₀₀₀ to this reaction mixture might have caused lipids to organize into micelles using this liposome preparation technique since DSPE-PEG₂₀₀₀ has the potential to form micelles [43]. Furthermore, TEM observations showed a remarkably low MNP encapsulation into these micelles despite the high encapsulation efficacy suggested by ICP-OES. This could be caused by a partial dissociation of iron oleate complexes from the C18:1 MNPs in the 60 °C ethanol, which could still be detected by ICP-OES, thereby giving a false positive result on encapsulated MNPs in disc-shaped micelles.

Table 2. MNP crystal diameter (core plus amorphous layer) distribution based on TEM observations and estimated increase in diameter based on the chemical structures of C10:0, C14:0 or C18:0 surface coatings. The sizes marked in green represent the particle sizes below the cut-off for liposome membrane incorporation of 6.5 nm.

Crystal diameter (nm)	%	Crystal diameter + C10:0 (nm)	Crystal diameter + C14:0 (nm)	Crystal diameter + C18:0 (nm)
3	14	5.25	6.25	7.25
4	28	6.25	7.25	8.25
5	36	7.25	8.25	9.25
6	18	8.25	9.25	10.25
7	3	9.25	10.25	11.25
8	1	10.25	11.25	12.25

Next to MNP surface modification and liposome preparation methods, also the size of the MNPs plays an important role in successful embedment into the liposome bilayer. From several TEM images of the C18:1 MNPs, we established a crystal diameter distribution profile (Table 2). Given these data, 96 % of all MNPs would be below the ~6.5 nm cut off range for liposome membrane incorporation [27-29]. However, the increase in size of the MNP including the surface coating reduces the amount of MNPs that meet this criterion. In these conditions, none of the C18:0 coated MNPs would be sufficiently small for bilayer embedment. Furthermore, the double bond in the carbon tail of C18:1 coated MNPs could also create steric hindrance for effective embedment into a C18:0 lipid membrane.

Our experiments for the incorporation of hydrophilic, TEPSA coated MNPs into the aqueous core of the liposome were successful, but with a very low yield of MNPs per liposome. We aimed to make 200 μ mol batches of MLs, which would be sufficient for a substantial amount of consecutive animal studies. However, with the current MNP loading efficacy, follow up studies are not realistic. Therefore, we required highly more concentrated TEPSA MNP batches for lipid film hydration and realizing MLs with a higher MNP loading efficacy, which were not available at this time. MLs with hydrophilic MNPs in the aqueous core are often produced by hydrating fewer lipids in a more concentrated MNP solution [24, 44, 45]. Nevertheless, for intensive (large) animal studies or clinical trials, more effective methodologies need to be investigated to obtain adequate ML batch sizes.

We were not successful in realizing an ML with a high quantity of MNPs in the bilayer. The hydrophobic MNPs used in this study can interact with lipids and detergents but are rather incorporated into micelles instead of embedded into liposomal bilayers. TEPSA-MNPs were successfully loaded into the aqueous core of the liposome, but the loading efficacy was too low to conduct further studies. Nevertheless, the presented results give insight into the pitfalls of effective ML production with high MNP loading efficacy and the feasibility of clinical transfer of this technology.

REFERENCES

1. R.D. Issels, L.H. Lindner, J. Verweij, P. Wust, P. Reichardt, B.C. Schem, S. Abdel-Rahman, S. Daugaard, C. Salat, C.M. Wendtner, Z. Vujaskovic, R. Wessalowski, K.W. Jauch, H.R. Durr, F. Ploner, A. Baur-Melnyk, U. Mansmann, W. Hiddemann, J.Y. Blay, P. Hohenberger, Neoadjuvant chemotherapy alone or with regional hyperthermia for localised high-risk soft-tissue sarcoma: a randomised phase 3 multicentre study, *The Lancet. Oncology*, 11 (2010) 561-570.
2. J. van der Zee, D. Gonzalez Gonzalez, G.C. van Rhoon, J.D. van Dijk, W.L. van Putten, A.A. Hart, Comparison of radiotherapy alone with radiotherapy plus hyperthermia in locally advanced pelvic tumours: a prospective, randomised, multicentre trial. Dutch Deep Hyperthermia Group, *Lancet (London, England)*, 355 (2000) 1119-1125.
3. M. Hiraoka, S. Jo, K. Akuta, Y. Nishimura, M. Takahashi, M. Abe, Radiofrequency capacitive hyperthermia for deep-seated tumors. I. Studies on thermometry, *Cancer*, 60 (1987) 121-127.
4. S.A. Curley, Radiofrequency Ablation of Malignant Liver Tumors, *Annals of Surgical Oncology*, 10 (2003) 338-347.
5. C.R. Hill, G.R.t. Haar, High intensity focused ultrasound—potential for cancer treatment, *The British Journal of Radiology*, 68 (1995) 1296-1303.
6. J.E. Kennedy, High-intensity focused ultrasound in the treatment of solid tumours, *Nature reviews. Cancer*, 5 (2005) 321-327.
7. S. Laurent, S. Dutz, U.O. Hafeli, M. Mahmoudi, Magnetic fluid hyperthermia: focus on superparamagnetic iron oxide nanoparticles, *Advances in colloid and interface science*, 166 (2011) 8-23.
8. C.L. Dennis, R. Ivkov, Physics of heat generation using magnetic nanoparticles for hyperthermia, *International journal of hyperthermia : the official journal of European Society for Hyperthermic Oncology, North American Hyperthermia Group*, 29 (2013) 715-729.
9. S. Tong, C.A. Quinto, L. Zhang, P. Mohindra, G. Bao, Size-Dependent Heating of Magnetic Iron Oxide Nanoparticles, *ACS nano*, (2017).
10. J. Pearce, A. Giustini, R. Stigliano, P. Jack Hoopes, Magnetic Heating of Nanoparticles: The Importance of Particle Clustering to Achieve Therapeutic Temperatures, *Journal of Nanotechnology in Engineering and Medicine*, 4 (2013) 0110071-01100714.
11. L.C. Branquinho, M.S. Carrião, A.S. Costa, N. Zufelato, M.H. Sousa, R. Miotto, R. Ivkov, A.F. Bakuzis, Effect of magnetic dipolar interactions on nanoparticle heating efficiency: Implications for cancer hyperthermia, *Scientific Reports*, 3 (2013) 2887.
12. S. Ruta, R. Chantrell, O. Hovorka, Unified model of hyperthermia via hysteresis heating in systems of interacting magnetic nanoparticles, *Scientific Reports*, 5 (2015) 9090.
13. H.F. Dvorak, L.F. Brown, M. Detmar, A.M. Dvorak, Vascular permeability factor/vascular endothelial growth factor, microvascular hyperpermeability, and angiogenesis, *The American journal of pathology*, 146 (1995) 1029-1039.
14. H. Hashizume, P. Baluk, S. Morikawa, J.W. McLean, G. Thurston, S. Roberge, R.K. Jain, D.M. McDonald, Openings between defective endothelial cells explain tumor vessel leakiness, *The American journal of pathology*, 156 (2000) 1363-1380.
15. T.M. Allen, P.R. Cullis, Drug delivery systems: entering the mainstream, *Science (New York, N.Y.)*, 303 (2004) 1818-1822.
16. C.S. Kumar, F. Mohammad, Magnetic nanomaterials for hyperthermia-based therapy and controlled drug delivery, *Advanced drug delivery reviews*, 63 (2011) 789-808.

17. A. Hervault, N.T. Thanh, Magnetic nanoparticle-based therapeutic agents for thermo-chemotherapy treatment of cancer, *Nanoscale*, 6 (2014) 11553-11573.
18. T. Lammers, F. Kiessling, W.E. Hennink, G. Storm, Drug targeting to tumors: principles, pitfalls and (pre-) clinical progress, *Journal of controlled release : official journal of the Controlled Release Society*, 161 (2012) 175-187.
19. Q. Zhao, L. Wang, R. Cheng, L. Mao, R.D. Arnold, E.W. Howerth, Z.G. Chen, S. Platt, Magnetic Nanoparticle-Based Hyperthermia for Head & Neck Cancer in Mouse Models, *Theranostics*, 2 (2012) 113-121.
20. J. Kolosnjaj-Tabi, R. Di Corato, L. Lartigue, I. Marangon, P. Guardia, A.K. Silva, N. Luciani, O. Clement, P. Flaud, J.V. Singh, P. Decuzzi, T. Pellegrino, C. Wilhelm, F. Gazeau, Heat-generating iron oxide nanocubes: subtle “deconstructors” of the tumoral microenvironment, *ACS nano*, 8 (2014) 4268-4283.
21. B. Kneidl, M. Peller, G. Winter, L.H. Lindner, M. Hossann, Thermosensitive liposomal drug delivery systems: state of the art review, *International journal of nanomedicine*, 9 (2014) 4387-4398.
22. Z. Al-Ahmady, K. Kostarelos, Chemical Components for the Design of Temperature-Responsive Vesicles as Cancer Therapeutics, *Chemical reviews*, 116 (2016) 3883-3918.
23. C.D. Landon, J.-Y. Park, D. Needham, M.W. Dewhirst, Nanoscale Drug Delivery and Hyperthermia: The Materials Design and Preclinical and Clinical Testing of Low Temperature-Sensitive Liposomes Used in Combination with Mild Hyperthermia in the Treatment of Local Cancer, *The open nanomedicine journal*, 3 (2011) 38-64.
24. P. Pradhan, J. Giri, F. Rieken, C. Koch, O. Mykhaylyk, M. Doblinger, R. Banerjee, D. Bahadur, C. Plank, Targeted temperature sensitive magnetic liposomes for thermo-chemotherapy, *Journal of controlled release : official journal of the Controlled Release Society*, 142 (2010) 108-121.
25. R. Di Corato, G. Bealle, J. Kolosnjaj-Tabi, A. Espinosa, O. Clement, A.K. Silva, C. Menager, C. Wilhelm, Combining magnetic hyperthermia and photodynamic therapy for tumor ablation with photoresponsive magnetic liposomes, *ACS nano*, 9 (2015) 2904-2916.
26. D. Calle, V. Negri, P. Ballesteros, S. Cerdan, Magnetoliposomes loaded with poly-unsaturated fatty acids as novel theranostic anti-inflammatory formulations, *Theranostics*, 5 (2015) 489-503.
27. V.V. Ginzburg, S. Balijepalli, Modeling the thermodynamics of the interaction of nanoparticles with cell membranes, *Nano letters*, 7 (2007) 3716-3722.
28. W. Haeng Sub, L. Kyuyong, P. Hyuk Kyu, Interfacial energy consideration in the organization of a quantum dot-lipid mixed system, *Journal of Physics: Condensed Matter*, 20 (2008) 494211.
29. O. Bixner, E. Reimhult, Controlled magnetosomes: Embedding of magnetic nanoparticles into membranes of monodisperse lipid vesicles, *Journal of colloid and interface science*, 466 (2016) 62-71.
30. M.R. Preiss, G.D. Bothun, Stimuli-responsive liposome-nanoparticle assemblies, *Expert opinion on drug delivery*, 8 (2011) 1025-1040.
31. S. Belaid, S. Laurent, M. Vermeesch, L. Vander Elst, D. Perez-Morga, R.N. Muller, A new approach to follow the formation of iron oxide nanoparticles synthesized by thermal decomposition, *Nanotechnology*, 24 (2013) 055705.
32. J.L. Bridot, D. Stanicki, S. Laurent, S. Boutry, Y. Gossuin, P. Leclere, R. Lazzaroni, L. Vander Elst, R.N. Muller, New carboxysilane-coated iron oxide nanoparticles for nonspecific cell labelling, *Contrast media & molecular imaging*, 8 (2013) 466-474.

33. Y. Maitani, H. Soeda, W. Junping, K. Takayama, MODIFIED ETHANOL INJECTION METHOD FOR LIPOSOMES CONTAINING beta-SITOSTEROL beta-D-GLUCOSIDE, *Journal of liposome research*, 11 (2001) 115-125.
34. Y. Maitani, Lipoplex formation using liposomes prepared by ethanol injection, *Methods in molecular biology* (Clifton, N.J.), 605 (2010) 393-403.
35. W.J. Lokerse, E.C. Kneepkens, T.L. ten Hagen, A.M. Eggermont, H. Grull, G.A. Koning, In depth study on thermosensitive liposomes: Optimizing formulations for tumor specific therapy and in vitro to in vivo relations, *Biomaterials*, 82 (2016) 138-150.
36. E. Amstad, T. Gillich, I. Bilecka, M. Textor, E. Reimhult, Ultrastable iron oxide nanoparticle colloidal suspensions using dispersants with catechol-derived anchor groups, *Nano letters*, 9 (2009) 4042-4048.
37. E. Amstad, J. Kohlbrecher, E. Muller, T. Schweizer, M. Textor, E. Reimhult, Triggered release from liposomes through magnetic actuation of iron oxide nanoparticle containing membranes, *Nano letters*, 11 (2011) 1664-1670.
38. G.A. van Tilborg, W.J. Mulder, N. Deckers, G. Storm, C.P. Reutelingsperger, G.J. Strijkers, K. Nicolay, Annexin A5-functionalized bimodal lipid-based contrast agents for the detection of apoptosis, *Bioconjugate chemistry*, 17 (2006) 741-749.
39. Y. Namiki, T. Namiki, H. Yoshida, Y. Ishii, A. Tsubota, S. Koido, K. Nariai, M. Mitsunaga, S. Yanagisawa, H. Kashiwagi, Y. Mabashi, Y. Yumoto, S. Hoshina, K. Fujise, N. Tada, A novel magnetic crystal-lipid nanostructure for magnetically guided in vivo gene delivery, *Nature nanotechnology*, 4 (2009) 598-606.
40. M. De Cuyper, M. Joniau, Magnetoliposomes. Formation and structural characterization, *European biophysics journal : EBJ*, 15 (1988) 311-319.
41. W. Jiskoot, T. Teerlink, E.C. Beuvery, D.J. Crommelin, Preparation of liposomes via detergent removal from mixed micelles by dilution. The effect of bilayer composition and process parameters on liposome characteristics, *Pharmaceutisch weekblad. Scientific edition*, 8 (1986) 259-265.
42. R. Schubert, Liposome preparation by detergent removal, *Methods in enzymology*, 367 (2003) 46-70.
43. B. Ashok, L. Arleth, R.P. Hjelm, I. Rubinstein, H. Onyuksel, In vitro characterization of PE-Gylated phospholipid micelles for improved drug solubilization: effects of PEG chain length and PC incorporation, *Journal of pharmaceutical sciences*, 93 (2004) 2476-2487.
44. A. Wijaya, K. Hamad-Schifferli, High-density encapsulation of Fe₃O₄ nanoparticles in lipid vesicles, *Langmuir : the ACS journal of surfaces and colloids*, 23 (2007) 9546-9550.
45. D. Frascione, C. Diwoky, G. Almer, P. Opriessnig, C. Vonach, K. Gradauer, G. Leitinger, H. Mangge, R. Stollberger, R. Prassl, Ultrasmall superparamagnetic iron oxide (USPIO)-based liposomes as magnetic resonance imaging probes, *International journal of nanomedicine*, 7 (2012) 2349-2359.

CHAPTER 7

General Discussion



CURRENT STATUS OF THERMOSENSITIVE LIPOSOMES FOR SOLID TUMOR THERAPY

The research to improve current systemic chemotherapy with respect to target-specificity and side effects, led to clinical approval of several nanoparticles for drug delivery [1, 2]. For example, Doxil®, DaunoXome™ and Onivyde™ are liposomal formulations that have shown improved safety profiles but demonstrated only in few applications improved efficacy [3, 4]. The latter is hampered by the slow diffusion driven release of the parental drug from its liposomal carrier, limiting the bioavailability [5-7]. The concept of temperature-induced drug release from thermosensitive liposomes (TSLs) has been introduced to counter this problem. Although drug encapsulation in TSLs may not be as stable as in non-TSL formulations such as Doxil® [8-11], the intravascular drug release in the heated tumor ensures a greater efficiency in drug delivery to the tumor cell [12]. Ever since the first description by Yatvin and Weinstein [13, 14], TSLs have been under continuous development and optimization. However, the only TSL formulation to have reached clinical trials remains the Doxorubicin (Dox)-loaded, lysolipid-based TSL (LTSL) developed by Needham & Dewhirst [15, 16]. This LTSL formulation has been evaluated in clinical trials conducted by Celsion Corporation under the commercial name of ThermoDox (Table I). Their first clinical studies focused on locally recurrent breast cancer (phase I/ II) and liver cancer (phase I/ III). For the breast cancer study, a microwave heating device was used, which is practical for heating of superficial tumors to mild hyperthermia (HT, 40-43 °C). Conversely, the liver cancer study made use of a radiofrequency (RF) applicator that is invasively placed into the center of the tumor for ablation at higher temperatures (> 60 °C; RFA). In this case, the periphery of the tumor is expected to be heated to temperatures closer to the mild HT range. The TSLs consequently deliver Dox to the tumor periphery and rim, which often constitutes the part of the lesion with occult cancer cells that escape thermal ablation. The clinical trial for breast cancer showed that ThermoDox can be administered multiple times at a maximum tolerated dose of 50 mg/ m², generating a local overall response rate of 48% [17].

Furthermore, toxicity levels were considerably lower than what is commonly observed in free Dox infused patients. The completed phase III trial for the treatment of hepatocellular carcinoma with RFA and LTSLs showed no increase in overall survival compared to RFA treatment alone. Here, LTSLs are infused at least 15 min prior to RFA treatment which lasted for 12-60 min, depending on the size of the heated lesion [18]. The problem that caused these disappointing findings was found in the duration of the RFA treatment since consecutive RFA treatments that lasted > 45 min in combination with infused LTSLs did result in increased survival for more than two years for a subgroup of patients [19-21]. Nevertheless, not for all cancers a superficial or invasive HT treatment is an option and therefore more sophisticated heating techniques should be investigated.

Table 1: Overview of clinical trials performed with ThermoDox

Study No	Start/ End year	Status	Cancer type	Heating method	Goals/ Results
1	2006/ 2016	Terminated	Breast cancer	Microwave	Phase I: Side effects and optimal dosing for therapy (Nolen Breast Cancer Res 2008; Zagar IJH 2014)
2	2007/ 2016	Completed	Primary and metastatic liver cancer	Radiofrequency ablation (RFA)	Phase I: Dose escalation study
3	2008/ 2014	Unknown	Hepatocellular carcinoma	RFA	Phase III: Therapeutic efficacy and safety
4	2009/ 2016	Completed	Breast cancer	Microwave	Phase I/II: Determine maximum tolerated dose, safety, pharmacokinetics, therapeutic efficacy (Zagar IJH 2014)
5	2011/ 2016	Terminated	Colon cancer liver metastasis	RFA	Phase II: Therapeutic efficacy and safety
6	2012/ 2016	Withdrawn	Painful bone metastases	MRI-guided high intensity focused ultrasound (MR-HIFU)	Phase II: Therapeutic efficacy and safety
7	2014/ -	Recruiting	Hepatocellular carcinoma	RFA	Phase III: Therapeutic efficacy and safety
8	2014/ -	Recruiting	Liver cancer	Focused ultrasound (FUS)	Phase I: Proof of concept; enhanced accumulation in tumors
9	2015/ -	Recruiting	Pediatric cancer	MR-HIFU	Phase I: Determine maximum tolerated dose and recommended Phase II dose
10	2016/ -	Not yet recruiting	Breast cancer	Microwave	Phase II: Therapeutic efficacy and safety

Heating by focused ultrasound is one technique which is non-invasive, can be used for deeper seated tumors and is currently being used in ThermoDox clinical trials for liver and pediatric cancers [22, 23]. This heating method, in combination with TSL-based drug delivery, has shown increased intratumoral drug levels versus free Dox treatment, as well as improved tumor growth delay in various preclinical tumor models [24-26].

The above mentioned results summarize the potential of LTSL-based therapies; however this particular formulation of TSL using lysolipids has also some shortcomings. LTSLs are relatively unstable compared to other TSL formulations in biological media [27] and have demonstrated lower therapeutic efficacy compared to formulations that lack lysolipid [28]. Furthermore, it has been suggested that the lysolipids dissociate from LTSLs in the blood stream, thereby lowering the systemic circulation time of the particles and encapsulated drug [10]. These findings may have contributed to the lack of therapeutic benefit in adding LTSLs to standard RFA treatment for hepatocellular

carcinoma [29]. Optimizing heating protocols may lead to higher therapeutic response [30]; however, a class of alternative TSL formulations warrants further investigation in the clinical setting, given the above mentioned disadvantages of the LTSL formulation.

OPTIMIZATION OF THERMOSENSITIVE LIPOSOMAL FORMULATIONS

Optimization of TSL formulations has been performed by many groups and continues to take place for novel TSLs and compounds. The basis for this can be found in the choice and ratio of lipids that determine the bulk transition temperature (T_m) of the particle [11, 31]. However, similar to the LTSL, most groups have added unique lipids to the formulation in order to achieve the optimal balance between TSL stability and circulation time at 37 °C, and fast release at 41-42 °C. For example, the inclusion of a select amount of DSPE-PEG₂₀₀₀ to a DPPC/ DSPC formulation can yield a TSL with reasonable stability and drug release characteristics, as has been shown by Hossann et al [32] and Li et al [33]. These formulations mainly exhibit lower drug leakage at temperatures below 41 °C, thereby improving drug circulation time [10, 11]. Another approach which is quite similar to the LTSL is the addition of Brij78 instead of lysolipid to the main lipid composition [34, 35]. Brij78 is a surfactant with a PEG₈₀₀ structure connected to a single acyl chain, which is also capable to form pores within the lipid bilayer for enhanced drug release. The PEG chain would stabilize the pore similarly as described for LTSL [36, 37], but is in this case linked to the same structure which facilitates the pore. In a comparison with LTSL, it was shown that Dox pharmacokinetic profiles were similar, while Dox release rates and intratumoral accumulation was slightly higher for Brij78-containing TSLs [34]. However, similar findings between lysolipid and Brij78 were found on dissociation from TSLs in biological media [10, 34]. Another example of a TSL bearing optimal circulation and release properties owing to a single component of the formulation is the 1,2-dipalmitoyl-sn-glycero-3-phosphodiglycerol (DPPG₂)-TSL described by Lindner et al [38]. The reported circulation half-life of 5.0 ± 0.9 h (carboxyfluorescein readout) in rats is remarkably longer than that of LTSLs which exhibit a half-life of approximately 1.3 h (radiolabeled lipid readout) [10]. This has likely been attributed to a higher systemic stability at 37 °C, while maintaining fast drug release properties [32]. However, a direct comparison between LTSL and DPPG₂-TSL has not been performed so far. Other examples of strategies that establish fast drug release from TSLs are the incorporation of thermosensitive polymers [39, 40] or polypeptides [31, 41] which undergo conformational changes at HT and destabilize the TSL membrane, thereby facilitating drug release. The polypeptide-TSL showed an almost threefold greater circulation time and significantly higher therapeutic response versus LTSL in a murine model of squamous cell carcinoma.

These above-mentioned examples indicate next to LTSL, other TSL formulations are also worthwhile to investigate pre-clinically and clinically. Other formulations have shown mainly higher stability and improved circulation time, which frequently resulted in higher intratumoral drug accumulation and therapeutic effect. We have shown in Chapter 2 that with a variety of relatively stable Dox-loaded TSLs, a significant therapeutic response can be achieved. Needham and Dewhirst based the potential success of the LTSL on a model where a particle would need 50-100 s to travel in a perfect horizontal line from one side to the other of a 1 cm diameter tumor with normal blood circulation and that the drug release has to take place within this timeframe [12]. In practice, the vascularization of the tumor is more complex and the TSL transition time is probably longer than what is expected according to the above mentioned model. However, there are several other parameters which were not considered. The first aspect is that *in vitro* release profiles were used as a predictor of how drug release would take place *in vivo*. We have shown in Chapter 2 that for TSL stability, *in vitro* plasma incubations only provide preliminary information on Dox retention and release characteristics. Upon systemic administration, many other factors have an impact on the particle, further compromising its integrity. Although this has not been investigated so far, this is likely also the case for Dox release at HT. Furthermore, the suggested dissociation of lysolipids from LTSL in circulation by Banno et al. [10] will certainly alter the Dox release profile *in vivo*. In Chapter 5 we have indicated that an infused bolus of TSLs likely passes through the tumor vasculature in low quantities per passage, and that the bulk amount of the injected dose stays in the main circulation. We have not evaluated LTSLs in this study; however, our findings imply that a considerable amount of passages are required to obtain typical intratumoral Dox levels that are found for TSL and HT based treatments [42]. These findings also suggest that longer circulating TSLs might be more effective for solid tumor therapy than LTSLs.

FACTORS WHICH LEAD TO ENHANCED THERAPEUTIC EFFECT

Next to the composition of the particle, the biology of the tumor must also be considered in order to optimize TSL therapy. At this point, the tumor has largely been considered as a mass of cancer cells supplied by a network of blood vessels for the delivery of nutrients and oxygen. However, there are some aspects of tumor physiology that need to be well-understood in order to properly interpret preclinical and clinical results of nanomedicine therapy [43]. For *in vitro* cancer cell cultures, factors such as growth kinetics, protein expression and sensitivity to cytotoxic agents are well-defined and reproducible characteristics that can be maintained through multiple passages. These cultures provide an adequate means to obtain preliminary assessment on the feasibility

of a given therapy in order to proceed to more complex, *in vivo* studies. For instance, cells that are located in the tumor core may not receive sufficient oxygen and nutrients since the area is often poorly vascularized. These cells are therefore termed hypoxic and can alter their proteome, which often negatively affects drug efficacy [44]. Conversely, tumor cells located in the periphery are in close proximity to functional blood vessels, and therefore are more viable and more likely to possess similar characteristics to those observed in culture [45, 46]. The vasculature of a tumor is often chaotically organized, tortuous and lacks structural integrity such as pericyte coverage, basement membrane and perivascular smooth muscle [47, 48]. Furthermore, the endothelial lining of tumor blood vessels can contain gaps up to several micrometers in size, which can be exploited for nanoparticle accumulation in tumors [49]. The so-called enhanced permeability and retention (EPR) effect is more effective for smaller-sized compounds [50], but can be increased by HT, especially for nanoparticles in the liposome size range (i.e., ~100 nm) [51, 52]. Despite these pathophysiological features which may enable drug delivery to solid tumors, there are some aspects of the tumor microenvironment that also hinder drug delivery. The lack of lymphatic drainage contributes to increased interstitial fluid pressure (IFP), which reduces the influx of nanoparticles into the tumor interstitium [53]. Moreover, tumors frequently contain a considerable amount of stroma, which can greatly influence metastatic potential [24, 54]. Tumor stroma is associated with increased levels of fibroblasts and extracellular matrix which can significantly hamper the transport of cytotoxic compounds towards the tumor cell [55, 56].

The above-mentioned tumor microenvironmental factors differ between tumor types and within the same tumor; heterogeneity is ubiquitous. The clinical impact of this observation on nanoparticle delivery to solid tumors has been thoroughly described in the studies of Harrington and coworkers [57]. Their findings have indicated that patients with head and neck cancers accumulate more radiolabeled liposomes ($33.0 \pm 15.8\%$ ID/kg), with a similar lipid composition to Doxil®, than patients with lung ($18.3 \pm 5.7\%$ ID/kg) or breast ($5.3 \pm 2.6\%$ ID/kg) tumors. In the preclinical setting, differences in nanoparticle accumulation between tumor types [58] and heterogeneous uptake within tumors has been observed [59]. However, it is important to consider that when using animal tumors, the growth rate is relatively higher than in humans, and tumors therefore have a higher potential of accumulating particles through the EPR effect. The B16 tumor model described in Chapter 3 constitutes a representative example of this phenomenon. EPR-mediated drug accumulation in this family of murine tumors was found to be highly pronounced, leading to the superior performance of a Doxil®-like liposome over that of an LTSL [60]. In xenograft models, this result has only been shown when tumors were subjected to 3 min RFA treatment prior to Doxil® injection versus LTSL injection performed 15 min prior to the same RFA treatment [61]. The therapeutic efficacy of LTSL in different subcutaneous tumor models has been extensively investigated by Yarmolenko

et al [62]. They found that slower growing cancer cells *in vitro* have a larger likelihood to therapeutically respond to TSL and HT therapy *in vivo*. We (Chapter 3) and others [58] have claimed that more invasive tumors accumulate more liposomes by the EPR effect. In Chapter 4, we observed a lower therapeutic response for slowly growing T-47D tumors relatively to fast growing MDA-MB-231, which contradicts the findings of Yarmolenko et al. In this case, we hypothesize that the high differentiation and relatively mature extracellular matrix of the orthotopic T-47D tumor model may limit effective drug accumulation. Conversely, the rapid development of MDA-MB-231 tumors may yield more permeable conduits for drug delivery. Overall, these findings suggest that the efficacy of cancer nanomedicines may require a prior identification of tumors that meet select criteria for therapeutically significant drug delivery, a concept also known as personalized medicine [63, 64]. Nevertheless, the above-mentioned observations indicate that it is likely that the scope of tumors that respond to therapy may prove broader for TSL- and HT-based drug delivery than for therapies that rely on stable systemic circulation and tumor accumulation.

THE NEXT LEVEL OF THERMOSENSITIVE LIPOSOMES AND ASPECTS TO BE INVESTIGATED

Nanoparticle-based drug delivery is a field wherein intensive research has been conducted for the past decades. A significant number of strategies, nanoparticles and targeting principles have been described throughout the literature over these years [65]. This raises the question as to whether a saturation level has been reached in optimizing nanoparticles and in developing correspondingly novel and clinically relevant treatments.

In Chapter 6, we investigated the development of liposomes incorporating magnetic nanoparticles for heat-triggered drug release when exposed to an alternating magnetic field. While the concept provided an attractive platform for *in vivo* MR-guided interventions, the poor scalability in the formulation process limited further development and translation of this research. Nanoparticle research should therefore be performed with both specific and realistic aims; the goal of clinical translation can be achieved through the development of scalable formulations that prove superior to standard of care. Conversely, basic research is critical to the fundamental understanding of nanoparticle performance and interactions *in vivo*. For TSLs, much research has been performed on optimal formulation development and rendering particles more target-specific [66, 67]. Optimizing formulations has been described above and is absolutely relevant concerning the limitations of LTSLs. For instance, the feasibility of molecularly targeting TSLs to specific cell populations is a question that has yet to be addressed. *In vitro*, targeting

of TSLs to major histocompatibility complex (MHC) class I [68], folate receptors [69], human epidermal growth factor receptor 2 (HER2) [70] or hydroxyapatite [71] on cancer cells resulted in enhanced intracellular drug levels and cytotoxic effect. However, *in vivo* studies showing enhanced drug accumulation via TSL targeting have only been described by Al-Ahmady et al [72] and Yang et al [73]. The results of the former study indicated that intratumoral Dox accumulation could be enhanced by targeting TSLs to tumor cells by an α -MUC1 antibody using specific HT regimes. The latter study did not perform drug accumulation studies, but therapeutic efficacy could be enhanced when TSLs contained a NGR-peptide residue. However, the doses between targeted, non-targeted and free drug groups were inconsistent and hence this result should be interpreted with caution. The lack of therapeutic benefit of targeted TSLs is likely caused by the significant amount of time required for the particles to accumulate in the tumor by the EPR effect. We have shown in Chapter 3 that TSLs are too unstable for particle accumulation-based studies as the drug leakage is too substantial within the time needed for the TSLs to reach their target in sufficient quantities. Furthermore, *in vitro* binding studies are often performed in serum-free conditions while it has been shown that serum component interactions can greatly inhibit targeted nanoparticle binding potential [74, 75]. Targeting TSLs to the tumor neovasculature has also been investigated by the incorporation of cationic lipids [76] or targeting peptides to the formulation [77, 78]. The results for these two targeting ligands were remarkably similar, with increased *in vitro* and *in vivo* affinity to the endothelium. Yet, the therapeutic benefit of vascular targeting for TSLs remains to be demonstrated [79]. Recently, one study showed a significant increase in therapeutic response when clotted plasma proteins in solid tumors were targeted by a peptide-conjugated TSL [80]. Overall, these results indicate that introducing targeting ligands to TSLs provides little benefit and that intravascular drug release remains the best option for effective solid tumor treatment [81].

These findings on optimization of TSLs and efforts to make the particles more target-specific might suggest that a saturation level in TSL research has been reached. However, key aspects of this delivery methodology still require further investigation in order to generate positive and sustained treatment outcomes in patient populations that are most likely to respond. We have previously addressed the importance of focusing on TSL formulations with higher systemic stability than LTSL; however, a more comprehensive understanding of how the drug delivery mechanism functions *in vivo* is required. This is particularly important when considering disparate tumor microenvironments and how these might influence drug potency. Few studies have been aimed at further characterizing the delivery method. For example, murine dorsal skinfold window chamber studies have been used to study drug release kinetics from TSLs in circulation, extravasation of the drug into the tumor interstitium and how effectively it is taken up by the tumor cell [28, 82]. However, for these models, aggressively growing murine or xenograft tumors

are used which grow only in two dimensions and therefore key microenvironmental factors such as hypoxic areas and extracellular matrix might not be representative compared to 3D developing tumors. Furthermore, quantitative drug accumulation in the tumor cannot be determined by this method. Accordingly, Dewhirst and coworkers have conducted pioneering research in “dose painting”- a method where a MRI contrast agent is co-encapsulated with Dox to image, in real-time, the deposition of a released compound from a TSL in a heated tumor [83, 84]. Their methods focused on the use of manganese as a MRI contrast agent, which was found to correlate remarkably well with Dox accumulation in solid tumors. Owing to these studies, the optimal HT regimen of heating during the LTSL administration was described using this dose painting approach. More recently, the accuracy of dose painting could be reproduced in other animal models, heating methodologies, and using gadolinium as a MRI contrast agent [24, 54, 81, 85, 86]. In conjunction with the determination of drug uptake rates by cells, Dox release rates by LTSLs, and tumor perfusion data, computational models have been constructed that better explain heat-triggered drug delivery to solid tumors by RFA and high intensity focused ultrasound (HIFU) treatments [87, 88].

These data have proven useful in interpreting the results of the therapy as a whole; however, what really transpires at the micro-scale in the solid tumor is not yet fully understood, leaving several questions that remain unanswered: How much of the drug is effectively released upon passage through the tumor vasculature? How much of the liposomes actually travel through the heated tumor and how much circulation time is required in order to obtain maximal drug accumulation? How much of the released drug is retained in the tumor and how much is washed out by blood flow-mediated convection? With the isolated limb infusion model described in Chapter 5, we describe a model which may address these questions. Although our PEG₂₀₀₀-TSL formulation was not directly compared to LTSL, the model indicated that a single passage of the particles through the heated tumor was not sufficient to deliver more Dox than infused free drug. These findings indicate that longer circulating TSLs might be more effective in delivering high drug doses to solid tumors than LTSLs. Taken together, it is plausible that the efficacy of drug delivery by TSLs yields is still suboptimal compared to standard of care. Nevertheless, with continued optimization of therapy regimens and formulation properties (e.g. LTSL), as well as the identification of likely responders and corresponding prognostic factors, significant advances are imminent.

CLINICAL TRANSLATION OF THERMOSENSITIVE LIPOSOME THERAPY

So far we have mostly focused on future investigation of TSLs in a pre-clinical setting. However, research that focuses on aspects directly linked to clinical application are es-

essential for successful clinical introduction of the therapy. The earlier-mentioned clinical trials show that optimal heating protocols have to be designed to establish maximal efficacy for TSL treatments [18-21]. Today, the focus of clinical HT is highly on HIFU and trials with this heating methodology in combination with LTSL therapy have recently been initiated [23]. One good example on investigation of optimal heating protocols with TSLs and HIFU has been recently described by Hijnen and Kneepkens et al [54]. Here, rhabdomyosarcoma-inoculated rats were i.v. injected with TSLs followed by a treatment regimen of two times 15 min mild HT and tumor ablation versus ablation alone. Their results show that Dox accumulation in tumors can be increased when giving additional mild HT treatments prior to ablation, which resulted in improved therapeutic efficacy. The potential cause for this finding was that first the local mild hyperthermia causes increased intratumoral particle and drug accumulation and that vascular shut-down induced by ablation afterwards results in a reduced efflux of these from the tumor interstitial space. This example indicates that studies that focus on optimal treatment protocols are important for successful translation of the treatment to the clinic [30, 54, 89]. Furthermore, more investigation has to be performed on repetitive treatments using this methodology, as this more closely represents clinical practice and as a set of previous studies have shown total tumor regression doing so [90, 91].

Given the above-mentioned results, it appears that with the right pre-clinical studies, treatments of tumors with TSL and HT is steadily approaching clinical introduction in an optimized fashion. However, there are some aspects that have to be carefully considered before this can be realized. The TSL as a carrier is biodegradable and therefore, does not induce long-term toxicity. But on short-term, adverse effects can occur such as complement activation-related pseudoallergy (CARPA), which is potentially lethal. This phenomenon has been extensively described for Doxil® in pig and human studies [92, 93] and only in pigs so far for LTSLs [30]. Furthermore, some Doxil® treated patients showed palmar-plantar erythrodysesthesia, which manifests itself as a skin rash, mainly on the hands and feet which has been suggested to be caused by Dox secreted in sweat [94-97]. Therefore, a careful assessment has to be made for each patient whether these side effects are manageable during treatment. Heating of tumors by HIFU is currently restricted to volumes of approximately 15 mm in diameter and larger volumes have to be heated by consecutively heating subareas [98, 99]. Therefore, research is being conducted on making the HIFU technology capable of heating more clinically relevant tissue volumes [100]. Because of the optimization required for the TSL formulation, heating protocol and heating equipment, successful clinical introduction of TSL and HT therapy is dependent on translational research at a drug-device combination level.

REFERENCES

1. A.C. Anselmo, S. Mitragotri, Nanoparticles in the clinic, *Bioengineering & Translational Medicine*, 1 (2016) 10-29.
2. J.I. Hare, T. Lammers, M.B. Ashford, S. Puri, G. Storm, S.T. Barry, Challenges and strategies in anti-cancer nanomedicine development: An industry perspective, *Advanced drug delivery reviews*, (2016).
3. A. Udhrain, K.M. Skubitz, D.W. Northfelt, Pegylated liposomal doxorubicin in the treatment of AIDS-related Kaposi's sarcoma, *International journal of nanomedicine*, 2 (2007) 345-352.
4. A.N. Gordon, J.T. Fleagle, D. Guthrie, D.E. Parkin, M.E. Gore, A.J. Lacave, Recurrent Epithelial Ovarian Carcinoma: A Randomized Phase III Study of Pegylated Liposomal Doxorubicin Versus Topotecan, *Journal of Clinical Oncology*, 19 (2001) 3312-3322.
5. K.M. Laginha, S. Verwoert, G.J. Charrois, T.M. Allen, Determination of doxorubicin levels in whole tumor and tumor nuclei in murine breast cancer tumors, *Clinical cancer research : an official journal of the American Association for Cancer Research*, 11 (2005) 6944-6949.
6. A.L. Seynhaeve, B.M. Dicheva, S. Hoving, G.A. Koning, T.L. ten Hagen, Intact Doxil is taken up intracellularly and released doxorubicin sequesters in the lysosome: evaluated by in vitro/in vivo live cell imaging, *Journal of controlled release : official journal of the Controlled Release Society*, 172 (2013) 330-340.
7. A.L. Seynhaeve, S. Hoving, D. Schipper, C.E. Vermeulen, G. de Wael-Ambagtsheer, S.T. van Tiel, A.M. Eggermont, T.L. Ten Hagen, Tumor necrosis factor alpha mediates homogeneous distribution of liposomes in murine melanoma that contributes to a better tumor response, *Cancer research*, 67 (2007) 9455-9462.
8. A. Gabizon, H. Shmeeda, Y. Barenholz, Pharmacokinetics of pegylated liposomal Doxorubicin: review of animal and human studies, *Clinical pharmacokinetics*, 42 (2003) 419-436.
9. A. Gabizon, R. Catane, B. Uziely, B. Kaufman, T. Safra, R. Cohen, F. Martin, A. Huang, Y. Barenholz, Prolonged circulation time and enhanced accumulation in malignant exudates of doxorubicin encapsulated in polyethylene-glycol coated liposomes, *Cancer research*, 54 (1994) 987-992.
10. B. Banno, L.M. Ickenstein, G.N. Chiu, M.B. Bally, J. Thewalt, E. Brief, E.K. Wasan, The functional roles of poly(ethylene glycol)-lipid and lysolipid in the drug retention and release from lysolipid-containing thermosensitive liposomes in vitro and in vivo, *Journal of pharmaceutical sciences*, 99 (2010) 2295-2308.
11. W.J. Lokerse, E.C. Kneepkens, T.L. ten Hagen, A.M. Eggermont, H. Grull, G.A. Koning, In depth study on thermosensitive liposomes: Optimizing formulations for tumor specific therapy and in vitro to in vivo relations, *Biomaterials*, 82 (2016) 138-150.
12. G. Kong, G. Anyarambhatla, W.P. Petros, R.D. Braun, O.M. Colvin, D. Needham, M.W. Dewhirst, Efficacy of liposomes and hyperthermia in a human tumor xenograft model: importance of triggered drug release, *Cancer research*, 60 (2000) 6950-6957.
13. M.B. Yatvin, J.N. Weinstein, W.H. Dennis, R. Blumenthal, Design of liposomes for enhanced local release of drugs by hyperthermia, *Science (New York, N.Y.)*, 202 (1978) 1290-1293.
14. J.N. Weinstein, R.L. Magin, M.B. Yatvin, D.S. Zaharko, Liposomes and local hyperthermia: selective delivery of methotrexate to heated tumors, *Science (New York, N.Y.)*, 204 (1979) 188-191.

15. G.R. Anyarambhatla, D. Needham, Enhancement of the Phase Transition Permeability of DPPC Liposomes by Incorporation of MPPC: A New Temperature-Sensitive Liposome for use with Mild Hyperthermia, *Journal of Liposome Research*, 9 (1999) 491-506.
16. D. Needham, G. Anyarambhatla, G. Kong, M.W. Dewhirst, A new temperature-sensitive liposome for use with mild hyperthermia: characterization and testing in a human tumor xenograft model, *Cancer research*, 60 (2000) 1197-1201.
17. T.M. Zagar, Z. Vujaskovic, S. Formenti, H. Rugo, F. Muggia, B. O'Connor, R. Myerson, P. Stauffer, I.C. Hsu, C. Diederich, W. Straube, M.K. Boss, A. Boico, O. Craciunescu, P. Maccarini, D. Needham, N. Borys, K.L. Blackwell, M.W. Dewhirst, Two phase I dose-escalation/pharmacokinetics studies of low temperature liposomal doxorubicin (LTLTD) and mild local hyperthermia in heavily pretreated patients with local regionally recurrent breast cancer, *International journal of hyperthermia : the official journal of European Society for Hyperthermic Oncology, North American Hyperthermia Group*, 30 (2014) 285-294.
18. Celsion, Phase 3 Study of ThermoDox With Radiofrequency Ablation (RFA) in Treatment of Hepatocellular Carcinoma (HCC), in, *ClinicalTrials.gov* NCT00617981, 2008.
19. Celsion, Study of ThermoDox With Standardized Radiofrequency Ablation (RFA) for Treatment of Hepatocellular Carcinoma (HCC) (OPTIMA), in, *ClinicalTrials.gov* NCT02112656, 2014.
20. Celsion, Celsion Corporation's ThermoDox® HEAT Study Findings Reviewed at the International Liver Cancer Association (ILCA) 2013 Annual Conference in Washington, D.C. on September 14, 2013, in, 2013.
21. Celsion, Celsion Announces Updated Overall Survival Data from HEAT Study of ThermoDox® in Primary Liver Cancer, (2014).
22. U.o. Oxford, Targeted Chemotherapy Using Focused Ultrasound for Liver Tumours (TARDOX), in, *ClinicalTrials.gov* NCT02181075, 2014.
23. AeRang-Kim, A Phase I Study of Lyso-thermosensitive Liposomal Doxorubicin and MR-HIFU for Pediatric Refractory Solid Tumors, in, *ClinicalTrials.gov* NCT02536183, 2015.
24. M. de Smet, E. Heijman, S. Langereis, N.M. Hijnen, H. Grull, Magnetic resonance imaging of high intensity focused ultrasound mediated drug delivery from temperature-sensitive liposomes: an in vivo proof-of-concept study, *Journal of controlled release : official journal of the Controlled Release Society*, 150 (2011) 102-110.
25. S. Dromi, V. Frenkel, A. Luk, B. Traugher, M. Angstadt, M. Bur, J. Poff, J. Xie, S.K. Libutti, K.C. Li, B.J. Wood, Pulsed-high intensity focused ultrasound and low temperature-sensitive liposomes for enhanced targeted drug delivery and antitumor effect, *Clinical cancer research : an official journal of the American Association for Cancer Research*, 13 (2007) 2722-2727.
26. R.M. Staruch, M. Ganguly, I.F. Tannock, K. Hynynen, R. Chopra, Enhanced drug delivery in rabbit VX2 tumours using thermosensitive liposomes and MRI-controlled focused ultrasound hyperthermia, *International journal of hyperthermia : the official journal of European Society for Hyperthermic Oncology, North American Hyperthermia Group*, 28 (2012) 776-787.
27. M. Hossann, Z. Syunyaeva, R. Schmidt, A. Zengerle, H. Eibl, R.D. Issels, L.H. Lindner, Proteins and cholesterol lipid vesicles are mediators of drug release from thermosensitive liposomes, *Journal of controlled release : official journal of the Controlled Release Society*, 162 (2012) 400-406.
28. L. Li, T.L. ten Hagen, M. Hossann, R. Suss, G.C. van Rhooon, A.M. Eggermont, D. Haemmerich, G.A. Koning, Mild hyperthermia triggered doxorubicin release from optimized stealth ther-

- mosensitive liposomes improves intratumoral drug delivery and efficacy, *Journal of controlled release : official journal of the Controlled Release Society*, 168 (2013) 142-150.
29. R. Lencioni, D. Cioni, RFA plus lyso-thermosensitive liposomal doxorubicin: in search of the optimal approach to cure intermediate-size hepatocellular carcinoma, *Hepatic Oncology*, 3 (2016) 193-200.
 30. C.E. Swenson, D. Haemmerich, D.H. Maul, B. Knox, N. Ehrhart, R.A. Reed, Increased Duration of Heating Boosts Local Drug Deposition during Radiofrequency Ablation in Combination with Thermally Sensitive Liposomes (ThermoDox) in a Porcine Model, *PloS one*, 10 (2015) e0139752.
 31. S.M. Park, J.M. Cha, J. Nam, M.S. Kim, S.J. Park, E.S. Park, H. Lee, H.R. Kim, Formulation optimization and in vivo proof-of-concept study of thermosensitive liposomes balanced by phospholipid, elastin-like polypeptide, and cholesterol, *PloS one*, 9 (2014) e103116.
 32. M. Hossann, M. Wiggenghorn, A. Schwerdt, K. Wachholz, N. Teichert, H. Eibl, R.D. Issels, L.H. Lindner, In vitro stability and content release properties of phosphatidylglyceroglycerol containing thermosensitive liposomes, *Biochimica et biophysica acta*, 1768 (2007) 2491-2499.
 33. L. Li, T.L. ten Hagen, D. Schipper, T.M. Wijnberg, G.C. van Rhooen, A.M. Eggermont, L.H. Lindner, G.A. Koning, Triggered content release from optimized stealth thermosensitive liposomes using mild hyperthermia, *Journal of controlled release : official journal of the Controlled Release Society*, 143 (2010) 274-279.
 34. T. Tagami, M.J. Ernstring, S.D. Li, Efficient tumor regression by a single and low dose treatment with a novel and enhanced formulation of thermosensitive liposomal doxorubicin, *Journal of controlled release : official journal of the Controlled Release Society*, 152 (2011) 303-309.
 35. T. Tagami, M.J. Ernstring, S.D. Li, Optimization of a novel and improved thermosensitive liposome formulated with DPPC and a Brij surfactant using a robust in vitro system, *Journal of controlled release : official journal of the Controlled Release Society*, 154 (2011) 290-297.
 36. L.M. Ickenstein, M.C. Arfvidsson, D. Needham, L.D. Mayer, K. Edwards, Disc formation in cholesterol-free liposomes during phase transition, *Biochimica et biophysica acta*, 1614 (2003) 135-138.
 37. D. Needham, J.Y. Park, A.M. Wright, J. Tong, Materials characterization of the low temperature sensitive liposome (LTSL): effects of the lipid composition (lysolipid and DSPE-PEG2000) on the thermal transition and release of doxorubicin, *Faraday discussions*, 161 (2013) 515-534; discussion 563-589.
 38. L.H. Lindner, M.E. Eichhorn, H. Eibl, N. Teichert, M. Schmitt-Sody, R.D. Issels, M. Dellian, Novel temperature-sensitive liposomes with prolonged circulation time, *Clinical cancer research : an official journal of the American Association for Cancer Research*, 10 (2004) 2168-2178.
 39. K. Kono, T. Ozawa, T. Yoshida, F. Ozaki, Y. Ishizaka, K. Maruyama, C. Kojima, A. Harada, S. Aoshima, Highly temperature-sensitive liposomes based on a thermosensitive block copolymer for tumor-specific chemotherapy, *Biomaterials*, 31 (2010) 7096-7105.
 40. M. van Elk, R. Deckers, C. Oerlemans, Y. Shi, G. Storm, T. Vermonden, W.E. Hennink, Triggered release of doxorubicin from temperature-sensitive poly(N-(2-hydroxypropyl)-methacrylamide mono/dilactate) grafted liposomes, *Biomacromolecules*, 15 (2014) 1002-1009.
 41. S.M. Park, M.S. Kim, S.J. Park, E.S. Park, K.S. Choi, Y.S. Kim, H.R. Kim, Novel temperature-triggered liposome with high stability: formulation, in vitro evaluation, and in vivo study combined with high-intensity focused ultrasound (HIFU), *Journal of controlled release : official journal of the Controlled Release Society*, 170 (2013) 373-379.

42. N. Hijnen, S. Langereis, H. Grull, Magnetic resonance guided high-intensity focused ultrasound for image-guided temperature-induced drug delivery, *Advanced drug delivery reviews*, 72 (2014) 65-81.
43. O. Tredan, C.M. Galmarini, K. Patel, I.F. Tannock, Drug resistance and the solid tumor micro-environment, *Journal of the National Cancer Institute*, 99 (2007) 1441-1454.
44. J.M. Brown, Tumor hypoxia in cancer therapy, *Methods in enzymology*, 435 (2007) 297-321.
45. A.I. Minchinton, I.F. Tannock, Drug penetration in solid tumours, *Nature reviews. Cancer*, 6 (2006) 583-592.
46. I.F. Tannock, The relation between cell proliferation and the vascular system in a transplanted mouse mammary tumour, *British journal of cancer*, 22 (1968) 258-273.
47. P. Carmeliet, Angiogenesis in life, disease and medicine, *Nature*, 438 (2005) 932-936.
48. F. Danhier, O. Feron, V. Preat, To exploit the tumor microenvironment: Passive and active tumor targeting of nanocarriers for anti-cancer drug delivery, *Journal of controlled release : official journal of the Controlled Release Society*, 148 (2010) 135-146.
49. H. Hashizume, P. Baluk, S. Morikawa, J.W. McLean, G. Thurston, S. Roberge, R.K. Jain, D.M. McDonald, Openings between defective endothelial cells explain tumor vessel leakiness, *The American journal of pathology*, 156 (2000) 1363-1380.
50. Z. Popovic, W. Liu, V.P. Chauhan, J. Lee, C. Wong, A.B. Greytak, N. Insin, D.G. Nocera, D. Fukumura, R.K. Jain, M.G. Bawendi, A nanoparticle size series for in vivo fluorescence imaging, *Angewandte Chemie (International ed. in English)*, 49 (2010) 8649-8652.
51. G. Kong, R.D. Braun, M.W. Dewhirst, Characterization of the effect of hyperthermia on nanoparticle extravasation from tumor vasculature, *Cancer research*, 61 (2001) 3027-3032.
52. T. Lammers, P. Peschke, R. Kuhnlein, V. Subr, K. Ulbrich, J. Debus, P. Huber, W. Hennink, G. Storm, Effect of radiotherapy and hyperthermia on the tumor accumulation of HPMa copolymer-based drug delivery systems, *Journal of controlled release : official journal of the Controlled Release Society*, 117 (2007) 333-341.
53. C.H. Heldin, K. Rubin, K. Pietras, A. Ostman, High interstitial fluid pressure - an obstacle in cancer therapy, *Nature reviews. Cancer*, 4 (2004) 806-813.
54. N. Hijnen, E. Kneepkens, M. de Smet, S. Langereis, E. Heijman, H. Grull, Thermal combination therapies for local drug delivery by magnetic resonance-guided high-intensity focused ultrasound, *Proceedings of the National Academy of Sciences of the United States of America*, 114 (2017) E4802-e4811.
55. P.A. Netti, D.A. Berk, M.A. Swartz, A.J. Grodzinsky, R.K. Jain, Role of extracellular matrix assembly in interstitial transport in solid tumors, *Cancer research*, 60 (2000) 2497-2503.
56. I.F. Tannock, C.M. Lee, J.K. Tunggal, D.S. Cowan, M.J. Egorin, Limited penetration of anti-cancer drugs through tumor tissue: a potential cause of resistance of solid tumors to chemotherapy, *Clinical cancer research : an official journal of the American Association for Cancer Research*, 8 (2002) 878-884.
57. K.J. Harrington, S. Mohammadtaghi, P.S. Uster, D. Glass, A.M. Peters, R.G. Vile, J.S. Stewart, Effective targeting of solid tumors in patients with locally advanced cancers by radiolabeled pegylated liposomes, *Clinical cancer research : an official journal of the American Association for Cancer Research*, 7 (2001) 243-254.
58. M. Bolkestein, E. de Blois, S.J. Koelewijn, A.M. Eggermont, F. Grosveld, M. de Jong, G.A. Kon- ing, Investigation of Factors Determining the Enhanced Permeability and Retention Effect in Subcutaneous Xenografts, *Journal of nuclear medicine : official publication, Society of Nuclear Medicine*, 57 (2016) 601-607.

59. S.N. Ekdawi, J.M. Stewart, M. Dunne, S. Stapleton, N. Mitsakakis, Y.N. Dou, D.A. Jaffray, C. Allen, Spatial and temporal mapping of heterogeneity in liposome uptake and microvascular distribution in an orthotopic tumor xenograft model, *Journal of controlled release : official journal of the Controlled Release Society*, 207 (2015) 101-111.
60. W.T. Al-Jamal, Z.S. Al-Ahmady, K. Kostarelos, Pharmacokinetics & tissue distribution of temperature-sensitive liposomal doxorubicin in tumor-bearing mice triggered with mild hyperthermia, *Biomaterials*, 33 (2012) 4608-4617.
61. A.V. Andriyanov, E. Koren, Y. Barenholz, S.N. Goldberg, Therapeutic efficacy of combining pegylated liposomal doxorubicin and radiofrequency (RF) ablation: comparison between slow-drug-releasing, non-thermosensitive and fast-drug-releasing, thermosensitive nano-liposomes, *PloS one*, 9 (2014) e92555.
62. P.S. Yarmolenko, Y. Zhao, C. Landon, I. Spasojevic, F. Yuan, D. Needham, B.L. Viglianti, M.W. Dewhirst, Comparative effects of thermosensitive doxorubicin-containing liposomes and hyperthermia in human and murine tumours, *International journal of hyperthermia : the official journal of European Society for Hyperthermic Oncology, North American Hyperthermia Group*, 26 (2010) 485-498.
63. T. Lammers, L.Y. Rizzo, G. Storm, F. Kiessling, Personalized nanomedicine, *Clinical cancer research : an official journal of the American Association for Cancer Research*, 18 (2012) 4889-4894.
64. S.N. Ekdawi, D.A. Jaffray, C. Allen, Nanomedicine and tumor heterogeneity: Concept and complex reality, *Nano Today*, 11 (2016) 402-414.
65. J. Shi, P.W. Kantoff, R. Wooster, O.C. Farokhzad, Cancer nanomedicine: progress, challenges and opportunities, *Nature reviews. Cancer*, 17 (2017) 20-37.
66. B. Kneidl, M. Peller, G. Winter, L.H. Lindner, M. Hossann, Thermosensitive liposomal drug delivery systems: state of the art review, *International journal of nanomedicine*, 9 (2014) 4387-4398.
67. Z. Al-Ahmady, K. Kostarelos, Chemical Components for the Design of Temperature-Responsive Vesicles as Cancer Therapeutics, *Chemical reviews*, 116 (2016) 3883-3918.
68. S.M. Sullivan, L. Huang, Enhanced delivery to target cells by heat-sensitive immunoliposomes, *Proceedings of the National Academy of Sciences of the United States of America*, 83 (1986) 6117-6121.
69. M.H. Gaber, Modulation of doxorubicin resistance in multidrug-resistance cells by targeted liposomes combined with hyperthermia, *Journal of biochemistry, molecular biology, and biophysics : JBMBB : the official journal of the Federation of Asian and Oceanian Biochemists and Molecular Biologists (FAOBMB)*, 6 (2002) 309-314.
70. B. Smith, I. Lyakhov, K. Loomis, D. Needle, U. Baxa, A. Yavlovich, J. Capala, R. Blumenthal, A. Puri, Hyperthermia-triggered intracellular delivery of anticancer agent to HER2(+) cells by HER2-specific affibody (ZHER2-GS-Cys)-conjugated thermosensitive liposomes (HER2(+) affisomes), *Journal of controlled release : official journal of the Controlled Release Society*, 153 (2011) 187-194.
71. H. Song, J. Zhang, X. Liu, T. Deng, P. Yao, S. Zhou, W. Yan, Development of a bone targeted thermosensitive liposomal doxorubicin formulation based on a bisphosphonate modified non-ionic surfactant, *Pharmaceutical development and technology*, 21 (2016) 680-687.
72. Z.S. Al-Ahmady, O. Chaloin, K. Kostarelos, Monoclonal antibody-targeted, temperature-sensitive liposomes: in vivo tumor chemotherapeutics in combination with mild hyperthermia,

- Journal of controlled release : official journal of the Controlled Release Society, 196 (2014) 332-343.
73. Y. Yang, Y. Yang, X. Xie, X. Cai, H. Zhang, W. Gong, Z. Wang, X. Mei, PEGylated liposomes with NGR ligand and heat-activable cell-penetrating peptide-doxorubicin conjugate for tumor-specific therapy, *Biomaterials*, 35 (2014) 4368-4381.
 74. A. Salvati, A.S. Pitek, M.P. Monopoli, K. Prapainop, F.B. Bombelli, D.R. Hristov, P.M. Kelly, C. Aberg, E. Mahon, K.A. Dawson, Transferrin-functionalized nanoparticles lose their targeting capabilities when a biomolecule corona adsorbs on the surface, *Nature nanotechnology*, 8 (2013) 137-143.
 75. M. Hadjidemetriou, Z. Al-Ahmady, M. Mazza, R.F. Collins, K. Dawson, K. Kostarelos, In Vivo Biomolecule Corona around Blood-Circulating, Clinically Used and Antibody-Targeted Lipid Bilayer Nanoscale Vesicles, *ACS nano*, 9 (2015) 8142-8156.
 76. B.M. Dicheva, T.L. ten Hagen, L. Li, D. Schipper, A.L. Seynhaeve, G.C. van Rhooen, A.M. Eggermont, L.H. Lindner, G.A. Koning, Cationic thermosensitive liposomes: a novel dual targeted heat-triggered drug delivery approach for endothelial and tumor cells, *Nano letters*, 13 (2013) 2324-2331.
 77. M.S. Kim, D.W. Lee, K. Park, S.J. Park, E.J. Choi, E.S. Park, H.R. Kim, Temperature-triggered tumor-specific delivery of anticancer agents by cRGD-conjugated thermosensitive liposomes, *Colloids and surfaces. B, Biointerfaces*, 116 (2014) 17-25.
 78. B.M. Dicheva, T.L. ten Hagen, A.L. Seynhaeve, M. Amin, A.M. Eggermont, G.A. Koning, Enhanced Specificity and Drug Delivery in Tumors by cRGD-Anchoring Thermosensitive Liposomes, *Pharmaceutical research*, 32 (2015) 3862-3876.
 79. B.M. Dicheva, A.L. Seynhaeve, T. Soulie, A.M. Eggermont, T.L. Ten Hagen, G.A. Koning, Pharmacokinetics, Tissue Distribution and Therapeutic Effect of Cationic Thermosensitive Liposomal Doxorubicin Upon Mild Hyperthermia, *Pharmaceutical research*, 33 (2016) 627-638.
 80. C. Wang, X. Wang, T. Zhong, Y. Zhao, W.Q. Zhang, W. Ren, D. Huang, S. Zhang, Y. Guo, X. Yao, Y.Q. Tang, X. Zhang, Q. Zhang, The antitumor activity of tumor-homing peptide-modified thermosensitive liposomes containing doxorubicin on MCF-7/ADR: in vitro and in vivo, *International journal of nanomedicine*, 10 (2015) 2229-2248.
 81. E. Kneepkens, E. Heijman, J. Keupp, S. Weiss, K. Nicolay, H. Grull, Interleaved Mapping of Temperature and Longitudinal Relaxation Rate to Monitor Drug Delivery During Magnetic Resonance-Guided High-Intensity Focused Ultrasound-Induced Hyperthermia, *Investigative radiology*, (2017).
 82. A.A. Manzoor, L.H. Lindner, C.D. Landon, J.Y. Park, A.J. Simnick, M.R. Dreher, S. Das, G. Hanna, W. Park, A. Chilkoti, G.A. Koning, T.L. ten Hagen, D. Needham, M.W. Dewhirst, Overcoming limitations in nanoparticle drug delivery: triggered, intravascular release to improve drug penetration into tumors, *Cancer research*, 72 (2012) 5566-5575.
 83. B.L. Viglianti, A.M. Ponce, C.R. Michelich, D. Yu, S.A. Abraham, L. Sanders, P.S. Yarmolenko, T. Schroeder, J.R. MacFall, D.P. Barboriak, O.M. Colvin, M.B. Bally, M.W. Dewhirst, Chemosimetry of in vivo tumor liposomal drug concentration using MRI, *Magnetic resonance in medicine*, 56 (2006) 1011-1018.
 84. A.M. Ponce, B.L. Viglianti, D. Yu, P.S. Yarmolenko, C.R. Michelich, J. Woo, M.B. Bally, M.W. Dewhirst, Magnetic resonance imaging of temperature-sensitive liposome release: drug dose painting and antitumor effects, *Journal of the National Cancer Institute*, 99 (2007) 53-63.

85. M. de Smet, S. Langereis, S. van den Bosch, K. Bitter, N.M. Hijnen, E. Heijman, H. Grull, SPECT/CT imaging of temperature-sensitive liposomes for MR-image guided drug delivery with high intensity focused ultrasound, *Journal of controlled release : official journal of the Controlled Release Society*, 169 (2013) 82-90.
86. M. Peller, L. Willerding, S. Limmer, M. Hossann, O. Dietrich, M. Ingrisich, R. Sroka, L.H. Lindner, Surrogate MRI markers for hyperthermia-induced release of doxorubicin from thermosensitive liposomes in tumors, *Journal of controlled release : official journal of the Controlled Release Society*, 237 (2016) 138-146.
87. A. Gasselhuber, M.R. Dreher, A. Negussie, B.J. Wood, F. Rattay, D. Haemmerich, Mathematical spatio-temporal model of drug delivery from low temperature sensitive liposomes during radiofrequency tumour ablation, *International journal of hyperthermia : the official journal of European Society for Hyperthermic Oncology, North American Hyperthermia Group*, 26 (2010) 499-513.
88. A. Gasselhuber, M.R. Dreher, A. Partanen, P.S. Yarmolenko, D. Woods, B.J. Wood, D. Haemmerich, Targeted drug delivery by high intensity focused ultrasound mediated hyperthermia combined with temperature-sensitive liposomes: computational modelling and preliminary in vivo validation, *International journal of hyperthermia : the official journal of European Society for Hyperthermic Oncology, North American Hyperthermia Group*, 28 (2012) 337-348.
89. Y. Dou, K. Hynynen, C. Allen, To heat or not to heat: Challenges with clinical translation of thermosensitive liposomes, *Journal of controlled release : official journal of the Controlled Release Society*, 249 (2017) 63-73.
90. S. Rizzitelli, P. Giustetto, D. Faletto, D. Delli Castelli, S. Aime, E. Terreno, The release of Doxorubicin from liposomes monitored by MRI and triggered by a combination of US stimuli led to a complete tumor regression in a breast cancer mouse model, *Journal of controlled release : official journal of the Controlled Release Society*, 230 (2016) 57-63.
91. A. Kheirloomoom, C.Y. Lai, S.M. Tam, L.M. Mahakian, E.S. Ingham, K.D. Watson, K.W. Ferrara, Complete regression of local cancer using temperature-sensitive liposomes combined with ultrasound-mediated hyperthermia, *Journal of controlled release : official journal of the Controlled Release Society*, 172 (2013) 266-273.
92. J. Szebeni, P. Bedocs, Z. Rozsnyay, Z. Weiszhar, R. Urbanics, L. Rosivall, R. Cohen, O. Garbuzenko, G. Bathori, M. Toth, R. Bunger, Y. Barenholz, Liposome-induced complement activation and related cardiopulmonary distress in pigs: factors promoting reactogenicity of Doxil and AmBisome, *Nanomedicine : nanotechnology, biology, and medicine*, 8 (2012) 176-184.
93. J. Szebeni, L. Baranyi, S. Savay, J. Milosevits, R. Bunger, P. Laverman, J.M. Metselaar, G. Storm, A. Chanan-Khan, L. Liebes, F.M. Muggia, R. Cohen, Y. Barenholz, C.R. Alving, Role of complement activation in hypersensitivity reactions to doxil and hynic PEG liposomes: experimental and clinical studies, *J Liposome Res*, 12 (2002) 165-172.
94. B. Uziely, S. Jeffers, R. Isacson, K. Kutsch, D. Wei-Tsao, Z. Yehoshua, E. Libson, F.M. Muggia, A. Gabizon, Liposomal doxorubicin: antitumor activity and unique toxicities during two complementary phase I studies, *Journal of clinical oncology : official journal of the American Society of Clinical Oncology*, 13 (1995) 1777-1785.
95. D. Lorusso, A. Di Stefano, V. Carone, A. Fagotti, S. Pisconti, G. Scambia, Pegylated liposomal doxorubicin-related palmar-plantar erythrodysesthesia ('hand-foot' syndrome), *Annals of oncology : official journal of the European Society for Medical Oncology*, 18 (2007) 1159-1164.

96. N. Yokomichi, T. Nagasawa, A. Coler-Reilly, H. Suzuki, Y. Kubota, R. Yoshioka, A. Tozawa, N. Suzuki, Y. Yamaguchi, Pathogenesis of Hand-Foot Syndrome induced by PEG-modified liposomal Doxorubicin, *Human cell*, 26 (2013) 8-18.
97. J. Kubicka-Wołkowska, M. Kędzierska, M. Lisik-Habib, P. Potemski, Skin toxicity in a patient with ovarian cancer treated with pegylated liposomal doxorubicin: A case report and review of the literature, *Oncology Letters*, 12 (2016) 5332-5334.
98. R. Staruch, R. Chopra, K. Hynynen, Localised drug release using MRI-controlled focused ultrasound hyperthermia, *International journal of hyperthermia : the official journal of European Society for Hyperthermic Oncology, North American Hyperthermia Group*, 27 (2011) 156-171.
99. A. Partanen, M. Tillander, P.S. Yarmolenko, B.J. Wood, M.R. Dreher, M.O. Köhler, Reduction of peak acoustic pressure and shaping of heated region by use of multifoci sonications in MR-guided high-intensity focused ultrasound mediated mild hyperthermia, *Medical Physics*, 40 (2013) 013301-n/a.
100. M. Tillander, S. Hokland, J. Koskela, H. Dam, N.P. Andersen, M. Pedersen, K. Tanderup, M. Ylihautala, M. Kohler, High intensity focused ultrasound induced in vivo large volume hyperthermia under 3D MRI temperature control, *Med Phys*, 43 (2016) 1539-1549.

Summary and future perspectives

Samenvatting en toekomstperspectief



SUMMARY

The treatment of cancer has been a topic for scientific research for many decades. Especially in recent years, many new findings are described on the tumor biology and therapy methods. However, in the clinic the “classical” chemotherapy and radiotherapy are still most frequently applied. These treatments often go together with severe side effects because these are not fully tumor directed. In this thesis, cancer therapy using drug containing nanoparticles has been described to make the treatment more targeted and reduce side effects. Liposomes are nanoparticles which are already clinically applied and Doxil®, a liposome that contains the chemotherapeutic Doxorubicin, is the best example for this. Doxil® can be very effective in reducing the side effects of Doxorubicin and these nanoparticles of approximately 100 nm in diameter can accumulate in the tumor by gaps in the endothelial lining of associated blood vessels. Nevertheless, this accumulation does not always induce a significant therapeutic response because the encapsulated Doxorubicin cannot leave the liposome effectively to be taken up by cancer cell nuclei in the tumor. Because of these reasons, thermosensitive liposomes were designed that can release their chemotherapeutic payload when exposed to mild hyperthermia (40-43 °C). These thermosensitive liposomes have shown to cause a higher Doxorubicin accumulation in tumors relatively to the free drug and Doxil®. These findings have resulted in the initiation of several clinical trials for cancer treatment using thermosensitive liposomes, which are currently on going. However, these liposomes can improved, especially the stability in the blood stream. Moreover, the therapeutic response has proven to be variable.

In this thesis the optimization of thermosensitive liposomes is described, which treatments in combination with hyperthermia give the best therapeutic effect, which tumor types are most likely to give a positive therapeutic response to the treatment and a new model is analyzed for a better understanding of the drug delivery mechanism by thermosensitive liposomes. Moreover, a feasibility study is presented for the development of liposomes that are loaded with magnetic nanoparticles for drug delivery by MRI-guidance. A general introduction concerning all these topics is given in **Chapter 1**.

In **Chapter 2**, the analysis of thermosensitive liposomes with different lipid compositions and Doxorubicin loading techniques is described. After the determination of the *in vitro* stability and drug release characteristics at mild hyperthermia, *in vivo* experiments concerning pharmacokinetics, intravital microscopy and therapeutic efficacy were conducted and an attempt to correlate the results between all experiments was made. The results show that *in vitro* analyses are a good measure to compare liposomal formulations, but that these cannot be correlated to *in vivo* outcome.

In **Chapter 3**, two different tumor treatment strategies are compared in two different tumor types. The first strategy is a “1-step” therapy where thermosensitive liposomes are

intravenously administered while the tumor is heated. The second strategy is a "2-step" therapy where the tumor is pre-heated to induce a higher accumulation of thermosensitive liposomes into the tumor, followed by a second heating treatment to cause a drug release in the tumor interstitial space. SPECT/CT analysis shows that preheating induces a higher nanoparticle accumulation, however highly dependent on the tumor type. The results of the therapeutic study implicate that a 1-step therapy is more potent in eliciting a therapeutic response than a 2-step therapy for both tumor types. This was most likely caused by the insufficient accumulation of liposomes in the tumor and the leakage of the drug from the liposomes during the accumulation time.

Chapter 4 describes a comparative study on the therapeutic efficacy of thermosensitive liposomes for two subtypes of breast cancer. It concerns a study in an orthotopic xenograft model that shows that aggressive and less differentiated breast cancers are more prone to respond to treatment with thermosensitive liposomes and hyperthermia than slowly progressing and well differentiated breast cancers. We give a hypothesis that extracellular matrix in the tumor stroma forms an important barrier for effective Doxorubicin delivery to the cancer cell.

In order to better understand the delivery of Doxorubicin *in vivo*, a novel isolated limb infusion model in rats was investigated, which is described in **Chapter 5**. The amount of Doxorubicin that can be delivered after a single passage through a heated tumor can be analyzed in this way. The model shows that a considerable amount of passages are required to obtain similar intratumoral Doxorubicin levels as described in most preclinical studies. This implicates that thermosensitive liposomes with a longer circulation time might be favourable for optimal drug delivery to solid tumors. However, future studies have to investigate this hypothesis.

Chapter 6 describes the production of liposomes that are loaded with magnetic nanoparticles for drug release when exposed to alternating magnetic fields and can be traced *in vivo* by MRI. We have attempted to incorporate the magnetic nanoparticles in the liposomal bilayer or inside the aqueous core of the liposome. Despite using various liposomal preparation techniques, we were not successful in obtaining liposomes with a high loading efficacy.

FUTURE PERSPECTIVES

Thermosensitive liposomes are currently investigated by many groups and with LTSL, there is a formulation which currently tested in clinical trials. The therapeutic results that were found with LTSL can be considered variable and many studies describe the short circulation time and low stability of this formulation in circulation as problematic. With the described results in this thesis, we intend to establish a better image on the aspects of thermosensitive liposomes that are effective and non-effective for optimal tumor therapy. Moreover, we have attempted to also obtain more understanding on the drug delivery mechanics *in vivo* and what could be improved in order to treat a broader group of patients effectively.

In the coming years, thermosensitive liposomes could be a realistic option for clinical cancer treatment. However, more research on these nanoparticles is required in order to improve therapy and make it more patient specific.

SAMENVATTING

De behandeling van kanker is een onderwerp waar al vele decennia onderzoek naar wordt gedaan. Zeker in de recente jaren volgen nieuwe bevindingen over de biologie van kanker en nieuwe therapie methoden elkaar in rap tempo op. Desondanks worden in de kliniek nog met de grootste regelmaat de “klassieke” chemotherapie en radiotherapie toegepast. Dit gaat vaak gepaard met grootschalige bijwerkingen omdat de therapie niet volledig tumor-gericht is. In dit proefschrift is de behandeling van tumoren met behulp van nanodeeltjes die chemotherapeutica bevatten beschreven, om chemotherapie doelgericht te maken en bijwerkingen tegen te gaan. Liposomen zijn nanodeeltjes die al in de kliniek worden toegepast en Doxil®, een liposoom dat het chemotherapeuticum Doxorubicine bevat is hier het beste voorbeeld van. Doxil® kan zeer effectief de bijwerkingen van Doxorubicine tegengaan en deze nanodeeltjes van ca 100 nm in diameter kunnen in de tumor ophopen door openingen in het endotheel van de geassocieerde bloedvaten. Deze ophoping zorgt alleen niet altijd voor een hoger therapeutisch effect omdat het geïncorporeerde Doxorubicine het liposoom niet effectief kan verlaten, om vervolgens opgenomen te worden door de kernen van de kanker cellen in de tumor. Om deze reden zijn thermosensitieve liposomen ontwikkeld, die chemotherapeutica vrij kunnen geven bij blootstelling aan milde hyperthermie (40-43 °C). Deze thermosensitieve liposomen hebben laten zien dat ze voor een hogere accumulatie van Doxorubicine in tumoren en therapeutisch effect zorgen dan het vrije chemotherapeuticum of Doxil®. Dit heeft ervoor gezorgd dat op dit moment, diverse klinische studies lopen met thermosensitieve liposomen voor kanker behandeling. Desondanks kunnen deze liposomen verbeterd worden, met name de stabiliteit in de bloedbaan. Daarnaast is de therapeutische respons is variabel gebleken.

In dit proefschrift wordt de optimalisatie van thermosensitive liposomen beschreven, welke behandelingen in combinatie met hyperthermie het beste therapeutische resultaat geven, in welke tumoren de beste therapeutische effecten verwacht kunnen worden en word een nieuwe methode geanalyseerd om het chemo afgifte systeem met thermosensitive liposomen beter te kunnen begrijpen. Daarnaast wordt een haalbaarheidstudie beschreven voor de ontwikkeling van liposomen die beladen zijn met magnetische nanodeeltjes voor visualisatie met behulp van MRI. Een overkoepelende introductie betreffende deze onderwerpen is beschreven in **Hoofdstuk 1**.

In **Hoofdstuk 2** is de analyse van thermosensitieve liposomen met verschillende lipide samenstellingen en Doxorubicine ladingstechnieken beschreven. Nadat *in vitro* de stabiliteit en vrijgave van Doxorubicine bij milde hyperthermie is bepaalt, worden *in vivo* farmacokinetiek, intravitale microscopie en therapie resultaten hiermee vergeleken. De resultaten laten zien dat *in vitro* analyses een goede graadmeter zijn voor vergelijkingen

van liposomale formulaties, maar dat deze niet gekoppeld kunnen worden aan *in vivo* resultaten.

In **Hoofdstuk 3** zijn twee verschillende tumor behandelingsstrategieën in twee verschillende tumor types vergeleken. De eerste strategie is een zogenaamde “1-staps” therapie waarbij thermosensitieve liposomen in de bloedbaan geïnjecteerd worden terwijl de tumor verwarmd wordt. De tweede strategie is een “2-staps” therapie waarbij de tumor voorverwarmd wordt waardoor thermosensitieve liposomen beter kunnen ophopen in de tumor, gevolgd door een tweede verwarmings stap om het chemotherapeuticum vrij te geven in het interstitium. SPECT/CT analyse laat zien dat de voorverwarming van tumoren zorgt voor een hogere ophoping van de liposomen, al is de hoeveelheid hiervan zeer afhankelijk van het tumor type. De resultaten van therapeutische studies impliceren dat de 1-staps therapie een hogere therapeutische respons induceert dan de 2-staps variant in beide tumor types. Dit resultaat is hoogstwaarschijnlijk veroorzaakt door onvoldoende ophoping van de liposomen en lekkage van het chemotherapeuticum uit de liposomen gedurende de periode die nodig is voor ophoping.

Hoofdstuk 4 beschrijft een vergelijkend onderzoek naar de therapeutische effectiviteit van thermosensitieve liposomen in twee verschillende borstkanker types. Het betreft een studie in een orthotoop muizen model die laat zien dat agressieve en minder gedifferentieerde borsttumoren beter reageren op therapie met thermosensitieve liposomen en hyperthermie dan langzaam ontwikkelende en beter gedifferentieerde tumoren. We beschrijven een hypothese dat de extracellulaire matrix in het stroma van de tumor een belangrijke barrière vormt voor effectieve afgifte van Doxorubicine aan de tumor cel.

Om de afgifte van Doxorubicine door thermosensitieve liposomen *in vivo* beter te kunnen begrijpen is in **Hoofdstuk 5** een geïsoleerde poot perfusie model in ratten beschreven. De hoeveelheid Doxorubicine die in een tumor ophoopt na één passage van de liposomen in een verwarmde tumor is hier geanalyseerd. De resultaten laten zien dat in dit model, vele passages nodig zijn om een gelijkwaardige hoeveelheid Doxorubicine aan een tumor af te geven dan wat regelmatig gevonden wordt in diverse preklinische studies. Dit impliceert dat thermosensitieve liposomen met een langere circulatietijd wellicht effectiever kunnen zijn in optimale chemo afgifte aan een tumor. Desalniettemin moeten toekomstige studies deze hypothese onderzoeken.

Hoofdstuk 6 beschrijft de productie en potentieel van liposomen die beladen zijn met magnetische nanodeeltjes voor chemo vrijgave door alternerende magnetische velden en die in het lichaam gevolgd kunnen worden met behulp van MRI. We hebben getracht de magnetische nanodeeltjes in de liposomale bilaag of in de kern van het liposoom in te kapselen. Ondanks dat veel liposomale bereidingstechnieken zijn getest, zijn we niet succesvol gebleken om deze liposomen met een hoge beladingsgraad te realiseren.

TOEKOMSTPERSPECTIEF

Thermosensitieve liposomen worden tegenwoordig door vele groepen onderzocht en met de LTSL is er een formulatie die op dit moment in klinische studies wordt getest. De therapeutische resultaten van de LTSL zijn variabel te noemen en diverse studies beschrijven de korte circulatietijd en lage stabiliteit van deze formulatie in de bloedbaan als problematisch. Met de beschreven resultaten in dit proefschrift willen we een beter beeld schetsen in de succesvolle en minder succesvolle aspecten van het gebruik van thermosensitieve liposomen voor kanker therapie. Daarnaast hebben we getracht om mechanismen achter chemo afgifte met behulp van thermosensitieve liposomen aan tumoren beter te kunnen begrijpen en wat er verbeterd zou kunnen worden om een bredere groep patiënten effectief te kunnen behandelen.

In de komende jaren kunnen thermosensitieve liposomen een reële optie worden voor kanker behandeling in de kliniek. Desalniettemin is meer onderzoek naar deze nanodeeltjes nodig om de therapie te verbeteren en meer patiënt specifiek te maken.

LIST OF PUBLICATIONS

In depth study on thermosensitive liposomes: Optimizing formulations for tumor specific therapy and in vitro to in vivo relation

Wouter J.M. Lokerse, Esther C.M. Kneepkens, Timo L.M. ten Hagen, Alexander M.M. Eggermont, Holger Gröll & Gerben A. Koning
Biomaterials 2016

Investigation of particle accumulation, chemosensitivity and thermosensitivity for effective solid tumor therapy using thermosensitive liposomes and hyperthermia

Wouter J.M. Lokerse, Michiel Bolkestein, Timo L.M. ten Hagen, Marion de Jong, Alexander M.M. Eggermont, Holger Gröll & Gerben A. Koning
Theranostics 2016

Comparing the therapeutic potential of thermosensitive liposomes and hyperthermia in two distinct subtypes of breast cancer

Wouter J.M. Lokerse, Michiel Bolkestein, Simone U. Dalm, Alexander M.M. Eggermont, Marion de Jong, Holger Gröll & Gerben A. Koning
Journal of Controlled Release 2017

Development and validation of an isolated limb infusion model for investigation of drug delivery kinetics to solid tumors by thermosensitive liposomes and hyperthermia

Wouter J.M. Lokerse, Alexander M.M. Eggermont, Holger Gröll & Gerben A. Koning
Submitted

Feasibility study on magnetic nanoparticle-entrapping liposomes for localized hyperthermia and image-guided drug delivery to solid tumors

Wouter J.M. Lokerse, Sophie Laurent, Sarah Belaïd, Alexander M.M. Eggermont, Holger Gröll, Robert N. Muller & Gerben A. Koning
In Preparation

Formulation and optimization of idarubicin thermosensitive liposomes provides ultrafast triggered release at mild hyperthermia and improves tumor response

Tao Lu, Wouter J.M. Lokerse, Ann L.B. Seynhaeve, Gerben A. Koning & Timo L.M. ten Hagen
Journal of Controlled Release 2015

PHD PORTFOLIO

Summary of PhD training and teaching

Erasmus MC Department:	Department of Surgery
Research School:	Molecular Medicine
PhD period:	May 2011 – November 2015
Promoters:	Prof. Dr. A.M.M. Eggermont, Prof. Dr. H. Grüll
Copromotor:	Dr. G.A. Koning

Courses	Year	ECTS
Anatomy & Physiology (Utrecht University)	2011	7.5
Animal Experimentation (Article 9)	2011	3.0
Biomedical Research Techniques (MolMed)	2011	1.5
In Vivo Imaging (MolMed)	2011	1.8
Advanced Drug Delivery & Drug Targeting (Leiden University)	2011	1.8
Translational Imaging Workshop by AMIE (MolMed)	2012	1.4
Translational Oncology (MolMed)	2012	1.8
Basic DLS & Zeta Potential (Sysmex Etten-Leur)	2012	0.3
NanoNextNL IP Awareness & Valorization (Leiden)	2012	1.0
Scientific Integrity (Erasmus MC)	2014	0.3
NanoNextNL RATA Course (Soesterberg)	2014	1.0
Advanced Immunology (Erasmus MC)	2014	3.0
InDesign C6 Workshop (MolMed)	2014	0.2
Writing Successful Grant Proposals (MolMed)	2014	0.5

Conferences	Year	ECTS	Contribution
MicroNano Conference (Ede)	2011	0.6	
ILS Liposome Advances (London, UK)	2011	1.0	
Mountain & Sea Liposome Workshop (Ameland)	2012	1.0	Presentation
COST TD1004 Group Meeting (London, UK)	2012	1.0	Poster
NanoNextNL Drug Delivery Meeting (Enschede)	2012	0.3	Presentation
Molecular Medicine Day	2013	0.3	Poster
EMIM 2013 (Turin, Italy)	2013	1.0	Poster
NanoNextNL Drug Delivery Meeting (Utrecht)	2013	0.3	Presentation
ESHO 2013 (Munich, Germany)	2013	1.0	Presentation
ECCO 2013 (Amsterdam)	2013	1.0	Poster

NanoNextNL Nanomedicine Day (Amsterdam)	2013	0.3	Poster
MicroNano Conference (Ede)	2013	0.6	Presentation
Molecular Medicine Day	2014	0.3	Poster
ESCDD 2014 (Egmond aan Zee)	2014	1.0	Poster
NanoNextNL Drug Delivery Meeting (Utrecht)	2014	0.3	Presentation
EMIM 2014 (Antwerp, Belgium)	2014	1.0	Presentation
ESHO 2014 (Turin, Italy)	2014	1.0	Presentation
CRS 2014 (Chicago, USA)	2014	1.0	Poster
COST TD1004 Group Meeting (Istanbul, Turkey)	2014	1.0	Presentation
Nanocity 2014 (Utrecht)	2014	1.0	Poster
EMIM 2015 (Tübingen, Germany)	2015	1.0	Poster
ESHO 2015 (Zurich, Switzerland)	2015	-	Presentation
NanoNextNL Nanomedicine Day (Amsterdam)	2015	0.3	Poster

TEACHING ACTIVITIES

Supervision of bachelor student Roos Bakker (Hogeschool Rotterdam) for 4 months

AWARDS

Young investigator travel award (ESHO 2013; Munich, Germany)

Poster award (EMIM 2017; Cologne, Germany)

GRANTS

COST TD1004 Short Term Scientific Mission as visiting researcher to University of Mons, Belgium (February 2012).

ACKNOWLEDGEMENTS

Ik wil als eerste mijn directe begeleider en copromotor **Gerben** bedanken. Vanaf de eerste dag heb ik me altijd onder zijn begeleiding op mijn gemak gevoeld en de open stijl van werk bespreken beviel mij ook zeer. Nieuwe inzichten, maar een kritische kijk op zaken werd altijd op prijs gesteld. Dat we samen met wat goed denkwerk en een realistische kijk op de haalbaarheid van projecten, het onderzoek naar magnetoliposomen hebben omgezet naar alternatieven is daarom ook illustratief te noemen en succesvol gebleken. Maar ook heel informeel even het voetbalweekend doornemen was niet ongebruikelijk en bijzonder prettig. Daarnaast wil ik hem ook bedanken voor alle gelegenheden die hij me heeft aangereikt om met andere mensen binnen het veld samen te kunnen werken en te ontmoeten op congressen, ik heb er mijn huidige baan ook aan te danken. Het is daarom ook bijzonder triest dat ik hem nooit in persoon heb kunnen laten weten hoe dankbaar ik ben voor al het boven genoemde. Ondanks de progressie van zijn ziekte, bleef hij op afstand, tot waar dat kon betrokken. Ik ben ook blij dat hij in alle rust en vrede, in de nabijheid van familie zijn laatste jaar heeft kunnen doorbrengen. Ik hoop dat ik met het afgeronde werk aan zijn verwachtingen heb kunnen voldoen en ik zal zijn aangename persoonlijkheid en onderzoeksgesest nooit vergeten.

Als tweede wil ik mijn promotor **Holger** bedanken. Toen ik je vroeg om de begeleiding van mijn promotietraject van Gerben over te nemen en je daarmee instemde was ik daar zeer blij mee. Dit was van essentieel belang en ondanks dat ik je af en toe wat moeilijk te pakken kon krijgen als ik weer een manuscript had liggen, kan ik het wel ontzettend waarderen dat je deze last vrijwillig hebt gedragen. Ik weet niet of ik ooit zoveel geduld zal krijgen als jij, maar ik heb wel veel van je geleerd, evenals jouw oog voor detail. De overstap van Eindhoven naar Keulen was niet eenvoudig te noemen maar toch kon ik je af en toe even bellen voor een snelle vraag of update. Ik kan met volle overtuiging zeggen dat jouw begeleiding, ondanks op afstand, zeer prettig en effectief was en daar ben ik dankbaar voor. Daarnaast wil ook mijn tweede promotor **Lex** bedanken. Hoewel onze ontmoetingen en gesprekken op twee handen te tellen zijn, maakt het ze niet minder effectief. Jouw directe aanpak van zaken en no-nonsense mentaliteit hebben mij altijd erg aangesproken en na elk gesprek had ik de indruk dat we goede stappen vooruit hadden gemaakt. Die link heeft misschien te maken met jouw Zeeuwse achtergrond waar je me ooit over verteld hebt. De wetenschap dat je op de achtergrond altijd aanwezig was als er belangrijke beslissingen genomen moesten worden was van grote waarde voor mij.

Ook wil ik graag **Joke** bedanken voor alle steun en vertrouwen. Toen de situatie van Gerben aan het licht kwam en er een contractverlenging moest komen om mijn promotie tot een goed einde te brengen, ben ik door jou persoonlijk uitgenodigd om op gesprek te komen over de situatie. Om even bij het afdelingshoofd op gesprek te komen is niet niks, maar direct kreeg ik de indruk dat je vertrouwen had in de plannen die ik had gemaakt

en ik ben daarom ook zeer dankbaar dat ik langer kon blijven om mijn werk succesvol af te ronden.

Mijn naaste collega's op de werkvloer wil ik een dankwoord geven voor de prettige samenwerking en plezierige tijd. Ten eerste **Michiel**, de enige andere Nederlandse promovendus in onze groep. We hebben goed samen gewerkt op twee hoofdstukken van dit proefschrift waar we denk ik met trots op terug kunnen kijken. Daarnaast hebben we ook vele congressen bezocht die ook altijd erg gezellig waren. Of het nu Egmond aan zee of Chicago was, altijd konden we er met een biertje erbij er een prima avond van maken. Secondly, I would like to thank **Asha** for the nice times in the lab. Although we did not really work together much, it was always nice to see you come in during the work in the weekends and have a chat about all kinds of things, it was nice to have you around. **Sara**, a.k.a. Granjera, thanks for all the nice chats and company during our simultaneous liposome prepping. I hope you currently are having good times back in Spain. But also my apartment neighbor **Mesha** I would like to thank for nice times. We always had nice conversations about work, Pakistani stuff or little Ari that was hanging around at my side of the balcony. **Lilia** and **Bilyana**, you graduated halfway my PhD period but it was enough for me to acknowledge you here. Conferences in London and Turin, respectively, were very nice, I had a good time with you there.

De analisten binnen onze groep verdienen natuurlijk ook een groot dankwoord. **Joost** uiteraard als eerste. Altijd positief gestemd en erg behulpzaam, twee aspecten die het lab absoluut vorm gaven. En als er dan even iets tegen zat, dan was met een half uurtje foute muziek weer alles goed. Natuurlijk wil ik je ook bedanken voor alle dingen die je me in en om het lab heb geleerd, het was essentieel en ik heb daar nu nog profijt van. Ik wens je dan ook veel succes toe met je nieuwe baan. Ook **Cindy** wil ik heel erg bedanken voor alles. Het is ook hier bijzonder triest dat ik dit niet in persoon kan doen. Ze was zeer behulpzaam en wist met een kritische noot altijd experimenten optimaal te krijgen. Als we samen dierexperimenten in het weekend moesten doen, was dat geen probleem voor haar. In de vroege zondagochtend, zelfs na een feest avond of voor een actieve dag met de kinderen was niet te gek voor haar. Mede dankzij haar is dit proefschrift nu afgerond en daar ben ik erg dankbaar voor. Daarnaast ook **Thomas** en **Csilla** bedankt voor de hulp en gezelligheid in het lab.

Collega's van groepen waar ik mee samen gewerkt heb wil ik ook graag bedanken. Ten eerste de mensen van de Nucleaire geneeskunde & Radiologie onder leiding van **Marion**. Ik heb veel profijt gehad van jullie kennis en expertise, wat terug te zien is in hoofdstuk 3 & 4. In het bijzonder wil ik **Simone** bedanken voor de hulp met het opzetten van het borstkanker model, dit hoofdstuk had geen vorm gekregen zonder jouw adviezen. Ook wil ik mijn dankwoord geven aan de burens, het lab van **Ron**. Even een snelle vraag of als ik wat nodig had was nooit te veel bij **Gisela** en **Sandra**. I would also like to thank the group of Prof **Robert Muller** for hosting me back in February 2012 at the University

of Mons. Although our project did not give the success that we initially hoped for, my time at your lab was informative and I definitely made use of that in my later research. **Esther** wil ik ook hartelijk danken voor de prettige samenwerking. Jouw oog voor detail was van grote waarde in ons eerste paper en mede daardoor is het ook goed ontvangen in het drug delivery wereldje. Ik wens je veel succes met je toekomstige baan en ben er van overtuigd dat je ook daar goed zal scoren. Andere collega's van de TU Eindhoven en Philips, bijzonder bedankt voor de prettige samenwerking en de mooie resultaten die we samen geboekt hebben.

Ik wil mijn ouders, familie en vrienden bedanken voor de support en er altijd te zijn als dat nodig was. Vooral mijn **vader en moeder, Rudy, Ivo en Nadia**. Ik weet dat ik jullie af en toe overrompelde met de verhalen over mijn promotietraject waarmee ik over de vloer kwam, maar dat is nu eindelijk voorbij. Jullie nuchtere repsons op mijn verhalen bracht vaak perspectief dat andere zaken in het leven veel belangrijker zijn, iets wat ik soms tijdens mijn promotietraject dreigde te vergeten. Bijzonder bedankt voor al deze onvoorwaardelijke steun, ik had hier niet gestaan zonder jullie.

And lastly, **Sandra**, I cannot really put in words show much you have meant to me in the last three years. Of course your brightness and eternal motivation were of major help to me in completing this thesis. We could even have deep discussions about a new chapter that I wrote, how to make it as best as possible. But what is much more important is the feeling that you were always next to me, every single day, that support is worth so much more. I am really blessed with someone like you by my side.

CURRICULUM VITAE

Wouter Lokerse was born on the 26th of February 1986 in Terneuzen, the Netherlands. He attended secondary education at the Buys Ballot College in Goes where he completed his HAVO degree. Consecutively, he got his Bachelor degree in Biochemistry at the HZ university of applied sciences in Vlissingen, the Netherlands and gained experience in high throughput drug screening by a one year internship at Organon N.V. in Oss, the Netherlands. Afterwards, he entered Utrecht University to obtain a master degree in Molecular & Cellular Life Sciences. In that period, internships were followed at the Proteomics Center at Utrecht University where protein turnover was analyzed using mass spectrometry and at Intervet B.V. in Boxmeer, the Netherlands, where work on novel DNA vaccines was conducted for effective parasite treatment in cattle. After completing his master thesis on drug delivery through epithelial and endothelial barriers in the group of Prof. Dr. van Bergen en Henegouwen, he joined the group of Experimental and Surgical Oncology at the Erasmus Medical Center in 2011 to start a PhD project under supervision of Dr. Gerben Koning. His doctoral thesis focused on the optimization of thermosensitive liposomes, providing detailed analysis on *in vitro* testing procedures and preclinical models for better interpretation of the delivery strategy and therapeutic response. Since January 2016, he continued the research on thermosensitive liposomes in the group of Prof. Dr. Lars Lindner at the Ludwig Maximilian University of Munich, Germany.